Structure-function analyses of the ribosome-associated chaperone NAC (nascent polypeptide-associated complex) in *Saccharomyces cerevisiae*

Dissertation zur Erlangung des akademischen Grades eines Doktors der Naturwissenschaften (Dr. rer. nat.)

vorgelegt von

Locher, Lisa

an der

Mathematisch-Naturwissenschaftliche Sektion

Fachbereich Biologie

11.08.2016

1. Referentin: Prof. Elke Deuerling

2. Referentin: Prof. Karin Hauser

Table of contents

1. Abbreviations

Å	Ångström
aa	amino acid
AAA+	ATPases associated with diverse cellular activities
ACD	α-crystallin domain
Acetyl-CoA	Acetyl-Coenzyme A
ADP	Adenosine diphosphate
ALP	Autophagy lysosome pathway
Amp	Ampicillin
ATP	Adenosine triphosphate
BSA	Bovine serum albumin
CD	Circular dichroism
C. elegans	*Caenorhabditis elegans*
CFTR	Cystic fibrosis membrane regulator
CHIP	C-terminus of Hsc70-interacting protein
CLANS	Cluster analysis of sequences
Cm	Chloramphenicol
Cryo-EM	Cryo-electron microscopy
CS	Citrate synthase
CTD	C-terminal domain
CTS	C-terminal sequence
Da	Dalton
D. melanogaster	*Drosophila melanogaster*
DMSO	Dimethyl sulfoxide
DNA	Deoxyribonucleic acid
dNTP	Deoxynucleotide
DTT	Dithiothreitol
E. coli	*Escherichia coli*
EDTA	Ethylene-diamine-tetraacetic acid
ER	Endoplasmic reticulum
ES	Expansion element
fMet	N-formylated methionine
G6PDH	Glucose-6-phosphate dehydrogenase
HEPES	4-(2-hydroxyethyl)piperazine-1-ethanesulfonic acid
HMM	Hidden Markov Model
H. sapiens	*Homo sapiens*

HPD-motif	Histidine-proline-aspartate-motif
HPLC	High-performance liquid chromatography
Hsc	Constitutively expressed heat shock protein
Hsp	Heat shock protein
Hyg B	Hygromycin B
INQ	Intra-nuclear quality control compartment
IPOD	Insoluble protein deposit
IPTG	Isopropyl *β*-D-1-thiogalactopyranoside
JUNQ	Juxta-nuclear quality control compartment
Kan	Kanamycin
kDa	Kilo Dalton
L-Can	L-Canavanine
Luci	Luciferase
MAP	Methionine aminopeptidase
MDa	Mega Dalton
MetAP	Methionine aminopeptidase
M. jannaschii	*Methanocaldococcus jannaschii*
MOPS	3-(N-morpholino)propanesulfonic acid
mRNA	Messenger ribonucleic acid
MS	Mass spectrometry
NAC	Nascent polypeptide-associated complex
NAT	N-acetyltransferase
NBD	Nucleotide-binding domain
NC	Nascent polypeptide chain
NEF	Nucleotide exchange factor
NES	Nuclear export sequence
NMR	Nuclear magnetic resonance
NRMSD	Normalized root mean square deviation
NTD	N-terminal domain
NTS	N-terminal sequence
OD	Optical density
P-bodies	Processing bodies
pBpa	para-benzoylphenylalanine
PCR	Polymerase chain reaction
PDF	Peptide deformylase
PDI	Protein disulphide isomerase
PMSF	Phenylmethylsulfonyl fluoride

PPI	Peptidyl-prolyl cis-trans isomerase
Prot. K	Proteinase K
PSI-BLAST	Position Specific Iterative-Basic Local Alignment and Search Tool
PTC	Peptidyltransferase centre
RAC	Ribosome-associated complex
RNA	Ribonucleic acid
RNase A	Ribonuclease A
RNC	Ribosome nascent-chain complex
RP	Ribosomal protein
rRNA	Ribosomal nucleic acid
RT	Room temperature
SAXS	Small-angle X-ray scattering
S. cerevisiae	*Saccharomyces cerevisiae*
SBD	Substrate-binding domain
SDS-PAGE	Sodium dodecyl sulfate polyacrylamide gel electrophoresis
SG	Stress granule
SH3	Src-homology 3
sHsp	Small heat shock protein
SMA	Super-molecular assembly
Spec	Spectinomycin
S. pombe	*Schizosaccharomyces pombe*
SR	SRP receptor
SRP	Signal recognition particle
SS	Signal sequence
Ssb	Stress-seventy subfamily B
T. aestivum	*Triticum aestivum*
TCA	Trichloroacetic acid
TF	Trigger Factor
tRNA	Aminoacyl-transfer ribonucleic acid
UBA	Ubiquitin associated
UPS	Ubiquitin proteasome system
UPR	Unfolded protein response
Wt	Wild type
yEGFP	yeast enhanced green fluorescent protein
ZHD	Zuotin homology domain
Zuo	Zuotin

2. Summary

2.1 Summary (English version)

Correct folding of newly synthesized proteins is one of the main functions of the cellular proteostasis system. To uphold this system, a widespread network of different proteins with a multitude of functions has evolved in pro- and eukaryotes. One important part of this network are molecular chaperones. Two classes can be distinguished: cytosolic and ribosome-associated chaperones. They exert multiple functions and reflect a conserved strategy to support the process of protein folding. When localized at the ribosome they bind near the exit tunnel where they contact newly synthesized nascent chains. They are not only involved in the process of folding but also modulate the translation activity thereby regulating the influx of new proteins into the cellular proteome. In yeast two chaperone complexes associate with the ribosome: The tripartite Ssb-RAC (ribosome associated complex) system, and the nascent polypeptide-associated complex (NAC).
Eukaryotic NAC is a heterodimer (αβ-NAC) known to participate in multiple processes in the cell. Its mechanisms of action, however, are still poorly understood. This work deals with the principles of NAC interaction with aggregating proteins and other substrates.

Apart from its functions on ribosomes, NAC was found associated with artificial protein aggregates in mammalian cells as well as various aggregates in *C. elegans*. In yeast, simultaneous deletion of NAC and Ssb leads to an enhanced protein aggregation compared to cells lacking Ssb only. One aim of this work was to better understand the interaction of NAC with aggregating proteins. In contrast to *C. elegans*, no co-localization of NAC was detected with heat shock induced protein aggregates in yeast. When pelleting the aggregates before heat shock, directly afterwards and during recovery, a slight increase of NAC was observed in the pellet fraction upon recovery. This points towards a role of NAC in protein disaggregation rather than to a role during the aggregation of formerly native proteins. This finding was supported by the positive effect of NAC on the reactivation of luciferase. Interestingly, NAC increased the aggregation levels of model proteins *in vitro*. The mechanism behind this unexpected effect remains elusive so far.

In yeast, two different NAC heterodimers exist, αβ and αβ'. All subunits contain a NAC domain responsible for dimerization. The α-subunit contains an additional UBA domain at its C-terminus. Using X-ray crystallography, only the structure of the dimerization and the UBA domain of archaea NAC and human αβ-NAC was determined so far (Spreter et al., 2005; Liu et al., 2010; Wang et al., 2010). By performing bioinformatics analyses, conserved regions in the sequences of the NAC subunits were identified. When investigating the C-termini of the

two β-subunits present in yeast, obvious differences were detected. These may account for a different substrate specificity of the two heterodimeric NAC complexes present in yeast. Parts of this analysis were published in Ott et al. (2015). In addition, a structure model of yeast NAC was constructed using the dimerization domain of human NAC as template to allow further analyses. Using circular dichroism measurements structural changes induced by different deletions of the UBA domain and the adjacent linker region connecting the UBA and the NAC domains of α-NAC were visualized. The deletion of these regions seemed to have an influence on the remaining structure of the NAC heterodimer.

Although NAC is known to interact with a variety of proteins and nascent chains no binding site(s) has been identified so far. To identify this region(s), *in vivo* crosslinking experiments with the zero-space crosslinker para-benzoylphenylalanine (pBpa) were designed. Two criteria were applied to determine suitable positions for pBpa incorporation: location in a hydrophobic patch or surface exposure of the residue. Using the results of the bioinformatics analyses, hydrophobic patches were identified on the surface of the dimerization and the UBA domain of NAC. Using the structure model of yeast NAC, possible positions for the incorporation of the unnatural amino acid pBpa were investigated. First experiments showed the successful incorporation of pBpa into the NAC proteins at most positions tested. Additionally, two different specific crosslinks of NAC with other proteins were determined *in vivo*.

Ott A-K, Locher L, Koch M, Deuerling E (2015) Functional Dissection of the Nascent Polypeptide-Associated Complex in *Saccharomyces cerevisiae*. *PLoS ONE* 10: e0143457

2.2 Zusammenfassung (Deutsche Version)

Die Faltung neuer Proteine ist eine der Hauptaufgaben der zellulären Proteostase. Um dieses System aufrecht zu erhalten, hat sich sowohl in Pro- als auch in Eukaryonten ein umfangreiches Netzwerk von verschiedensten Proteinen mit unterschiedlichen Aufgaben entwickelt. Ein Hauptbestandteil dieses Netzwerks sind molekulare Chaperone. Diese können entweder frei im Zytosol vorkommen oder gebunden an Ribosomen. Am Ribosom interagieren sie mit naszierenden Ketten und helfen den neu-synthetisierten Polypeptiden ihre native Struktur zu erreichen. Außerdem spielen sie eine Rolle bei der Regulation der Translationsaktivität des Ribosoms. Dadurch können sie die Menge an neu-synthetisierten Proteinen steuern. In *S. cerevisieae* existieren zwei unterschiedliche ribosomenassoziierte Systeme: Das Ssb-RAC (ribosome associated complex) System sowie NAC (nascent polypeptide associated complex). NAC ist in allen Eukaryonten hochkonserviert und scheint an einer Vielzahl zellulärer Prozesse beteiligt zu sein. Wie genau NAC in diese Prozesse eingreift, ist allerdings noch größtenteils unbekannt. In dieser Arbeit lag darum der Fokus auf der Analyse der Interaktion von NAC mit Substraten inklusive aggregierenden Proteinen.

Eukaryontisches NAC ist ein Heterodimer (αβ-NAC) und hat unter anderem eine Funktion als Chaperon, zum einen am Ribosom aber wahrscheinlich auch im Zytosol an Aggregaten. Es wurde beispielsweise sowohl an artifiziellen Aggregaten in Säugerzellen als auch an Aggregaten unterschiedlichen Ursprungs in *C. elegans* gefunden. In Hefezellen führt eine simultane Deletion von NAC und Ssb zu einer verstärkten Aggregation im Vergleich zu Zellen, denen lediglich Ssb fehlt. Ein Ziel dieser Arbeit war es, diese direkte Interaktion besser zu verstehen. In *in vivo*-Experimenten mit Hefe konnte allerdings, im Vergleich zu Experimenten in *C. elegans*, keine Kolokalisierung von NAC mit Hitzeschockaggregaten festgestellt werden. Pelletierung der Aggregate vor dem Hitzeschock, direkt danach oder während der Erholungsphase zeigte einen leichten Anstieg der Menge an NAC in der Pelletfraktion erst mit Beginn der Erholungsphase. Dies deutet darauf hin, dass NAC eher eine Rolle bei der Disaggregation von Proteinen spielt und nicht in den eigentlichen Aggregationsprozess ehemals nativer Proteine eingreift. Diese Annahme wird durch den positiven Effekt von NAC auf die Reaktivierung von Luciferase unterstützt. War NAC während des Hitzeschocks von Modellproteinen zugegen, führte dies zu einem Anstieg der Aggregation im Vergleich zum Verhalten der Proteine ohne NAC. Der Grund für diesen Effekt ist bisher unklar.

In Hefe existieren zwei heterodimere NAC-Komplexe, αβ und αβ‘. Alle Untereinheiten besitzen eine NAC-Domäne, welche verantwortlich für die Dimerisierung ist. Die α-Untereinheit besitzt eine zusätzliche UBA-Domäne in ihrem C-Terminus. Bisher konnten

lediglich die Dimerisierungsdomäne und die UBA-Domäne von NAC aus Archaeen und von humanem αβ-NAC kristallisiert werden (Spreter et al., 2005; Liu et al., 2010; Wang et al., 2010). Um weitere Einblicke in die Struktur zu gewinnen, wurden in dieser Arbeit bioinformatische Analysen durchgeführt. Dadurch konnten einerseits konservierte Regionen in den Sequenzen der NAC Untereinheiten identifiziert werden, andererseits war es möglich, ein Strukturmodell von Hefe-NAC zu erstellen, wobei die kristallisierte Dimerisierungsdomäne von humanem NAC als Vorlage genutzt wurde. Große Unterschiede in der Sequenz der C-Termini der beiden in Hefe vorhandenen β-Untereinheiten wurden festgestellt. Diese Unterschiede könnten die verschiedenen Substratspezifitäten der beiden in Hefe vorkommenden heterodimeren NAC Komplexe erklären. Strukturelle Veränderungen, die durch verschiedene Deletionen der UBA-Domäne und Teile der Linkerregion zwischen der UBA- und der NAC-Domäne in NAC hervorgerufen wurden, wurden mittels zirkularem Dichroismus gemessen. Die Deletion dieser Regionen scheint die Struktur des restlichen Heterodimers zu beeinflussen. Teile dieser Analysen sind publiziert in Ott et al. (2015).

NAC interagiert mit einer Vielzahl unterschiedlicher Proteine und naszierender Ketten. Nichtsdestotrotz sind die Substratbindestelle(n) bisher unbekannt. Zur Identifizierung der Substratbindestelle(n) sind *in vivo* Crosslinking-Experimente geplant. Dazu muss die unnatürliche, UV-aktivierbare Aminosäure para-Benzoylphenylalanin (pBpa) in NAC eingebaut werden. pBpa besitzt keinen Linker, das bedeutet, dass ein möglicher Bindungspartner nur detektiert wird, wenn er direkt mit NAC interagiert. Die Positionen für die Inkorporation von pBpa in die Proteinstruktur von NAC wurden mittels zwei Kriterien ausgewählt: Lokalisation in einem hydrophoben Bereich oder Oberflächenexposition. Mittels des Strukturmodells von Hefe-NAC wurden mehrere hydrophobe Bereiche auf der Oberfläche der Dimerisierungs- sowie der UBA-Domäne identifiziert. In diesen Bereichen wurden Aminosäuren ausgewählt, die durch pBpa ersetzt werden konnten. Erste *in vivo* Experimente zeigen eine erfolgreiche Inkorporation von pBpa in die Struktur von NAC an der Mehrzahl der ausgewählten Stellen. Bisher konnten zwei spezifische, unterschiedliche Crosslinks von NAC mit anderen Proteinen detektiert werden.

Ott A-K, Locher L, Koch M, Deuerling E (2015) Functional Dissection of the Nascent Polypeptide-Associated Complex in *Saccharomyces cerevisiae*. *PLoS ONE* 10: e0143457

3. Introduction

Protein synthesis requires the transcription of the information encoded on the DNA to mRNA (messenger RNA) and subsequent translation by ribosomes. By folding into a three-dimensional structure, a functional protein is formed (Hutt et al., 2009). Due to their chemical properties proteins are prone to misfolding. The cell has developed an extensive quality control system to maintain protein homeostasis (proteostasis, Fig. 1) (Powers et al., 2009). During productive folding, newly synthesized proteins reach their native structures assisted by molecular chaperones. Most of them pass one or multiple folding intermediates on the way. These folding intermediates have a tendency to misfold. If this happens, they can either be refolded by molecular chaperones or they are targeted to the ubiquitin proteasome system (UPS) for degradation. The UPS is also responsible for the degradation of native proteins when required. Misfolded and unfolded proteins can form different kinds of aggregates when coming in close proximity. They are distinguished in amorphous aggregates which are rather disordered, oligomers and amyloid fibrils which are composed of multiple oligomers. Cells have evolved two major pathways to deal with aggregated proteins. In some cases, chaperones are able to dissolve the aggregates and the extracted proteins are either refolded or targeted for degradation by the UPS. If this is not possible, the aggregates are targeted for autophagy.

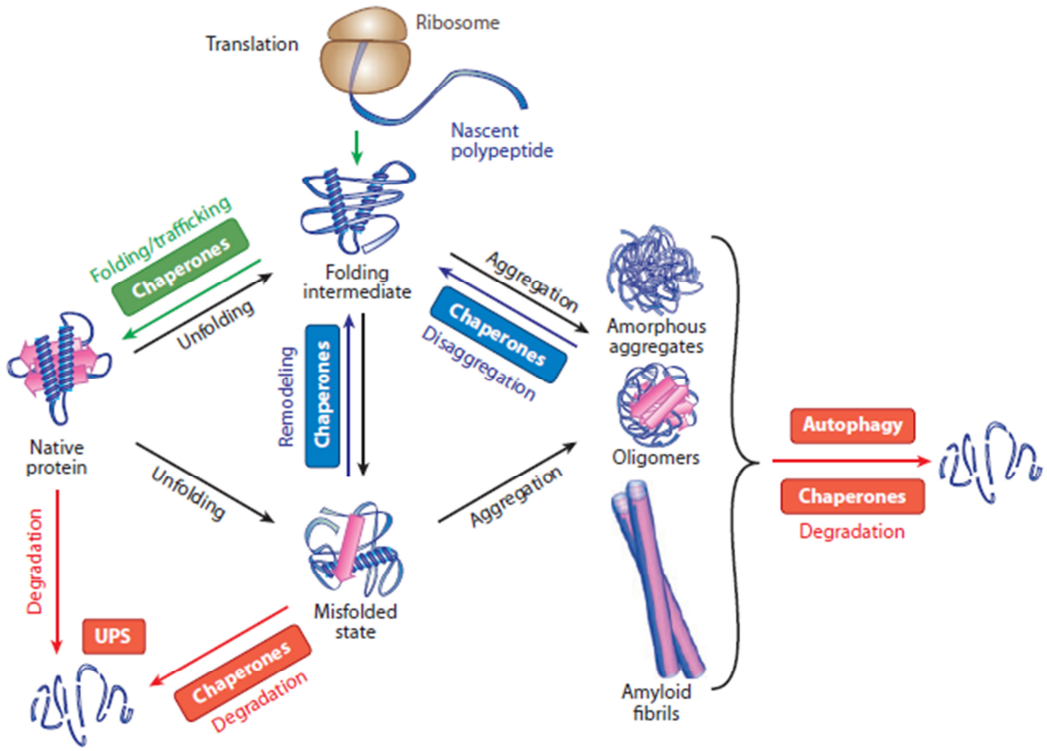

Fig. 1: Model of the proteostasis network. Overview of the different pathways and possibilities newly folded proteins can take upon synthesis and afterwards. UPS: ubiquitin proteasome system. Figure was taken from Kim et al. (2013).

Upon different kinds of stresses like heat shock or nutrient deprivation, proteostasis is impaired. The balance of the system is shifted towards protein aggregation. After an acute stress situation has passed, the cell is able to regenerate and to dissolve or degrade the aggregates. Under persistent stress conditions the system might collapse, which can eventually lead to apoptosis.

Protein misfolding and aggregation have been associated with a variety of neurodegenerative diseases (Powers et al., 2009; Douglas and Dillin, 2010) like Chorea Huntington (Maiti et al., 2014), Parkinson's disease (Gundersen, 2010) or Alzheimer's disease (Xu et al., 2002). Molecular chaperones play a major role in the concept of proteostasis. They help newly synthesized proteins to fold into their native conformations, play a role in targeting proteins to their point of destination, help with degradation and are even able to reactivate aggregated proteins.

3.1 The ribosome: structure and function

Protein biosynthesis is accomplished by ribosomes. The translation rate of ribosomes differs considerably between bacterial and eukaryotic cells. In bacteria, ribosomes translate at a speed of 15 – 20 aa/sec, whereas in eukaryotes, 5 – 7 aa/sec are translated (Wegrzyn and Deuerling, 2005; Bashan and Yonath, 2008).

The overall architecture and function of ribosomes is highly conserved in pro- and eukaryotes. The highest sequence conservation is found in the stretch encoding the functional central core that comprises the catalytically active site, the PTC (peptidyl transferase centre) (Bashan and Yonath, 2008). Ribosomes consist of a small and a large subunit, whose sizes differ between pro- and eukaryotes. In bacteria, the small 30S and the large 50S subunit comprise the functional 70S ribosome (~ 2.4 MDa). It consists of three ribosomal RNAs (rRNAs) – 5S, 23S and 16S – and 55 ribosomal proteins. In eukaryotes, the 80S ribosome (~ 4 MDa) is formed by the small 40S and the large 60S subunit. The ribosome consists of 4 rRNAs (5S, 28S, 5.8S and 18S) and 82 proteins. In contrast to the prokaryotic ribosome, the eukaryotic one contains multiple long additional rRNA expansion elements (ES) (Wilson and Nierhaus, 2005; Bashan and Yonath, 2008; Yusupova and Yusupov, 2014). Recently it was shown, that the composition of ribosomes and their translational specificity varies depending on the translational status (monosomes vs. polysomes) in yeast and mouse cells. The stoichiometry among ribosomal proteins correlates to the growth rate and depends on the number of ribosomes bound per mRNA as well as on the growth conditions (Slavov et al., 2015).

X-ray crystallographic analysis and cryo-electron microscopy (cryo-EM) performed in recent years allowed the determination of ribosomal structures thereby allowing deeper insights into protein biosynthesis. Using cryo-EM, initial information about the structure of the bacterial ribosome was gained (Frank et al., 1995, Stark et al., 1997; Agrawal et al., 1998). These analyses were followed by X-ray crystallization of the 30S subunit of *Thermus thermophilus*, the 50S subunit of *Haloarcula marismortui* and the entire 70S subunit of *Thermus thermophilus* (Cate et al., 1999; Ban et al., 2000; Wimberly et al., 2000; Yusupov et al., 2001). Nowadays the structures of the 70S ribosome of *E. coli* and the 80S ribosomes of *S. cerevisiae*, *D. melanogaster* and *H. sapiens* have been solved via X-ray crystallography (Fig. 2) (Ben-Shem et al., 2010; Anger et al., 2013; Khatter et al., 2015).

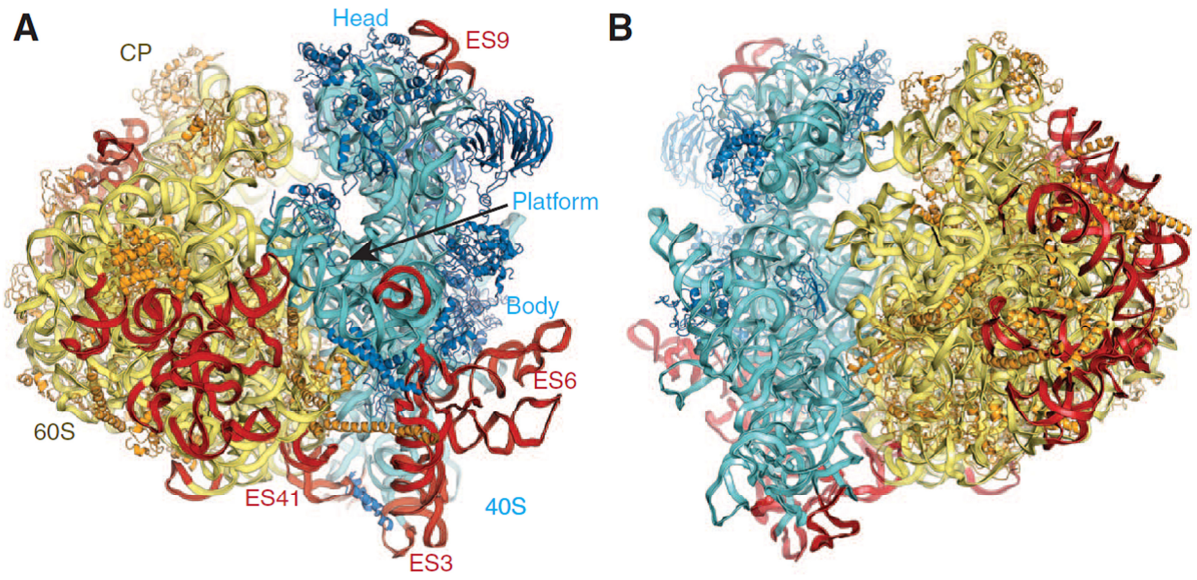

Fig. 2: Crystal structure of the *S. cerevisiae* 80S ribosome. (A) View on the ribosome from the E-site of the PTC. (B) View from the A-site of the PTC. The proteins and mRNA in the 40S subunit are coloured dark and light blue, respectively. In the 60S subunit, proteins and mRNA are coloured dark and pale yellow, respectively. Expansion segments are marked in red. Figure was taken from Ben-Shem et al. (2010).

The ribosome is considered to be a ribozyme: The interface of the two subunits, which holds all active sites, is mainly composed of rRNA as is the peptidyl transferase centre (PTC), which is the catalytically active core responsible for peptide bond formation (Nissen et al., 2000; Bashan and Yonath, 2008).

The different roles in polypeptide synthesis are divided between the two ribosomal subunits. The small ribosomal subunit binds the mRNA, contains the decoding centre and controls the fidelity and accuracy of translation. The large ribosomal subunit contains the PTC and the ribosomal exit tunnel where the nascent chain leaves the ribosome (Bashan and Yonath, 2008). This tunnel crosses through the complete subunit, thereby reaching a length of 80 – 100 Å, bridging the distance between the PTC and the cytosolic environment. Its diameter

varies from 20 Å at the widest point to 10 Å at the narrowest with an average diameter of 15 Å (Malkin and Rich, 1967; Blobel and Sabatini, 1970; Smith et al., 1978; Bernabeu and Lake, 1982; Yonath et al., 1987; Ban et al., 2000; Nissen et al., 2000; Gabashvili et al., 2001; Spahn et al., 2001; Voss et al., 2006; Wilson and Beckmann, 2011). In an extended conformation around 30 amino acids are able to fit into the tunnel. If the amino acids adopt an α-helical conformation, the tunnel can hold twice as much (Picking et al., 1992; Ban et al., 1999; Nissen et al., 2000).

α-helical structures at the C-termini of emerging nascent chains can form in the ribosomal tunnel near the PTC as well as in the lower 20 – 30 Å vestibule region of the tunnel (Lim and Spirin, 1986; Kosolapov et al., 2004; Woolhead et al., 2004; Lu and Deutsch, 2005a/b; Woolhead et al., 2006; Bhushan et al., 2010; Tu and Deutsch, 2010; Wilson and Beckmann, 2011; Tu et al., 2014; Holtkamp et al., 2015). Recently it was shown, that ARD1, a small zinc-finger domain, folds deep inside the ribosomal exit tunnel. Using single molecule measurements it was determined, that a pulling force prevents ribosome stalling (Nilsson et al., 2015).

In accordance with that, numerous reconstitutions of 70S and 80S ribosomes via cryo-EM revealed a limited flexibility of the ribosomal tunnel which renders it unlikely that apart from α-helices other secondary structure conformations are formed within the tunnel (Halic et al., 2006 a/b; Chandramouli et al., 2008; Becker et al., 2009; Seidelt et al., 2009; Taylor et al., 2009). It was further shown, that the ribosomal tunnel is involved in the regulation of protein synthesis by modulating the activity of the PTC (Mankin, 2006; Beringer, 2008; Ito et al., 2010; Ramu et al., 2011). Additional functions are its involvement in early protein folding, its regulation of translation speed and its recruitment of targeting factors as well as chaperones to the exit site (Wilson and Beckmann, 2011).

The tunnel wall is primarily formed by a negatively charged rRNA (23S rRNA in prokaryotes, 25S rRNA in eukaryotes) and non-globular segments of ribosomal proteins (uL4, uL22, and uL23). The rRNA lining the tunnel lacks extended hydrophobic patches which allows for every polypeptide to pass through the tunnel without getting stuck. uL4 and uL22 form the most narrow constriction in the tunnel, located approximately 30 Å downstream of the PTC (Ban et al., 2000; Nissen et al., 2000; Kramer et al., 2009; Rabl et al., 2011; Wilson and Beckmann, 2011; Wilson et al., 2011). The end of the ribosomal tunnel widens up into a vestibule (Ban et al., 2000; Nissen et al., 2000; Lu et al., 2007; Lu and Deutsch, 2008; Kosolapov and Deutsch, 2009). It was shown to be flanked by rRNA and the ribosomal proteins uL22, uL23, uL24 and uL29 together with further kingdom-specific proteins (Jenni and Ban, 2003; Wilson and Beckmann, 2011). Cryo-EM studies together with molecular simulations of nascent chains inside the ribosomal exit tunnel predicted minimalist tertiary

structure formation near the exit site (Bhushan et al., 2010 a; O'Brien et al., 2010; Tu et al., 2014). The exit site itself is thought to provide a defined environment in which emerging nascent chains can interact with downstream factors which are necessary for the maturation of new proteins (Giglione et al., 2009). Such factors are for example molecular chaperones like trigger factor (TF) in bacteria or NAC in eukaryotes and archaea (Preissler and Deuerling, 2012) as well as the targeting factor SRP (signal recognition particle) (Rapoport, 2007).

3.2 Co-translational processes

Maturation processes of newly synthesized proteins not only include correct folding, but also covalent modifications and/or transport to different compartments or the cell membrane. Consequently, there are factors associated with the ribosome that are responsible for N-terminal deformylation, methionine excision and N-acetylation (Zhang and Ignatova, 2011).

The N-terminal methionine is removed by methionine aminopeptidases (MAPs) from 30 – 60% of newly synthesized nascent chains (Ball and Kaesberg, 1973; Meinnel and Giglione, 2008) with the excision being essential in bacteria and higher eukaryotes (Lowther and Matthews, 2002; Giglione et al., 2004; Ross et al., 2005). However, in bacteria and eukaryotic organelles the first amino acid is not a regular methionine but an N-formylated one (fMet) (Meinnel et al., 1990). The N-formyl group needs to be removed co-translationally by a peptide deformylase (PDF) before the methionine can be cleaved off (Fry and Lamborg, 1967; Adams, 1968; Pine, 1969; Leeds and Dean, 2006; Bingel-Erlenmayer et al., 2008; Kramer et al., 2009). MAPs interact with ribosomes through the ribosomal proteins uL23 and uL29 (Vetro and Chang, 2002; Raue et al., 2007; Nyathi and Pool, 2015).

In eukaryotes 60 – 80% of newly synthesized proteins are N-α-acetylated (Polevoda and Sherman, 2000; Falb et al., 2006; Martinez et al., 2008; Arnesen et al., 2009; Polevoda et al., 2009; Soppa, 2010; Van Damme et al., 2011). The process is carried out by N-acetyltransferases (NATs). They exist as hetero-oligomeric enzyme complexes, whose only function is to transfer the acetate moiety of acetyl-CoA to the N-α-amino group of a polypeptide (Meinnel and Giglione, 2008). An essential role of N-acetylation was reported for human cells and in the development of nematodes (Starheim et al., 2008; Gromyko et al., 2010; Rope et al., 2011; Chen et al., 2014). In contrast, NATs are not essential in lower eukaryotes (Meinnel and Giglione, 2008). Little is known about the concrete functional relevance of N-acetylation. One described function concerns the creation of a specific degron which triggers proteasome dependent degradation (Hwang et al., 2010; Shemorry et al.,

2013; Kim et al., 2014). NATs were found to associate with ribosomes and crosslinks to nascent chains of 40 – 70 amino acids were detected (Pestana and Pitot, 1975; Green et al., 1978; Palmiter et al., 1978; Yamamuda and Bradshaw, 1991; Gautschi et al., 2003; Polevoda et al., 2008). In yeast, NATs interact with ribosomes possibly through the proteins uL23 and uL29 of the large ribosomal subunit which are located close to the exit site (Gautschi et al., 2003; Polevoda et al., 2008).

Another co-translational modification, which only occurs in eukaryotes, is myristoylation. However, only 1 – 4% of all eukaryotic proteins are affected by this modification (Boutin, 1997; Rajala et al., 2000; Farazi et al., 2001; Selvakumar et al., 2007; Martinez et al., 2008). They are mainly targeted to lipid membranes and suggested to play a role in the cellular communication network (Giglione et al., 2015).

~30% of synthesized protein species are destined for incorporation into membranes or have to transit one to reach their destination. Hence, an efficient targeting and transport system is vital for the cell (Wallin and von Heijne, 1998). Targeting of these proteins to the endoplasmic reticulum (ER) in eukaryotes or the plasma membrane in prokaryotes can occur co-translationally via the universal targeting system comprised of the signal recognition particle (SRP) and the Sec-translocon (Walter and Blobel, 1980; Walter and Blobel, 1982; Luirink and Sinning, 2004; Cross et al., 2009). SRP scans nascent polypeptides for an emerging hydrophobic signal sequence (SS) (Keenan et al., 2001) and upon detection binds to the nascent chain of the so called ribosome nascent chain complex (RNC). The RNC is then delivered to the ER membrane in eukaryotes via an interaction of SRP with its receptor (SRP receptor = SR). Upon this attachment, the RNC is transferred to the Sec61 translocon and the growing nascent chain is translocated across the membrane into the ER lumen (Cross et al., 2009). SRP itself binds to ribosomes close to the tunnel exit via uL23 of the large ribosomal subunit. This position enables SS recognition and binding (Halic et al., 2004; Halic et al., 2006 a/b; Schaffitzel et al., 2006).

3.3 Protein folding

3.3.1 Principles of protein folding

First experiments concerning protein structure formation were done in 1973. Ribonuclease was denatured *in vitro* and then subjected to conditions where refolding was possible. From this experiment Anfinsen concluded, that the structure of a protein is determined by its amino acid sequence (Anfinsen, 1973). Since then, a lot of experiments have been performed to

prove this assumption, but it is still not clear, how the primary amino acid sequence determines the final structure of a protein (Hartl and Hayer-Hartl, 2009; Cubrita et al., 2010; Hingorani and Gierasch, 2014).

One model of protein folding is based on energy landscapes (Fig. 3). The theory is that free energy is minimized during the process of folding which runs along a funnel-like energy landscape. On the way to their native state proteins are expected to pass one or more folding intermediates. It is assumed that they are surrounded by an aqueous environment which leads them to bury their hydrophobic residues. During the collapse into a folding intermediate or molten globule it is presumed that certain native contacts are already formed. The native structure is supposed to be located at the bottom of the funnel, where entropy and free energy are at their minimum. In the presence of other molecules that need to fold, unfavourable contacts between these molecules can occur during the process. This would lead to another unwanted but energetically favourable pathway that results in aggregation (Bryngelson et al., 1995; Wolynes et al., 1995; Onuchic et al., 1996; Onuchic et al., 1997). *In vitro*, small proteins were observed to fold spontaneously in seconds or even faster (Jackson, 1998; Kubelka et al., 2004). In contrast, large multidomain proteins can take hours to fold with the possibility to never reach their native state (Herbst et al., 1998).

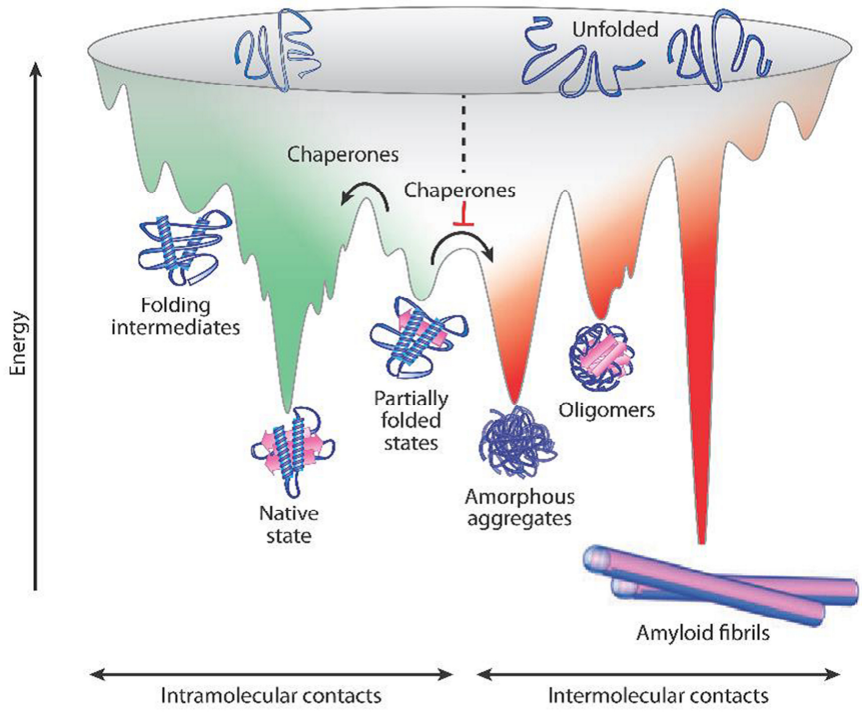

Fig. 3: Energy landscape of protein folding. The free-energy landscape of proteins is supposed to be funnel-shaped. Proteins are proposed to reach their final structure by passing different folding intermediates. These intermediates can be kinetically trapped and the free-energy barriers need to be overcome to reach the final destination. This can be helped by chaperones. When not only one molecule is present, the formation of intermolecular contacts is possible which may lead to the aggregation of folding proteins into amorphous aggregates, toxic oligomers or into ordered amyloid fibrils. Chaperones are able to prevent such misleading intermolecular contacts. Figure was taken from Kim et al. (2013).

The environment in a cell, however, is determined by molecular crowding. 300 – 400 mg/ml is the cytosolic concentration of proteins and other macromolecules found in living cells (Zimmermann and Trach, 1991). Thus, the cytoplasm does not possess the qualities of an ideal fluid making folding *in vivo* and *in vitro* fundamentally different (Gershenson and Gierasch, 2011; Hingorani and Gierasch, 2014). *In* vivo, hardly any protein showed an ideal folding behaviour. Even for small single-domain proteins folding intermediates have been observed (Teilum et al., 2002; Neuweiler et al., 2005; Brockwell and Radford, 2007).

The cell shows a preference for compact forms of proteins and macromolecular associations over large and less ordered structures. This is a direct consequence of the excluded volume effect with the excluded volume being the volume of a molecule a second one cannot enter (Minton, 1980; Minton, 2001; Minton, 2005). This effect also increases the tendency of structurally flexible as well as non-native proteins to aggregate (Ellis and Minton, 2006). Despite these observations, intrinsically disordered proteins are observed in cells. They exhibit high dynamics and flexibility which enables them to interact with various different proteins. Consequently, they are mainly found in signalling pathways of regulatory processes (Tompa et al., 2015). When a binding partner is found, the disordered regions start to adopt a (partially) stable conformation. Prominent examples for this kind of proteins are the tumour suppressor p53 (Wright and Dyson, 2015), α-synuclein which plays a role in Parkinson's disease (Drescher et al., 2012) and the Aβ-peptide with a role in Alzheimer's disease (Cuchillo and Michel, 2012). Around 20 – 30% of proteins in a mammalian cell are reported to possess these qualities (Dunker et al., 2008).

According to Levinthal's paradox, a protein cannot adopt its native structure by scanning through all possible ones during the process of folding. For a protein of 101 amino acids this would take 10^{27} years assuming a sampling rate of 3x 10^{20} per year. Hence, a pre-determined folding pathway has to exist with mechanisms that speed up the process (Zwanzig et al., 1992; Karplus, 1997; Kubelka et al., 2004; Gruebele et al., 2005; Buchner et al., 2011). Translation is a vectorial process. It starts at the N-terminus and proceeds to the C-terminus. Thus, the entire sequence information required for folding is not available until the whole protein chain is synthesized and present outside the ribosomal exit tunnel. In addition, the process of translation is inhomogenous: It displays varying translation rates which are quite slow in comparison to folding kinetics (Varenne et al., 1984; Zwanzig, 1992; Jackson, 1998; Kubelka et al., 2004; Wegrzyn and Deuerling, 2005; Hartl and Hayer-Hartl, 2009; Ingolia et al., 2011; Holtkamp et al., 2015). This highlights, that proteins are especially prone to misfolding and aggregation during their biosynthesis. It is, therefore, necessary to avoid premature folding as well as off-pathway reactions. This is achieved by a highly

specialized quality control system. One class of molecules working in this system are molecular chaperones which can interact co-translationally with nascent chains (Hartl et al., 2011; Preissler and Deuerling, 2012; Gloge et al., 2014).

Many studies in recent years focused on the investigation of co-translational protein folding at the ribosome and in this context on the role of molecular chaperones (Komar et al., 2009; Kim et al., 2013).

3.3.2 Concepts of *de novo* folding in the cell

De novo folding was assumed to be more efficient than *in vitro* folding (Ellis, 1996; Naylor and Hartl, 2001). And indeed, experiments with luciferase revealed, that albeit folding upon translation is very rapid and efficient, refolding of denatured luciferase *in vitro* is much slower and results in a lower yield of active protein (Frydman et al., 1999; Kolb et al., 2000). When comparing refolding of misfolded or aggregated proteins and co-translational *de novo* folding, *de novo* folding is generally faster and more efficient making it energetically more favourable (Fedorov and Baldwin, 1999; Frydman et al., 1999; Kolb et al., 2000; Katranidis et al., 2009; Ugrinov and Clark, 2010).
The first hint that proteins can fold co-translationally emerged in the 1960s (Cowie et al., 1961; Kiho and Rich, 1964). As nascent chains need more and more conformational space and energy as they grow, co-translational folding seems to be beneficial (Fedorov and Baldwin, 1997; Baldwin, 1999). The formation of secondary structures of nascent polypeptides at the ribosome was investigated using a multitude of techniques: Usage of limited proteolysis, conformation specific antibodies and the investigation of correct disulphide bridge formation led to the detection of secondary structure elements of nascent chains emerging from the ribosome. Additionally, enzymatic activity and ligand binding ability of completely synthesized ribosome-bound nascent chains were detected. This confirmed that proteins can adopt a native conformation while still attached to ribosomes (Hamlin and Zabin, 1972; Bergman and Kuehl, 1979; Kudlicki et al., 1995; Makeyev et al., 1996; Komar et al., 1997; Netzer and Hartl, 1997; Frydman et al., 1999; Land et al., 2003; Kleizen et al., 2005; Komar, 2009). Recent computational analyses showed that a high translational speed is able to increase the probability of co-translational protein folding (Wang et al., 2015).

Three main concepts are proposed for d*e novo* folding of newly synthesized polypeptides (Fig. 4): Co-translational, co-translational domainwise and post-translational. The co-translational concept states, that proteins start to fold into their native tertiary structure as

soon as the chain emerges from the ribosome. Formation of folding intermediates is possible but no necessary requirement.

The second concept focuses on larger and more complex proteins, like multidomain proteins. There, folding is proposed to occur co-translational and domainwise (Netzer and Hartl., 1997; Frydman et al., 1999; Deuerling and Bukau, 2004; Kleizen et al., 2005; Zhang and Ignatova, 2011). It was proposed, that domainwise folding would prevent a collision of domains (Netzer and Hartl., 1997; Bukau et al., 2000). However, Borgia et al. showed that neighbouring domains diverge in their sequence. To avoid permanent misfolding, the sequence identity has to be below 40%. Apparently, transient misfolded intermediates resembling intramolecular amyloid-like states are formed during the folding process. They disappear much more rapidly when neighbouring domains have low sequence identity as compared to having a high one (Borgia et al., 2011; Borgia et al., 2015). The mechanism that allows such domainwise folding is proposed to originate in a local attenuation of translation that is initiated by clusters of rare codons between the structural elements (Komar, 2009; Zhang et al., 2009; Novoa and Ribas de Pouplana, 2012). If a protein contains long-range contacts, meaning contacts between distant sites of the protein, these need to be formed later in translation or even after the release of the polypeptide chain from the ribosome (Krishna and Englander, 2005).

The third concept describes post-translational folding. This pathway is supposed to be the one primarily used in bacteria (Netzer and Hartl, 1997). Mainly small proteins are subjected to this folding process. However, also for some larger proteins post-translational folding is known to occur.

The number of proteins and the exact mechanism that underlies the process of co-translational folding is still unclear. However, several studies in recent years tried to investigate them more closely by using nuclear magnetic resonance (NMR) spectroscopy of artificially arrested polypeptides *in vitro* and *in vivo*. New insights into the dynamics and structures of nascent chains were gained (Evans et al., 2005; Hsu et al., 2007; Rutkowska et al., 2008; Hsu et al., 2009; Cabrita et al., 2010; Eichmann et al., 2010). Recently, a new technique has been published to study co-translational folding. It is based on limited proteolysis coupled with MS evaluation (Rajabi et al., 2015 a/b). Free and ribosome-bound polypeptides of SH3 (Src-homology) and an unfolded counterpart were investigated showing that the ribosome protects the nascent chain. Rajabi et al. were able to distinguish the peptides generated by the polypeptides from peptides originating from the ribosome thereby providing a fast and sensitive method for the study of RNCs.

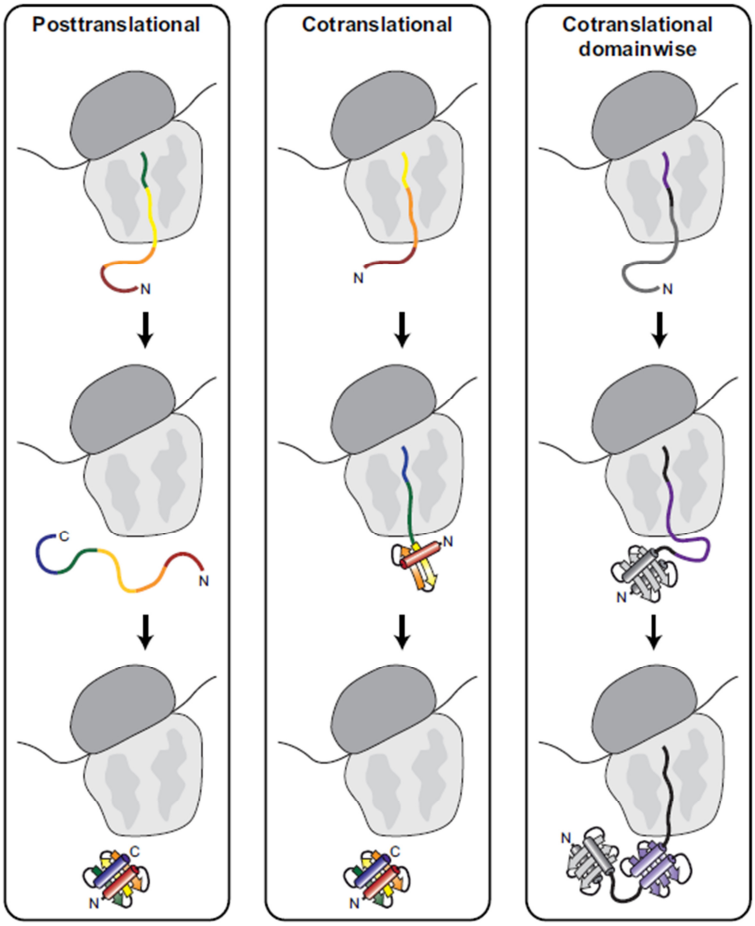

Fig. 4: Concepts of *de novo* protein folding. Three different concepts for the folding of newly synthesized proteins have been proposed. First, proteins may need to be completely synthesized before the folding starts → post-translational. In the second model, proteins start to fold as soon as the first amino acids leave the ribosomal exit tunnel → co-translational. In the third and last model, which mainly concerns multidomain proteins, a domainwise folding is proposed. Domains are expected to fold as soon as the complete information is synthesized and the next domain folds when its information is available → co-translational domainwise. Figure is based on Deuerling and Bukau, 2004 and was taken from Preissler (2011).

3.4 Protein aggregation

The concept of proteostasis not only involves protein biogenesis but also the folding of newly synthesized proteins as well as protein targeting in cells. The aim is to prevent protein misfolding and in later stages the formation of toxic aggregates (Hipp et al., 2014). However, acute stress can disturb this balance which leads to reduced translation rates and the induction of the heat shock response and the UPR (unfolded protein response) in the ER with the goal of disaggregation or degradation of misfolded protein species. If a stress situation persists the cells suffer from chronic stress conditions. This is the case during ageing or certain diseases which go hand in hand with the production of aggregates that deplete proteins from the proteostasis network. This leads to increased misfolding and aggregation until the proteostasis system is overloaded and collapses. Apoptosis is the general response to the collapse (Hipp et al., 2014). The process of proteostasis collapse can be enhanced by environmental effects like heat shock or mutations affecting either the

stability of a substrate protein or a component of the proteostasis network itself. In ageing cells, protein quality control slowly declines which also increases misfolding (Tyedmers et al., 2010). Protein aggregates are associated in humans with diseases like Alzheimer's disease, Parkinson's disease or Huntington's disease. They are all marked by proteins which fail to adopt or to remain in their native conformation, thereby overloading the proteostasis system and finally inducing the disease (Xu et al., 2002; Chiti and Dobson, 2006; Powers et al., 2009; Douglas and Dillin, 2010; Gundersen, 2010; Maiti et al., 2014).

Two morphologically different aggregates exist: Amorphous and disordered aggregates which do not display any structural organisation and highly ordered amyloid-like ones (Tyedmers et al., 2010). Amyloid fibrils are characteristic for many neurodegenerative diseases (Chiti and Dobson, 2006). They are rich in β-sheets which assemble into long fibres (Sunde et al., 1997; Rubin et al., 2008). Formation starts by a so called seed which is one misfolded protein. This misfolded protein sequesters further proteins into the fibre leading to a loss of function of this protein which in turn disturbs the whole cellular system (Gidalevitz et al., 2006; Kitamura and Kubota, 2010). In recent years evidence was gained, that the fibre is not the toxic species but the oligomeric intermediates formed during the process (Chiti and Dobson, 2006; Kitamura and Kubota, 2010).

Aggregated proteins are deposited in certain 'compartments' in the cell. This is supposed to facilitate the handling of the aggregated proteins. This process seems to be evolutionarily conserved, even though the way of sequestration differs (Sontag et al., 2014). Bacteria tend to form 1 – 2 inclusion bodies which are located at one cell pole. This allows for asymmetric division producing aggregation-free daughter cells (Lindner et al., 2008; Tyedmers et al., 2010). This asymmetric aggregate inheritance was also observed in ageing yeast cells (Aguilaniu et al., 2003; Nyström, 2005; Henderson and Gottschling, 2008; Liu et al., 2010 a). If cells have a shorter expected life span, protein deposits are also asymmetrically inherited in higher eukaryotes (Rujano et al., 2006; Fuentealba et al., 2008). Similar deposits like in bacteria are found in all yeast and mammalian cells near the nucleus. They are called aggresomes and contain misfolded as well as ubiquitinated proteins. This structure is associated with diseases and the expression of heterologous proteins (Johnston et al., 1998; García-Mata et al., 1999).

Another sort of deposit arises if the proteasomal degradation is the limiting factor during stress conditions. It contains misfolded but soluble ubiquitinated proteins. When discovered it was named JUNQ for juxta-nuclear quality control compartment. It is thought to be a fusion of the stress foci emerging directly after stress exposure (also named Q-bodies or CytoQ)

(Kaganovich et al., 2008; Specht et al., 2011; Malinovska et al., 2012; Escusa-Toret et al., 2013). Recently, however, JUNQ was demonstrated to have a nuclear rather than a juxta-nuclear localization (Miller et al., 2015). It was therefore renamed to INQ (intra-nuclear quality control compartment). Misfolded cytosolic proteins are transported into the nucleus via the nuclear pore. This process involves the Hsp40 Sis1 in yeast and other still unknown factors (Park et al., 2013; Miller et al., 2015). Proteins containing disordered and low complexity sequences were shown to be sequestered and mislocalized upon aggregation in the cytoplasm but not in the nucleus. It seems likely, that the impairment of nucleo-cytoplasmic transport might contribute to the cellular pathology of several aggregate deposition diseases (Woerner et al., 2016). Amyloid aggregates were found to accumulate in another structure, the insoluble protein deposit (IPOD) which is located adjacent to the vacuole (Kaganovich et al., 2008; Sontag et al., 2014).

P-bodies (processing bodies) and stress granules (SGs) were described to be further deposits present in the cell. They are conserved in eukaryotes and contain mainly non-translating mRNA together with associated proteins (Eulalio et al., 2007; Kedersha and Anderson, 2009; Decker and Parker, 2012). Upon induction of several different stresses, these structures are formed within minutes in the cytoplasm (Teixeira et al., 2005; Brengues et al., 2005; Garmendia-Torres et al., 2014). Interestingly, the appearance of these foci correlates with translational arrest (Holcik and Sonenberg, 2005; Kedersha and Anderson, 2009; Simpson and Ashe, 2012). The exact composition and the assembly kinetics vary in a stress-related manner (Buchan et al., 2011). The core proteins forming P-bodies have roles in mRNA decay (Sheth and Parker, 2003; Buchan et al., 2010). In contrast, SGs mainly consist of translation initiation factors and other mRNA binding proteins (Hoyle et al., 2007; Buchan et al., 2008; Liu et al., 2010 a; Decker and Parker, 2012; Kedersha et al., 2013). A role for the Hsp40 protein Ydj1 in P-body assembly was proposed recently (Cary et al., 2015). In SGs, Hsp70 was found to accumulate together with Ydj1 and Sis1. Ydj1 seems to promote the disassembly of SGs to stimulate translation and Sis1 seems to play a role in the targeting of SGs to the vacuole (Walters et al., 2015).

To adapt to stress, reduction of translation or reducing the number of ribosomes seem to be effective measures (Kirstein-Miles et al., 2013; Guerra-Moreno et al., 2015). Recently it was discovered in mammalian cells that MRPL18, a cytosolic isoform of a mitochondrial ribosomal protein generated upon stress, incorporates into the cytosolic ribosome thereby generating a hybrid that has other translational properties (Zhang et al., 2015 b).

In yeast, disaggregation is carried out by cooperation of Hsp104, the Hsp70 Ssa1 and the Hsp40 Ydj1. Ssa1/Ydj1 extract proteins from the aggregates and hand them to Hsp104 which unfolds the aggregated proteins by threading them through a translocation pore in an ATP-dependent manner (Tyedmers et al., 2010; Mogk et al., 2015). Higher eukaryotes do not possess Hsp100 chaperones. It was suggested, that the Hsp70/40 system cooperates with the Hsp110s (NEFs) to disassemble protein aggregates. However, this process proved to be inefficient *in vitro* and only occurred on the surface of aggregates (Shorter, 2011). When this system was analysed in nematodes and human cells *in vivo* it proved to be quite efficient. Importantly, complex formation of class A and B J-proteins is required. They act in a synergistic manner to extract proteins from various aggregates. (Rampelt et al., 2012; Nillegoda et al., 2015; Yu et al., 2015).

Marking proteins for degradation is the role of the ubiquitin proteasome system (UPS) (Hershko and Ciechanover, 1992; Nijholt et al., 2011; Kaushik and Cuervo, 2015). Neurodegenerative diseases and ageing cells are associated with a decline in the UPS (Gaczynska et al., 2001; Ciechanover and Brundin, 2003). If proteins are stuck in aggregates which can no longer be dissolved they are instead targeted to the autophagy lysosome pathway (ALP). The aggregates are engulfed by autophagosomes which then fuse with lysosomes where the aggregates are digested (Kundu and Thomposon, 2008; Kettern et al., 2010). Impaired autophagy is associated with neurodegenerative diseases (Kundu and Thompson, 2008). Chaperones help factors of the UPS and the ALP to ensure efficient clearance of aggregates. For example, to efficiently ubiquitinate aggregation prone proteins in protein misfolding diseases the E3 ubiquitin ligase CHIP (C-terminus of Hsc70-interacting protein) of the UPS tightly cooperates with the Hsp70/90 system (Kettern et al., 2010). An example in the ALP pathway is the Hsp70 co-chaperone BAG3 which enables the interaction of chaperones and an ubiquitin adaptor molecule that leads to lysosomal degradation (Kettern et al., 2010). Mechanisms for an ubiquitin-independent chaperone-assisted transport of aggregated proteins for degradation also exist (Kettern et al., 2010).

The major risk for neurodegenerative diseases is ageing. There, the accumulation of protein aggregates in neurons together with a deficiency in proteostasis leads to the onset of these diseases. To find molecules that boost the proteostasis system could be a major step forward in conquering these diseases (Hipp et al., 2014; Brandvold and Morimoto, 2015; Kaushik and Cuervo, 2015).

3.5 Molecular chaperones

Without help, newly synthesized proteins tend to collapse into compact but not yet native structures to bury their hydrophobic amino acids. This leads to a tendency for unproductive folding, misfolding or, in the end, to aggregation. Furthermore, the native structures of proteins are not invariable. They need a certain degree of flexibility to fulfil their biological functions (Jahn and Radford, 2008; Richter et al., 2010). Two different classes of specialized proteins help other proteins to fold into their native conformation without being integrated into the folded molecule itself. These are folding helper enzymes and molecular chaperones (Buchner, 1996; Bukau and Horwich, 1998; Ellis and Hartl, 1999; Hartl and Hayer-Hartl, 2009).

Folding helper enzymes are able to catalyse slow steps in the folding process and thereby minimize the accumulation of intermediates. They are able to help with the formation of covalent bonds and can even restructure them if there has been a mistake (Schiene and Fischer, 2000). Two of these foldases exist: the protein disulphide isomerase (PDI) and the peptidyl-prolyl cis-trans isomerase (PPI). The PDI was shown to catalyse the correct formation of disulphide bridges (Oka and Bulleid, 2013). The PPI is responsible for the isomerization of ribosome-incorporated trans-proline to cis-proline. This step would otherwise be very slow and rate-limiting for folding (Braakman and Hebert, 2013).

In contrast to folding helper enzymes, chaperones have broad substrate specificity and can basically help all proteins to reach their native conformation. Apart from folding, they also play important roles in complex assembly, disaggregation, protein transport, unfolding and the targeting of misfolded proteins to the proteasome system (Hartl and Hayer-Hartl, 2009; Kim et al., 2013). Chaperones are ubiquitously expressed in cells and interact transiently with their clients in a stoichiometric ratio (Hartl, 1996; Hartl and Hayer-Hartl, 2009; Kim et al., 2013).
Upon increased stress levels heat shock proteins (Hsps) are transcriptionally or translationally upregulated to counteract the destabilization of existing proteins and misfolding (Richter et al., 2010; Saibil, 2013). This heat shock response is conserved in pro- and eukaryotes. The different chaperone families are classified according to their molecular weight: Hsp100, Hsp90, Hsp70, Hsp60, Hsp40 and small Hsp (sHsp). Hsps deal with protein folding, unfolding, disaggregation, targeting and other aspects of proteostasis not only under heat shock conditions, some of them also influence these processes under physiological conditions. These are, for example, constitutively expressed versions of Hsp70 and Hsp90 (Hsc) (Richter et al., 2010). Chaperones are able to recognize either specific peptide

sequences or surface exposed hydrophobic amino acids that are normally not exposed in correctly folded proteins (Richter et al., 2010; Kim et al., 2013).

An ATP-independent class of chaperones are the sHsps (Basha et al., 2012; Haslbeck and Vierling, 2015). They are the least conserved class of molecular chaperones even though they are present in all three kingdoms of life (De Jong et al., 1993; Kriehuber et al., 2010; Basha et al., 2012). sHsps are very ancient molecules as they were already present in the last common ancestor of pro- and eukaryotes (De Jong et al., 1993; Waters et al., 1996; Kappe et al., 2002).

Small heat shock proteins are known to be able to assemble into oligomeric structures whose architecture is very diverse between different sHsps. Monomers of sHsps build polydisperse symmetric oligomers that usually contain 4 – 18 dimers (Kim et al., 1998; Basha et al., 2012). However, all sHsps share the same domain structure: an N-terminal sequence (NTS), an α-crystallin domain (ACD) and a C-terminal sequence (CTS) (Fig. 5 A) (Hochberg and Benesch, 2014). The ACD is the conserved signature motif of sHsps. It has an approximate length of 94 amino acids and its compact β-sandwich structure resembles the immunoglobulin fold (Fig. 5 B and C): Two anti-parallel β-sheets are connected by a short inter-domain loop. One of this sheets consist of three β-strands, the other of four (van Montfort et al., 2001; van Montfort et al., 2002; Delbecq and Klevit, 2013).The ACD is responsible for dimerization, albeit not sufficient for higher oligomer formation (Bagneris et al., 2009; Laganowsky et al., 2010; Baranova et al., 2011; Clark et al., 2011). There are two different ways of dimerization known so far. One possible way to dimerize is reciprocal swapping of the β6-strands between the two monomers (Fig. 5 B) (Kim et al., 1998; van Montfort et al., 2001; Bepperling et al., 2012; Hanazono et al., 2013). The other dimerization technique uses a fusion of the β6- and the β7-strands into one elongated strand which forms the dimer with its counterpart from the other monomer (Fig. 5 C) (Jehle et al., 2009; Delbecq and Klevit, 2013). The flexible NTS and CTS are required for the formation of higher oligomers. The conserved I-x-I motif in the CTS binds to the hydrophobic groove formed by the β4- and β8-strands in the ACD of an adjacent monomer thereby leading to the formation of tetramers or hexamers. The NTS is then responsible for the formation of higher oligomers (Kim et al., 1998; van Montfort et al., 2001; van Montfort et al., 2002; Braun et al., 2011; Jehle et al., 2011; Delbecq et al., 2012; Delbecq and Klevit, 2013; Hanazono et al., 2013). However, so far only three crystal structures of oligomeric sHsps complexes exist (Fig. 5 D) (Kim et al., 1998; van Montfort et al., 2001; Hanazono et al., 2013). At equilibrium, sHsps tend to populate a range of oligomeric states (Stengel et al., 2010; Braun et al., 2011; Basha et al., 2012). The different oligomers exchange subunits constantly thereby rendering the oligomeric structures highly dynamic (Fig. 6). This ability correlates to the chaperone activity

observed for sHsps (Basha et al., 2012). A novel molecular mechanism for sHsp function has been identified recently. It was shown, that the oligomers of CeHSP17 from *C. elegans* formed large sheet-like super-molecular assemblies (SMAs) at high temperatures in contrast to the rather unordered structures observed before (Zhang et al., 2015 b).

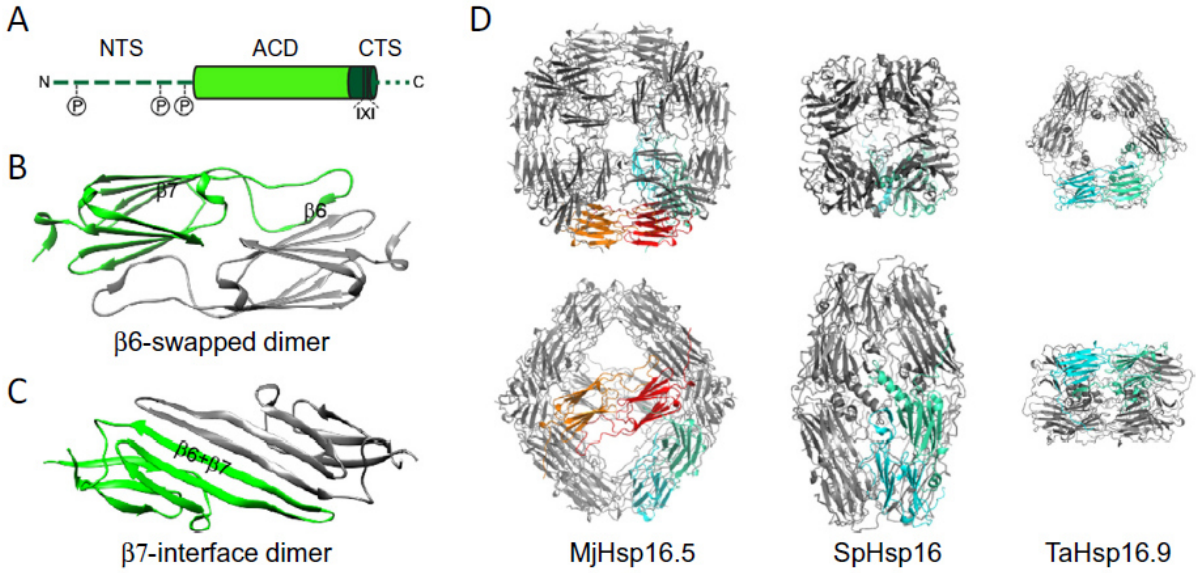

Fig. 5: Structural architecture of small Hsps. (A) Domains of sHsps. NTS (broken line in dark green) with possible phosphorylation sites; ACD (light green); CTS (dark green), the conserved I-x-I motif is highlighted. (B) Structure of the β6-swapped dimer of two ACDs of *M. jannaschii* Hsp16.5. (C) Structure of the β7-interface dimer of two ACDs of human αB-crystallin. (D) The three available oligomeric crystal strucutres of sHsps are depicted. Marked in green-cyan is the dimeric building block. Marked in orange-red is the equatorial protein axis forming an octahedron. MjHsp16.5: 24-mer from *M. jannaschii*; SpHsp16: 16-mer from *S. pompe*; TaHsp16.9: 12-mer from *T. aestivum*. Figure was taken from Haslbeck and Vierling (2015).

sHsps are mainly active upon stress induction (Das and Surewicz, 1995; Haslbeck et al., 1999; Richter et al., 2010; Hilton et al., 2013) and act as holdases. They interact with aggregating proteins to stabilize them in a refolding-competent state. Upon stress relief, the instable proteins are transferred to chaperones that can actively refold them or initiate targeting for degradation (Fig. 6) (Richter et al., 2010; Kim et al., 2013; Haslbeck and Vierling, 2015). The small heat shock protein Hsp26 from yeast was shown to be able to slow down the inactivation of the model protein citrate synthase. It was also able to protect citrate synthase from aggregation (Haslbeck et al., 1999). The protective function of Hsp26 on aggregating proteins was confirmed *in vivo* (Cashikar et al., 2005).

Even so no structures of sHsp/substrate complexes were resolved so far it is assumed, that the sHsps first dissociate into dimers upon stress induction freeing the NTS and then reassemble into oligomers which then also accommodate diverse non-native client proteins (Shashidharamurthy et al., 2005; Stengel et al., 2010; Braun et al., 2011; McHaourab et al., 2012; Hiltron et al., 2013; Peschek et al., 2013; Haslbeck and Vierling, 2015). To ensure efficient refolding of the substrates present in complex with the sHsps, the complex needs to be soluble. For this, stoichiometric or excess concentrations of sHsps in comparison to the

substrate need to be present. Otherwise large amorphous aggregates are formed in which the sHsps are incorporated. For resolubilization of these aggregates disaggregases are needed. The involved mechanism is conserved from bacteria to lower eukaryotes to higher plants (Mogk et al., 2003; Cashikar et al., 2005; Haslbeck et al., 2005; Lee et al., 2005; Ratajczak et al., 2009; Bepperling et al., 2012). Substrates unfolded or incorporated into aggregates in the absence of sHsps cannot be rescued by them (Haslbeck and Vierling, 2015). Four major regulatory mechanisms are proposed to be responsible for the shift of the equilibrium from higher oligomeric structures to dimers or small oligomers in sHsps. The first mechanism involves the presence of unfolded or partially unfolded substrates. The second mechanism is based on environmental changes in temperature. Post-translational modifications are responsible for the third mechanism and the fourth is based on the formation of hetero-oligomers with other sHsps (Haslbeck and Vierling, 2015). The major roles of sHsps in aggregation make them important for cell survival (Haslbeck et al., 2005; Tyedmers et al., 2010). They are proposed to serve as a buffer system which protects cells from irreversible aggregation upon stress (Fig. 6) (Haslbeck and Vierling, 2015). Deletion leads to an increased sensitivity of organisms to heat stress (Zhong et al., 2013). The deletion of the human HspB5 was linked to myopathies as well as to neurological disorders like Alzheimer's and Creuzfeldt-Jakob (Sun and MacRae, 2005).

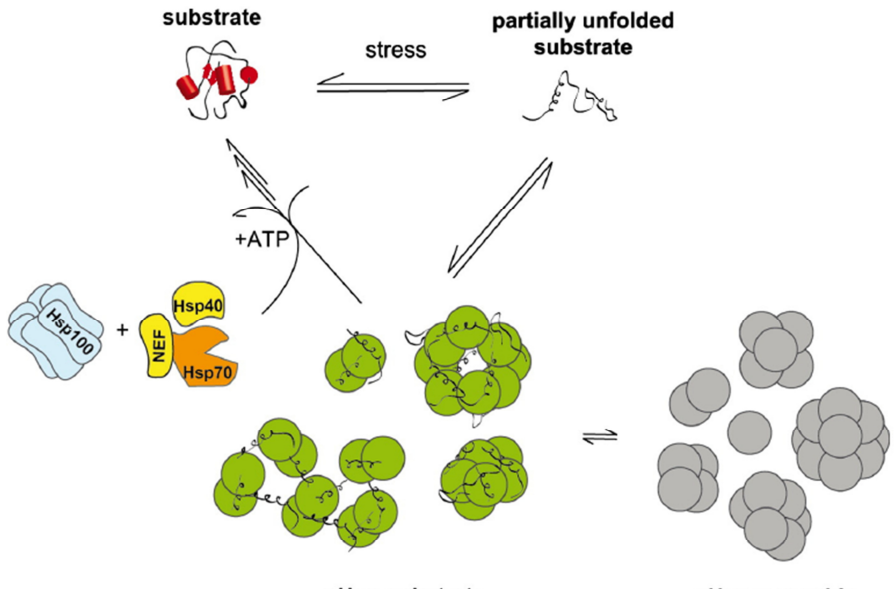

Fig. 6: Model of the chaperone function of most sHsps. The class of sHsps is known to bind to already partially unfolded substrates in an ATP-independent manner. The bound proteins are kept in a folding-competent state. When activation of sHsps, which are organized in oligomeric structures (grey), takes place, the majority dissociates into smaller structures (mainly dimers, green) which then interact with the substrate molecules. Some bound substrates may spontaneously refold, but the majority is kept in a stable complex. Via interaction with the Hsp70/40 system and, where available, an Hsp100 chaperone, substrates can be refolded or targeted for degradation. Figure was taken from Haslbeck and Vierling (2015).

So far it is unclear, which part of their substrates sHsps recognize. As larger proteins are less well protected, the mass ratio seems to play a role. This hints towards a charge-driven and/or hydrophobicity-driven interaction (Basha et al., 2012). The interaction with the non-native client proteins is proposed to be carried out by the highly flexible NTS (Koteiche et al., 2005; White et al., 2006; Jaya et al., 2009; Stengel et al., 2010; Jehle et al., 2011). It is highly variable in its length and sequence between different sHsps (Eifert et al., 2005; Sun and MacRae, 2005). However, substrate binding was also implicated for the ACD and the CTS, albeit the evidence is much weaker than for the NTS (Haslbeck and Vierling, 2015). As the NTS and the CTS have evolved independently, variations in substrate preferences for sHsps seem possible (Kriehuber et al., 2010).

ATP-dependent chaperones are able to actively fold unstructured proteins. Hsp60s, Hsp70s and Hsp90s all belong to this sort of chaperones. They display controlled cycles of client binding and release. Binding of ATP as well as hydrolysis affects the affinity towards their substrates and leads to structural rearrangements. These chaperones need to have a dynamic conformation to be able to fulfil their function (Mayer, 2010).

Hsp70s are essential in all living organisms. They are the most diverse class of chaperones and contribute to a lot of different cellular processes including folding of proteins, disassembly of protein aggregates, degradation of proteins, protein-protein interactions, transport across membranes and a general role in the protection of the proteome upon stress conditions (Hartl and Hayer-Hartl., 2002; Bukau, 2005; Mayer, 2010; Kim et al., 2013; Clerico et al., 2015; Mayer and Kityk, 2015; Yu et al., 2015). The Hsp70s depict a high sequence similarity across all species as well as a similar structural organisation. The nucleotide binding domain (NBD, ~43 kDa) is located in the N-terminus. It is followed by a flexible linker which, in turn, is followed by the substrate binding domain (SBD) and a variable C-terminal region (~27 kDa). The SBD is able to bind small hydrophobic segments of its client proteins in a cleft which is covered by a lid (Rüdiger et al., 1997; Mayer and Bukau, 2005; Kampinga and Craig, 2010; Mayer, 2013). The binding and release of substrates depends on ATP. The cycle of ATP binding and hydrolysis (Fig. 7) which is necessary for substrate interaction is regulated by various Hsp40 chaperones, the so called J-proteins, together with diverse nucleotide exchange factors (NEFs) (Kampinga and Craig, 2010). Binding of ATP reduces substrate affinity and goes along with rapid association and dissociation rates of potential substrates. The hydrolysis of ATP leads to a conformational change in the SBD, the lid closes. This stabilizes the substrate interaction (Zhu et al., 1996; Mayer et al., 2000; Vogel et al., 2006 a/b): Association and dissociation of client proteins is slowed down considerably when ADP is bound at the NBD (Slepenkov and Witt, 2002; Moro et al., 2004; Mayer, 2013).

Assuming no co-chaperones are present, ATP hydrolysis would be the rate-limiting step in the Hsp70 cycle. In the cell, Hsp40 chaperones not only recruit clients for Hsp70s but also stimulate the ATPase activity (Karzai and McMacken, 1996; Bukau and Horwich, 1998; Misselwitz et al., 1998; Laufen et al., 1999; Walsh et al., 2004). NEFs trigger the replacement of ADP with a new ATP molecule which releases the substrate so that the cycle can start anew (Bukau and Horwich, 1998; Walsh et al., 2004; Dragovic et al., 2006; Raviol et al., 2006).

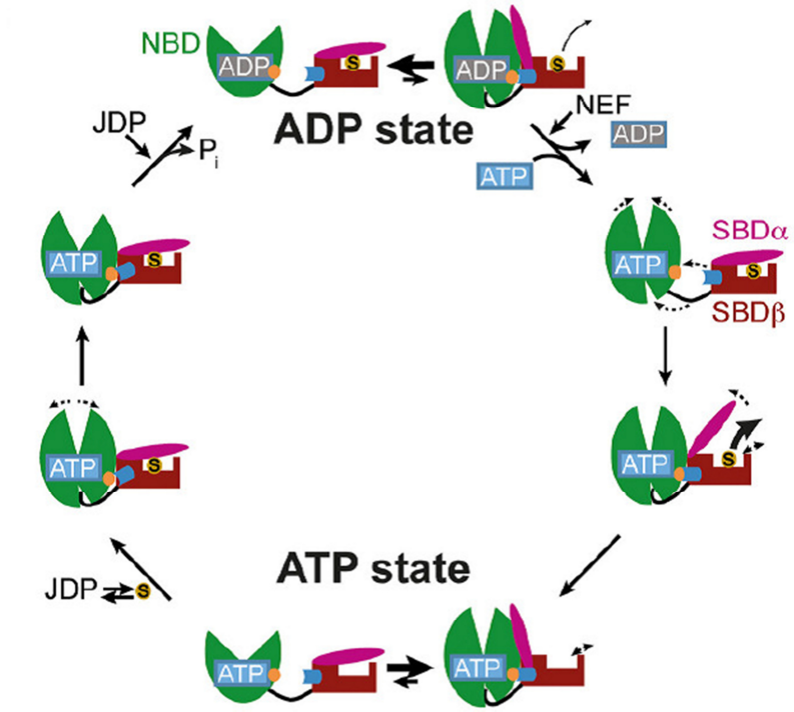

Fig. 7: Model of the substrate binding cycle of Hsp70s. In the ADP bound state an equilibrium exists between the closed conformation with the nucleotide binding domain (NBD, green) and the substrate binding domain (SBD, dark red) being connected by the conserved interdomain linker (black) and tightly bound substrate (S) and a very transient open conformation. Substrate dissociation in the ATP bound state only happens at very low rates. Nucleotide exchange factors (NEFs) catalyse ADP dissociation and ATP rebinding. This leads to a conformational change in the SBD, where the α-helical lid (magenta) opens. The substrate is released at high rates. In the ATP, as in the ADP bound state, an equilibrium exists, albeit between a very transient closed conformation and an open one. J-proteins (Hsp40s) play a role in the binding of new substrates and accelerate ATP hydrolysis. Figure was taken from Mayer and Kityk (2015).

The Hsp40 co-chaperones contain a so-called J-domain. It is 70 amino acids long and interacts specifically with Hsp70s. In its sequence it contains a conserved motif made up of a histidine, a proline and an aspartate (HPD-motif). This motif is important for the ability of Hsp40s to stimulate the ATPase activity of Hsp70s. Structurally the J-domain is made up of four α-helices (Szyperski et al., 1994; Wall et al., 1994; Pellecchia et al., 1996; Qian et al., 1996; Tsai and Douglas, 1996; Greene et al., 1998). Some Hsp40s have a substrate binding site on their own, but the main function is to ensure the contact between Hsp70s and their clients. This is achieved by either recruiting Hsp70 to the client or by bringing the client to the Hsp70 (Clerico et al., 2015).

Another important class are the Hsp100 chaperones. Homologues of the yeast Hsp104 exist in bacteria (ClpB) (Squires et al., 1991; Hanson and Whiteheart, 2005), mitochondria, chloroplasts (Hanson and Whiteheart, 2005) and in plants (Queitsch et al., 2000). They belong to the class of AAA+ ATPases (ATPases associated with diverse cellular activities) (Hanson and Whiteheart, 2005). The active conformation is a ring composed of six monomers with a central tunnel in the middle (Parsell et al., 1994 a). Each monomer consists of an N-terminal domain, two nucleotide binding domains (NBD-1 and NBD-2) as well as a C-terminal region (Doyle and Wickner, 2009). Hsp100s are able to unfold misfolded proteins and extract them from aggregates by threading them through their central pore in an ATP-dependent manner. This allows the refolding of the formerly aggregated proteins by other chaperones or their targeting for degradation (Parsell et al., 1994 b; Bosl et al., 2006; Doyle and Wickner, 2009; Mayer, 2010; Richter et al., 2010).

In the living cell, these different classes of chaperones cooperate to fulfil their functions. The activity of Hsp70s is influenced by Hsp40s, for instance (Mayer, 2013). In bacteria, fungi and plants, the Hsp100 disaggregases together with the Hsp70/40 chaperone system form a powerful system to resolubilize and reactivate aggregated proteins (Winkler et al., 2012; Mogk et al., 2015). In accordance, sHsps are reported to interact with Hsp100 and Hsp70s during disaggregation. sHsps keep the proteins in a folding-competent state thereby facilitating disaggregation by other chaperones (Richter et al., 2010). Furthermore, a synergistic effect between complexed Hsp40s was discovered recently. It promotes the disaggregation activity of the Hsp70 system in human cells and nematodes which lack powerful disaggregases of the Hsp100 family (Nillegoda et al., 2015; Yu et al., 2015). In *E. coli*, proteins of the Hsp70 and Hsp90 family cooperate to remodel proteins (Genest et al., 2015).

3.6 Ribosome-associated chaperones

In pro- as well as eukaryotes chaperone systems exist that directly bind to ribosomes to assist folding of newly synthesized proteins (Wegrzyn and Deuerling, 2005; Preissler and Deuerling, 2012). They can decelerate folding processes and shield hydrophobic amino acids (Kim et al., 2013). Though the principle of ribosome-associated chaperones is conserved, different systems have evolved independently in pro- and eukaryotes. Bacteria contain the ribosome-associated trigger factor (TF). In yeast, the system is more complex (Fig. 8). It consists of the nascent polypeptide-associated complex (NAC) and the ribosome associated complex (RAC, comprised of the Hsp70 Ssz and the Hsp40 Zuotin) together with the Hsp70 Ssb (Nelson et al., 1992; Huang et al., 2005; Conz et al., 2007; Preissler and

Deuerling, 2012). In mammals, the Ssz homologue Hsp70L1 and the Zuo-like protein MPP11 constitute the RAC complex (mRAC). No homologue to Ssb has been found in higher eukaryotes. Instead, mRAC recruits a cytosolic Hsp70 to nascent chains (Otto et al., 2005; Jaiswal et al., 2011).

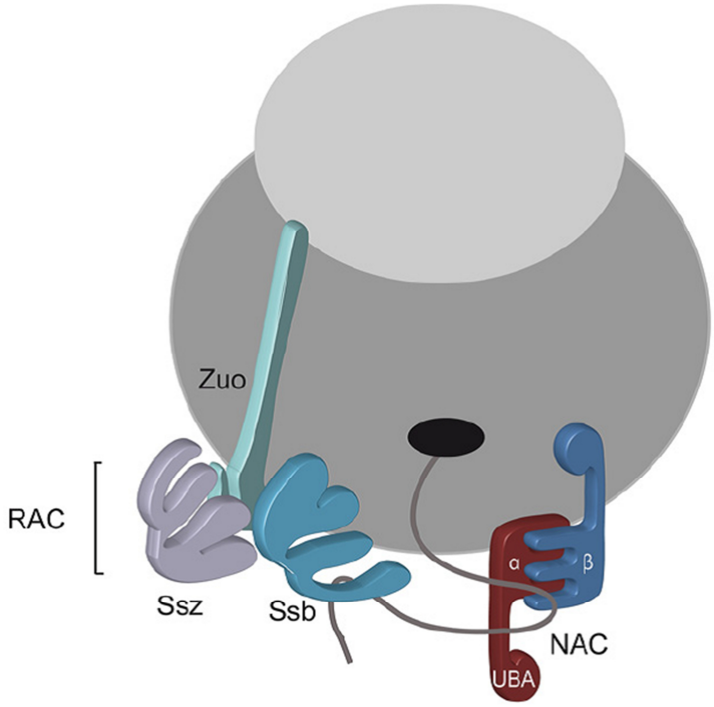

Fig. 8: Chaperone systems associated with the yeast ribosome. In yeast, different complexes and proteins associate with the ribosome. The Hsp70 Ssz (grey) forms a complex together with the Hsp40 Zuotin (Zuo, cyan) which spans the two ribosomal subunits. This complex is termed RAC (ribosome associated complex). RAC interacts with Ssb, another Hsp70, which is also localized directly at the tunnel exit (light blue). The second complex is the nascent polypeptide associated complex (NAC). It is a heterodimeric complex consisting of a β- (dark blue) and an α-subunit (red) which has an additional UBA domain (ubiquitin associated domain). Figure was taken from Ott et al. (2015).

3.6.1 The Hsp70/40 system at the ribosome

In eukaryotes, a ribosomal Hsp70/40 systems has evolved to assist in co-translational protein folding (Craig et al., 2003; Peisker et al., 2010). This system consists in yeast of Ssb and RAC. Ssb (stress-seventy subfamily B), an Hsp70 unique to yeast, directly binds to the ribosome (Gautschi et al., 2001; Gautschi et al., 2002; Huang et al., 2005). Two Ssb proteins exist: Ssb1 and Ssb2 (hereafter referred to as Ssb). The two proteins are highly homologous and differ in only four amino acids. Ssb shows the typical structure of the Hsp70 class: NBD – linker – SBD. Additionally, the C-terminus contains a nuclear export sequence (NES) (Shulga et al., 1999). It is present in a 1:1 stoichiometry to ribosomes and was crosslinked to short nascent chains. This indicates a ribosomal localization close to the exit site which is independent of RAC (Pfund et al., 1998; Hundley et al., 2002; Gautschi et al., 2002). The ATPase activity of Ssb is stimulated by RAC (Gautschi et al., 2001; Gautschi et al., 2002; Huang et al., 2005) and Sse1 and Fes1 act as its nucleotide exchange factors. RAC and Ssb

build a functional triad on the ribosome, but only Ssb has been shown to contact nascent chains (Conz et al., 2007). Loss of Ssb leads to the aggregation of newly synthesized polypeptides as well as of ribosomal particles and ribosomal biogenesis factors, thereby inducing a deficiency in ribosome biogenesis and an impairment of translation (Albanèse et al., 2010; Koplin et al., 2010). In addition, hypersensitivity to various cations, translation inhibitory drugs and low temperatures is induced. Ribosomal proteins are especially liable for aggregation when Ssb is missing, indicating that they are clients of Ssb. This implicates a role for it in ribosomal biogenesis (Nelson et al., 1992; Yan et al., 1998; Gautschi et al., 2001; Craig et al., 2003; Rakwalska and Rospert, 2004; Kim and Craig, 2005; Albanèse et al., 2010; Koplin et al., 2010; Peisker et al., 2010). By sequencing of mRNAs translated by Ssb associated ribosomes it was determined, that Ssb interacts with the majority of nascent proteins destined for the nucleus or cytosol. It apparently protects longer and aggregation-prone proteins where co-translationally folding proves to be difficult. This substrate specificity is regulated by RAC (Willmund et al., 2013).

Zuo and Ssz interact stably with each other, whereby Zuo is responsible for the ribosomal localization of the complex and the interaction with Ssb via its J-domain (Yan et al., 1998; Kaschner et al., 2015). Hydrogen-deuterium exchange experiments revealed that Zuo contacts the SBD as well as the NBD of Ssz via its N-terminal end (Fiaux et al., 2010). Cells lacking Ssz, Zuo or both proteins show similar phenotypes as cells lacking Ssb (Nelson et al.,1992; Yan et al., 1998; Gautschi et al., 2001; Craig et al., 2003; Rakwalska and Rospert, 2004; Kim and Craig, 2005; Peisker et al., 2010). Stimulation of the ATPase domain of Ssb by Zuo depends on its interaction with Ssz (Gautschi et al., 2002; Huang et al., 2005). Ssz is a rather unusual Hsp70. It does not bind or hydrolyse ATP (Huang et al., 2005) and its SBD is shorter than that of other Hsp70s (Hundley et al., 2002). It was also revealed, that Ssz lacks three residues which are critical for ATP hydrolysis in other Hsp70s. This explains the inactivity of Ssz, which can theoretically bind but not hydrolyse ATP (Gautschi et al., 2001; Huang et al., 2005; Leidig et al., 2013). In addition, the SBD is not necessary for Ssz function (Hundley et al., 2002). It was speculated, that Ssz might regulate conformational rearrangements in the J-domain of Zuo (Fiaux et al., 2010) and that it might act as a holdase which guides nascent chains towards Ssb (Leidig et al., 2013).
Small-angle X-ray scattering (SAXS) together with cryo-EM analysis enabled first insights into structure and ribosome binding of RAC in *Saccharomyces cerevisiae* and *Chaetomium thermophilum* (Leidig et al., 2013; Zhang et al., 2014). Zuotin was shown to possess an elongated α-helical structure of about 180 – 190 Å which spans the two ribosomal subunits. The NTD and CTD of Zuotin were found to be responsible for ribosome binding of RAC (Peisker et al., 2010; Leidig et al., 2013; Zhang et al., 2014). Three contact points of Zutoin

with the ribosome exist, involving five distinct ribosomal components. Two of these contact sites are situated at the 60S subunit and one at the 40S subunit (Fig. 9). The first contact site on the 60S subunit involves H59 and uL22 (Fig. 9 A and B). The second contact site on the 60S subunit involves H101 and eL31 (Fig. 9 A and B). The contact site at the 40S subunit is mediated via ES12 (Fig. 9 C and D). uL22 and eL31 are both located near the exit site of the ribosomal tunnel. RAC seems to be hunched over the exit site, positioned ideally to interact with nascent chains (Gautschi et al., 2001; Huang et al., 2005; Leidig et al., 2013; Zhang et al., 2014).

A model was proposed which is based on the characterization of different conformations of RAC on the ribosome. It seems that RAC stabilizes the ribosome in a non-rotated state. This may enable RAC to directly regulate protein translation by coupling co-translational folding and peptide elongation in a mechanic way (Huang et al., 2005; Zhang et al., 2014). The RAC complex is conserved in higher eukaryotes. mRAC was reported to cooperate with a cytosolic Hsp70 as no Ssb homologue is conserved in higher eukaryotes (Hundley et al., 2005; Otto et al., 2005; Jaiswal et al., 2011). The knockdown of human MPP11 (Zuo-homologue) caused similar effects in cells concerning growth and drug sensitivity as was observed for the loss of Zuo in yeast (Jaiswal et al., 2011). The conserved co-translational role of RAC was demonstrated by the partial complementation of the loss of yeast RAC by mRAC which was independent of Ssb but dependent on the cytosolic Ssa chaperones (Hundley et al., 2005; Otto et al., 2005).

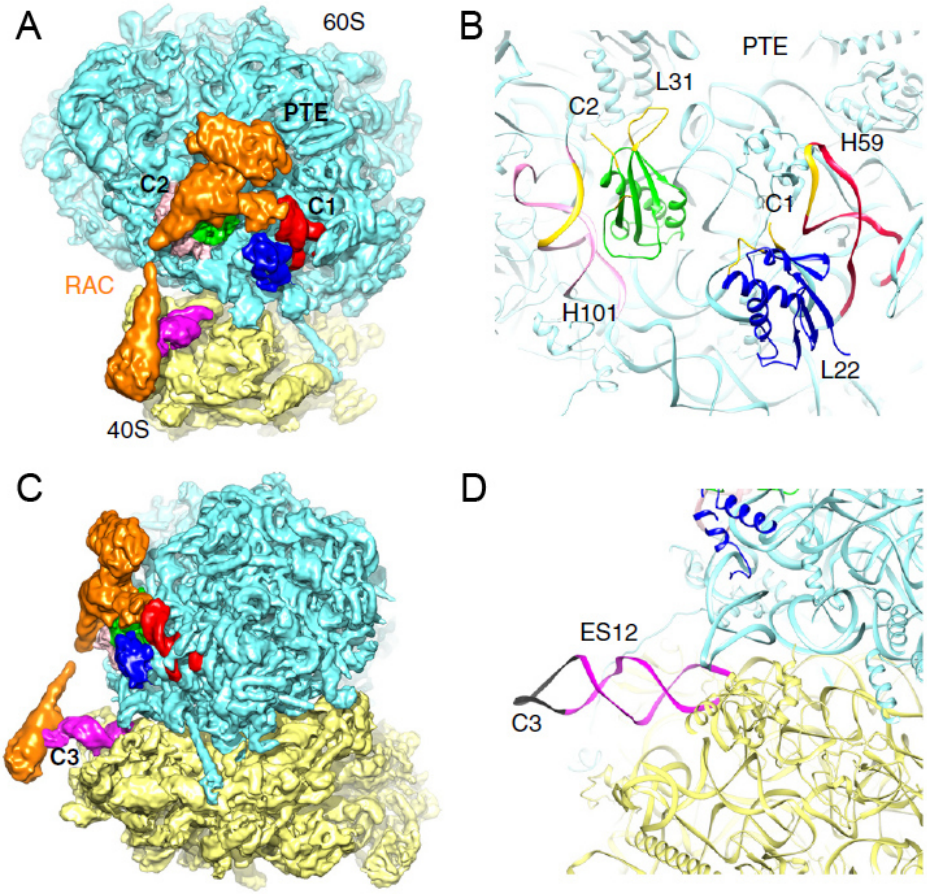

Fig. 9: Interaction sites of Zuotin with the ribosome. (A) and (C) Cryo-EM density maps with the 4.9 Å density map being filtered to 6 Å resolution. It depicts the 80S-RAC complex in the non-rotated state. The 60S subunit is coloured in cyan, the 40S subunit is coloured in yellow and RAC is coloured in orange. The three ribosomal interaction sites are marked with C1-C3. (B) and (D) Detailed view of the Zuotin interaction sites with the ribosome. (B) Ribosomal component in direct contact with Zuotin is highlighted in yellow. (D) Ribosomal component in direct ccontact with Zuotin is highlighted in gray. Figure was taken from Zhang et al. (2014).

3.6.2 NAC

The nascent polypeptide-associated complex (NAC) was first described in 1994 (Wiedmann et al., 1994). It was identified when analysing a protein crosslinked to emerging nascent chains. However, the β-subunit of the complex was discovered much earlier (Zheng et al., 1987; Zheng et al., 1990). It was reported to form a stable complex with RNA Polymerase B (II) and a function as initiation factor of transcription was proposed. In 1992, the β-subunit of NAC was found in a bandshift assay to enhance Gal4 DNA binding and was afterwards named Egd1 (enhancer of Gal4 DNA binding) (Parthun et al., 1992). Wiedmann et al. (1994) then identified Egd1 as being the β-subunit of NAC. A second β-subunit was identified in yeast and named Btt1 (BTf Three, β') (Hu and Ronne, 1994). In yeast, Egd2 was found to be the homologue of the human α-NAC subunit (Shi et al., 1995) (Fig. 8).

Characterization of yeast NAC led to the discovery of two heterodimeric complexes, one formed by Egd1 and Egd2 (αβ) and the other by Btt1 and Egd2 (αβ') (Reimann et al., 1999; Ghaemmaghami et al., 2003). The Egd1-Egd2 complex was identified to be the one responsible for NAC function. As Btt1 is around 100-fold less expressed than Egd1, the complex of Btt1-Egd2 is also much less abundant (Reimann et al., 1999). The two complexes were also shown to display different substrate specificities. Egd1-Egd2 was shown to preferentially interact with RNCs translating metabolic enzymes as well as membrane proteins and proteins destined for secretion. In contrast, the Btt1-Egd2 complex was found associated with RNCs translating ribosomal as well as nuclear-encoded mitochondrial proteins (del Alamo et al., 2011). It was speculated, that differences in the C-termini of the two β-subunits present in yeast may account for this different substrate specificity (Ott et al., 2015). The intracellular concentration of human NAC was predicted to range between 3 – 10 µM (Möller et al., 1998 a) and, therefore, a stoichiometric balance or excess in comparison to ribosomes exists (Wang et al., 1995; Powers and Walter, 1996; Raue et al., 2007).

Ribosome binding of NAC is mediated via the β-subunit in a salt sensitive manner (Reimann et al., 1999). Binding was shown to be abolished when the first 11 amino acids of the β-subunit were missing (Franke et al., 2001). In 2006, Wegrzyn and colleagues identified a ribosomal binding motif in the N-terminus of β-NAC, the RRK$(X)_n$KK motif that starts at position 24 in Egd1 and Btt1 (Fig. 10). This motif localizes in a potential loop region that is

situated between two predicted α-helices. A crosslink between this region and the ribosomal protein uL23 was detected. They speculated that the deletion of the first 11 amino acids might lead to structural rearrangements of the complex and thereby abolish ribosome binding (Wegrzyn et al., 2006). However, the sole responsibility of this motif for ribosome binding was challenged. It was proposed, that the positive charges located in the extreme N-terminus might also contribute to ribosome binding (Panasenko et al., 2009). Pech et al. (2010) found, that the first 23 amino acids of Egd1 were sufficient for ribosome binding. They exchanged ^{6}EKL^{8} and ^{10}KLQ^{12} with alanines which greatly reduced ribosome association of NAC. Furthermore, they identified different interactions sites on the ribosome than Wegrzyn et al. (2006). They proposed an interaction of Egd1 with eL31, a ribosomal protein unique to eukaryotes and archaea. They also identified uL22 as a possible interaction site for α-NAC on the ribosome.

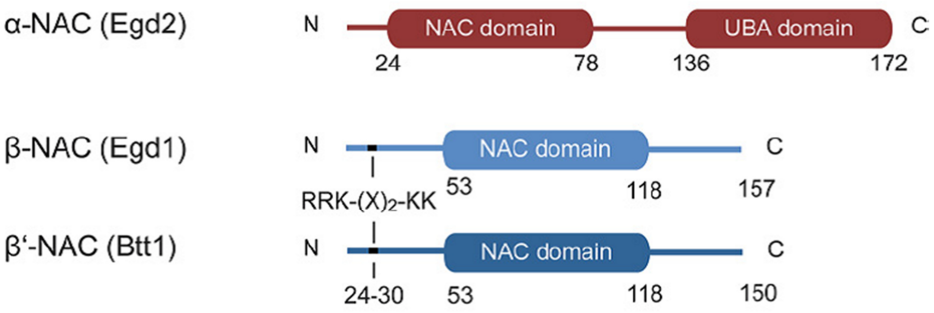

Fig. 10: Domain architecture of the yeast NAC complex. All three subunits contain a NAC domain which mediates dimerization. Egd2 contains a UBA domain in addition. The ribosome binding motif is indicated in Egd1 and Btt1. Figure was taken from Ott et al. (2015).

All subunits of NAC contain a so called NAC domain which is unique to them and responsible for dimerization (Spreter et al., 2005; Liu et al., 2010 b; Wang et al., 2010). The first structure resolved was that of the dimerization domain of archaeal NAC (Spreter et al., 2005). In archaea, NAC is a homodimer of two α-subunits (Macario and Conway De Macario, 2001; Spreter et al., 2005). In these α-subunits the presence of a C-terminal UBA-domain was detected, but no function could be assigned to it. The structure of the dimerization domain of human NAC was published in 2010 (Fig. 11) (Liu et al., 2010 b; Wang et al., 2010). Although in these studies the authors attempted to crystallize the complete NAC complex, only the dimerization domain was found to crystallize even after 6 months. The NAC domains of α- and β-NAC displayed a similar fold although the electric charge distribution on the NAC interface differed between the two subunits. This difference might explain the increased stability of hetero- over homodimers (Wang et al., 2010). The dimerization site built by the two NAC domains displays a six-stranded β-barrel like structure (Liu et al., 2010 b; Wang et

al, 2010). Because of unsaturated hydrogen bonding potential and an extensively exposed hydrophobic surface, monomers of the subunits are unlikely to be stable in solution (Wang et al., 2010). Furthermore, a potential nucleic acid binding region on the α-subunit was identified (Liu et al., 2010 b). However, the identified region is buried inside the NAC complex upon heterodimerization (Liu et al., 2010 b).

The UBA-domain found in α-NAC has always been an object of great interest. UBA-domains are present in diverse proteins, which are involved in protein degradation, cell cycle control and DNA-repair. They have been shown to be able to bind ubiquitin as well as polyubiquitin via a hydrophobic patch (Wilkinson et al., 2001; Mueller et al., 2004; Raasi et al., 2005). For the UBA-domain present in α-NAC, no interaction with ubiquitin was detected (Raasi et al., 2005; Andersen et al., 2007). However, the kind of UBA-domain present in α-NAC seems to be an ancient and distinct subgroup of this family. Thus, in evolution, this UBA-domain precedes ubiquitin as binding partner (Andersen et al., 2007). It is therefore likely, that it may function independently of the ubiquitin-proteasome system. One possible role for this UBA-domain might be the regulation of Egd2 and subsequently Egd1 stability in yeast (Panasenko et al., 2006). Recently, we were able to elucidate another possible role for the UBA-domain as a negative regulator of the NAC chaperone activity *in vivo* (Ott et al., 2015). Although the UBA-domain does not interact with ubiquitin, ubiquitination was proposed for NAC (Panasenko et al., 2006; Panasenko et al., 2009; Hiraishi et al., 2009) and in the course of this an interaction with the Ccr4-Not complex (Panasenko et al., 2006). However, this finding is still controversial.

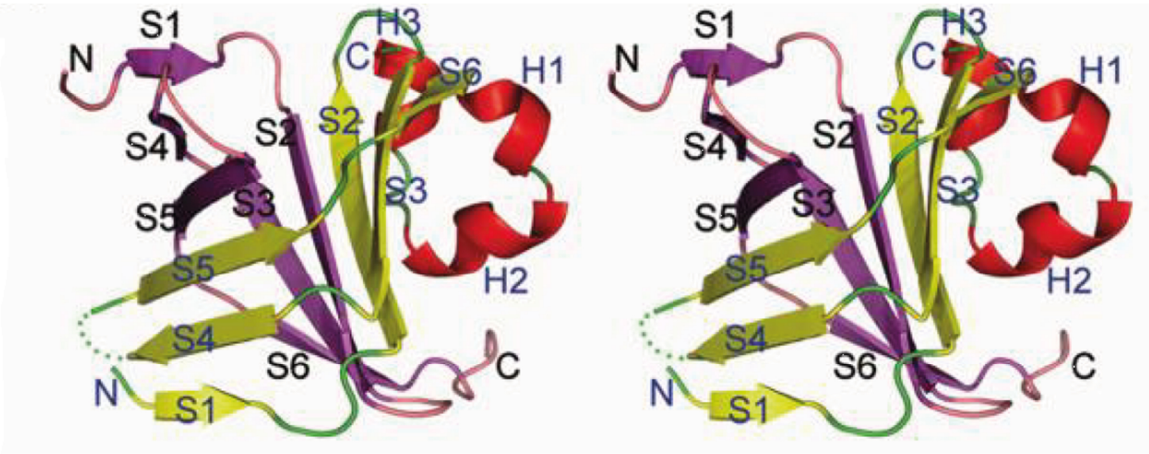

Fig. 11: Crystal structure of the dimerization domain of human NAC. The dimerization domain is shown in a stereochemical view. α-NAC is coloured in purple, β-NAC is coloured in yellow (β-sheets) and red (α-helices). S = β-sheet, H = α-helix. Figure was taken from Liu et al. (2010 b).

NAC is highly conserved from archaea to humans with especially the NAC domain being highly similar. In yeast, deletion of NAC does not result in drastic phenotypes under optimal

growth conditions. However, deletion of both β-subunits abolished growth at 37°C. This effect was attributed to a potentially toxic gain of function of the remaining α-subunit. Loss of one subunit generally led to a downregulation of the remaining ones (Reimann et al., 1999). In contrast to yeast, deletion in higher eukaryotes like *C. elegans*, fruit flies or mice led to severe embryonic defects or lethality (Deng and Behringer, 1995; Markesich et al., 2000; Bloss et al., 2003). Hence, yeast seems to have developed some backup mechanisms to compensate for the loss of NAC.

Various functions have been proposed for the single subunits of NAC. As mentioned, the first function proposed for Egd1 (β-NAC) was a role as transcriptional activator (Zheng et al., 1987; Zheng et al., 1990; Parthun et al., 1992). It was also proposed to interact with a translation initiation factor in *Arabidopsis thaliana* (Freire et al., 2005) and to be a novel activator of cell wall integrity signalling (Krause et al., 2008). During an induced misbalance of the two NAC subunits in cells, formation of *EGD1* granules was observed. They contain *EGD1* mRNA, and Egd1 as well as P-body components were found to associate with them. This mechanism was proposed to be a novel microtubule-dependent mechanism for controlling NAC by RNA localization (Hayashi et al., 2011). β-NAC was also proposed to function in the apoptotic pathway of cells and human β-NAC was identified to be a substrate of caspase3 (Brockstedt et al., 1999; Bloss et al., 2003; Thiede et al., 2001). Additionally, Egd1 in yeast was shown to be sufficient for complementing the pleiotropic growth defect of *nacΔssbΔ* cells back to the level of *ssbΔ* cells (Ott et al., 2015).

A multitude of different functions were proposed for the α-NAC subunit. In 1996, Yotov and St-Arnaud identified a muscle specific isoform of α-NAC which they named skNAC. It is expressed in differentiated myotubes and activates transcription from the myoglobin promoter, which is involved in normal cell differentiation. It was also shown, that skNAC is upregulated in differentiating myoblasts and osteoblasts as well as in cells involved in wound healing (Yotov and St-Arnaud, 1996; Moreau et al., 1998; Yotov et al., 1998; Munz et al., 1999). α-NAC seems to play a role in the differentiation of human erythroid cells as well (Lopez et al., 2005). Apart from this, it was suggested to be involved in the apoptotic pathways of different cells (Stilo et al., 2003; Quélo et al., 2004 a/b; Yoshida et al., 2005; Hotokezaka et al., 2009; Hotokezaka et al., 2015). In mammalian cells, a role for α-NAC in immune response was identified, which was independent of β-NAC (Baghdoyan et al., 2000; Goatley et al., 2002; Al-Shanti et al., 2004; Li et al., 2005; Al-Shanti and Aldahoodi, 2006; Arsenovic et al., 2012; Hradetzky et al., 2013; Li et al., 2015). For example, α-NAC was postulated to be a negative regulator in the proliferation, differentiation and cytosolic activation of CD8(+) T-cells (Al-Shanti et al., 2004; Al-Shanti and Aldahoodi, 2006). In

accordance with these findings, α-NAC was also found to interact with various disease related proteins (Goatley et al., 2002; Mossabeb et al., 2002; Li et al., 2005; Mittermann et al., 2008).
But, as stated before, single subunits are unlikely to occur *in vivo* (Wang et al., 2010). The existence of homodimers in living cells is, therefore, more likely than the existence of single subunits. However, the *in vivo* existence of these is also under debate. In some studies, the existence of homodimers under normal *in vivo* conditions is confirmed (Yotov et al., 1998; del Alamo et al., 2011), whereas others state, that NAC is solely present as a heterodimer. According to these studies, only an induced imbalance of the two subunits would lead to homodimer formation (Reimann, et al., 1999; Beatrix et al., 2000; Franke et al., 2001).

As for the single subunits, various functions have been proposed for the whole complex. Apart from its many cytosolic functions, NAC was proposed to have an additional role in the nucleus (Wool, 1996). This was supported by Yotov et al. (1998), who detected α-NAC in the nucleus upon serum starvation of an osteogenic cell line. However, Reimann et al. (1999) found no evidence for NAC in the nucleus using immunofluorescence experiments. Later, single subunits of yeast NAC were found to be actively transported into the nucleus but this was only observed when ribosome binding of NAC was abolished (Franke et al., 2001). Based on these observations a model was proposed: Newly synthesized NAC components are assumed to be transported into the nucleus where they bind to ribosomal subunits and then leave the nucleus together with them (Franke et al., 2001).

One cytosolic role of NAC that was debated concerned its interplay with the signal recognition particle (SRP). When the complex was first described, a role of NAC in the regulation of the specificity of SRP was already proposed (Wiedmann et al., 1994). This was supported by further findings, that NAC prevents inappropriate SRP binding and sterically blocks the interaction of ribosomes with the Sec61-translocon in the ER-membrane. Blocking can be overcome by SRP (Kalies et al., 1994; Walter and Johnson, 1994; Lauring et al., 1995 a/b; Möller et al., 1998 a/b; Reimann et al., 1999). This role for NAC was challenged, however, by other studies, which claimed that ribosome nascent chain complexes (RNCs) could bind independently of SRP to the ER-membrane, also in the presence of NAC (Neuhof et al., 1998; Raden and Gilmore, 1998). Further evidence for a modulation of SRP specificity and fidelity was gained by the analysis of mRNAs associated with RNCs bearing a signal sequence. A partial overlap between the proteins interacting with SRP and NAC was identified and some even seemed to require NAC in order to interact with SRP (del Alamo et al., 2011). Additionally, the early recruitment of SRP to RNCs containing a signal sequence within the ribosomal tunnel seems to be NAC dependent (Zhang et al., 2012). However, no

visible defects in SRP targeting were observed in yeast lacking NAC (Dalley et al., 2008). In contrast, depletion of NAC in *C. elegans* shortened the life span of the worm, was responsible for a global mistargeting of translating ribosomes to the ER and led to incorrect import of mitochondrial proteins into the ER-lumen (Fig. 12) (Gamerdinger et al., 2015). These effects strongly impaired proteostasis in the ER and mitochondria, supporting a suppressor role of NAC in *C. elegans*. It was also shown to block the autonomous high-affinity binding of ribosomes to the translocon. This antagonistic targeting activity is fundamentally important to sustain the correct protein sorting in the worm (Gamerdinger et al., 2015). In addition to SRP, NAC also seems to be responsible for regulating the access of the methionine aminopeptidase (MetAP) to the ribosome as SRP and MetAP otherwise seem to antagonize each other (Nyathi and Pool, 2015). SRP and the Sec61-translocon were both identified to contact the ribosome via uL23. This is the binding site for NAC identified by Wegrzyn et al. (2006). In contrast, the contact site for Egd1 identified by Pech et al. (2010), eL31, is supposed to be the contact site for the SRP receptor (SR) and RAC (Halic et al., 2006; Peisker et al., 2008). Taking into account the observed functions for NAC in regulating targeting, all proposed contact sites are theoretically possible. Multiple interactions could allow a better regulation, as the loss of one contact point would not abolish ribosome association completely.

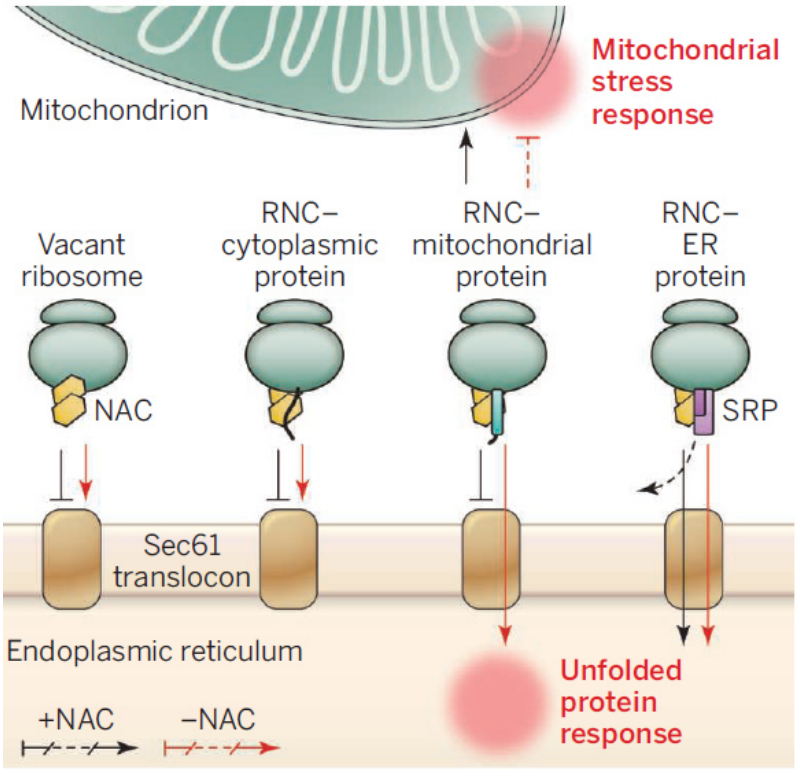

Fig. 12: NAC prevents disordered targeting of newly synthesized proteins in *C. elegans*. Targeting of vacant ribosomes or RNCs encoding for cytoplasmic or mitochondrial proteins to the ER-membrane is prevented by NAC. Depletion of NAC leads to mistargeting and translocation of some mitochondrial proteins resulting in ER stress and mitochondrial stress. Figure was taken from Kramer et al. (2015).

Apart from targeting to the ER, NAC was also suggested to play a role in mitochondrial targeting. First, NAC was merely assumed to provide a secure environment for mitochondrial targeting sequences to fold, thereby enhancing the targeting efficiency (George et al., 1998; George et al., 2002). Fünfschilling and Rospert (1999) supported such a role for NAC. They presented evidence for a function of NAC in facilitating the recognition of nascent chains by the import machinery of mitochondria. Further support for a role of NAC in mitochondrial targeting came from data showing that its depletion reduced the rate of translocated fumarase (Yogev et al., 2007). Screening for strains that display a defect in mitophagy also yielded a strain lacking Egd1. This strain had a reduced Pho8Δ60 activity (Kanki et al., 2009). Recently, a receptor for NAC on the outer membrane of mitochondria was identified by Lesnik et al. (2014): OM14. The authors of this study stated that OM14 dependent import necessitates NAC and found increased levels of Tom20 in cells depleted of NAC which they attributed to a compensatory mechanism.

NAC seems to be the first non-ribosomal protein to contact nascent chains (Wiedmann et al., 1994). Both subunits were crosslinked to newly emerging polypeptides with a length ranging from 17 to 100 amino acids (Wiedmann et al., 1994; Wang et al., 1995). In addition, NAC was not only shown to interact with these nascent chains but also to be able to protect them from proteolysis. Polypeptide chains with a length of up to ~30 amino acids were protected from digestion with proteinase K (Wiedmann et al., 1994; Wang et al., 1995; Powers and Walter, 1996). This led to the assumption that NAC might act as a molecular chaperone during translation. However, no capability of NAC to prevent protein aggregation was observed and NAC was only found to contact nascent chains while they were bound to the ribosome (Wiedmann et al., 1994; Plath and Rapoport, 2000). The assumption of a chaperone activity of NAC was first supported by the finding, that NAC displays a functional connection to the Ssb-RAC system at the ribosome and to the cytosolic chaperone network (Koplin et al., 2010). As already mentioned above, the deletion of Ssb severely affected yeast cells. All phenotypes observed in these cells were enhanced by an additional loss of NAC. This suggests a role of NAC in ribosome biogenesis together with Ssb (Koplin et al., 2010). Deletion of NAC in yeast was shown to result in more heavily ubiquitinated nascent chains which were also more aggregation prone and contained a higher β-sheet propensity (Duttler et al., 2013). This indicates a role of NAC in the stabilization and protection of newly synthesized proteins and supports a role of it as molecular chaperone. In Ott et al. (2015) we determined a role for NAC in the prevention of aggregation in yeast cells. Different NAC variants were able to reduce the amount of aggregating proteins when expressed in *nacΔssbΔ* cells. A NAC variant lacking the UBA domain even reduced the amount of aggregated proteins beyond the level observed in *ssbΔ* cells. Investigation of artificially

constructed amyloid fibrils or aggregates induced by the metalloid arsenite revealed the association of NAC with these aggregates (Olzscha et al., 2011; Jacobson et al., 2012) again supporting a role for NAC in the process of protein aggregation.

First indications for a chaperone function in *C. elegans* were found in 2012. Loss of NAC in adult worms triggered ER-stress and the unfolded protein response (UPR) (Arsenovic et al., 2012). In addition to the expression of ER stress marker proteins, NAC depletion also induced the expression of mitochondrial stress marker proteins (Guo et al., 2014). Kirstein-Miles et al. (2013) established NAC as a sensor for proteostasis in *C. elegans* (Fig. 13). NAC relocalized from ribosome to aggregates under acute as well as chronic stress conditions. This relocalization reduced the translation rate and thereby the influx of new proteins into the cell providing a regulatory mechanism, where the folding state of the proteome contributes to the control of translational activity. Upon acute stress conditions like heat shock, NAC relocalized to ribosomes once the stress passed. This is in contrast to chronic stress conditions induced for example by ageing or upon expression of polyQ proteins or the Aβ-peptide, where NAC is sequestered permanently to aggregates. This leads to a permanent reduction in protein synthesis.

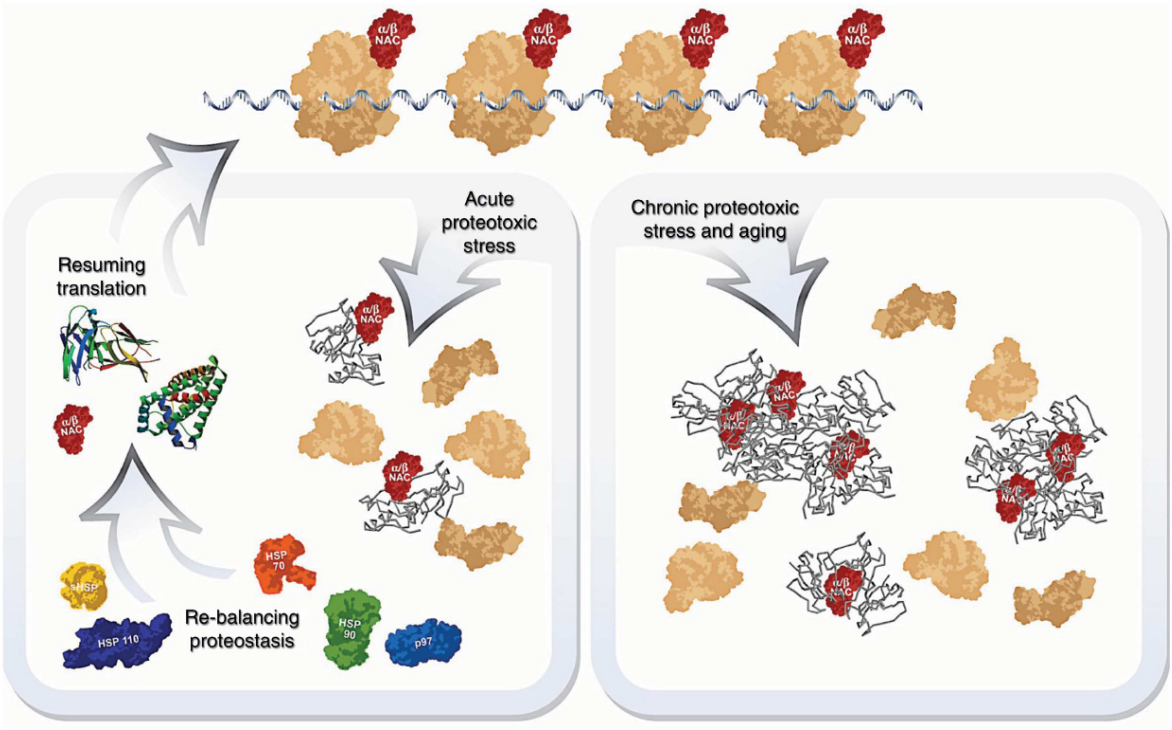

Fig. 13: NAC acts as a proteostasis sensor in *C. elegans*. Acute proteotoxic stress conditions (left site) lead to a timely restricted sequestration of NAC from ribosomes by misfolded and aggregated proteins. This reduces the translational activity. When the balance is restored, NAC shifts back to ribosomes. Under chronic stress conditions (right site) NAC is sequestered permanently to misfolded and aggregated proteins, which in turn leads to a persistent decrease in protein synthesis. Figure was taken from Kirstein-Miles et al. (2013).

4. Aims of this work

The folding of newly synthesized proteins is a complex and error-prone process. Molecular chaperones have evolved to assist proteins in reaching their native conformation. Chaperones can be bound to ribosomes or freely accessible in the cytosol. Positioning at the ribosomal exit tunnel enables the interaction with nascent chains, thereby preventing unfavourable interactions and providing assistance in folding. One important eukaryotic chaperone associated with ribosomes is the nascent polypeptide-associated complex (NAC). Amongst other proposed functions, it was reported to interact with nascent chains during translation and to play a role in the accuracy and fidelity of protein targeting to different compartments. Recent findings support a role for NAC as a molecular chaperone: It was found to associate with artificial aggregates and aggregates originating from different stress conditions in *C. elegans*. However, the mechanisms of action of NAC are still elusive. To analyse this function of NAC in more detail, 3 major goals were pursued in this thesis.

1)
The first goal was to analyse the functional interaction of NAC with potential substrate proteins and aggregates. To this end, different *in vivo* and *in vitro* experiments were performed. Purified NAC was tested for its ability to prevent the inactivation of citrate synthase and to promote the reactivation of luciferase. Its direct effect on the aggregation of these model substrates was examined as well. The nature of the interaction between NAC and the model substrates was analysed using size exclusion chromatography.
In Ott et al. (2015) we recently discovered a negative regulatory role for the UBA domain of Egd2 in prevention of protein aggregation. To analyse this effect in more detail, *in vitro* aggregation prevention experiments with different ΔUBA variants were performed.
NAC was found to co-localize with different sorts of aggregates in *C. elegans* including aggregates arising from heat shock. To determine if this association is evolutionarily conserved, *in vivo* experiments were performed in yeast to analyse the localization of NAC during heat shock.

2)
Second, structure-function analyses of NAC were performed to better understand the interactions between the different domains of NAC. The complete structure of NAC has not been elucidated so far. It was only possible to crystallize the dimerization and the UBA domain of the complex. Analysis of the crystallized structure revealed the existence of the unique NAC domains present in the subunits. Together they form a flattened β-barrel-like structure. The remainder of the structure, apart from the UBA domain, seems to be too

flexible to be suitable for crystallization. To understand the structure of NAC and to judge conformational changes introduced by mutations, circular dichroism measurements were performed. In a second approach, the purified complex was digested with proteinase K to determine, which parts of the structure are easily accessible and if these regions change in a concentration-dependent way. Additionally, bioinformatics analyses were performed to determine conserved regions in the sequence and to construct a structure model of yeast NAC.

3)

The third goal was to identify potential substrate binding sites of NAC. The complex is known to contact nascent chains and to interact with aggregates. However, the site(s) responsible for these interactions has not been identified till now. The bioinformatics analyses provided valuable information for the screening for these potential binding sites. Furthermore, positions in the NAC complex were determined which were suitable for the incorporation of the zero-space crosslinker para-benzoylphenylalanine (pBpa). Using this crosslinker, interactions between NAC and its partners can be investigated *in vivo*.

5. Results

5.1 NAC does not act like a small heat shock protein

In this study, the function of NAC in yeast was analysed. It was investigated, if it behaves in a similar way as *C. elegans* NAC. In *S. cerevisiae*, three subunits of NAC exist: Two β-subunits, Egd1 and Btt1, with Egd1 being the more abundant one and one α-subunit, Egd2 (Wiedmann et al., 1994; Reimann et al., 1999).

In a recent study of our lab we showed that NAC is not only actively recruited to heat shock and ageing dependent aggregates in *C. elegans* but also supports disaggregation (Kirstein-Miles et al., 2013). Furthermore, Olzscha et al. (2011) identified an interaction of NAC with artificial protein aggregates. This activity is reminiscent to that described for the small heat shock protein Hsp26 (Haslbeck et al., 1999; Haslbeck, 2002; Cashikar et al., 2005). This chaperone acts independently of ATP. It associates with proteins during the aggregation process and keeps them in a folding competent state. Thereby it facilitates disaggregation by Hsp104 and Ssa1/Ydj1in yeast. We now speculated that a possible chaperone function of NAC might be similar to the one observed for Hsp26.

5.1.1 Shift of Hsp26 to the aggregate fraction as described in Cashikar et al. (2005)

Cashikar et al. (2005) analysed the *in vivo* role of Hsp26 in yeast. They showed that after a sublethal heat shock (30 min at 37°C followed by 30 min at 46°C) the majority of Hsp26 shifted to the insoluble fraction. Resolubilization upon recovery depended on Hsp104 (Fig. 14).

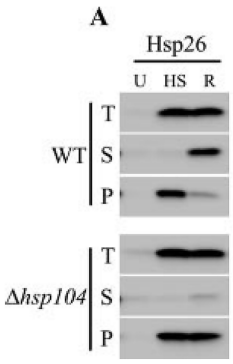

Fig. 14: Solubility of Hsp26 after a sublethal heat shock in wt and *hsp104Δ* cells. (A) Western Blot detected with Hsp26 antibody. Cells (untreated → U) were subjected to heat shock (30 min at 37°C followed by 30 min at 46°C → HS) and allowed to recover (30°C for 1 h → R). Total lysates (T) were centrifuged to separate supernatant (SN) and pellet (P). Figure taken from Cashikar et al. (2005).

In a first step we established the protocol of Cashikar et al. (2005) in our lab. Wt, *hsp104Δ* and *nacΔ* cells were subjected to thermotolerance with subsequent heat shock and samples were prepared as described in Cashikar et al. (2005). The *nacΔ* strain was included to investigate, whether the lack of NAC influences the behaviour of Hsp26. In both, wt and *hsp104Δ* cells, the distribution of Hsp26 was identical to the one described in Cashikar et al. (2005). Under untreated conditions, expression of Hsp26 was relatively low and it was found in the soluble fraction (Fig. 15 A and B). Upon thermotolerance and subsequent heat shock, the expression of Hsp26 increased and it shifted to the insoluble fraction. In wt cells, Hsp26 shifted back to the soluble fraction upon recovery (Fig. 15 A). In *hsp104Δ* cells aggregates can no longer be resolved efficiently (Parsell et al., 1994 b). As Hsp26 is associated with these aggregates it stayed in the pellet fraction even upon recovery (Fig. 15 B). Hsp26 is not influenced by NAC as the results obtained with *nacΔ* were comparable to wt (Fig. 15 C). In untreated cells Hsp26 was only weakly expressed and found in the soluble fraction. Upon heat shock, expression was upregulated and Hsp26 shifted to the pellet fraction. This was reversed upon recovery. The amount of Hsp26 in the pellet fractions of the three tested strains was quantified (Fig. 15 D). The shift of Hsp26 into the pellet fraction was statistically significant in all three strains (wt, *hsp104Δ*, *nacΔ*: $p<0.001$; analysed with one-way ANOVA with post hoc Holm-Sidak) as was the shift back to the soluble fraction in wt and *nacΔ* ($p<0.001$). The amount of Hsp26 present in the pellet fraction of *hsp104Δ* during recovery hardly changed.

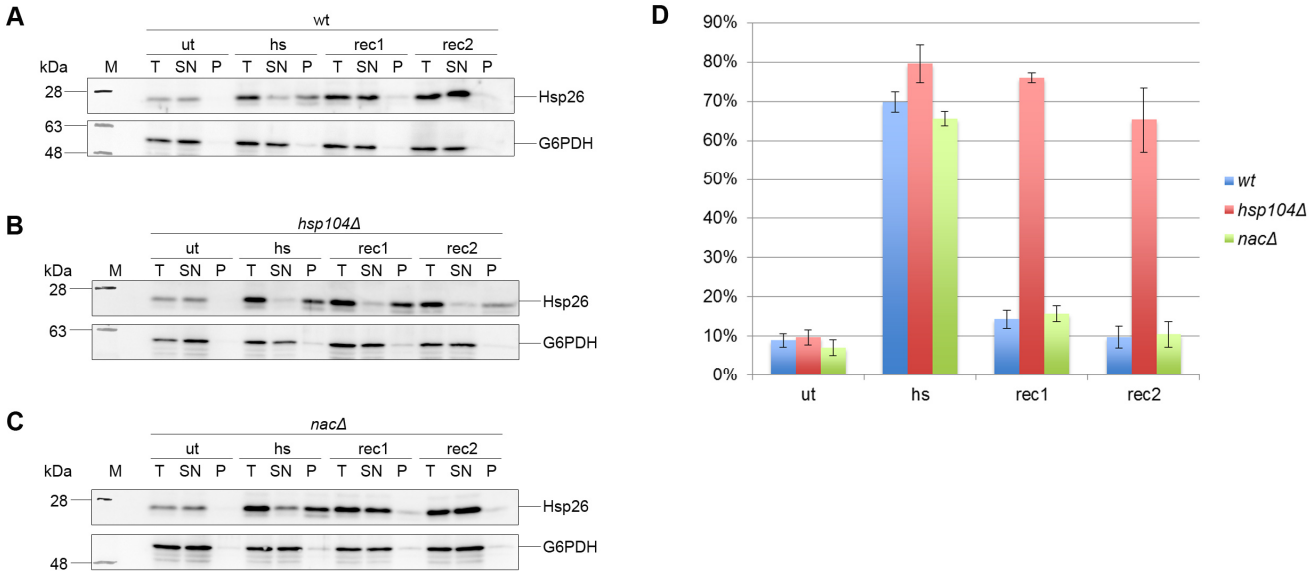

Fig. 15: Hsp26 behaves like described in Cashikar et al. (2005) and deletion of NAC does not influence the distribution of the small heat shock protein. Cells were grown at 30°C. Samples were taken before heat shock (ut), after heat shock (30 min at 37°C, 30 min at 45°C → hs) and after 1 h and 2 h of recovery (rec1 and rec2 respectively). Lysates (total → T) were centrifuged to separate them into supernatant (SN) and pellet (P). Samples were run on 12% SDS gels, blotted onto nitrocellulose membranes and probed with an antibody against Hsp26. G6PDH served as loading control. (A) wt, (B) *hsp104Δ*, (C) *nacΔ*. (D) Quantification of the pellet fractions of three independent experiments each. One-way ANOVA was performed with consecutive Holme-Sidak. Increase of Hsp26 in the pellet fraction of all three strains upon heat shock was significant ($p<0.001$) as was the decrease of Hsp26 in the pellet fraction upon recovery in wt and *nacΔ* ($p<0.001$). +/- mean standard deviation is shown.

5.1.2 NAC does not shift to aggregates like Hsp26

Using the established protocol it was analysed, if NAC shifts into the pellet fraction upon heat shock as Hsp26 does. Notably, the used NAC antibody detected Egd2 better than Egd1. In addition, an unspecific band with a molecular weight between the two subunits was always detected by the antibody.

In wt cells, no shift of Egd2 or Egd1 into the pellet fraction was observed upon heat shock (Fig. 16 A). After recovery, the amount of the two subunits in the pellet fraction seemed to increase slightly (Fig. 16 C and D), however, the observed differences were statistically insignificant. As in wt cells, no shift of the NAC subunits into the pellet fraction upon heat shock was observed in *hsp104Δ* cells (Fig. 16 B). The amount of Egd2 and Egd1 in the pellet fraction was slightly increased after recovery as observed in wt.

NAC did not shift to the pellet fraction as observed for Hsp26 which indicates different mechanisms of action of the two proteins.

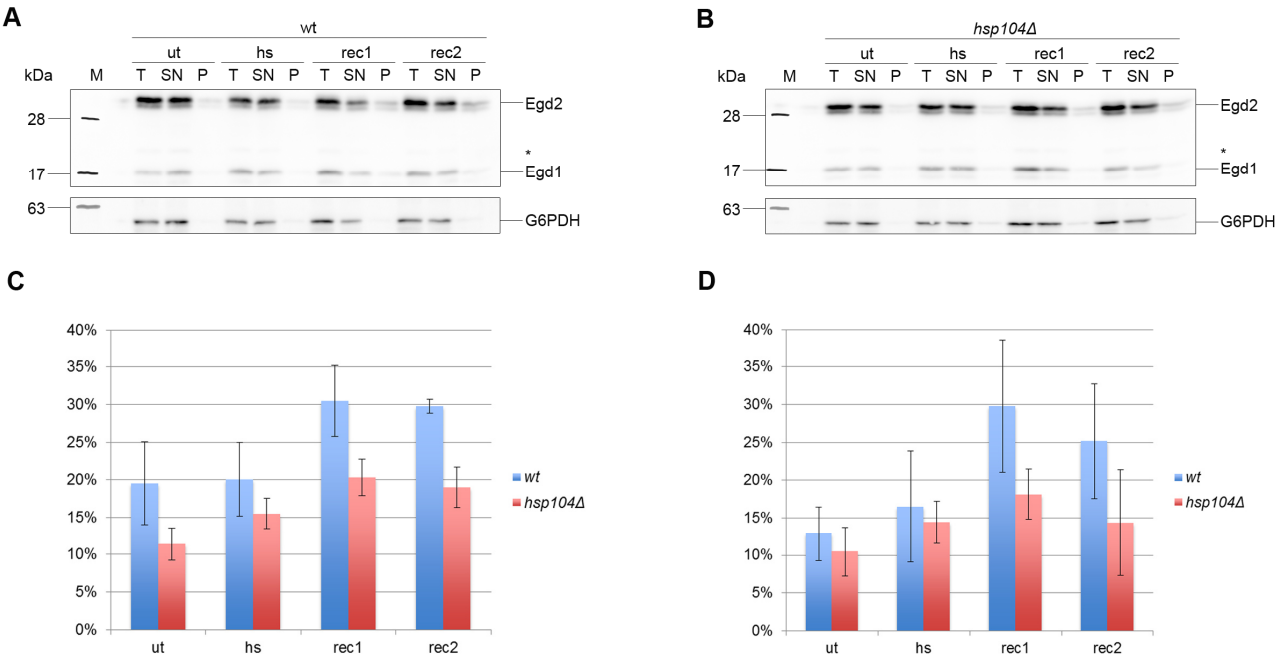

Fig. 16: NAC does not shift to the pellet fraction upon heat shock. Cells were grown at 30°C and samples were taken before (ut) and after heat shock (30 min at 37°C, 30 min at 45°C → hs) as well as after 1 h and 2 h of recovery (rec1 and rec2 respectively). Lysates (total → T) were centrifuged to separate them into supernatant (SN) and pellet (P). Samples were run on 12% SDS gels, blotted onto nitrocellulose membranes and probed with an antibody against NAC. G6PDH served as loading control. (A) wt, (B) *hsp104Δ*. (C) and (D) Quantification of the amount of Egd2 (C) and Egd1 (D) in the pellet fractions from three independent experiments each. One-way ANOVA was performed with consecutive Holme-Sidak. In *hsp104Δ* cells, there was significantly more Egd2 found in the rec1 fraction ($p = 0.017$) and the rec2 fraction ($p = 0.045$) compared to untreated cells (ut). +/- mean standard deviation is shown. *: unspecific band detected by the NAC antibody.

In *C. elegans* NAC is washed off ageing dependent aggregates in the presence of detergent in the buffer (Kirstein-Miles et al., 2013). To test for this possibility, detergent was omitted from the buffer and the fractionation experiment was repeated. Also under this experimental condition neither in wt nor in *hsp104Δ* cells a shift of NAC to the pellet fraction was observed (Fig. 17 A and B). This was confirmed by quantitative analysis (Fig. 17 C and D). Only a

slight redistribution of Egd2 and Egd1 to the pellet fraction upon recovery was observed but this shift was statistically insignificant. Hence, the presence or absence of detergents did not influence NAC behaviour in this experimental setup.

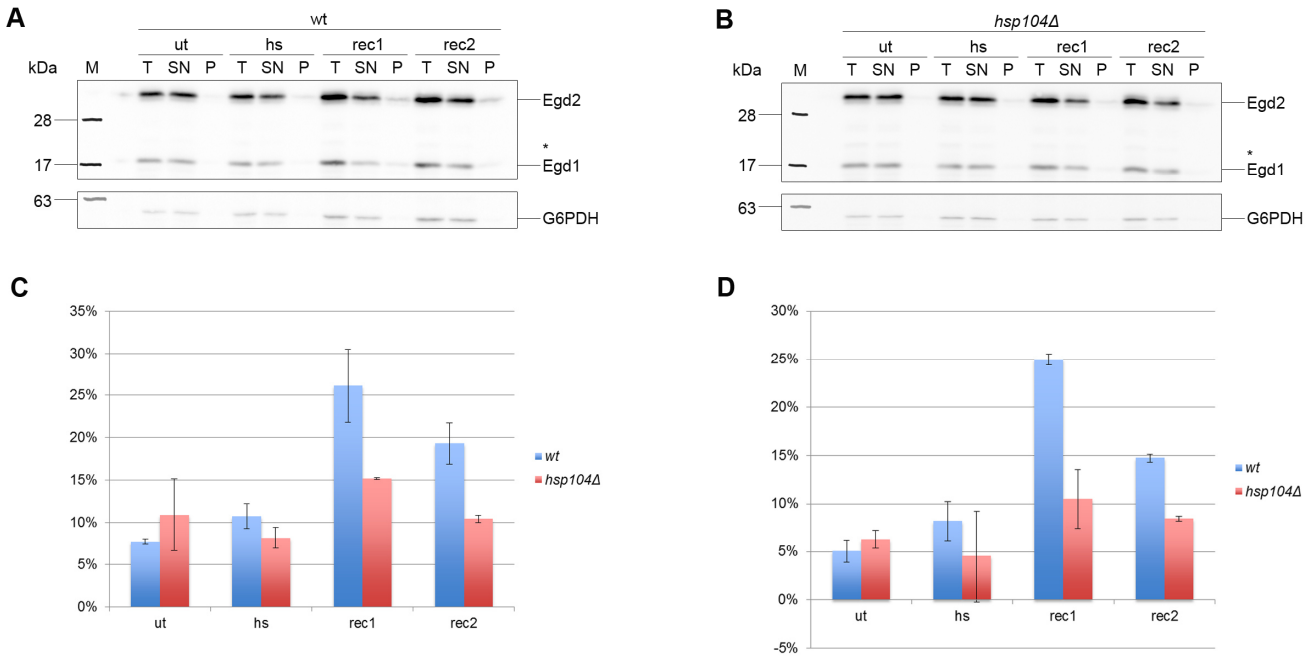

Fig. 17: NAC does not shift to the pellet fraction upon heat shock when using detergent-free buffer. Cells were grown at 30°C and samples were taken before (ut) and after heat shock (30 min at 37°C, 30 min at 45°C → hs) as well as after 1 h and 2 h of recovery (rec1 and rec2 respectively). Lysates (total → T) were centrifuged to separate them into supernatant (SN) and pellet (P). Samples were run on 12% SDS gels, blotted onto nitrocellulose membranes and probed with an antibody against NAC. G6PDH served as loading control. (A) wt, (B) *hsp104Δ*. (C) and (D) Quantification of the amount of Egd2 (C) and Egd1 (D) in the pellet fractions from two independent experiments each. One-way ANOVA was performed with consecutive Holme-Sidak. No statistically significant differences could be detected. +/- mean standard deviation is shown. *: unspecific band detected by the NAC antibody.

The absence of a shift of NAC to the pellet fraction might also be due to the experimental protocol. To exclude this possibility another method for the preparation of aggregates was used. The main differences in the protocols were the washing procedure of the cell pellet with NaN_3 before freezing it for storage and the washing steps applied to the pelleted aggregates (protocol 7.2.10.2 in comparison to 7.2.10.1). As can be seen in Fig. 14, no shift of NAC to the pellet fraction upon heat shock was detectable. The amount of Egd2 and Egd1 in the pellet fraction did only increase very slightly upon recovery in *hsp104Δ* cells but not in wt cells (Fig. 18 A and B). The quantification confirmed the absence of a clear shift of Egd2 or Egd1 to the pellet fraction. There were no statistically significant differences between untreated cells, heat shocked ones or cells after recovery (Fig. 18 C and D). Changing the technique of aggregate preparation did not lead to obvious differences in the obtained results.

In sum, unlike Hsp26 the chaperone NAC does not show redistribution to aggregates under the experimental conditions tested in *Saccharomyces cerevisiae*.

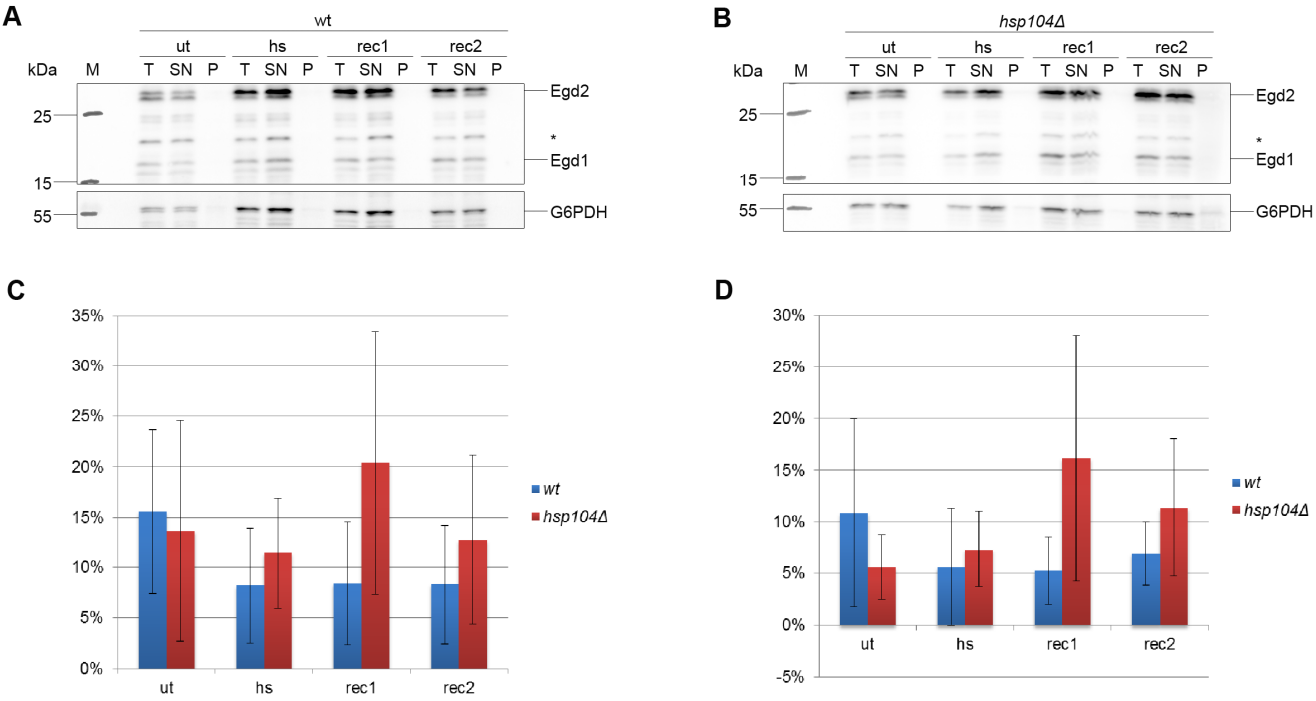

Fig. 18: No shift of NAC to the pellet fraction could be detected by using another method to prepare the aggregates. Cells were grown at 30°C and samples were taken before (ut) and after heat shock (30 min at 37°C, 30 min at 45°C → hs) as well as after 1 h and 2 h of recovery (rec1 and rec2 respectively). Lysates (total → T) were centrifuged to separate them into supernatant (SN) and pellet (P). Pellets were washed three times. Samples were run on 12% SDS gels, blotted onto nitrocellulose membranes and probed with an antibody against NAC. G6PDH served as loading control. (A) wt, (B) *hsp104Δ*. (C) and (D) Quantification of the amount of Egd2 (C) and Egd1 (D) in the pellet fractions from two independent experiments each. One-way ANOVA was performed with consecutive Holme-Sidak. No statistically significant differences could be detected. +/- mean standard deviation is shown. *: unspecific band detected by the NAC antibody.

5.1.3 Fluorescence microscopy shows that NAC does not co-localize with aggregates

5.1.5.1 Fluorescence tag does not alter NAC behaviour

Biochemical studies as described above gave no evidence for a stable association of NAC with heat-induced aggregates. It is possible that the interaction of NAC with aggregates is only weak or very transient. To analyse this, the localization of NAC during the process of aggregation was investigated by fluorescence microscopy. To visualize NAC in yeast cells it was C-terminally tagged with the fluorescent protein yEGFP. To investigate the functionality of the tagged NAC construct *nacΔssbΔ* cells were transformed with the plasmid encoding for Egd1-yEGFP-Egd2. *ssbΔ* cells display a phenotypic growth defect which is enhanced in *nacΔssbΔ* cells (Koplin et al., 2010). If the tagged NAC construct is functional, it will be able to complement the growth defect of *nacΔssbΔ* cells back to the level of *ssbΔ* cells. And indeed, the fluorescence tag did not negatively influence the ability of NAC to complement the pleiotropic growth defect (Fig. 19). When comparing the untagged version of NAC and the tagged version, no significant difference in the complementation of the growth defect on YPD, CM-URA-LEU, CM-URA-LEU + 0.4 M NaCl and CM-URA-LEU-ARG + 0.25 µg/ml L-canavanine plates was observed. Only when comparing the untagged and the tagged

version on the hygromycin B plate, a slight difference in complementation was detected. The tagged version could not complement the pleiotropic growth phenotype as well as the untagged one.

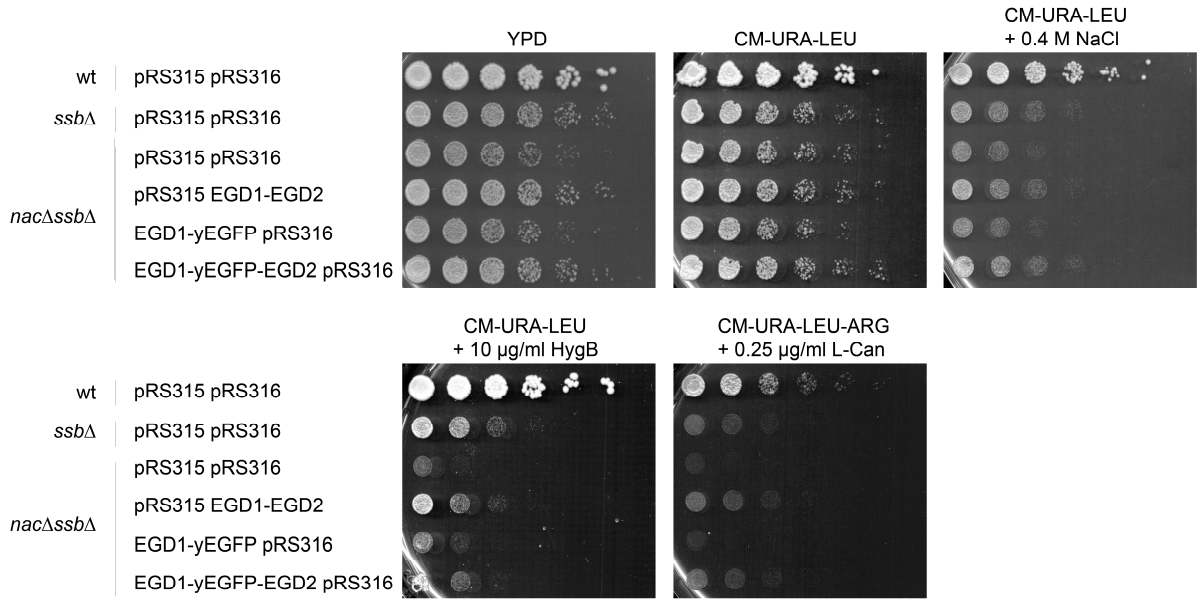

Fig. 19: Fluorescently labelled NAC complements the growth defect of *nacΔssbΔ* cells back to the level of *ssbΔ* cells. Cells were grown in CM-URA-LEU medium. 5-fold serial dilutions were spotted onto indicated selection plates and cells were grown at 30°C for 3 days. pRS315 and pRS316 are empty expression vectors with the auxotrophic markers for leucine and uracil, respectively. When using the arginine homologue L-canavanine, arginine was additionally omitted from the medium.

To analyse the expression level of the tagged construct alkaline lysis of the different yeast strains was performed. Samples were run on a 12% SDS gel and blotted on a nitrocellulose membrane which was probed with an antibody against NAC. The unspecific band detected by the used NAC antibody was also present in the *nacΔssbΔ* strain, proving that it is unspecific (Fig. 20, lane 3).

In wt and *ssbΔ* cells, the native NAC subunits Egd2 and Egd1 were detected (Fig. 20, lanes 1 and 2). When untagged NAC was expressed from a plasmid in *nacΔssbΔ* cells, the amount of detected protein was similar as in wt cells (Fig. 20, lane 4). Expressing the tagged Egd1 subunit alone resulted in a stronger signal for Egd1 compared to untagged one (Fig. 20, lane 5). The same was observed when Egd2 was expressed in addition (Fig.20, lane 6). In contrast to tagged Egd1, no difference in the intensity of the band corresponding to Egd2 was detected between the strains. It could either be that the tagged subunit is expressed in a higher amount or just more stable. Another possibility could be that the antibody detected the tagged version of Egd1 better than the untagged one.

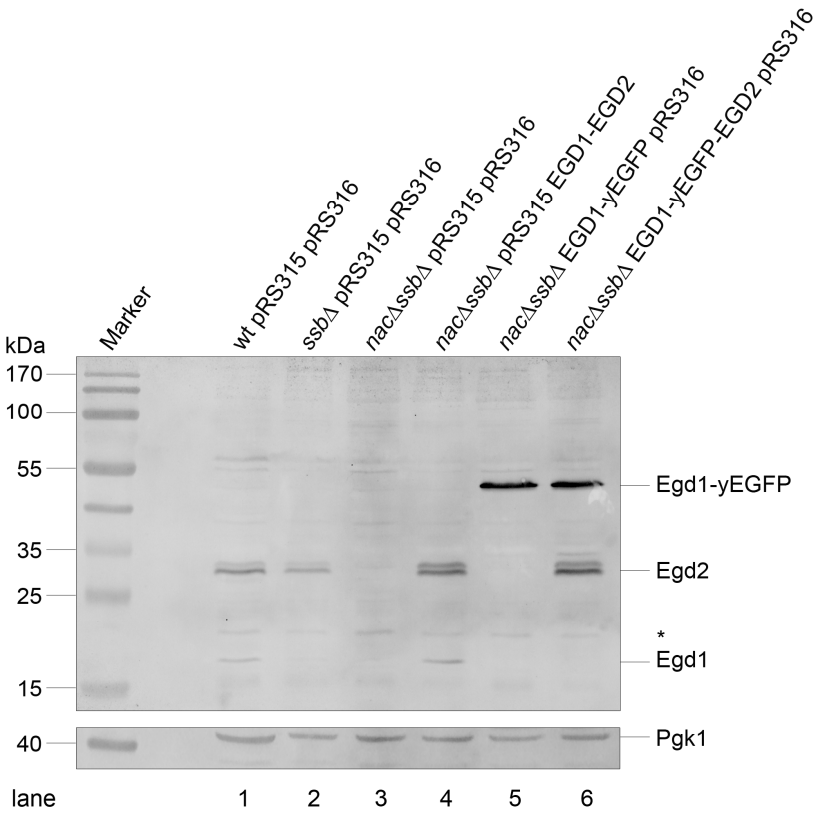

Fig. 20: Expression pattern of tagged and untagged NAC in different strains. Cells were grown in CM-URA-LEU medium and lysed using NaOH. Equal amounts were loaded onto a 12% SDS-gel. Western Blot was performed and the nitrocellulose membrane was probed with NAC antibody. Pgk1 was used as loading control. *: unspecific band detected by the NAC antibody.

NAC is known to bind to ribosomes via a conserved motif and probably an adjacent alpha helical structure present in the Egd1 subunit (Franke et al., 2001; Wegrzyn et al., 2006; Pech et al., 2010). To investigate if the fluorescence tag at the C-terminus of Egd1 might influence ribosome binding, an *ex vivo* ribosome sedimentation analysis was performed. In wt and *ssbΔ* cells, the majority of endogenous NAC was found in the pellet fraction (Fig. 21 A) which indicates a ribosomal localization of NAC. In the negative control (*nacΔssbΔ* cells with empty vectors) neither Egd2 nor Egd1 were detected (Fig. 21 B). In *nacΔssbΔ* cells supplemented with a plasmid encoding for native NAC, the subunits of the complex were detected mainly in the pellet fraction again indicating a ribosomal localization of the complex. However, in contrast to Egd1, Egd2 was also found to a great amount in the supernatant. When expressing the tagged NAC version in *nacΔssbΔ* cells, the majority of Egd1-yEGFP and Egd2 was found in the pellet fraction. Still, as in the cells expressing the untagged NAC construct, a fair amount of NAC was detected in the supernatant.

In summary, the C-terminally tagged version of the *S. cerevisiae* NAC complex is fully functional.

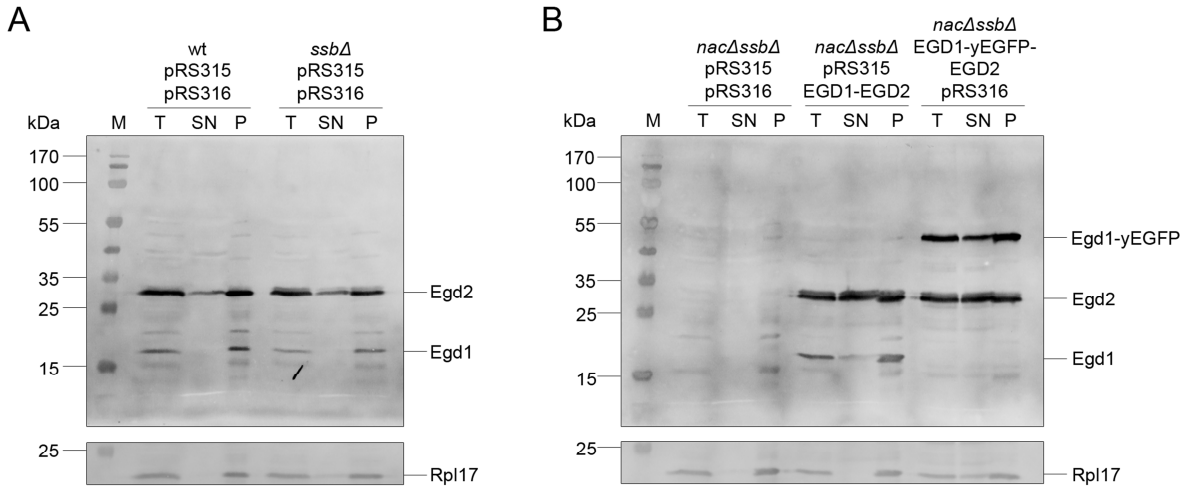

Fig. 21: Fluorescently labelled NAC binds to ribosomes. Cells were grown in CM-URA-LEU medium to an OD_{600} of 0.8 – 1. Cells were disrupted via glass bead lysis. Total lysates (T) were centrifuged through a 20% sucrose cushion to isolate ribosomes (P). Samples were also taken from the supernatant after the centrifugation step (SN). The samples were loaded onto 12% SDS-gels, blotted onto nitrocellulose membranes and probed with an antibody against NAC. Rpl17 was used as loading control.

5.1.5.2 Co-expression of NAC with tagged luciferase during heat shock

To monitor the behaviour of NAC upon heat shock, it was co-expressed with an aggregation prone protein, namely luciferase. Luciferase was tagged with mCherry (Bachelor Thesis Lisa Maria Haiber, 2015) to follow the aggregation by fluorescence microscopy. For the experiment *nacΔ* cells were transformed with two plasmids, one encoding for the yEGFP tagged NAC and one for the mCherry tagged luciferase. In contrast to NAC, which was expressed under its endogenous promoter, luciferase was under control of a CUP1 promoter. The expression was induced by the addition of 50 µM copper sulphate. *nacΔ* cells expressing the two proteins were grown to an OD_{600} of 0.6 and subjected to thermotolerance at 37°C with a subsequent heat shock at 45°C. Afterwards they were allowed to recover for 90 min at 30°C. As negative control yEGFP under control of the *EGD1* promoter was used and as positive control GFP-tagged Hsp104. Hsp104 is known to interact with aggregates. It is responsible for the resolubilization of aggregated proteins together with the Hsp70/40 system in yeast (Parsell et al., 1994 b).

Prior to heat shock, Hsp104 and luciferase were evenly distributed throughout the cytosol (Fig. 22, ut). Upon heat shock, luciferase aggregated and Hsp104 could be found co-localizing with these aggregates (Fig. 22, hs). After 30 min of recovery (Fig. 22, rec1) no change in the localization of luciferase and Hsp104 was detected. The amount of visible luciferase aggregates was reduced after 60 min of recovery (Fig. 22, rec2) and after 90 min, all aggregates were resolubilised. Hsp104 and luciferase were again evenly distributed throughout the cytosol (Fig. 22, rec3).

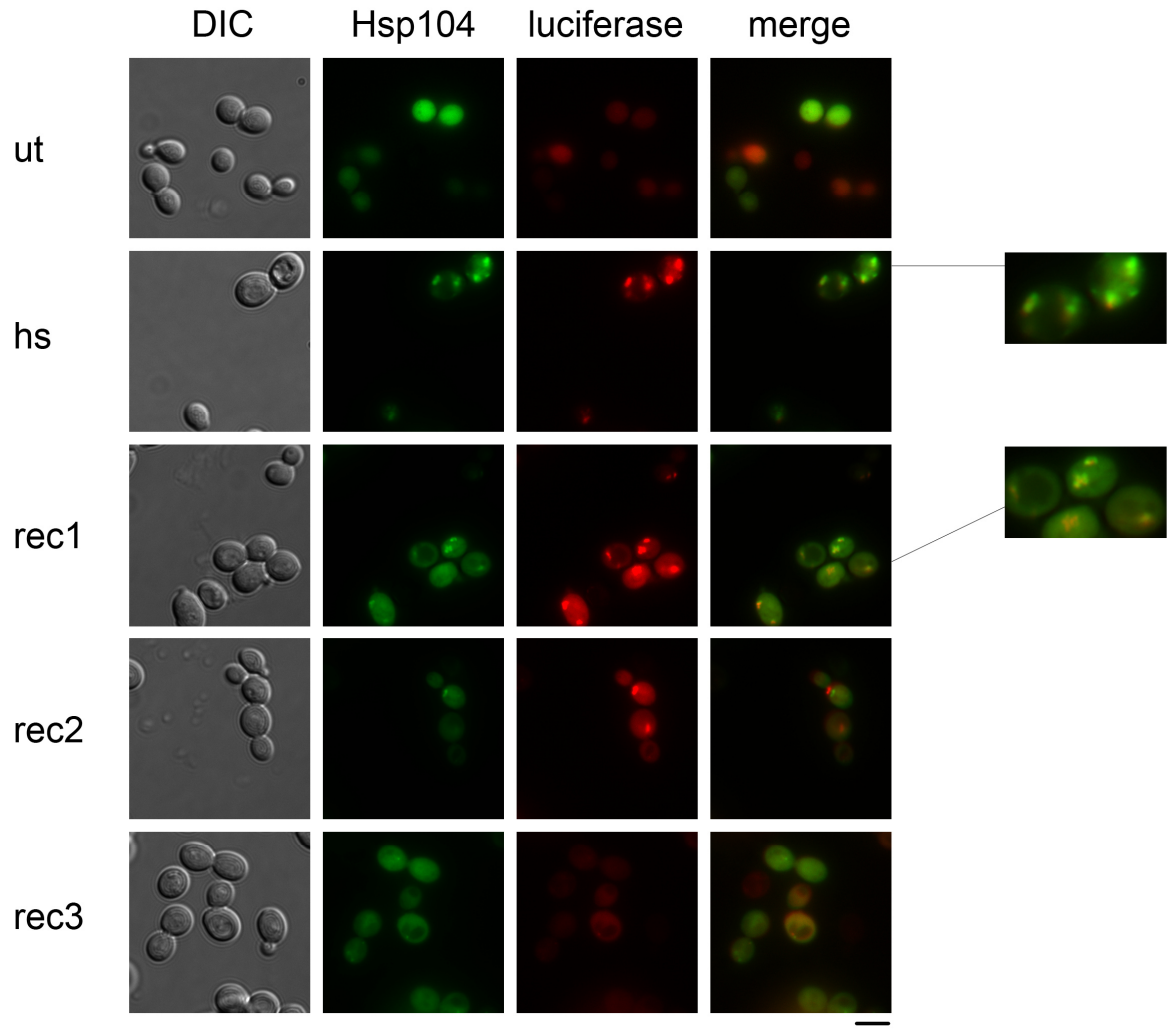

Fig. 22: Hsp104 co-localizes with aggregated luciferase. *Δnac* cells containing the plasmids encoding for luciferase and Hsp104 were grown in CM-URA-LEU medium supplemented with 50 µM copper sulphate for induction of luciferase expression. They were grown to an OD_{600} of 0.6, subjected to a sublethal heat shock (30 min at 37°C, 30 min at 45°C) and allowed to recover for 90 min at 30°C. Samples were taken before heat shock (ut), after heat shock (hs) and in 30 min intervals during the recovery period (rec1 – rec3). Co-localization of Hsp104 and luciferase is highlighted for hs and rec1 conditions. Scale bar = 5 µM.

As a control, the distribution of yEGFP was analysed to exclude the possibility that it aggregates on its own. At 30°C yEGFP as well as luciferase were both evenly distributed throughout the cytosol (Fig. 23, ut). After thermotolerance with subsequent heat shock at 45°C, luciferase re-localized to aggregates as observed before. In contrast, yEGFP did not shift to aggregates but remained evenly distributed (Fig. 23, hs). Upon recovery at 30°C, the aggregates containing luciferase were slowly resolubilised over the course of 90 min (Fig. 23, rec1 – rec3). yEGFP maintained its cytosolic localization. Therefore, a possible co-localization of NAC with luciferase aggregates would not be a result of the aggregation of its fluorescent tag.

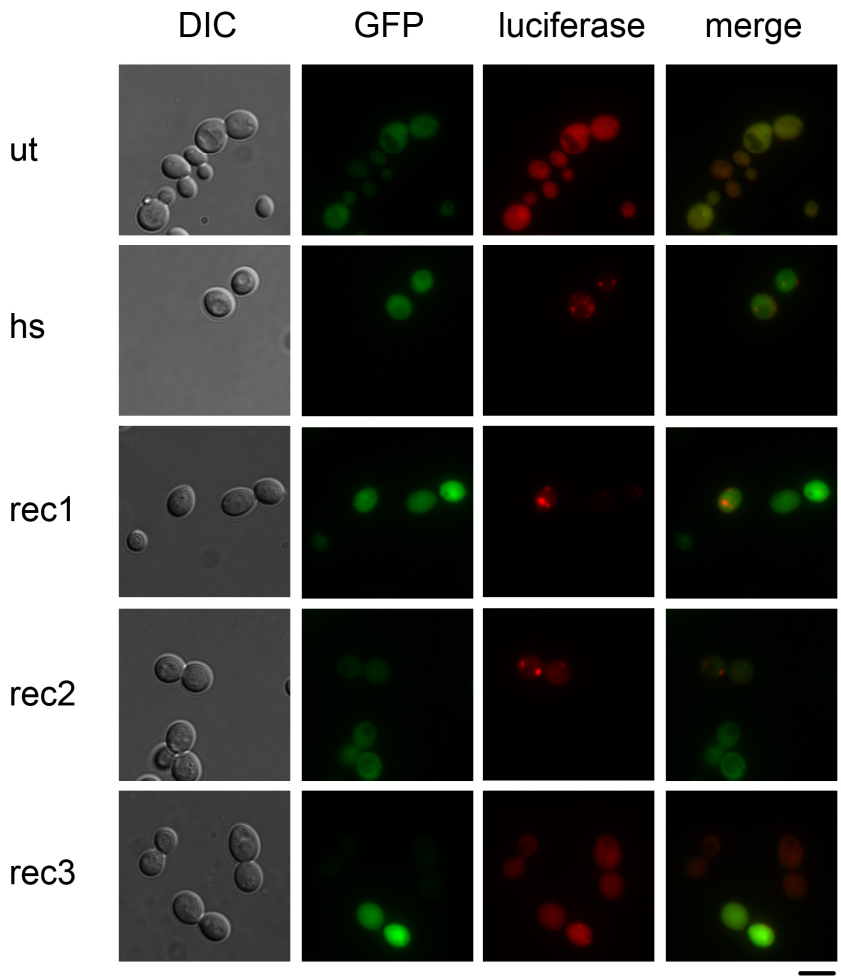

Fig. 23: No co-localization of yEGFP with aggregated luciferase was observed. *Δnac* cells containing the plasmids encoding for luciferase and yEGFP were grown in CM-URA-LEU medium supplemented with 50 µM copper sulphate for induction of luciferase expression. They were grown to an OD_{600} of 0.6, subjected to a sublethal heat shock (30 min at 37°C, 30 min at 45°C) and allowed to recover for 90 min. Samples were taken before heat shock (ut), after heat shock (hs) and in 30 min intervals during recovery (rec1 – rec3). Scale bar = 5 µM.

To analyse the localization of NAC during heat shock, *nacΔ* cells were transformed with plasmids encoding for yEGFP tagged NAC and mCherry tagged luciferase. Luciferase, as well as NAC, were both evenly distributed throughout the cytosol (Fig. 24, ut). Upon heat shock luciferase re-localized into aggregates whereas NAC stayed soluble (Fig. 24, hs). During the first 30 min of recovery, no change in the localization of luciferase and NAC occurred (Fig. 24, rec1). Resolubilization of luciferase aggregates started between 30 and 60 min after heat shock (Fig. 24, rec2). After 90 min, nearly all aggregates were resolubilised. However, a few cells containing one aggresome-like structure were still present.

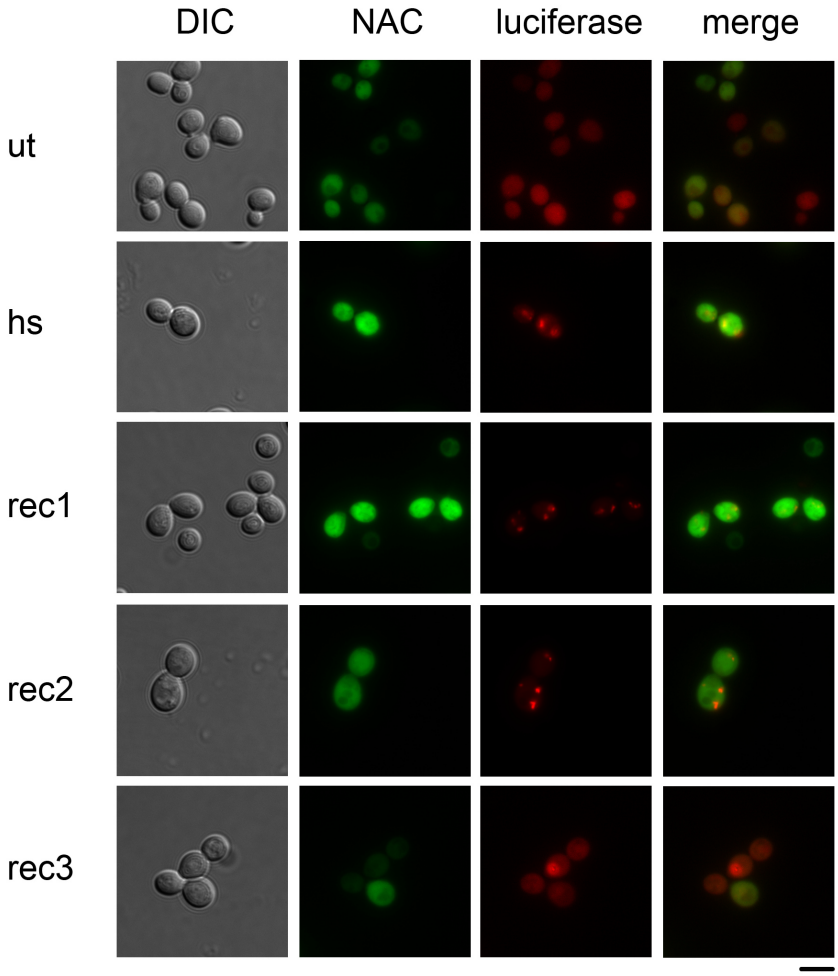

Fig. 24: NAC does not co-localize with aggregated luciferase. *Δnac* cells containing the plasmids encoding for luciferase and NAC were grown in CM-URA-LEU medium supplemented with 50 µM copper sulphate for induction of luciferase expression. They were grown to an OD_{600} of 0.6, subjected to a sublethal heat shock (30 min at 37°C, 30 min at 45°C) and allowed to recover for 90 min. Samples were taken before heat shock (ut), after heat shock (hs) and in 30 min intervals during recovery (rec1 – rec3). Scale bar = 5 µM.

In summary, no role of NAC during the aggregation of proteins in *S. cerevisiae* could be detected via the used biochemical methods and fluorescence microscopy. This result is contradictory to the observed NAC effects in *C. elegans* (Kirstein-Miles et al., 2013), suggesting functional differences between *C. elegans* and yeast NAC.

5.2 Effects of NAC on the aggregation of model substrates

In vivo, no direct interaction of yeast NAC with aggregates or the aggregation prone protein luciferase was detected. This might be due to the nature of the interaction. If it is very transient, it might not be detected with the methods applied so far. To investigate the possibility of such an interaction further, *in vitro* experiments with purified proteins were conducted. It was analysed, if NAC is able to interact with the model proteins citrate synthase and luciferase during inactivation, reactivation and aggregation. As positive control, the small heat shock protein Hsp26 was used (Haslbeck et al., 1999) and as negative control bovine serum albumin (BSA).

5.2.1 Purification of chaperones and stability tests

To conduct *in vitro* experiments, Hsp26, Hsp104, Ssa1, Ydj1, luciferase, NAC and different mutants thereof, were purified from *E. coli* cells. Citrate synthase was purchased from Sigma Aldrich.

First, the commonly used expression strain BL21* pRosetta was used for the expression of NAC. However, the two subunits Egd2 and Egd1 were not expressed in the same amount (data not shown). For *in vitro* experiments, the complex as such is needed which requires equal amounts of the two subunits. Thus, the expression strain was switched to MH1 pRosetta which is a protease deficient *E. coli* strain. When expressed in this strain, equal amounts of the two subunits were detectable in the gel (data not shown). For NAC purification, the lysate was first incubated with a Ni-IDA silica matrix using the His6-tag at the N-terminus of Egd2. Finally, ion exchange chromatography was performed. After purification 25.68 mg of highly pure NAC were gained (Fig. 25 A). To analyse NAC more closely, different variants thereof were purified:

1) NAC-RRK

To investigate if the ribosome binding ability of NAC might have an influence on the proposed chaperone activity, a ribosome binding deficient mutant was purified (Wegrzyn et al., 2006). The RRK motif in the ribosome binding site RRK-X_n-KK of Egd1 was substituted with three alanine residues. 22.4 mg of the mutant were purified and equal amounts of the two subunits were obtained (Fig. 25 B).

2) *C. elegans* NAC

Effects of NAC on protein aggregation processes were observed in the nematode *C. elegans* (Kirstein-Miles et al., 2013). To analyse this activity *in vitro*, *C. elegans* NAC was purified. The amount of NAC gained at the end of the purification process was not as high as for yeast

NAC with 2.8 mg, albeit sufficient for the *in vitro* experiments. It was quite pure and the subunits were present in equal amounts (Fig. 25 C).

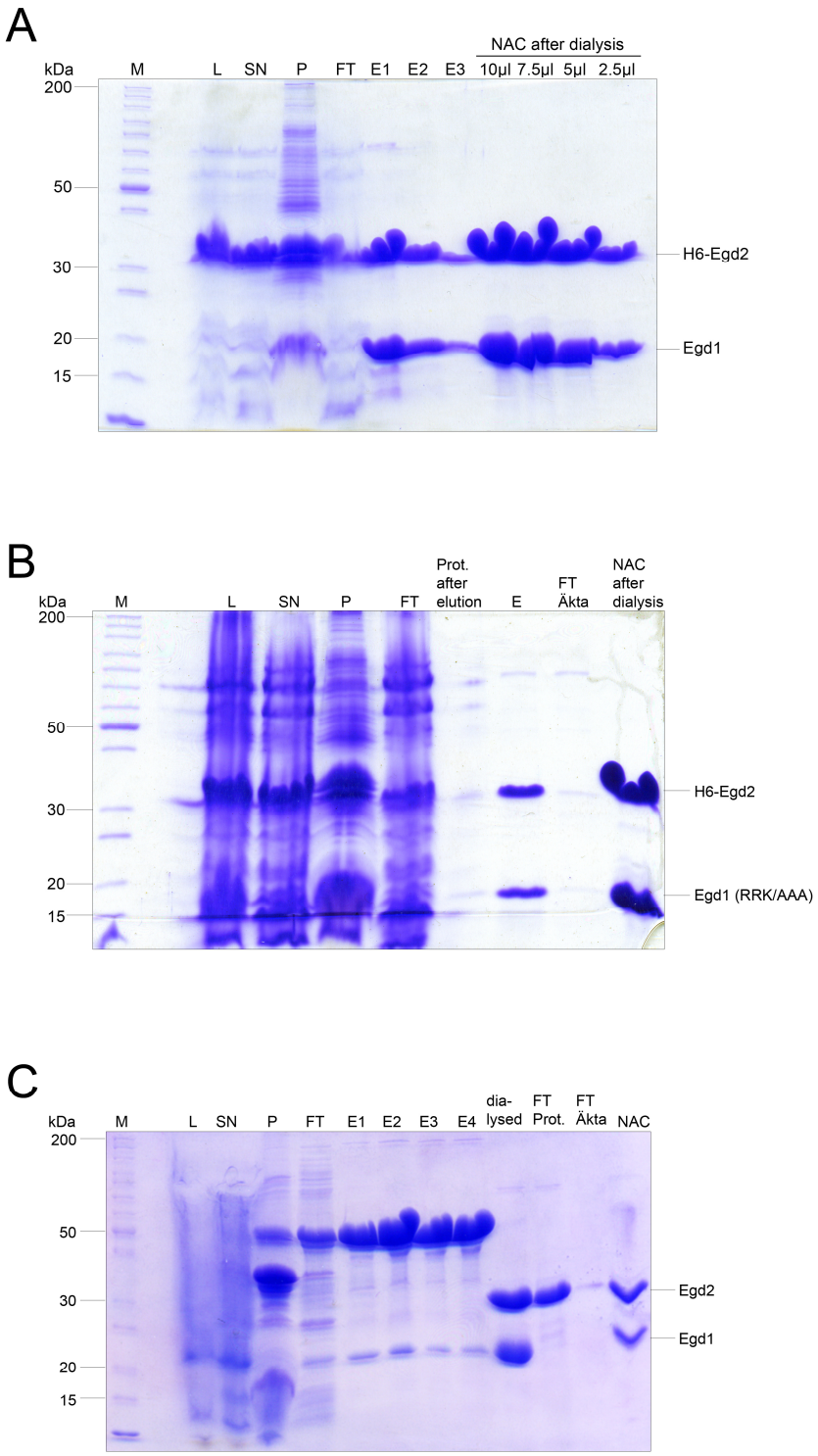

Fig. 25: Purification of the different NAC complexes. NAC complexes were purified as described in the respective sections in Material and Methods. L=lysate, SN=supernatant after the second centrifugation step, P=pellet after the second centrifugation step, FT=flowthrough of the NI-NDA protino matrix, Prot. after elution= sample of the NI-IDA protino matrix after elution, Ex=different elution fractions, FT Äkta= flowthrough of the ion exchange chromatography system (Äkta), NAC after dialysis=final protein solution which was frozen in aliquots. (A) NAC complex of *S. cerevisiae*; different amounts of the final protein were loaded. (B) NAC complex of *S. cerevisiae* containing the ribosome binding mutation RRK/AAA. (C) NAC complex of *C. elegans*. It was dialysed once before subjecting it to ion exchange chromatography to remove the His6-SUMO tag.

3) NACΔUBA

In Ott et al. (2015) our group showed, that the UBA domain of Egd2 plays a role for the *in vivo* chaperone activity of NAC. To analyse this possible effect *in vitro*, different mutants were purified.

First, a mutant lacking the UBA domain as well as the whole linker region connecting the UBA with the NAC domain was generated and purified out of MH1 pRosetta cells (Fig. 26 A). The mutant was purified in sufficient amounts (8.1 mg), high purity and with an equal ratio of the two subunits.

Egd2 consists of a total of 174 amino acids. The second mutant lacked the C-terminal UBA domain and a part of the linker region. It was cut at position 109, which is located at approximately the centre of the linker region. The cut in the linker region was determined by limited proteolysis using proteinase K (see 5.3.2). This complex was obtained in high purity, high amounts (20.4 mg) and with no imbalance in the subunit ratio (Fig. 26 B).

The third NAC mutant was constructed based on the one used for the *in vivo* studies in Ott et al. (2015). This mutant lacked the UBA domain and part of the linker region. It differs from the above described mutant by the cutting site in the linker region, which was shifted by one amino acid to position 108 (for more details see 5.3.4). The complex was, as the others, purified in sufficient quantity (14 mg), high purity and with both subunits present in equal amounts (Fig. 26 C).

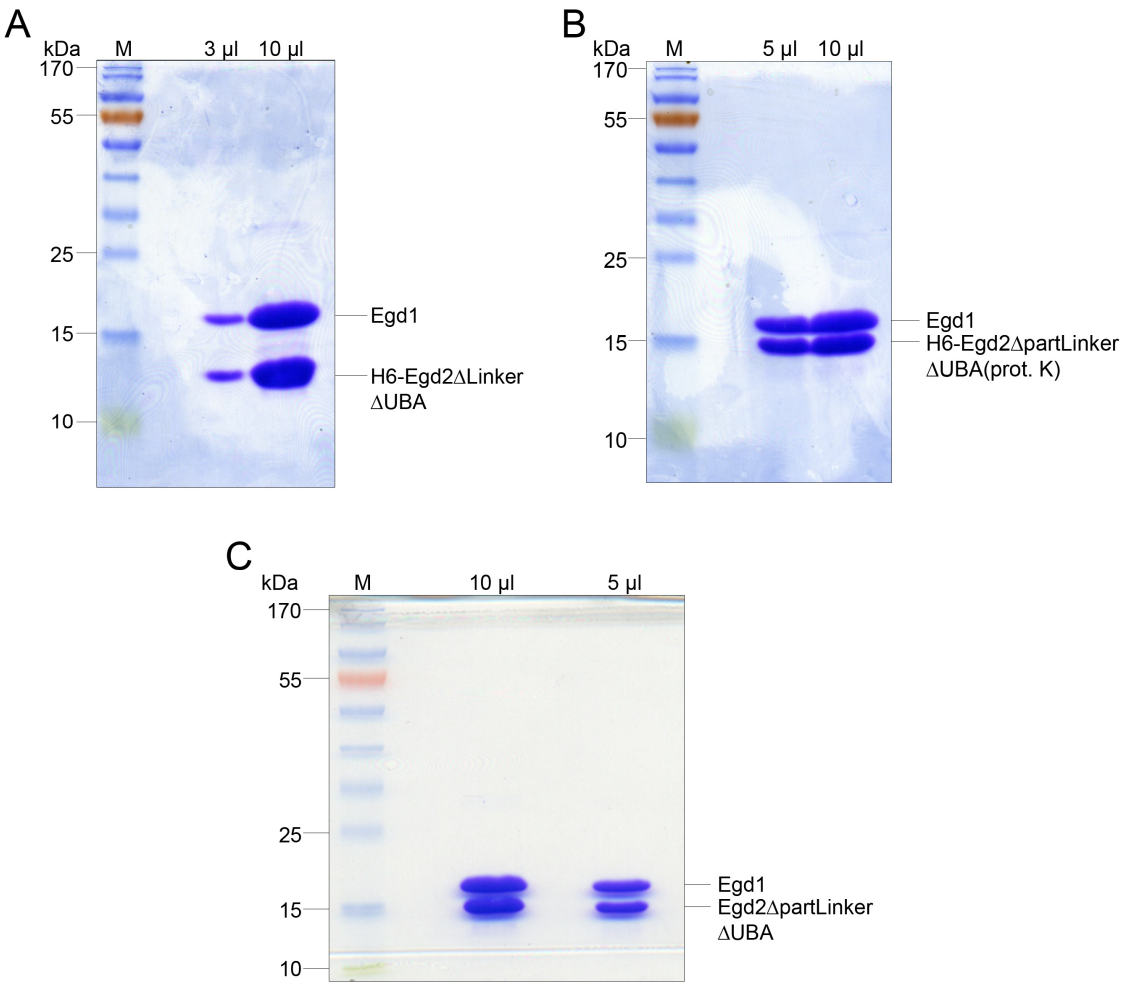

Fig. 26: Purification of the different NAC∆UBA mutants. NAC complexes were purified as described in the respective Material and Methods sections. (A) NAC version lacking the UBA domain and the complete linker region, (B) NAC version lacking the UBA domain and part of the linker region as determined by limited proteolysis of NAC with proteinase K, (C) NAC version lacking the UBA domain and part of the linker region as described in the *in vivo* version used in Ott et al. (2015).

As positive control for the *in vitro* experiments, Hsp26 was purified. It was described earlier to have a chaperone effect on different model proteins like citrate synthase and luciferase: Hsp26 slows down aggregation and inactivation when present during the aggregation process and speeds up disaggregation and reactivation. It also plays a role in aggregation processes *in vivo* where the *in vitro* effect could be reproduced (Haslbeck et al., 1999; Haslbeck et al., 2002; Cashikar et al., 2005). For purification, Hsp26 was expressed with an N-terminal His6-SUMO tag. Devising a strategy for the removal of the tag proved challenging, as Hsp26 forms higher oligomeric structures and, therefore, the access for the His6-Ulp1 protease to cleave the tag was restricted (Bentley et al., 1992; Haslbeck et al., 2005). The problem was solved by exchanging the dialysis buffer multiple times. During dialysis, His6-SUMO-Hsp26 was incubated with His6-Ulp1 protease. The repeated exchange of buffer seemed to have increased the dynamics of the exchange of subunits in the higher oligomers of Hsp26. Therefore, His6-Ulp1 was able to remove the tag from the majority of the Hsp26 molecules. Finally, Hsp26 could be purified in sufficient amounts (12 mg), albeit not to high purity (Fig. 27 B). Additionally, two stable degradation products of Hsp26 seem to be present after the purification process. Still, Hsp26 was able to fulfil its described functions without any restrictions (see 5.2.4; 5.2.5; 5.2.7).

For the reactivation experiments, Hsp104 was purified. It is the main disaggregase in yeast where it acts together with the Hsp70/40 system to resolubilise aggregated proteins (Parsell et al., 1994 b). When Hsp104 is absent, aggregates can no longer be resolved in an adequate time scale; the proteins are stuck in the aggregates (Cashikar et al., 2005). High amounts (53.9 mg) of relatively pure Hsp104 were gained after the purification procedure (Fig. 27 A).

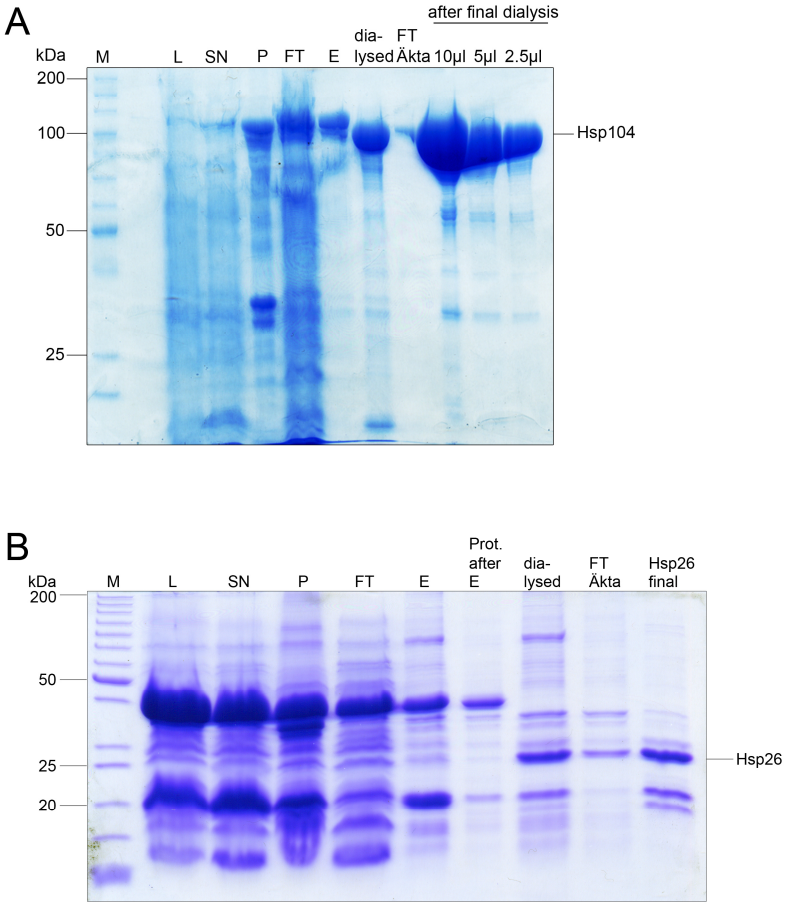

Fig. 27: Purification of Hsp104 and the small heat shock protein Hsp26. Proteins were purified as described in the respective Material and Methods sections. L=lysate, SN=supernatant after the second centrifugation step, P=pellet after the second centrifugation step, FT=flowthrough of the Ni-IDA protino matrix, E=combined elution fractions, Prot. after elution= sample of the Ni-IDA protino matrix after elution, dialysed=dialysis to remove the His6-SUMO tag, FT Äkta= flowthrough of the ion exchange chromatography system (Äkta), final=protein solution from which aliquots were frozen (A) Hsp104, different amounts of the final protein were loaded, (B) Hsp26.

To resolubilise aggregates, Hsp104 acts together with the Hsp70/40 system (Parsell et al., 1994 b). To achieve the best reactivation effects in the *in vitro* experiments, this system was purified in addition. Gaining sufficient amounts of the Hsp70 chaperone Ssa1 proved to be difficult. To increase the amount of purified protein, ATP was added to the buffers. As this interfered with the UV signal detection system of the Äkta purifier, every fraction collected during ion exchange chromatography was tested for Ssa1. In the end, Ssa1 was purified in decent amounts (3.5 mg) and with acceptable purity for the planned experiments (Fig. 28 A). The fractions were split into two pools, A and B, according to the different impurity patterns and amount of Ssa1 detectable in them.

To complement the system, the Hsp40 protein Ydj1 was purified. The protein was purified in high amounts (45.8 mg) with not much impurities being detectable (Fig. 28 B). The ion exchange chromatography fractions containing Ydj1 were again split into two pools according to the amount of Ydj1 and the detected impurities.

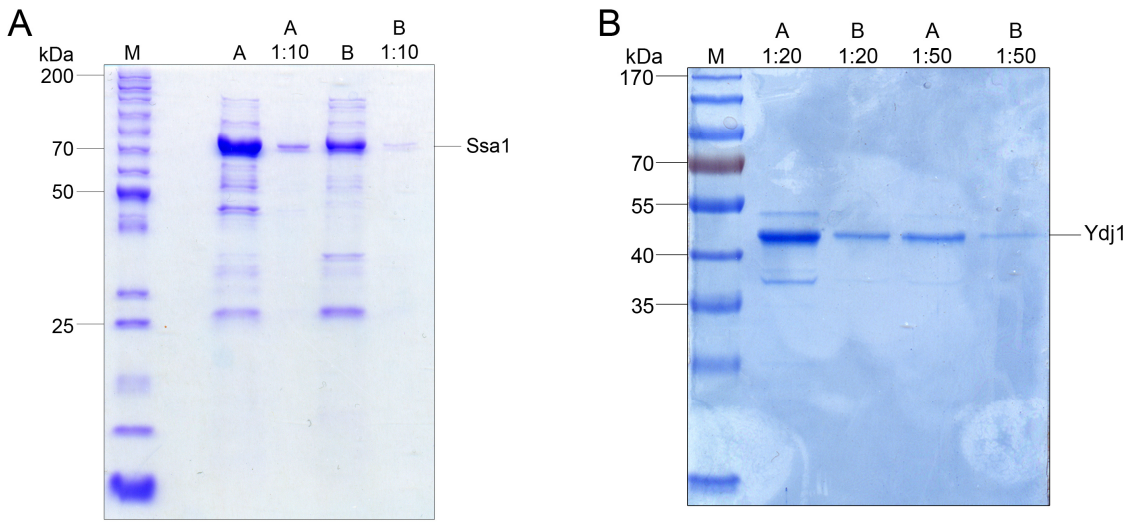

Fig. 28: Purification of the Hsp70 Ssa1 and the Hsp40 Ydj1. Proteins were purified as described in the respective Material and Methods sections. A and B in the figure legends correspond to two pools, where different fractions of the last purification step via ion exchange chromatography were united. (A) Ssa1, (B) Ydj1.

Luciferase and citrate synthase were chosen as aggregation prone model proteins. Whilst citrate synthase was bought from Sigma Aldrich, luciferase was purified out of *E. coli* cells. The plasmid was a kind gift of the lab of Bernd Bukau. To achieve sufficient amounts of luciferase with high purity, two purification steps on the Ni-IDA silica matrix were sufficient (Fig. 29). No additional purification step via ion exchange chromatography, which was inevitable for the other purified proteins, was needed. The elution fractions were again split into two pools according to the amount of purified luciferase detected in them. A contained 8.4 mg luciferase and B 2.72 mg.

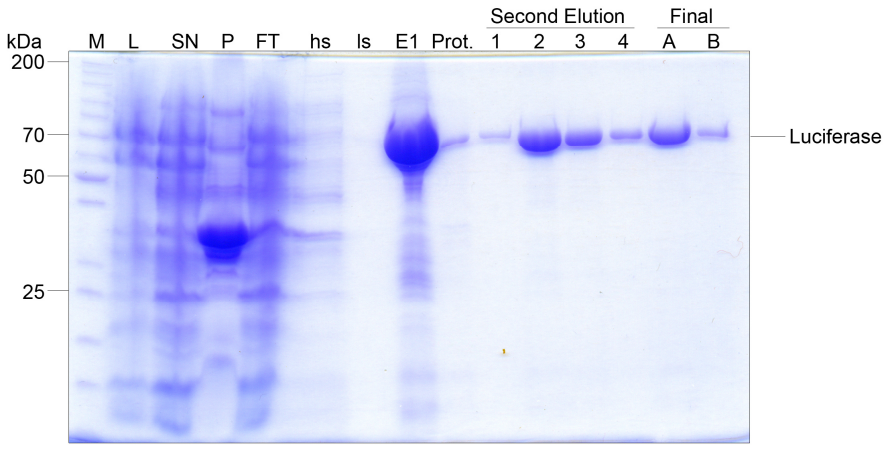

Fig. 29: Purification of the model protein luciferase. Luciferase was purified as described in the respective Material and Methods section. L=lysate, SN=supernatant after the second centrifugation step, P=pellet after the second centrifugation step, FT=flowthrough of the Ni-IDA protino matrix, hs=last washing step with high salt buffer, ls= last washing step with low salt buffer, E1=first elution fraction, Prot.= sample of the Ni-IDA protino matrix after elution, Second Elution=fractions of the first elution were pooled, incubated with Ni-IDA protino matrix for a second time and subjected to subsequent elution, Final=protein solutions from which aliquots were frozen; the final protein solutions were divided into two pools, A and B according to the amount of detectable luciferase.

To ensure, that no artefacts would arise in the *in vitro* experiments due to instability of the purified proteins, the stability of them was tested over time. They were either incubated for 2 h on ice or at 25 °C. Samples were taken after 10 min, 30 min, 1 h and 2 h. Citrate synthase was included in this experiment as well. As shown in Fig. 30, all proteins tested were stable over time. No degradation products appeared and the quantity of each protein remained the same. Therefore, the proteins could be used without restrictions for all experiments.

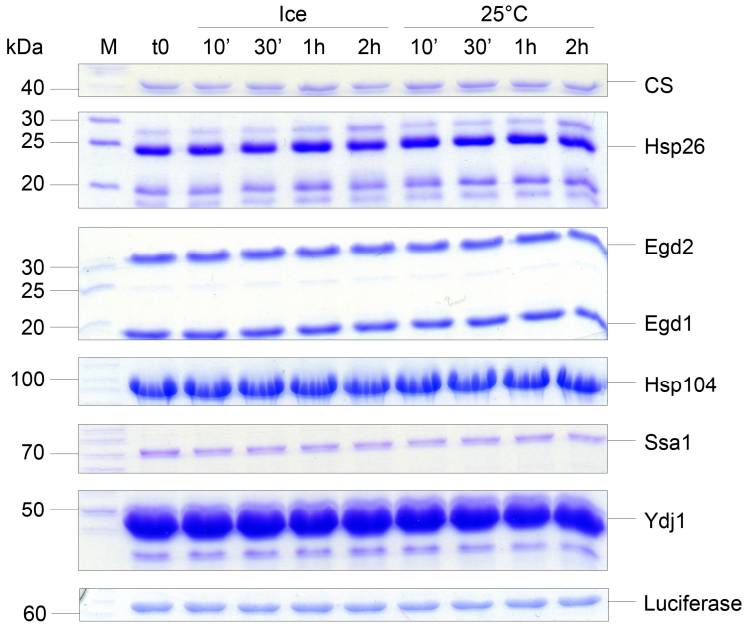

Fig. 30: Purified proteins are stable over time. Proteins were either incubated on ice or at 25°C for a time period of 2 h. Samples were taken at indicated time points, run on a 12% SDS gel and stained with Coomassie brilliant blue.

5.2.2 NAC is mainly present as a dimer

NAC is described to form a heterodimeric complex consisting of Egd2 (α-NAC) and Egd1/Btt1 (β/β'-NAC) (Wiedmann et al., 1994; Reimann et al., 1999; del Alamo et al., 2011). Dimerization is achieved by the NAC domains of Egd2 and Egd1/Btt1, which form a six-stranded flattened β-barrel-like structure (Spreter et al., 2005; Liu et al., 2010 b; Wang et al., 2010). Functions for individual NAC subunits have been described. Amongst others, roles for single α- and β-NAC subunits in transcription (Zheng et al., 1997, Zheng et al., 1990; Parthun et al., 1992; Hu and Ronne, 1994; Yotov et al., 1996; Moreau et al., 1998; Yotov et al., 1998; Munz et al., 1999; Akhouayn et al., 2005; Freire 2005) and apoptosis (Thiede et al., 2001; Bloss et al., 2003; Stilo et al., 2003) as well as a role for α-NAC in immunological processes (Baghdoyan et al., 2000; Goatley et al., 2002; Al-Shanti et al., 2004; Li et al., 2005; Arsenovic et al., 2012; Hradetzky et al., 2013; Zeng et al., 2014; Li et al., 2015) have been proposed. However, it seems that single subunits are only present in cells if the balance of α- and β-NAC is disrupted (Beatrix et al., 2000; Franke et al., 2001). Hence, the significance of an *in*

vivo role of single NAC subunits is still unclear. Higher oligomeric structures of NAC have not been described so far. Nevertheless it may be possible, that NAC is able to form higher oligomeric structures as described for Hsp26 (Haslbeck et al., 2002). To analyse if purified NAC mainly forms dimers or if single subunits or higher molecular weight structures exist as well, analytical ultracentrifugation was performed. This technique allows analysing the size-distribution of biological macromolecules in solution (Signer and Gross, 1934; Svedberg and Pederson, 1940; Bridgman, 1942; Baldwin and Williams, 1950; Vinograd and Bruner, 1966; Scholte, 1968; van Holde and Weischet, 1978; Stafford, 1992). When analysing purified NAC, the main peak of the spectrum correlated to a molecular weight of 46 kDa (Fig. 31). This mass corresponds to roughly the size of a heterodimer. No peaks corresponding to possible single subunits were detected. The presence of homodimers cannot be excluded as their mass approximately corresponds to the one observed for heterodimers. Two smaller peaks at 117 kDa and 220 kDa, respectively, were observed, which correlated to higher molecular weight states of NAC. The peak at 117 kDa might correspond to a dimer consisting of two heterodimeric complexes and the peak at 220 kDa might correspond to a tetramer of heterodimers.

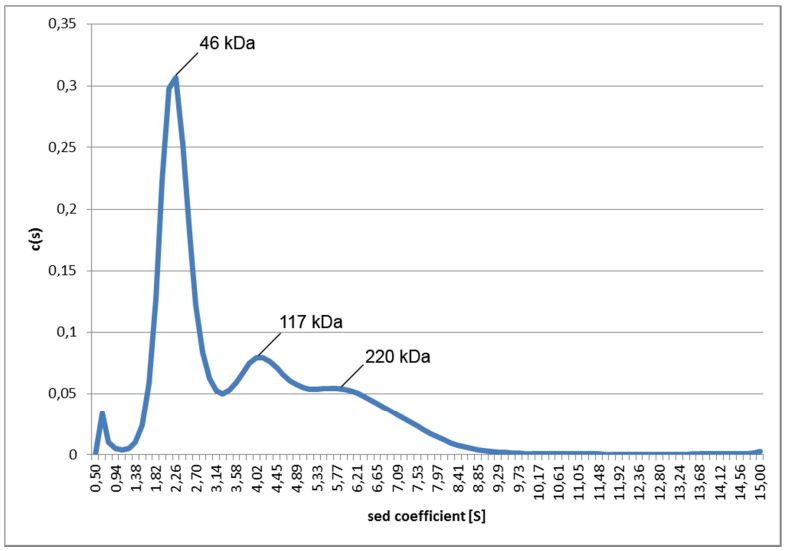

Fig. 31: Analytical ultracentrifugation of the purified NAC complex of *S. cerevisiae*. The purified NAC complex (0.87 mg/ml) was subjected to analytical ultracentrifugation. c(s) = differential sedimentation coefficient distribution where corrections for diffusion were made (Schuck, 2000). [S] = sedimentation coefficient.

5.2.3 Secondary structure analysis of NAC by circular dichroism

So far, only the UBA and the dimerization domain of the NAC complex could be crystallized (Spreter et al., 2005; Liu et al., 2010 b; Wang et al., 2010). Therefore it is difficult to monitor structural changes potentially initiated by mutations. To be able to detect such differences, circular dichroism spectroscopy of NAC was performed. The gained spectra were analysed using Dichroweb (Whitmore and Wallace, 2004; Whitmore and Wallace, 2008). One

parameter of the quality of a spectrum is the NRMSD value (Wallace et al., 2003). The value needs to be below 0.1 for a spectrum to be judged of good quality. However, this is just a necessary but not a sufficient condition for assessing a good quality spectrum (Brahms and Brahms, 1980). The parameters for the calculation of the NRMSD value were chosen as in Mao et al. (1982).

The spectrum for NAC was calculated using CDSSTR with SMP180 as reference dataset (Compton and Johnson, 1986; Manavalan and Johnson, 1987; Sreerama and Woody, 2000; Jones, 2008; Abdul-Gader et al., 2011). The NRMSD value of this spectrum was 0.000, so the spectrum was judged as being of good quality. Based on this spectrum (Fig. 32), Dichroweb predicted 10.8 helix segments throughout the whole NAC complex with an average length of 17.729 amino acids and 13.6 strand segments with an average length of 4.945 amino acids. The heterodimeric complex of NAC seems to have an excess of beta strands in comparison to alpha helices. One explanation for this might be the NAC domain, which consists mainly of β-sheets in both subunits.

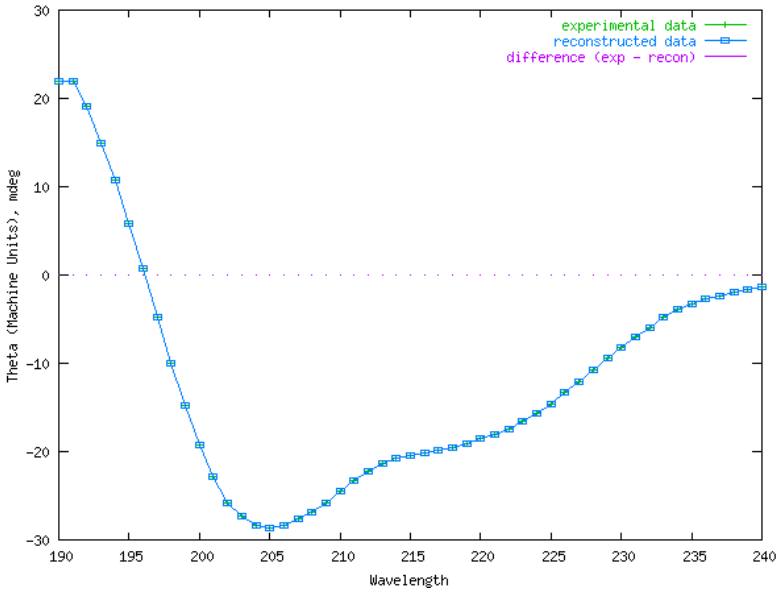

Fig. 32: Circular dichroism measurement of the purified NAC complex of *S. cerevisiae*. The purified NAC complex was subjected to circular dichroism measurement at 20°C. Analysis was performed using Dichroweb (Whitmore and Wallace, 2004; Whitmore and Wallace, 2008). NRMSD value = 0.000. Green=experimental data, blue=reconstructed data.

5.2.4 NAC binds transiently to model proteins

NAC was previously shown to act as a chaperone on different levels, to associate with artificial protein aggregates and to speed up disaggregation of heat shock or ageing dependent aggregates in *C. elegans* (Bukau et al., 2000; Hartl and Hayer-Hartl, 2002; Rospert et al., 2002; Wegrzyn and Deuerling, 2005; Olzscha et al., 2011; Kirstein-Miles et al., 2013). To investigate if NAC is able to bind to aggregation prone proteins, size exclusion

chromatography was performed. Citrate synthase and luciferase were chosen as model proteins. The model proteins were analysed alone or in combination with NAC at 25°C or 43°C, thereby testing for a possible interaction at heat shock temperatures. They were pre-incubated at the respective temperature and then subjected to size exclusion chromatography. The temperature of the column was adjusted accordingly. To verify the setup, Hsp26 was used as a control as it interacts with these model substrates (Haslbeck et al., 1999; Haslbeck et al., 2002). An interaction of the chaperones with the model substrates would result in a shift of the main peak of the spectrum towards higher molecular weight fractions upon heat shock. The peak height is a measure of the intrinsic fluorescence but does not give any information about the interaction of two proteins.

First, citrate synthase and Hsp26 were subjected to size exclusion chromatography. At 25°C, citrate synthase eluted in fractions corresponding to a molecular weight of 35 – 40 kDa (Fig. 33 A, orange), which is surprising concerning its theoretical molecular weight of approximately 52 kDa. Hsp26 eluted mainly at fractions corresponding to ~150 kDa (Fig. 33 A, grey). Small parts of the protein either eluted at even higher molecular weights (~670 kDa) or at fractions possibly representing the dimeric structure (~35 kDa). This is consistent with the assumption, that this small heat shock protein is mainly present in higher oligomeric structures at physiological temperatures. When incubating citrate synthase and Hsp26 together at 25°C, two peaks appeared (Fig. 33 A, blue). One, corresponding to Hsp26, was slightly shifted to lower molecular weights. The other peak appeared at approximately 44 kDa which is slightly shifted to higher molecular weights when compared to the native citrate synthase peak. This might indicate a transient interaction of Hsp26 and citrate synthase at 25°C. At 43°C, citrate synthase started to aggregated. One half eluted at fractions corresponding to ~670 kDa (Fig. 33 B, orange). The other half stayed soluble, but instead of one peak, two peaks appeared at a molecular weight of around 44kDa. The equilibrium of Hsp26 also shifted (Fig. 33 B, grey). One half dissociated into potentially dimeric structures eluting at about 35 kDa. The other half formed high molecular weight structures eluting at about 670 kDa. When incubating Hsp26 and citrate synthase together at 43°C, the main peak of the spectrum eluted at ~670 kDa, possibly representing the formation of large complexes or aggregates (Fig. 33 B, blue). Two small peaks were detected at ~44 kDa and ~35 kDa. They may represent still soluble forms of citrate synthase and Hsp26. The shift of the main peak of the spectrum of citrate synthase and Hsp26 incubated together at 43°C (Fig. 33 B, blue) to higher molecular weights when compared to the main peak at 25°C (Fig. 33 A, blue) indicates a direct interaction between Hsp26 and citrate synthase.

Next, the interaction between citrate synthase and NAC was analysed. Citrate synthase eluted again at fractions corresponding to a molecular weight of ~35 – 40 kDa when incubated at 25°C (Fig. 33 C, orange). NAC eluted at about 45 kDa (Fig. 33 C, grey), which

roughly corresponds to the size of the dimer measured by analytical ultracentrifugation. The main peak of the spectrum when incubating NAC and citrate synthase together at 25° was located at about 45 kDa as well (Fig. 33 C, blue), possibly representing both, NAC and citrate synthase. A second much smaller peak appeared at ~670 kDa. This could already represent some large complexes or even aggregates. At 43°C, one half of citrate synthase possibly formed aggregates and eluted at ~670 kDa (Fig. 33 D, orange). The other half formed two peaks at about 35 and 44 kDa, possibly representing still soluble citrate synthase. NAC stayed soluble at 43°C (Fig. 33 D, grey). The peak maximum shifted only slightly to a lower molecular weight of about 40 kDa. A small peak appeared at ~158 kDa maybe indicating the formation of higher oligomers of a minority of NAC. An even smaller peak appeared at ~670 kDa. When incubating NAC and citrate synthase together, the main peak of the spectrum eluted at ~42 kDa (Fig. 33 D, blue). A smaller peak was again detectable at ~670 kDa. Comparing the summit of the main peaks of the spectra generated by a combined exposition of NAC and citrate synthase at 43°C (Fig. 33 D, blue) and 25°C (Fig. 33 C, blue) revealed a slight shift to lower molecular weights. This might indicate a potential transient interaction of the two proteins upon heat shock.

To examine, if this transient interaction was specific for citrate synthase or occurred also with other model proteins, the experiment was performed again using luciferase. NAC and Hsp26 were again analysed together with luciferase at 25°C or 43°C. In Fig. 34 A the spectrum of luciferase and Hsp26 incubated together at 25°C is depicted. Luciferase alone eluted at fractions corresponding to a molecular weight of about 30 – 44 kDa (Fig. 34 A, orange). This is surprising as luciferase has a theoretical molecular weight of ~63 kDa. A small peak at ~670 kDa was already detectable. As luciferase is a very labile protein, this peak might already represent aggregated species of luciferase. Hsp26 was present in a mixture of species (Fig. 34 A, grey). The main peak eluted at fractions corresponding to ~150 kDa, possibly representing higher oligomers. A smaller peak appeared at ~670 kDa, possibly indicating large complexes. The third peak appeared at about ~35 kDa, which might account for dimeric structures of Hsp26. The main peak of the spectrum of the combined incubation of luciferase and Hsp26 at 25°C eluted at about 140 kDa (Fig. 33 A, blue). This was slightly shifted to the peak summit of Hsp26 incubated alone. Another smaller peak appeared at ~670 kDa like for the two proteins alone. Two further peaks appeared at lower molecular weights, possibly representing luciferase and dimeric Hsp26. Incubation of luciferase at 43°C led to the aggregation of the protein (Fig. 34 B, orange). At 43°C, one half of Hsp26 was present in very high oligomeric structures and eluted at ~670 kDa, whereas the other half eluted at fractions corresponding to the dimeric structures of the protein (Fig. 34 B, grey). The main peak of the spectrum of the combined incubation of luciferase and Hsp26 eluted at ~670 kDa (Fig. 34 B, blue), indicating the formation of large complexes. A smaller peak was

detectable at ~35 kDa, possibly representing still soluble Hsp26. Comparing the main peaks of the spectra of combined incubation of Hsp26 and luciferase at 25°C (Fig. 34 A, blue) and 43°C (Fig. 34 B, blue) reveals a shift of the main peak of the spectrum towards high molecular weights. This indicates a direct interaction between Hsp26 and luciferase.

Next, a possible interaction of NAC with luciferase was investigated. At 25°C luciferase eluted again at 30 – 44 kDa (Fig. 34 C, orange). A small additional peak eluted at ~670 kDa. NAC eluted at about 42 kDa with a very small additional peak at ~670 kDa (Fig. 34 C, grey). The main peak of the combined incubation of luciferase and NAC eluted at fractions corresponding to about 35 kDa (Fig. 34 C, blue). Another smaller peak appeared at ~670 kDa. When incubating luciferase at 43°C, aggregation took place (Fig. 34 D, orange). The main peak of NAC shifted slightly towards 40 kDa (Fig. 34 D, grey). The very small additional peak at ~670 kDa persisted. In addition, a small peak at around 158 kDa appeared which might indicate the formation of higher oligomeric structures of a minority of NAC. The main peak of the spectrum of NAC and luciferase incubated together shifted slightly towards 43 kDa (Fig. 34 D, blue) in comparison to the observed peak at 25°C (Fig. 34 C, blue). This might indicate a transient interaction of NAC with luciferase under the tested condition. Two very small additional peaks were observable: One at ~670 kDA and one at ~158 kDa.

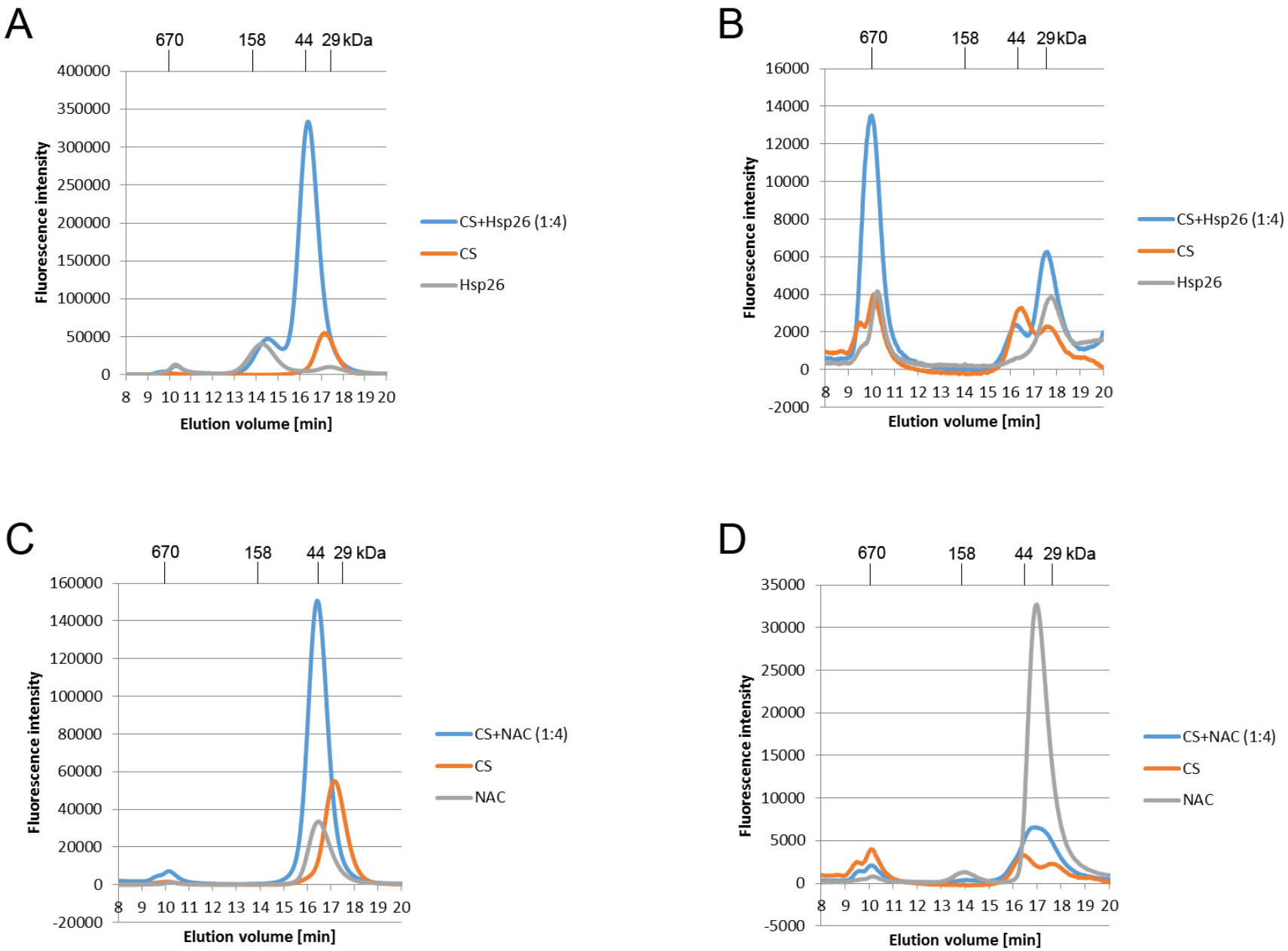

Fig. 33: Analysis of the interaction of NAC and citrate synthase (CS) via size exclusion chromatography. Purified NAC (9.6 M), Hsp26 (9.6µM) and CS (2.4 µM) were subjected to gel filtration analysis to check for an interaction of Hsp26 and NAC with the model protein CS. Proteins were pre-incubated at the respective temperature and the column was also adjusted to the used temperature during the experiment. (A) Hsp26 and CS incubated together at 25°C. (B) Hsp26 and CS incubated together at 43°C. (C) NAC and CS incubated together at 25°C. (D) NAC and CS incubated together at 43°C. Molecular weight controls are indicated.

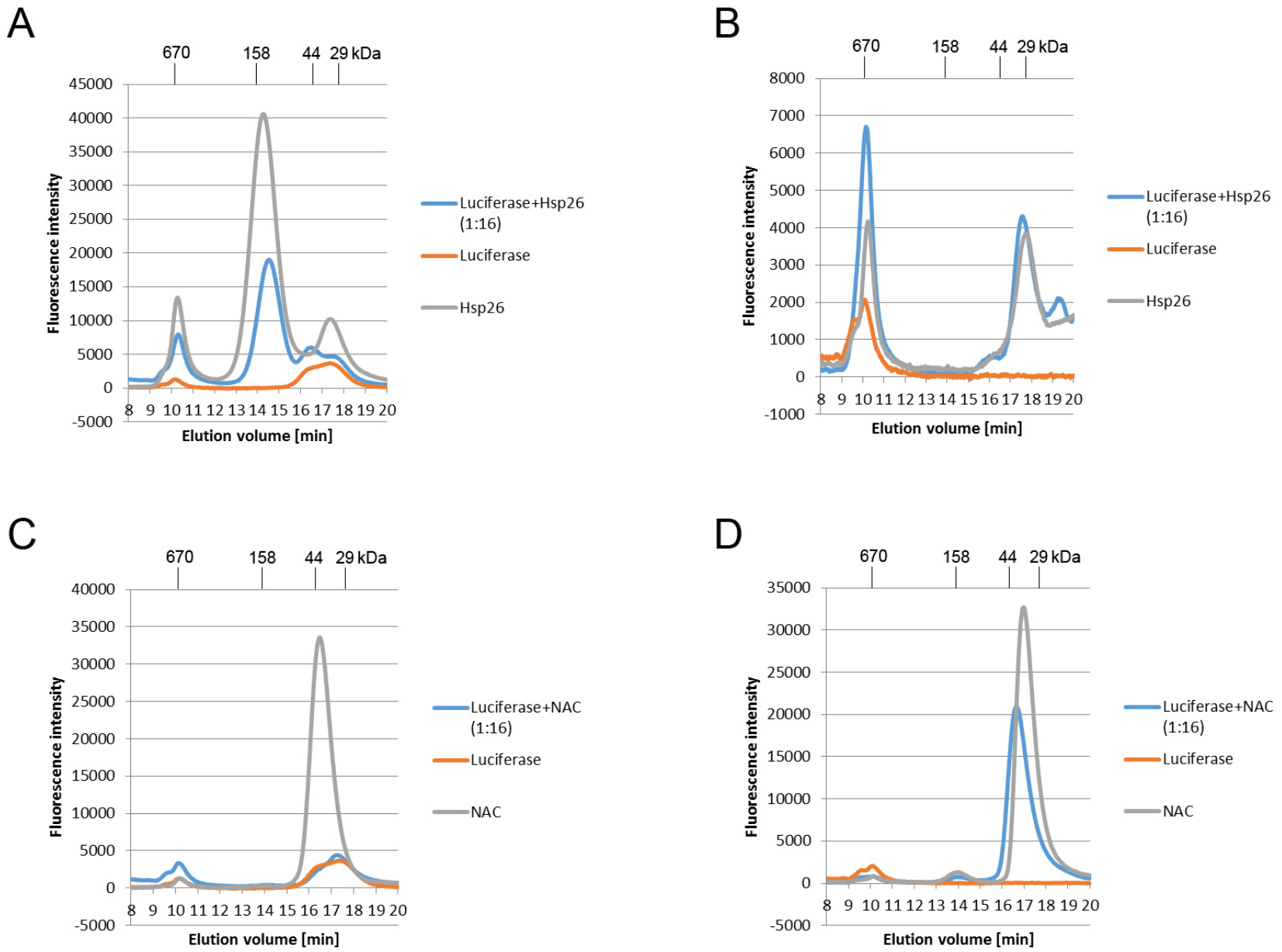

Fig. 34: Analysis of the interaction of NAC and luciferase via size exclusion chromatography. Purified NAC (9.6 µM), Hsp26 (9.6 µM) and luciferase (0.6 µM) were subjected to gel filtration analysis to check for an interaction of Hsp26 and NAC with the model protein luciferase. Proteins were pre-incubated at the respective temperature and the column was also adjusted to the used temperature during the experiment. (A) Hsp26 and luciferase were incubated together at 25°C. (B) Hsp26 and luciferase were incubated together at 43°C. (C) NAC and luciferase were incubated together at 25°C. (D) NAC and luciferase were incubated together at 43°C. Molecular weight controls are indicated.

5.2.5 Analysis of NAC effects on the inactivation of citrate synthase

As NAC seems to transiently interact with citrate synthase, a possible influence of it on the inactivation kinetics of citrate synthase was investigated. Again, Hsp26 was used as control as it is known to positively influence the inactivation kinetics of citrate synthase (Haslbeck et al., 1999). Inactivation of citrate synthase was performed by incubating it at 43°C, either alone or with an excess of NAC or Hsp26. Samples were taken at fixed time points and the activity of citrate synthase was measured. As described before (Haslbeck et al., 1999), a 4-fold excess of Hsp26 considerably slowed down the inactivation of citrate synthase (Fig. 35 A). Interestingly, the negative control bovine serum albumin (BSA) also showed a very slight positive effect. When citrate synthase was incubated with a 4-fold excess of NAC, inactivation was not slowed down to the same extent as observed with Hsp26 (Fig. 35 B). Increasing the amount of NAC to a 6-fold excess over citrate synthase did not result in a strong improvement (Fig. 35 C). Only if the excess of NAC was increased to 8-fold, inactivation of citrate synthase was visibly affected (Fig. 35 D). However, this effect was clearly not as prominent as the one observed with Hsp26.

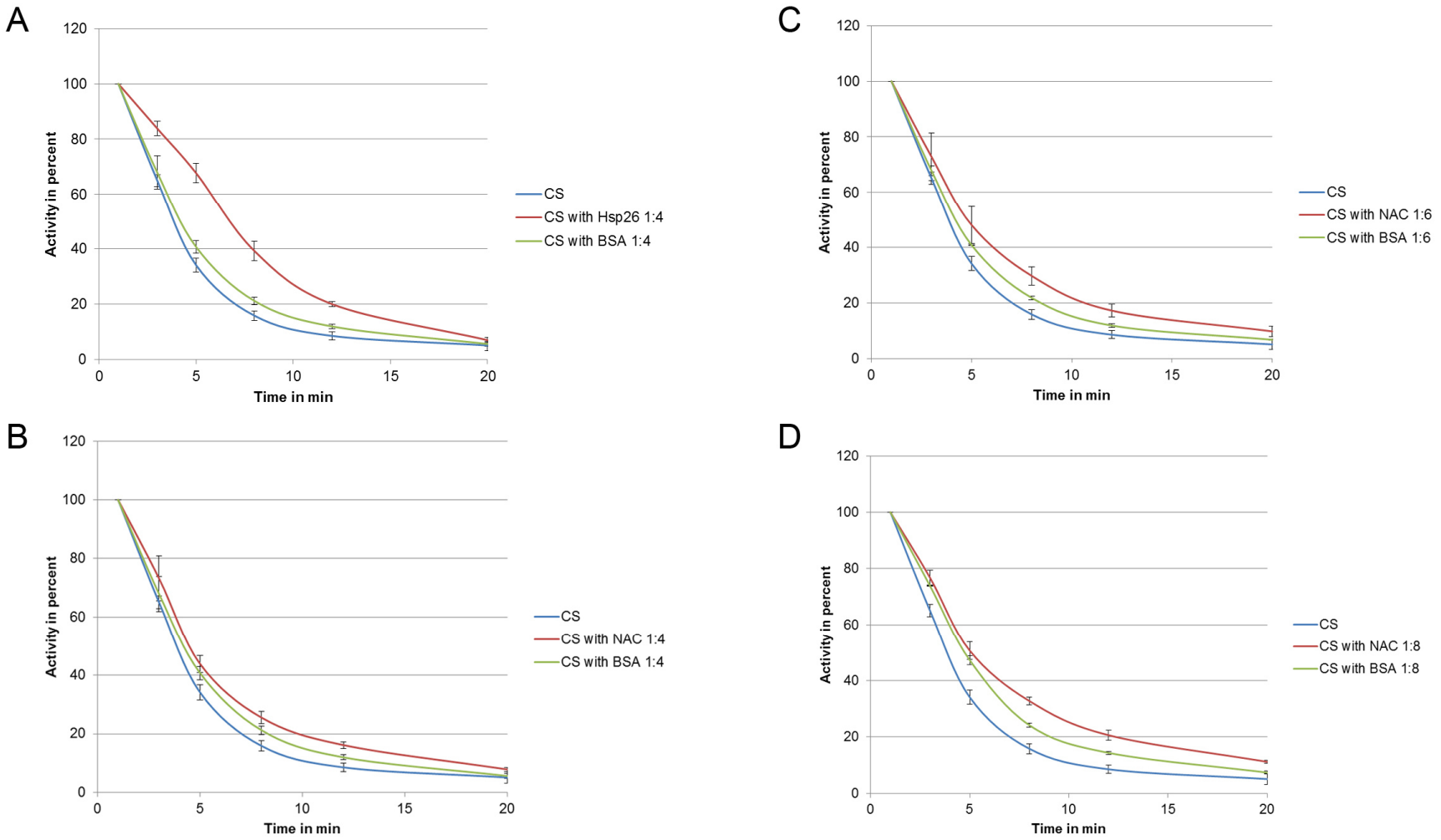

Fig. 35: Inactivation of citrate synthase (CS) in the presence of Hsp26 or NAC. Purified CS (1.2 µM) was inactivated thermally at 43°C alone or in the presence of Hsp26 or different concentrations of NAC. Samples were taken at indicated time points. Mean values of 4 independent experiments were taken and standard deviations at the different time points are indicated. BSA was used as negative control. (A) CS with a 4-fold excess of Hsp26. (B) CS with a 4-fold excess of NAC. (C) CS with a 6-fold excess of NAC. (D) CS with an 8-fold excess of NAC.

5.2.6 Analysis of NAC effects on the reactivation of luciferase

After the observed slightly positive effect on citrate synthase inactivation and considering the observation that NAC transiently interacts with luciferase upon heat shock it was tested, if NAC might have a positive effect on the reactivation process of luciferase. Luciferase was denatured chemically in 8 M guanidinium hydrochloride and then diluted into buffer. The buffer contained either no chaperones or different mixtures of them. Background fluorescence levels were determined with buffer and buffer containing NAC only (Fig. 36 A and B, purple). Dilution of luciferase into buffer led to a slight spontaneous reactivation (Fig. 36 A and B, blue). Addition of the Hsp70/40 system did not improve the reactivation (Fig. 36 A, green). This is contradictory to what is known about the function of the Hsp70/40 system. It might be that the formed aggregates were too tight to allow the resolubilization of the majority of luciferase. An improvement over the spontaneous reactivation would not be possible in that case. No improvement in luciferase activity was observed when Hsp104 was present in the buffer (Fig. 36 A, red). Incubation of luciferase with the whole reactivation machinery (Hsp104 and Hsp70/40) only slightly improved reactivation (Fig. 36 A, yellow), supporting an advanced aggregation of luciferase.

When NAC was present in addition to the Hsp70/40 system, a slight improvement in the reactivation of luciferase was observed (Fig. 36 B, green). This was not the case, when NAC was added to the disaggregase Hsp104 (Fig. 36 B, red). Addition of NAC to the whole reactivation machinery (Hsp104 and Hsp70/40) clearly augmented reactivation of luciferase (Fig. 36 B, yellow). Interestingly, reactivation of luciferase was already increased when only NAC was present in addition (Fig. 36 B, violet).

Taken together, a positive effect of NAC on the reactivation of luciferase was observed, especially when the Hsp70/40 system was present in addition. This might suggest an interaction of these proteins during the process of reactivation.

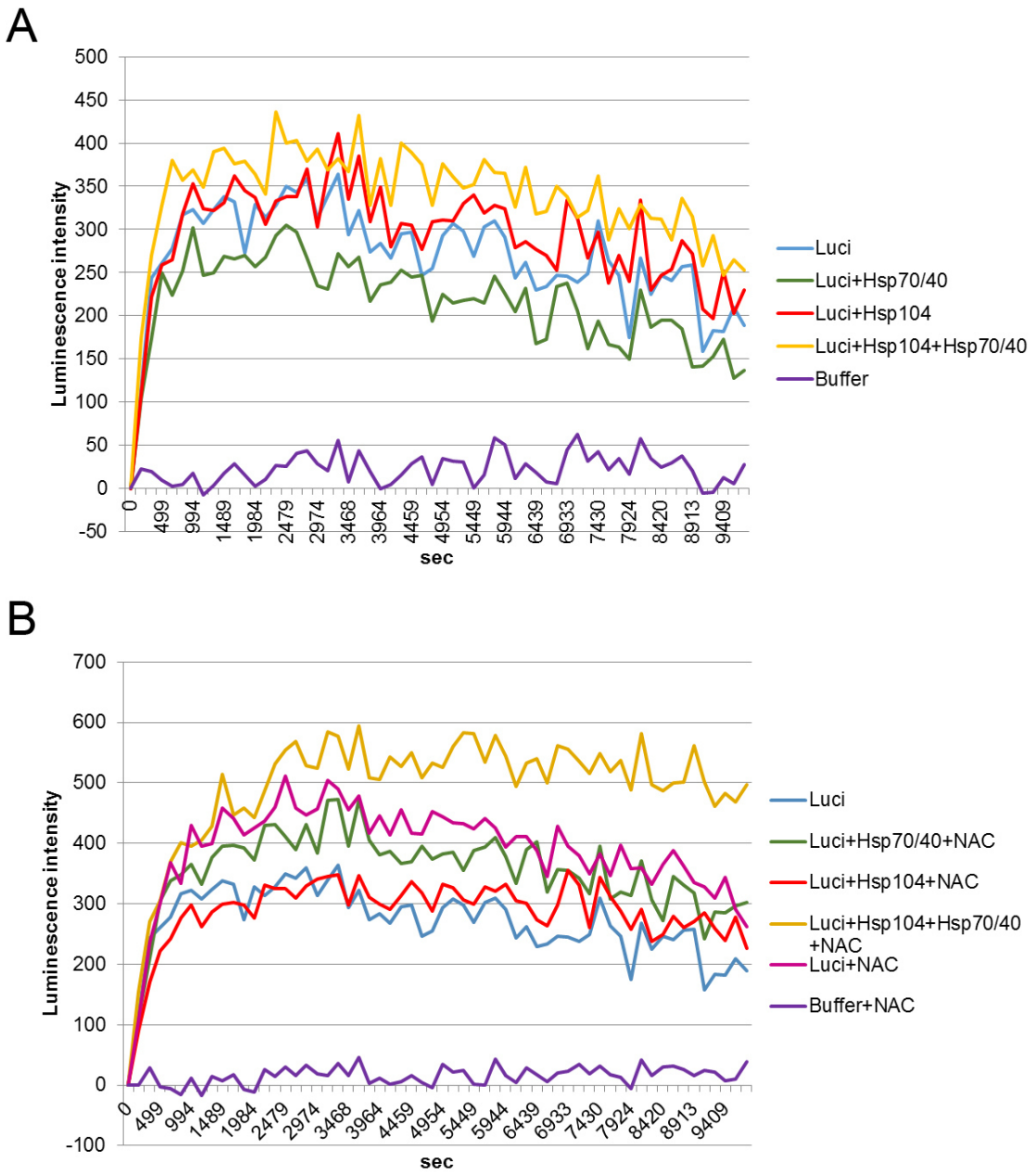

Fig. 36: Reactivation of luciferase in the presence of NAC. Purified luciferase (184 nM) was inactivated chemically in 8 M guanidinium hydrochloride. It was diluted into buffer containing either nothing or different combinations of 16-fold more NAC, 16-fold more Hsp104, 16-fold more Ssa1 (Hsp70) and 32-fold more Ydj1 (Hsp40). Mean values of triplicates are depicted.

5.2.7 NAC enhances aggregation of the model proteins

NAC had an effect on the inactivation of citrate synthase and the reactivation of luciferase. This effect might be due to an influence on the aggregation process. To study this in more detail, the aggregation process of the two model proteins was analysed in the presence of NAC using light scattering as readout of aggregation. A cuvette containing either citrate synthase or luciferase with or without additional proteins was heated to 43°C which allowed to directly monitor the aggregation process photometrically. When citrate synthase alone was subjected to heat shock, aggregation occurred (Fig. 37 A, blue) which was completely

prevented by Hsp26 (Fig. 37 A, red). Addition of NAC had the opposite effect. Instead of reducing aggregation, the levels were even enhanced. This was observed for all tested concentrations of NAC (Fig. 37 A, green, purple, pink and orange; 2-fold to 8-fold excess). When a 4-fold excess of both NAC and Hsp26 was present during the measurement, aggregation was blocked again (Fig. 37 A, grey).

To verify this unexpected behaviour of NAC, the model substrate luciferase was tested as well. As citrate synthase, luciferase aggregated upon heat shock (Fig. 37 B, blue). In presence of NAC the same effect as observed for citrate synthase was detected. At all concentrations of NAC tested (from 0.5-fold to 8-fold), aggregation of luciferase was increased (Fig. 37 B, red, green, purple, pink and orange). Further addition of Hsp26 blocked aggregation (Fig. 37 B, grey).

To test for an involvement of the ribosome binding motif in enhancement of aggregation, the ribosome binding deficient mutant AAA-X_n-KK was used (Wegrzyn et al., 2006). As shown in Fig. 37 C (red) this motif is not involved in aggregation, the effect was the same as for native NAC. As described in Ott et al. (2015), Egd2 alone had a slightly positive effect on aggregation prevention in *nacΔssbΔ* cells. However, Egd2 could not prevent luciferase aggregation *in vitro* (Fig. 37 C, green). It enhanced aggregation levels like native NAC. Finally, both native *C. elegans* NAC and a ribosome binding deficient mutant thereof enhanced the aggregation level of luciferase (Fig. 37 C, purple and pink), even so *C. elegans* NAC was shown to have a positive effect on aggregation *in vivo* (Kirstein-Miles et al., 2013).

Subjecting luciferase together with Hsp26 to heat shock resulted in strongly reduced aggregation (Fig. 37 D, red). Incubation of luciferase together with BSA slightly reduced the aggregation level of luciferase (Fig. 37 D, green). This is consistent with the slightly positive effect of BSA on the inactivation of citrate synthase observed before (5.2.5). Incubation at 43°C of Hsp26 (Fig. 37 D, purple) or NAC (Fig. 37 D, pink) alone did not induce aggregation of the proteins. It might be, that the enhancement of the aggregation level is a general effect of NAC on other proteins during heat stress. To test this, NAC and BSA were incubated together at concentrations equivalent to a 4-fold excess over luciferase (Fig. 37 D, orange), but no aggregation was induced. The effect of NAC seems to be specific for aggregation prone proteins.

As NAC shows a pro-aggregation activity on the model substrates it would be plausible, that it shifts to the aggregates. Hence it should be possible to pellet NAC together with the aggregates. Samples were taken before and after the light scattering measurements and aggregates were pelleted via centrifugation (16,000 x g, 30 min, 4°C). In all cases, no shift of NAC to the pellet fraction was detected (data not shown). These results are consistent with the ones obtained via size exclusion chromatography. Both indicate a transient interaction of NAC with aggregation prone proteins and/or aggregates.

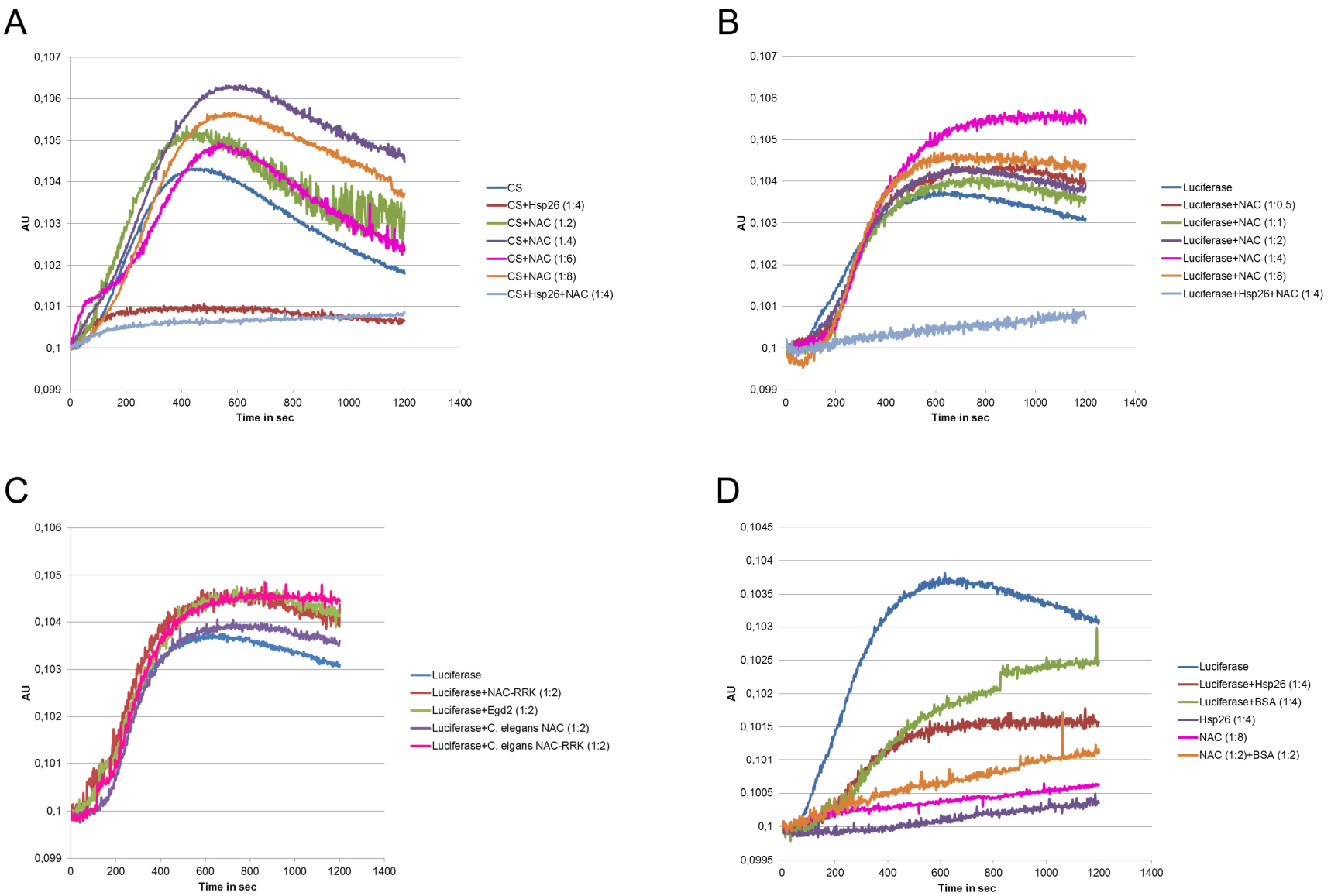

Fig. 37: Aggregation of citrate synthase (CS) and luciferase is enhanced by addition of NAC. Purified CS (600 nM) or luciferase (600 nM) was inactivated thermally at 43°C. Aggregation was monitored at 500 nm. Additional proteins were added as specified. (A) Light scattering of CS. (B) Light scattering of luciferase. (C) Testing of NAC variants on the light scattering of luciferase. (D) Controls for light scattering of luciferase.

5.3 Structure-function analysis of NAC

The heterodimeric NAC complex was first described in the early nineties (Wiedmann et al., 1994). So far, no complete structure of the complex exists, only the dimerization and the UBA domain could be resolved. The first resolved structure of the dimerization domain was that of archaeal NAC, which consists of two α-subunits which are similar to Egd2 of *S. cerevisiae* (Spreter et al., 2005). In 2010, the dimerization site of the human NAC complex was crystallized (Liu et al., 2010 b; Wang et al., 2010). Apart from this, not much is known about the structure of NAC. The α-subunit (Egd2 in yeast) contains a UBA domain at the C-terminus (Spreter et al., 2005; Liu et al., 2010 b; Wang et al., 2010). The β-subunit (Egd1 in yeast) mediates ribosome binding via a helix segment and the conserved RRK-X_n-KK motif in the N-terminus (Franke et al., 2001, Wegrzyn et al., 2006; Pech et al., 2010). Even so NAC was shown to interact with nascent chains and aggregates, the domain or motif responsible for these interactions could not be identified so far (Wiedmann et al., 1994; Wang et al., 1995; del Alamo et al., 2011; Olzscha et al., 2011; Kirstein-Miles et al., 2013).

5.3.1 Structure modelling of yeast NAC

In order to investigate the dimerization domain more closely, a structure model of yeast NAC was created based on the solved structure of the dimerization domain of human NAC (Liu et al., 2010 b; Wang et al., 2010). The bioinformatics analysis was already part of my Master Thesis which was prepared in the course of the Konstanz Fast Track Programme. First, alignments for both NAC subunits were generated, starting with a PSI-BLAST search using the NCBI database. The gained sequences were subjected to CLANS (Frickey and Lupas, 2004) and then aligned using ‘muscle’ (Edgar, 2004). Finally, an external hidden Markov model (HMM) was applied. An extract of the alignment of the β-subunits is given in Fig. 38, where the sequences of *H. sapiens*, *C. elegans* and *S. cerevisiae* are displayed. *S. cerevisiae* is the only organism known to contain two β-subunits, Egd1 (β-NAC) and Btt1 (β’-NAC). The ribosomal binding motif is highly conserved throughout all eukaryotes. Only the length of the amino acid stretch between the RRK and the KK motifs does vary slightly between different organisms. It ranges from 0 to 2 amino acids whereas higher eukaryotes tend to have 0 amino acids in between. The amino acid pattern in the NAC domain is also very similar throughout all eukaryotes. Comparing the *S. cerevisiae* NAC domain of β-NAC to the one of *C. elegans* and *H. sapiens* a similarity of ~56% and ~53% was detected respectively. The similarity between β and β’ in yeast was ~70%. Even β’-NAC displays a similarity of ~44% to *C. elegans* and ~45% to human NAC in this domain. Certain amino acids at defined positions in the sequences are highly conserved, especially in higher eukaryotes. Prominent differences in the protein sequences can be detected in the C-

terminus. While the C-terminus of *S. cerevisiae* β-NAC (Egd1) and the C-termini of *H. sapiens* and *C. elegans* are relatively similar, the C-terminus of β'-NAC (Btt1) differs considerably from all other C-termini. It could not even be aligned completely to all the other sequences. A very prominent motif in the C-termini of the β-subunits was the I/V-P-E/D-L-V motif. It is conserved throughout all eukaryotes. This indicates an important function for this part of the protein. Only β' does not display this motif.

Fig. 38: Extract of the alignment of all β-subunits. The sequences of the β-subunits of *S. cerevisiae*, *C. elegans* and *H. sapiens* as well as the β'-subunit of *S. cerevisiae* are depicted. The conserved ribosome binding motif, the NAC domain and a conserved motif in the C-terminus are highlighted. Amino acid sequences are depicted in the one-letter code. Small letters indicate inserted amino acids. Orange = small hydrophilics, green = small hydrophobics, red = bases, blue = aromatics, colourless = acids/amides and sulphhydrils.

An extract of the alignment of all α-subunits is shown in Fig. 39. Again the sequences of *S. cerevisiae*, *C. elegans* and *H. sapiens* are depicted. The NAC as well as the UBA domain are highlighted. The amino acids in the dimerization domain are highly conserved throughout all eukaryotic organisms. The yeast NAC domain displays a similarity of ~73% to the one of *C. elegans* and a similarity of ~67% to the human one. The amino acids in the UBA domain are also highly conserved, especially the hydrophobic ones. The linker region connecting the two domains is considerably less conserved between the different organisms. While this region is quite long in *S. cerevisiae*, it is markedly shorter in higher eukaryotes. Large parts are missing, but the pattern of small hydrophobic and small hydrophilic residues is conserved. The linker region of Egd2 displays a similarity of ~74% to the one in *C. elegans* and a ~64% similarity to the human one. In contrast to the C-terminus, which is quite conserved because of the UBA domain, the N-terminus shows a lot of variation. In higher eukaryotes, large extensions at this end of the protein were observed. These extensions seem to differ

considerably in their sequence as they could not be aligned to each other. The reason behind these long extensions is still obscure. The N-termini of yeast α-NAC and *C. elegans* α-NAC only display a similarity of ~11%. This decreases to ~4% between the N-termini of yeast α-NAC and the human one.

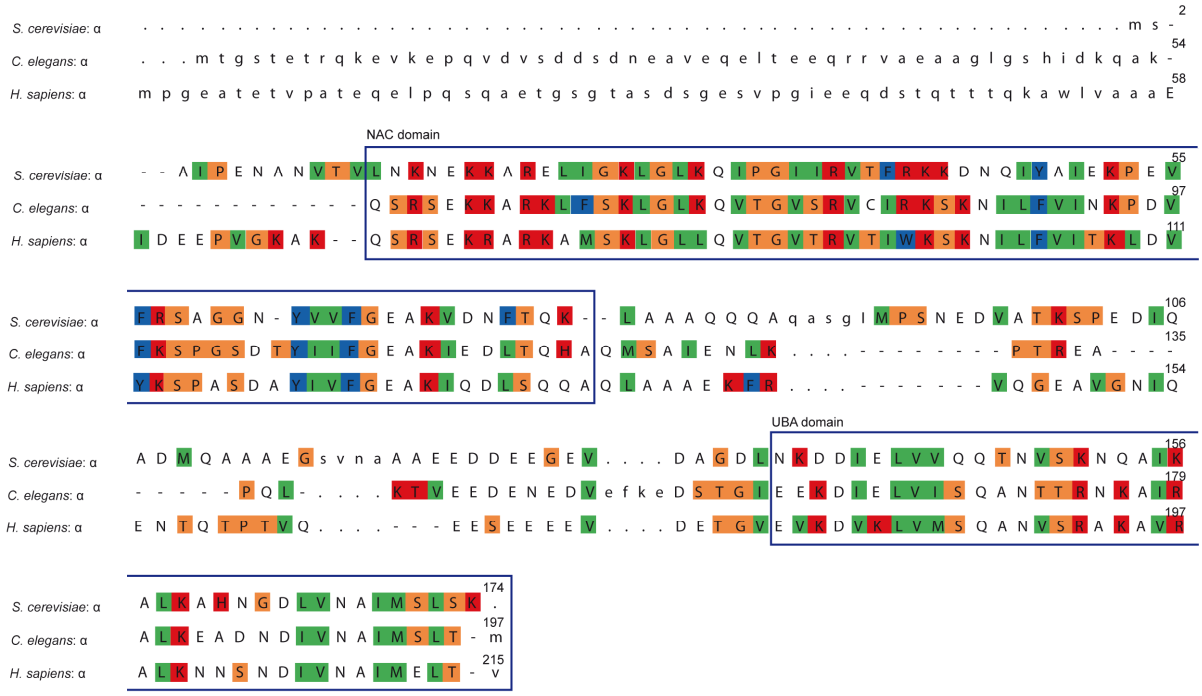

Fig. 39: Extract of the alignment of all α-subunits. The sequences of the α-subunits of *S. cerevisiae*, *C. elegans* and *H. sapiens* are depicted. The NAC domain and the UBA domain are highlighted. Amino acid sequences are depicted in the one-letter code. Small letters indicate inserted amino acids. Orange = small hydrophilics, green = small hydrophobics, red = bases, blue = aromatics, colourless = acids/amides and sulphhydrils.

To investigate the dimerization domain of *S. cerevisiae* NAC more closely, the actual structure model was constructed. The dimerization domain was modelled using HHPred which used the crystal structure of the human dimerization domain as template (Liu et al., 2010 b; Wang et al., 2010). The NAC domains of the two subunits form a flattened β-barrel-like structure (Fig. 40). One side is formed out of six β-strands, the opposite side of four. The strands on both sides are equally divided between the two subunits. The three strands of each subunit which make up the elongated side of the β-barrel are not situated directly behind each other on the protein sequence. The first two strands are encoded directly behind each other. However, the next two encoded β-sheets form the shorter side of the β-barrel. After these two strands sides are shifted again and the final β-strand on the elongated side of the β-barrel is encoded on the sequence. Apart from the β-strands, three short α-helices belong to the NAC domain of Egd1. They are located at the elongated site of the β-barrel and seem to interact with the β-strands (Liu et al., 2010 b; Wang et al., 2010).

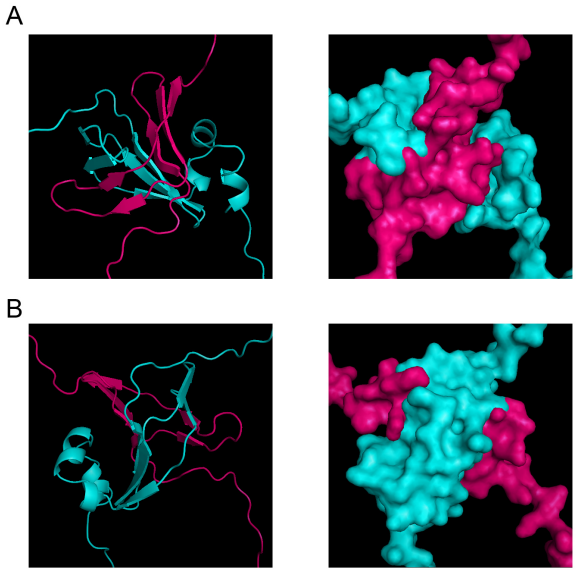

Fig. 40: Structure model of the *S. cerevisiae* NAC complex. The structure of yeast NAC was modelled according to the existing structure of the dimerization domain of the human NAC complex (Liu et al., 2010 b; Wang et al., 2010). Egd1 is depicted in cyan and Egd2 in pink. (A) View on the dimerization domain. (B) 180° spin of the structure depicted in (A).

5.3.2 Limited proteolysis of NAC with proteinase K

To learn more about the structure of NAC, limited proteolysis using proteinase K was performed. This proteinase predominantly cleaves at the peptide bond adjacent to the carboxyl group of aliphatic and aromatic amino acids with blocked alpha amino groups. Due to this broad specificity it is widely used (Ebeling et al., 1974; Kraus and Femfert, 1976; Lizardi and Engelberg, 1979). Purified NAC was subjected to digestion with proteinase K (Fig. 41 A and B). Samples were taken at different time points to monitor the course of digestion with mass spectrometric analysis. First, 0.5 mg/ml of NAC were used (Fig. 41 A). During the course of digestion, no bands were visible between those of Egd2 and Egd1. Only bands with a molecular weight equal or lower than that of Egd1 appeared. The same held true when 1 mg/ml of NAC was used (Fig. 41 B). Only fragments smaller than Egd1 appeared over time. After 180 min, the remaining fragments had a molecular weight of about 13 kDa. Various bands were cut out and sent to mass spectrometric analysis (marked by red numbers).

The most prominent cutting sites for proteinase K in the two NAC-subunits are marked in Fig. 41 C and D. When using 0.5 mg/ml NAC for the digestion, only the NAC domain remained stable in Egd1, the C- and N-terminal extensions were cleaved off (Fig. 41 C). In Egd2, the NAC domain also remained mostly stable as did nearly the complete UBA domain. However, cuts appeared at the very C-terminus (Fig. 41 C).

Using 1 mg/ml NAC for the digestion stabilized part of the N-terminus and the complete C-terminus of Egd1 (Fig. 41 D). Intriguingly, the cleavage pattern for Egd2 differed considerably from the one observed for 0.5 mg/ml NAC. It was now cleaved at the beginning of the NAC domain and in the middle thereof, generating a different fragment of the NAC domain. An

additional cleavage site appeared in the linker region between the NAC and the UBA domain (Fig. 41 D).

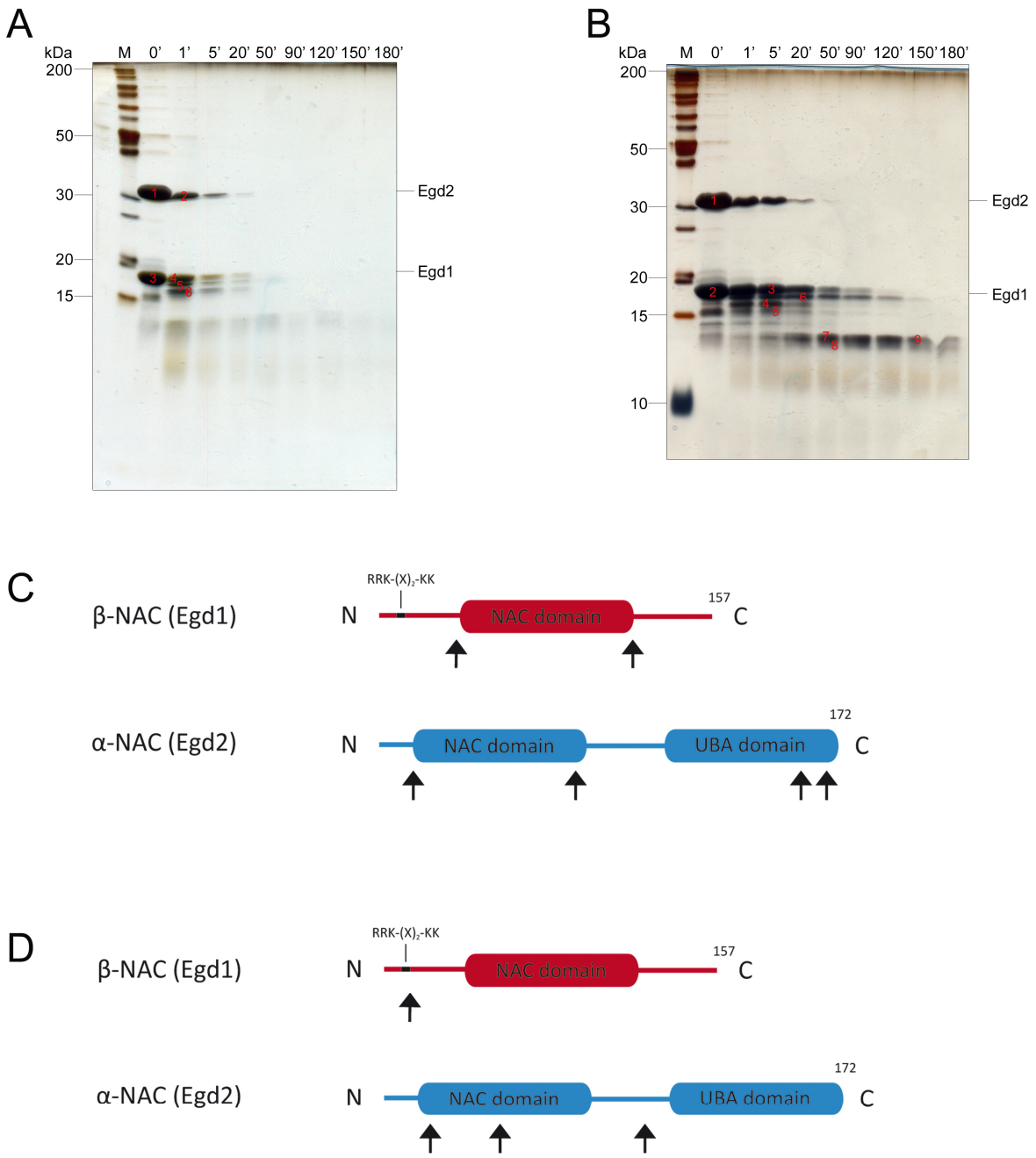

Fig. 41: Limited proteolysis of purified NAC. NAC was subjected to limited proteolysis with proteinase K. Samples were taken at the indicated time points. Red numbers mark the bands that were cut out and sent to analysis by mass spectrometry. (A) 0.5 mg/ml NAC, (B) 1 mg/ml NAC. (C) and (D) Overview of the most prominent cutting sites detected in the limited proteolysis experiment. (C) Pattern when 0.5 mg/ml NAC was used for digestion, (D) Pattern when 1 mg/ml NAC was used for digestion.

To analyse these observations in more detail, the fragments analysed by mass spectrometry were aligned to the full length sequence of the respective subunit. All the fragments detected in one of the bands marked in Fig. 41 A and B are labelled accordingly. Using 0.5 mg/ml

NAC, a clear cut was observed directly at the end of the NAC domain in Egd1 (Fig. 42). Another two cutting sites were detected in the fragments from band 6, approximately in the first half of the dimerization domain. It exactly cut out the middle β-strand of Egd1 on the elongated side of the flattened β-barrel of the dimerization domain. After this strand a short linker normally crosses to the other side of the β-barrel. In all gained fragments the N-terminus of Egd1 was completely digested up to a short stretch of amino acids directly in front of the NAC domain. The C-terminus was also very susceptible to proteinase K. Only a stretch containing the conserved I/V-P-E/D-L-V motif proved more resistant.

Fig. 42: Fragments of Egd1 generated by limited proteolysis of 0.5 mg/ml NAC and determined by mass spectrometry. Fragments generated by limited proteolysis with proteinase K were determined by mass spectrometry and aligned to the full length sequence at the top of the alignment. Domains present in the protein are indicated. Amino acid sequences are depicted in the one-letter code. Small letters indicate inserted amino acids. Orange = small hydrophilics, green = small hydrophobics, red = bases, blue = aromatics, colourless = acids/amides and sulphhydrils.

Interestingly, in Egd2 the linker region between the NAC domain and the UBA domain was way more stable than the NAC domain itself (Fig. 43). Even if the linker is shorter in higher eukaryotes and predicted to be disordered in yeast, it nevertheless seems to adopt a very stable conformation at least in *S. cerevisiae*. The UBA domain was also relatively stable. In the beginning, the fragments just lacked the short tail end. With ongoing digestion, the last two of the three α-helices in the UBA domain were cut off. The fragment found in band 4 lacked a part of the linker region as well as the complete UBA domain. This cutting site was used later for the generation of a ΔUBA variant of NAC. In the NAC domain, one region was

quite stable. This region includes the middle β-strand of Egd2 on the elongated side of the β-barrel, the linker between the two sides and the first β-strand of the shorter side of the β-barrel. The reason for the high stability of this region is unclear so far. As observed for Egd1, the residues directly before the dimerization domain were also preserved for a quite long time of the digestion process. A region at the beginning of the NAC domain containing a spot of basic residues was stable during the first minutes of digestion but cut out of the protein with ongoing digestion.

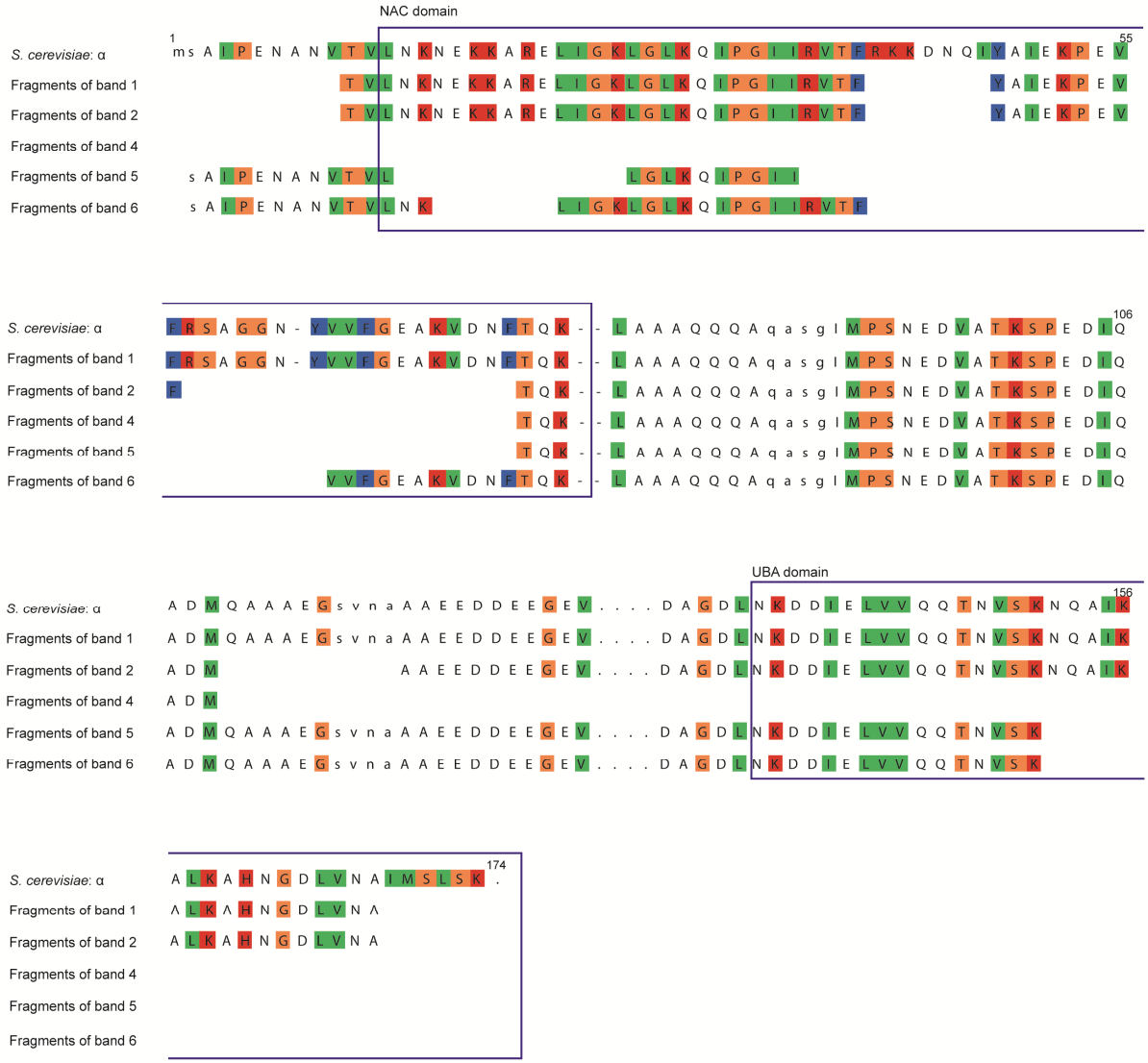

Fig. 43: Fragments of Egd2 generated by limited proteolysis of 0.5 mg/ml NAC and determined by mass spectrometry. Fragments generated by limited proteolysis with proteinase K were determined by mass spectrometry and aligned to the full length sequence at the top of the alignment. Domains present in the protein are indicated. Amino acid sequences are depicted in the one-letter code. Small letters indicate inserted amino acids. Orange = small hydrophilics, green = small hydrophobics, red = bases, blue = aromatics, colourless = acids/amides and sulphhydrils.

When using 1 mg/ml NAC, the NAC domain of Egd1 was still very stable indicating no conformational changes that would have allowed cleavage of the domain (Fig. 44). In line with this, the C-terminus took longer to be digested due to the increased amount of NAC

present. The same held true for the N-terminus of Egd1. Cleavage occurred directly after the suggested ribosomal binding motif (Wegrzyn et al., 2006). This motif seems to be prominently exposed and easily accessible for proteinase K.

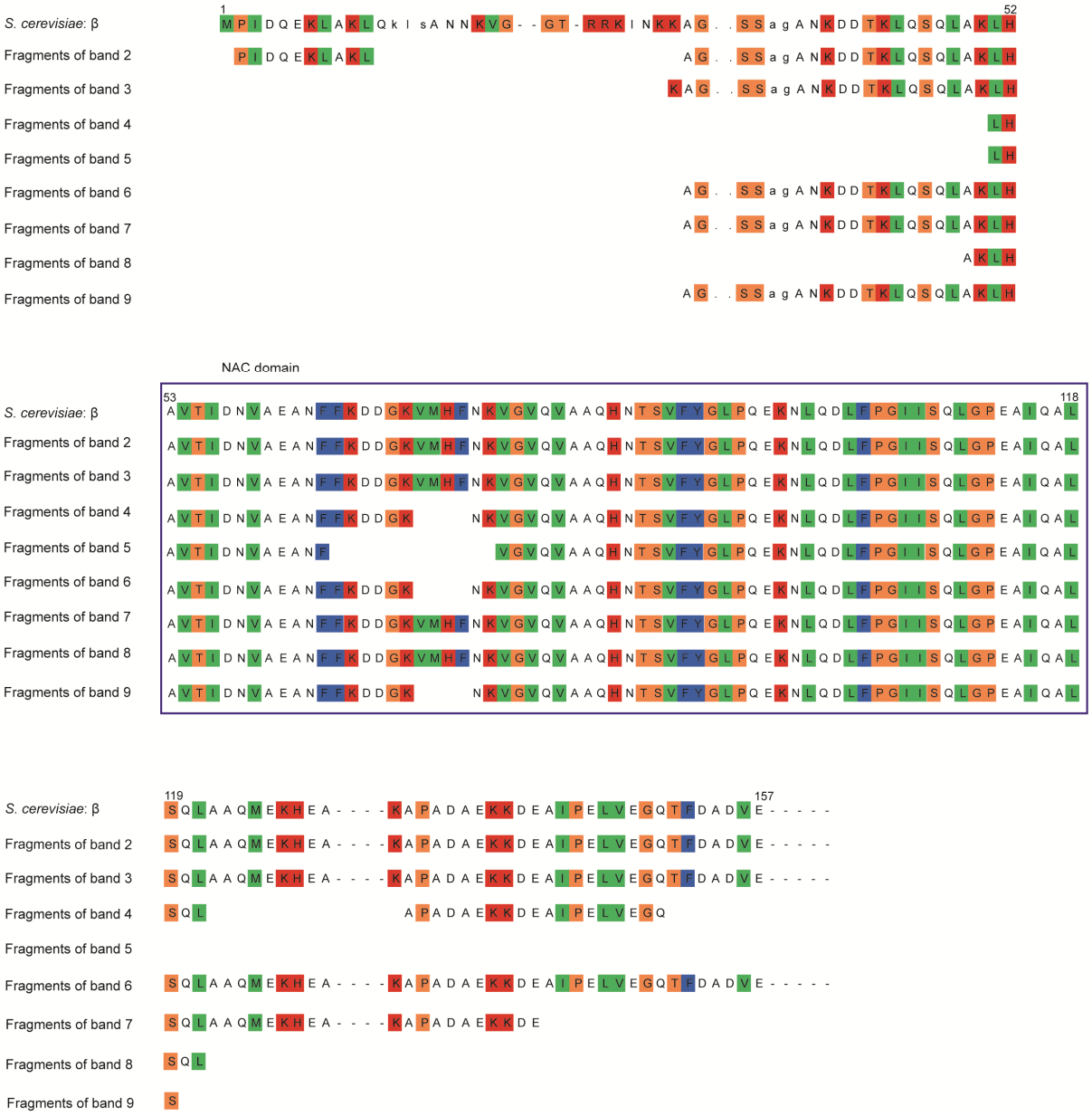

Fig. 44: Fragments of Egd1 generated by limited proteolysis of 1 mg/ml NAC and determined by mass spectrometry. Fragments generated by limited proteolysis with proteinase K were determined by mass spectrometry and aligned to the full length sequence at the top of the alignment. Domains present in the protein are indicated. Amino acid sequences are depicted in the one-letter code. Small letters indicate inserted amino acids. Orange = small hydrophilics, green = small hydrophobics, red = bases, blue = aromatics, colourless = acids/amides and sulphhydrils.

In contrast to Egd1, a different cleaving pattern of proteinase K was detected for Egd2 when 1 mg/ml NAC was used (Fig. 45). A part of the NAC domain, that was stable when 0.5 mg/ml was used, was cleaved out of the domain and the parts around that region were stabilized. Furthermore, the UBA domain was no longer stable, but missing completely in nearly all

fragments together with a part of the linker region between the NAC and the UBA domain. Interestingly, no cut at the interface of the linker region and the UBA domain was detected. Instead, when the UBA domain was missing, a part of the linker region was always missing as well. These observed differences may be caused by conformational changes in Egd2 when a higher amount of NAC is present during the experiment.

Fig. 45: Fragments of Egd2 generated by limited proteolysis of 1 mg/ml NAC and determined by mass spectrometry. Fragments generated by limited proteolysis with proteinase K were determined by mass spectrometry and aligned to the full length sequence at the top of the alignment. Domains present in the protein are indicated. Amino acid sequences are depicted in the one-letter code. Small letters indicate inserted amino acids. Orange = small hydrophilics, green = small hydrophobics, red = bases, blue = aromatics, colourless = acids/amides and sulphhydrils.

5.3.3 *In vivo* NAC lacking the UBA-domain and part of the linker region has a higher aggregation prevention activity

Beside NAC, another chaperone complex can be found at the ribosomal exit site: the Hsp70/Hsp40 system RAC together with the Hsp70 Ssb (Nelson et al., 1992; Huang et al., 2005; Conz et al., 2007; Preissler and Deuerling, 2012). If NAC is deleted in yeast cells, no increased protein aggregation can be observed. In contrast, deletion of Ssb leads to the accumulation of protein aggregates. However, when NAC is deleted in addition to Ssb, protein aggregation is even enhanced (Koplin et al., 2010). The level of aggregation in a *nacΔssbΔ* strain can be reduced to that of an *ssbΔ* strain when expressing the NAC complex from a plasmid. In a recent study of our group, different subunits and complexes of NAC were tested for their ability to complement the aggregation levels of a *nacΔssbΔ* strain to the levels of an *ssbΔ* strain (Ott et al., 2015). By preparing aggregates from *nacΔssbΔ* cells complemented with different plasmids Ann-Kathrin Ott could show, that a NAC variant lacking the UBA domain and part of the linker region was most potent in reducing the aggregation level (Fig. 46, lane 10). The levels fell even below the ones observed in *ssbΔ* cells (lane 2). Therefore, the UBA domain seems to play a role in the prevention of aggregation activity of NAC *in vivo*. This activity needs to be specified further.

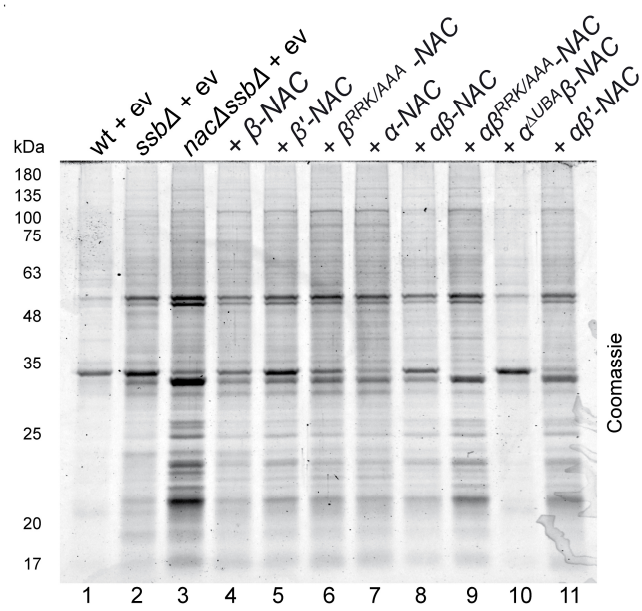

Fig. 46: NAC lacking the UBA domain and part of the linker region is most potent in preventing aggregation. Cells expressing different NAC variants were lysed when they reached the logarithmic phase and the aggregated protein material was prepared. Samples were separated by SDS gel electrophoresis and the gel was stained with Coomassie brilliant blue. Figure was taken from Ott et al. (2015).

5.3.4 Construction of different ΔUBA versions for *in vitro* analysis

To analyse the function of the UBA domain and the linker region of Egd2 in more detail, different deletion mutants for *in vitro* studies were generated (Fig. 47). The mutants were created using PCR. They were inserted in the same bacterial expression vector that was

used for native NAC. The first mutant was constructed according to the one used for the *in vivo* analyses in Ott et al. (2015), which allowed to compare the behaviour of this specific mutant to its *in vivo* activity. During the limited proteolysis experiments, a cutting site in the linker region between the NAC and the UBA domain was identified (Fig. 43). The cutting site identified was shifted by one amino acid compared to the mutant used in Ott et al. (2015). Last, the UBA domain as well as the complete linker region were deleted. As the version shown to have an effect *in vivo* lacked just part of the linker region, the mutant lacking the complete linker region enabled to investigate a possible role of this region in total.

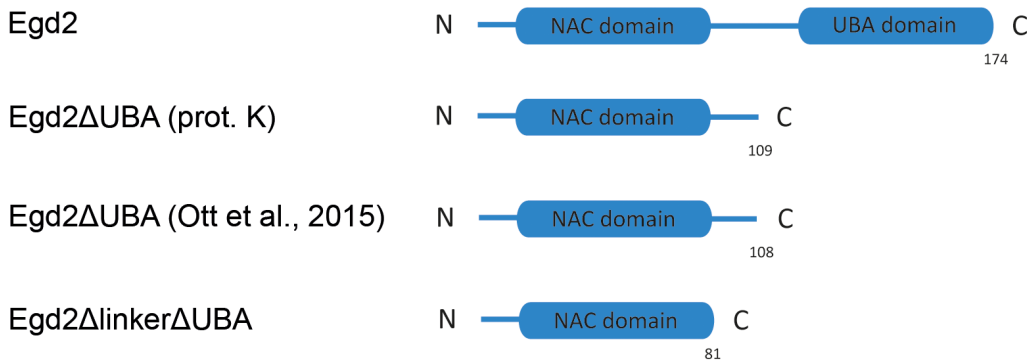

Fig. 47: Overview of the different NAC mutants used for analysis. Topmost is the native version of yeast Egd2. The next version depicted is the one where the cutting site was determined by limited proteolysis with proteinase K. The following mutant was constructed based on the one used in Ott et al. (2015) for the *in vivo* aggregation analyses. The last version lacks the UBA domain as well as the complete linker region.

5.3.4.1 Analysis by Circular Dichroism

Circular dichroism spectra of the three mutants were compared to the spectra obtained for native NAC. Differences in the secondary structure of the mutants could be visualized by this method. As the spectrum of native NAC (Fig. 48 D) is a mixture of β-strands, α-helices and random coils, it is difficult to assign any differences detected in the spectra to a specific secondary structure element. However, the predicted numbers for α-helices and β-sheets can be compared directly to the ones of native NAC.

When comparing the spectra of native NAC and the one for the mutant described in Ott et al. (2015), the first obvious difference is the reduced range covered on the y-axis (Fig. 48 A). Native NAC starts with a value of around 20 mdeg at 180 nm whereas the mutant starts at about 4 mdeg. This is an indication for a reduced amount of α-helices present in the mutant (Whitmore and Wallace, 2008) which is further strengthened by the altered minimum at 205 nm. Whereas native NAC has a minimum at -30 mdeg, the minimum of the mutant is situated at around -14 mdeg. Furthermore the minimum is shifted slightly to a lower wavelength. This might be due to a decreased share of α-helices in the protein and the supposedly unchanged amount of β-strands could shift the spectrum upwards at this position. Another reason could be an unchanged amount of random coils which could also be responsible for an upshift of the spectrum, even if the number of β-strands was reduced as

was the number of α-helices. The regional minimum at 220 nm was upshifted as well from -20 to -8 mdeg and located at a slightly lower wavelength. Dichroweb (Whitmore and Wallace, 2004; Whitmore and Wallace, 2008) predicted a total of 7.1 helix segments for the protein with an average length of 21.197 amino acids. Whereas around 4 α-helices less than in the native NAC complex were predicted, the helix segments themselves seem to be longer with average length of 21.197 amino acid per helix (native NAC: 10.8 α-helices with an average length of 17.729). This was consistent with the observed shifts in the spectrum. Interestingly, also a lower amount of β-sheets was predicted by Dichroweb (Whitmore and Wallace, 2004; Whitmore and Wallace, 2008). 9.6 β-strands with an average length of 4.811 amino acids were predicted in comparison to 13.6 β-strands with an average length of 4.945 amino acids for native NAC. A secondary structure prediction programme predicted the missing part of the linker region to be disordered and not to contain β-sheets. So apparently the missing UBA domain together with a part of the linker region has an influence on the overall structure of NAC.

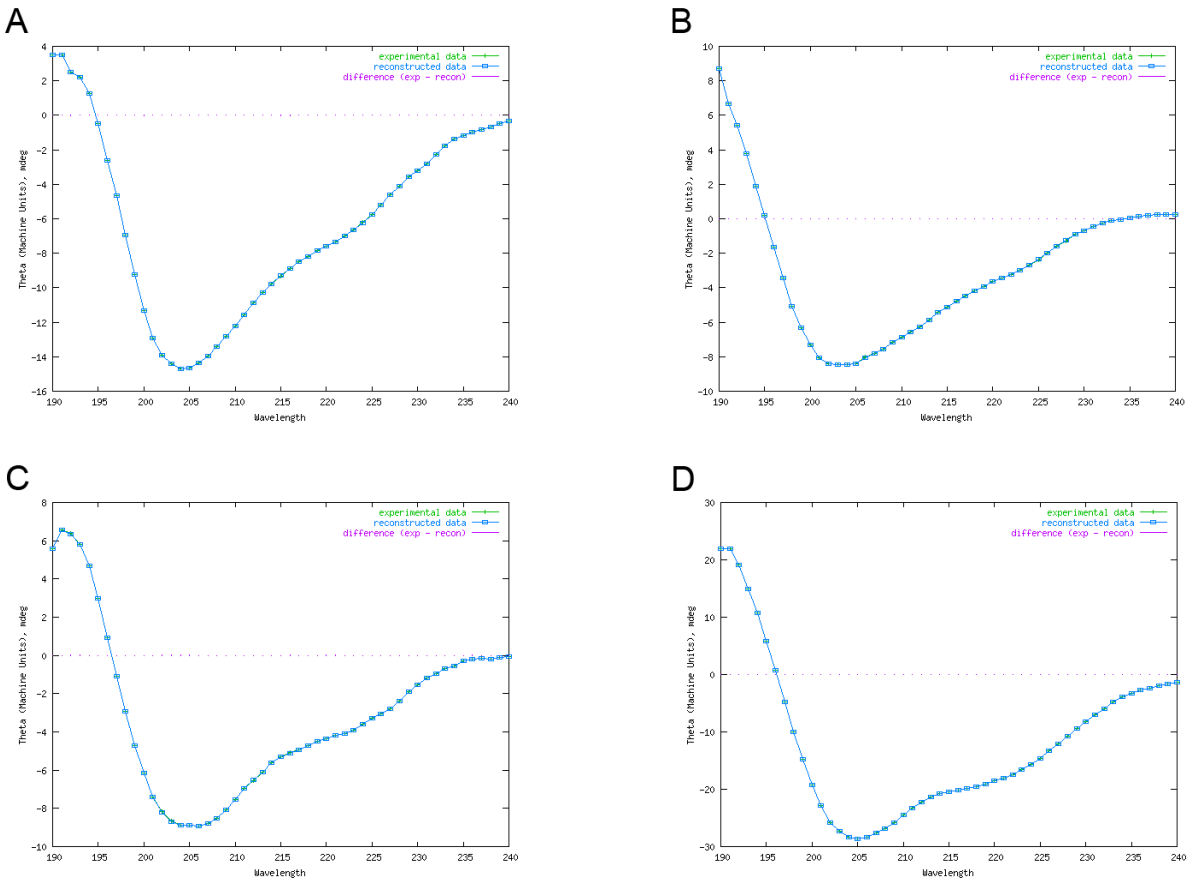

Fig. 48: Circular dichroism measurement of the purified NAC mutants. The purified NAC mutants were subjected to circular dichroism measurement at 20°C. Analysis was performed using Dichroweb (Whitmore and Wallace, 2004; Whitmore and Wallace, 2008). (A) Mutant corresponding to the version used in Ott et al. (2015); NRMSD value = 0.000. (B) Mutant constructed according to the cutting site of proteinase K; NRMSD value = 0.001. (C) Mutant lacking the UBA domain as well as the complete linker region; NRMSD value = 0.001. (D) CD-spectrum of native NAC; NRMSD value = 0.000.

The spectrum of the NAC version which was constructed based on the cutting site determined by limited proteolysis is depicted in Fig. 48 B. This mutant should be very similar to the one described in Fig. 44 A, as just one amino acid less of the linker region is missing. Interestingly, the spectrum started at 8 mdeg in comparison to the 4 mdeg of the mutant described before. Fittingly, the minimum at around 205 nm had a value of -8 mdeg instead of -14. However, the minimum at around 205 nm was also shifted slightly to a lower wavelength as was observed for the mutant described above. The regional minimum at around 220 nm was found at -5 instead of at -8 mdeg. The whole spectrum was shifted upwards in comparison to the spectrum of the mutant used by Ott et al. (2015). This indicates a lower amount of α-helices compared to β-strands. Indeed, the predicted number of α-helices was 7.1 with an average length of 18.790. Even though the number of predicted α-helices was the same, the predicted average length was shorter by about 3 amino acids. The predicted number of β-strands increased to 10.2, so more and also longer β-strands, with a predicted length of 5.087 amino acids per segment, were present in this mutant. One amino acid more in the linker region seems to be responsible for a visible difference in the secondary structure of the two mutants.

The spectrum of the mutant lacking the UBA domain as well as the whole linker region is shown in Fig. 48 C. The spectrum started at around 6 mdeg. The minimum was located directly at 205 nm like in native NAC and in contrast to the other two mutants. The minimum itself was reached at -9 mdeg. The local minimum was located at around 220 nm and -6 mdeg. These values are most similar to the ones observed for the proteinase K mutant described in Fig. 44 B. However, Dichroweb (Whitmore and Wallace, 2004; Whitmore and Wallace, 2008) predicted 9.4 α-helices with an average length of 16.522 amino acids. The number of helices was slightly reduced compared to native NAC but clearly higher than in the two other mutants. The average length of the α-helical segments was considerably shorter than the ones predicted for the other two mutants but similar to the one calculated for native NAC. The number of β-strands predicted was reduced to about half the amount present in native NAC (6.2 in comparison to 13.6). Furthermore, the β-sheets with an average length of 4.188 amino acids were considerably shorter than the ones in native NAC and the other mutants. The complete lack of the linker region seems to be responsible for large-scale changes in the secondary structure of the complex.

5.3.4.2 Effect of NAC mutants on luciferase aggregation

To determine if the mutants of NAC affected aggregation of luciferase differently than native NAC, light scattering experiments were performed. The mutant lacking the UBA domain and part of the linker region as described in Ott et al. (2015) was the most powerful NAC version in prevention of aggregation *in vivo*. Therefore, the purified NAC mutant was expected to

behave similarly *in vitro*, as was the one constructed according to the information gained by limited proteolysis. The version corresponding to the one used in Ott et al. (2015) was tested under the same conditions as native NAC. Luciferase was subjected to heat shock in the absence or presence of different concentrations of the mutant and aggregation levels were observed (Fig. 49 A). Surprisingly, the mutant showed the same behaviour as native NAC: It increased the aggregation levels of luciferase (red and green). When subjected to heat shock alone, the mutant did not aggregate (pink).

The same pattern was observed with the mutant cut at the site defined by limited proteolysis (Fig. 49 B). When added at 4-fold excess, the mutant again enhanced aggregation (green). Interestingly, if only a 2-fold excess of the mutant was added (red), the aggregation level was the same as for luciferase alone (blue). The mutant itself did not aggregate upon heat shock (pink). However, a probably artificial peak appeared in this curve during the measurement.

Finally, if luciferase was incubated with the NAC version lacking the UBA domain as well as the whole linker region, again an increase in the aggregation levels occurred (Fig. 49 C), irrespective of whether a 2-fold (pink) or a 4-fold excess (purple) of the mutant was added. Again, the mutant itself did not aggregate (grey).

Hsp26 reduced the aggregation level of luciferase as expected (Fig. 49 C, red). Native NAC as control showed the same behaviour as described earlier (green). Pelleting samples that had been taken before and after the light scattering experiments by centrifugation revealed no shift of the NAC mutants into the pellet fraction (data not shown). The same had been observed for native NAC.

In sum, the mutants showed the same behaviour as native NAC in the light scattering experiments. They increased the aggregation level of the model protein luciferase albeit a positive effect on aggregation was observed for one mutant *in vivo*. Thus, the light scattering experiments allow no conclusion about the differences between the mutants and native NAC.

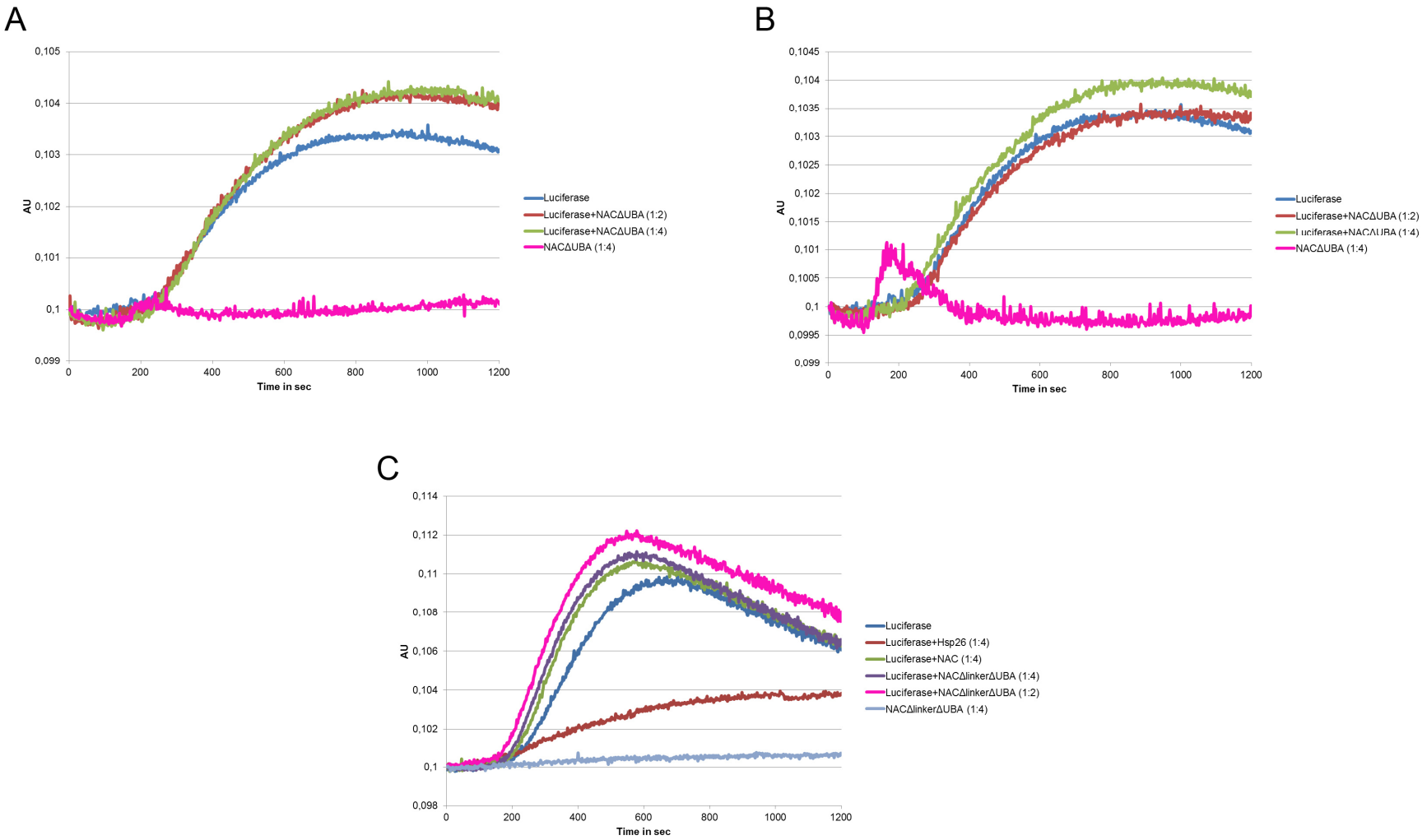

Fig. 49: The different purified NACΔUBA mutants did behave as native NAC in light scattering experiments. Luciferase was subjected to light scattering at 43°C with or without different concentrations of the different NAC mutants. (A) Mutant corresponding to the version used in Ott et al. (2015). (B) Mutant constructed according to the cutting site of proteinase K. A probably artificial peak appeared in the pink curve which depicts the behaviour of the mutant on its own at 43°C. (C) Mutant lacking the UBA domain as well as the complete linker region.

5.3.5 The C-termini of the different β-subunits of NAC seem to play a role in functionality

The heterodimeric NAC complex consists of two subunits, Egd2 and Egd1. However, in yeast a second β-subunit and thus a second heterodimeric complex exists. It is formed by Egd2 and Btt1. The complex of Egd2 and Egd1 is present in a 100-fold excess over the complex of Egd2 and Btt1 (Hu and Ronne, 1994; Shi et al., 1995; Reimann et al., 1999; Pech et al., 2010). The two complexes were reported to have different substrate specificities. Egd2-Egd1 was shown to preferentially associate with ribosomes translating metabolic enzymes as well as secretory and membrane proteins. In contrast, Egd2-Btt1 associated mainly with ribosomes translating ribosomal and mitochondrial proteins (del Alamo et al., 2011). In a recent study we could show, that Egd1 is sufficient to complement the growth deficit of *nacΔssbΔ* cells back to *ssbΔ* levels. This was no longer possible if Egd1 was expressed under the *BTT1* promoter. In contrast, Btt1 was not able to complement the growth deficit even when expressed under the *EGD1* promoter (Ott et al., 2015). These data demonstrate clear differences in the functionality of the two subunits which are probably represented in their protein sequences. To investigate these possible differences, the sequences of Egd1 and Btt1 were analysed in more detail. First, the overall similarity and identity were calculated. Egd1 and Btt1 shared a similarity of 64.3% and an identity of 46.5%. The biggest differences were observed in the C-termini of the two subunits (Fig. 50). When comparing only the C-termini, the similarity was reduced to 30.8% and the identity to even 10.3%. These values are much lower and well below the average of the ones obtained for the full length sequences. A further difference is the sequence length of the two proteins. Btt1 is 8 amino acids shorter than Egd1. Moreover, the last 16 amino acids of Btt1 showed no homology whatsoever to Egd1 or any other β-subunit present in eukaryotes. The two C-termini also exhibited differences in their net charge. Egd1 has 11 negatively (Asp and Glu) and 4 positively charged residues (Arg and Lys) in its C-terminus. The negative charge is higher than in Btt1 which has 5 negatively and 2 positively charged residues in its C-terminus. These observations support the experimentally observed differences between the two β-subunits in yeast.

Interestingly, the C-termini of all other eukaryotes were similar to Egd1 and not to Btt1. As this subunit fulfils functions different from those of Egd1 in yeast, its absence has to be compensated for either by the regular β-subunit or another protein in higher eukaryotes.

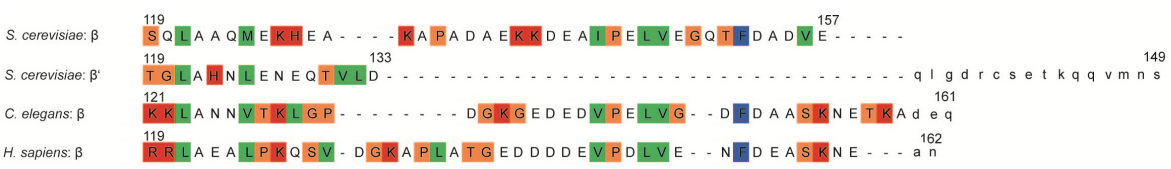

Fig. 50: C-termini of Egd1 and Btt1 differ considerably. Extract of an alignment of the C-termini of all eukaryotes. The C-terminal sequences of the β-subunits of *S. cerevisiae*, *C. elegans* and *H. sapiens* as well as the β'-subunit of *S. cerevisiae* are depicted. Amino acid sequences are depicted in the one-letter code. Small letters indicate inserted amino acids. Orange = small hydrophilics, green = small hydrophobics, red = bases, blue = aromatics, colourless = acids/amides and sulphhydrils.

5.4 Preliminary work for *in vivo* crosslinking of NAC with substrates and nascent chains

Even though NAC is known to interact with substrates, no substrate binding site(s) could be identified so far.

To identify the substrate binding site(s), the created structure model of yeast NAC was investigated more closely. For binding of nascent chains or aggregating proteins, hydrophobic patches on the surface of NAC are the most likely candidates. Highlighting hydrophobic amino acids on the surface of the NAC and the UBA domain in the structure model revealed three prominent hydrophobic patches (Fig. 51).

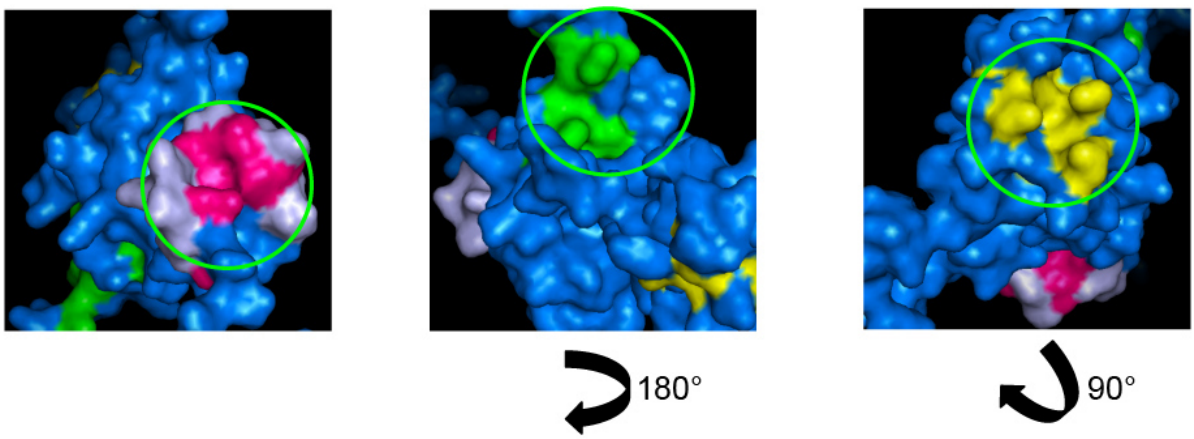

Fig. 51: Hydrophobic patches on the surface of NAC. Surface model of the yeast NAC complex. Coloured in blue are Egd1 and Egd2. Highlighted in light blue are the three short alpha helices of the dimerization domain of Egd1. Pink: hydrophobic patch on the surface of the dimerization domain of Egd1. Green: hydrophobic patch on the surface of the dimerization domain of Egd2. Yellow: hydrophobic patch on the surface of the UBA domain.

One patch was located on the surface of the dimerization domain of Egd1 (pink). The NAC domain of Egd1 not only consists of the β-strands that form the β-barrel-like structure, but in addition of three short α-helices which are positioned at the elongated site of the β-barrel with which they interact (Liu et al., 2010 b; Wang et al., 2010). The hydrophobic patch was positioned on the site of the α-helical structure that did not directly interact with the β-barrel. The second hydrophobic patch was located on the surface of the dimerization domain of Egd2 (green) on the other side of the dimerization domain. The last prominently exposed patch was located on the surface of the UBA domain of Egd2 (yellow). This patch was formed by three amino acids which protruded slightly.

To investigate, if NAC binds its substrates at any of these sites, the unnatural amino acid para-benzoylphenylalanine (pBpa) was incorporated into these patches. pBpa forms site specific zero-spacer crosslinks which enables to detect a direct interaction of NAC with substrates at these positions.

5.4.1 The tags do not alter NAC behaviour

As pBpa was planned to be incorporated into both subunits separately, a method to pull down the subunit crosslinked to a potential substrate was needed. To achieve this, the two subunits of NAC were differently tagged. Egd2 was tagged with 3xHA and Egd1 with Flag. First it was analysed if the tags had an influence on regular NAC behaviour.

Tagged NAC was first assayed for its potential to complement the pleiotropic growth defect of *nacΔssbΔ* cells back to the level of *ssbΔ* cells (Koplin et al., 2010). Untagged NAC (Fig. 52 A) complemented the growth defect of *nacΔssbΔ* cells back to *ssbΔ* levels. Interestingly, expression of the tagged version not only complemented the pleiotropic growth phenotype of *nacΔssbΔ* cells but the cells seemed to grow even better than the ones expressing the untagged version. This effect was observed on all plates tested: Cells expressing the tagged version always grew slightly better than cells expressing wt NAC.

One reason for the better complementation might be an increased expression of the tagged version over the untagged one. Analysis of protein levels revealed that this was not the case (Fig. 52 B): The expression levels of the tagged construct were around the same as the ones for wt NAC in the two control strains. As seen in Fig. 20, untagged NAC is also expressed around wt levels in *nacΔssbΔ* cells.

Finally, ribosome binding of the tagged NAC version was investigated. For this, an *ex vivo* ribosome sedimentation analysis was performed. Ribosomes were extracted from cells by centrifugation through a sucrose cushion. If the tagged complex still associates with ribosomes, it should be found in the same fraction when physiological salt concentrations are used. Indeed, it was detected predominantly in the pellet fraction together with ribosomes (Fig. 52 C). When the experiment was repeated using high salt concentrations, the tagged NAC was washed off the ribosomes (data not shown). These data show that the tags do not negatively influence ribosome binding of the complex and that the complex is fully functional.

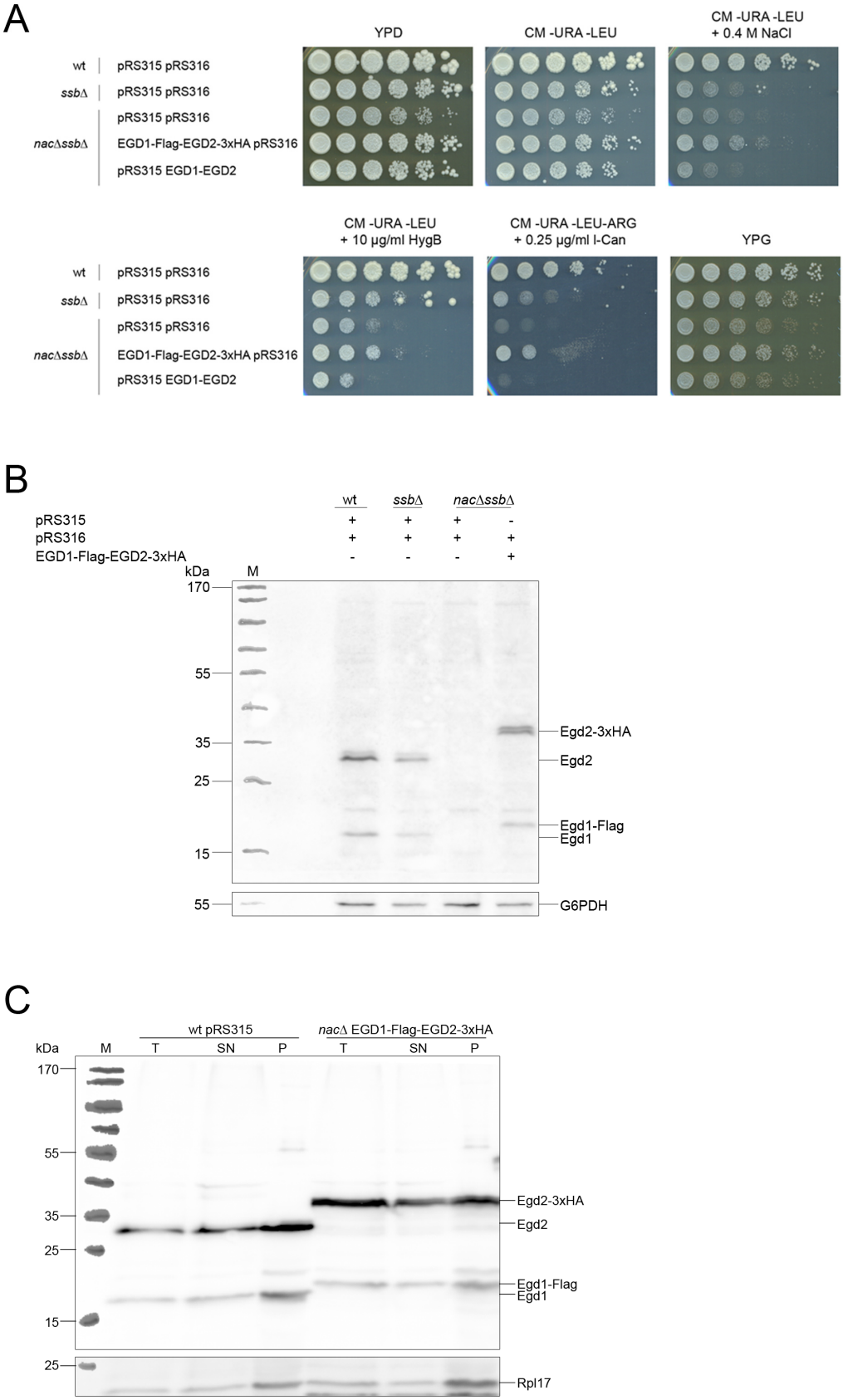

Fig. 52: The tags at the C-terminal ends of the two NAC subunits did not influence the behaviour of the NAC complex. Egd1 was tagged with a Flag-tag and Egd2 with a 3xHA-tag at their respective C-termini. (A) *nacΔssbΔ* cells were transformed with the tagged NAC construct and 5-fold serial dilutions were spotted on the indicated selection plates. (B) Alkaline lysis of yeast cells expressing the tagged NAC construct was performed. Samples were run on a 12% SDS-PAGE and blotted on a nitrocellulose membrane. It was probed with an antibody against NAC. G6PDH served as loading control. (C) Yeast lysates were subjected to centrifugation through a sucrose cushion to isolate ribosomes together with associated proteins. Samples were subjected to SDS-PAGE and western blotting. The membrane was probed with an antibody against NAC. Rpl17 was used as control. Experiments were performed by a student of mine, Annika Krüger.

5.4.2 Stop codons are incorporated at defined positions

For incorporation of pBpa into the tagged NAC constructs, amber stop codons had to be included into the protein sequence. Specific tRNAs recognizing the amber stop codon would then incorporate pBpa into the protein *in vivo*. As the natural stop codon of Egd1 is an amber stop codon it was changed into 'TAA' to avoid accidental incorporation of pBpa instead of stopping translation.

Small hydrophobic amino acids located mainly in the identified hydrophobic patches were chosen for substitution by pBpa. The structure model was investigated more closely to check, how a more bulky amino acid like pBpa would interact with the neighbouring residues at certain positions and if incorporation at the favoured positions would be possible. A total amount of 14 positions were chosen for incorporation and 14 different mutants were generated.

Three mutants were generated to analyse the hydrophobic patch present on the surface of the dimerization domain of Egd1 (Fig. 53 A). The three amino acids were positioned to one another in a triangular position in the α-helical patch of the NAC domain of Egd1. In mutant one, phenylalanine at position 103 was exchanged with an amber stop codon. The second mutant had the isoleucine at position 107 replaced and the last one the isoleucine at position 115.

In the hydrophobic patch on the surface of the dimerization domain of Egd2, a total of four amino acids were substituted (Fig. 53 B). One was located on a β-strand of the dimerization domain, one on a very short α-helix directly before the β-strands involved in dimerization and two in a region shortly before that. The two amino acids directly before the β-strands involved in dimerization were leucine at position 23 and isoleucine at position 24. The third amino acid was leucine at position 27 situated in the very short α-helix. The last amino acid replaced was the phenylalanine situated at position 66 in a β-strand of the dimerization domain.

The last prominent hydrophobic surface patch was identified in the UBA domain of Egd2 (Fig. 53 C). The chosen amino acids were again positioned in a triangle. The three selected amino acids were leucine at position 142, leucine at position 165 and methionine at position 170.

In addition to the amino acids that were replaced in the hydrophobic patches, four more were selected. Conserved regions in the alignments were identified for incorporation and positions well outside the dimerization domain were picked as controls. One of the chosen amino acids was leucine at position 27 in the Egd1 subunit (Fig. 53 D). It was directly located in the conserved ribosomal binding motif. If NAC interacts with aggregates, it would have to leave its position at the ribosome and the motif would generally be free to contact, for example, aggregates (Olzscha et al., 2011; Kirstein-Miles et al., 2013).

Two further stop codons were incorporated into the C-terminus of Egd1 (Fig. 53 E). As reasoned before, the C-terminus might be responsible for substrate interaction. The phenylalanine at position 152 is conserved throughout all eukaryotes. As substituting this amino acid might abolish a possible substrate binding, two other amino acids flanking the phenylalanine were chosen. These two were valines at positions 147 and 156.
Last, an amino acid directly at the beginning of the NAC domain in Egd2, which was not part of a hydrophobic patch, was substituted (Fig. 53 F); this was leucine at position 13.
All mutants described were constructed using site directed mutagenesis. They were all tested for expression with and without pBpa and checked for appearing crosslinks. Ribosome binding was tested as well (data not shown). Mutation of leucine at position 13 and methionine at position 170 in Egd2 abolished expression of NAC completely. In contrast, mutation of phenylalanine at position 66 abolished expression of Egd2 but not of Egd1. Mutating leucine at position 27 in Egd1 led to a sole expression of Egd2. Even though mutants at positions L142 in Egd2 as well as V147 and V156 in Egd1 were expressed and could still bind to ribosomes, no crosslinks were detectable. All other described mutants were expressed, able to bind to ribosomes and a crosslink appeared after UV irradiation.

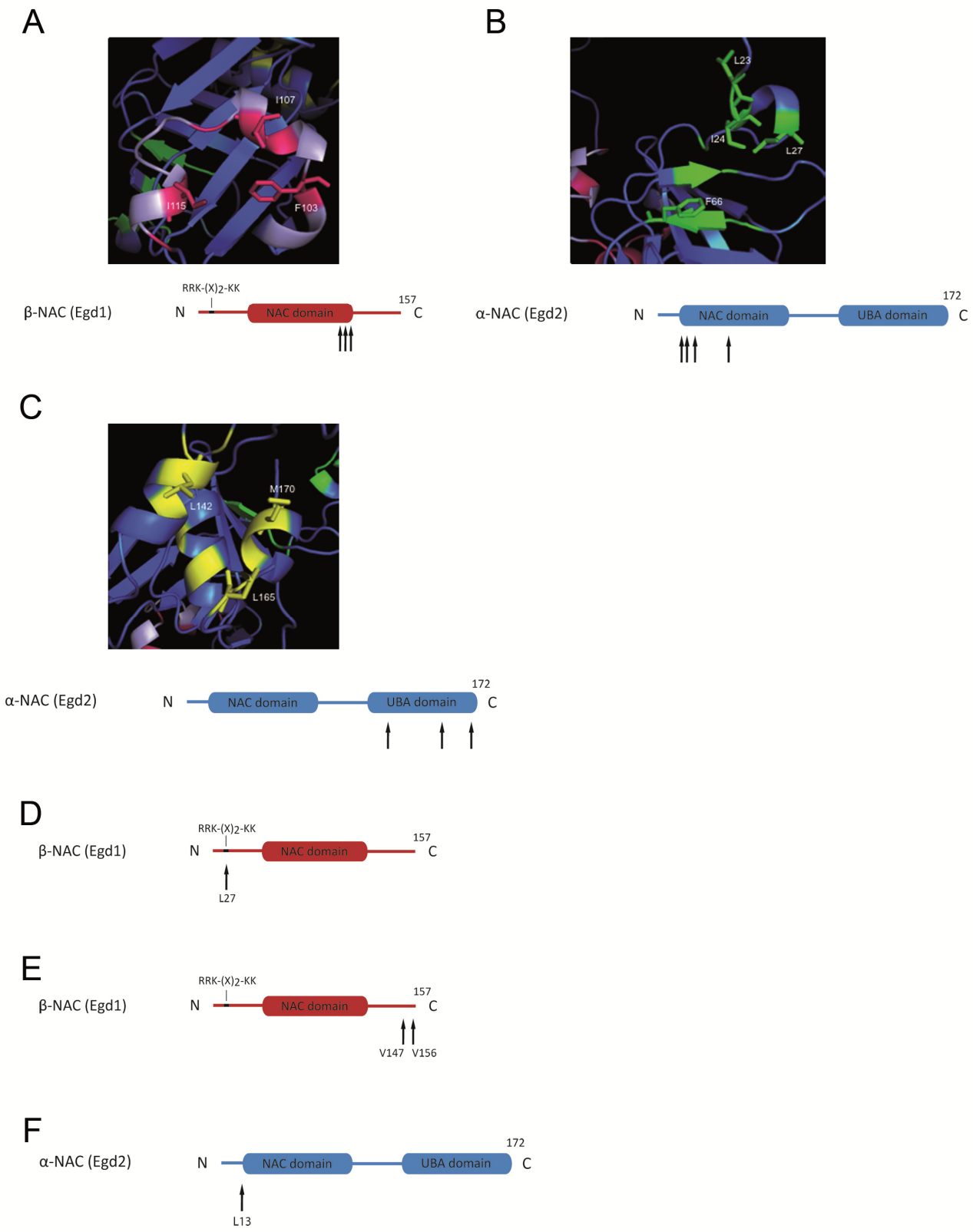

Fig. 53: Identification of the positions for the incorporation of the unnatural amino acid para-benzoylphenylalanine (pBpa). (A) NAC domain of Egd1. Three hydrophobic amino acids were replaced in separate mutants with an amber stop codon for pBpa incorporation (marked in pink): F103, I107 and I115. (B) NAC domain of Egd2. Four hydrophobic amino acids were replaced in separate mutants with an amber stop codon (marked in green): L23, I24, L27 and F66. (C) UBA domain of Egd2. Three hydrophobic amino acids were replaced in separate mutants with an amber stop codon (marked in yellow): L142, L165 and M170. (D) N-terminal region of Egd1. L27, directly situated in the ribosome binding domain of Egd1 (marked with an arrow) was replaced by an amber stop codon. (E) C-terminus of Egd1, which is possibly involved in substrate binding. The residues V147 and V156 were replaced in separate mutants by an amber stop codon (marked with arrows). (F) N-terminal region of Egd2. L13 at the beginning of the NAC domain but not part of a hydrophobic patch was replaced by an amber stop codon (marked with an arrow).

5.4.3 First detection of crosslinking products

The four constructs that showed the most promising crosslinking products during the test phase were investigated more closely. Two of them carried a mutation in Egd2 and two in Egd1. One of the mutations present in Egd2 was located at leucine 27 on the surface of the dimerization domain and the other one at leucine 165 on the surface of the UBA domain. The two mutations in the Egd1 subunit were both located on the surface of the dimerization domain. It was the phenylalanine at position 103 and the isoleucine at position 115.

For the analysis two cultures of each mutant were inoculated with and without pBpa. Each of these cultures was split in two parts with one being subjected to UV-light. This allowed analysing the specificity of the reaction, i.e. if the crosslinking product only appeared when the culture was grown in the presence of pBpa and subjected to UV-light. Samples were taken from each condition for each construct analysed. Western blotting of all tested constructs revealed a background expression level: The subunit, where pBpa should be incorporated was also detected when no pBpa was present in the medium (Fig. 54). This indicates that the expression conditions are not optimal so far. Nevertheless, expression generally increased when pBpa was present during growth.

The crosslink determined for the construct in which pBpa was incorporated at position L27 in Egd2 was specific; it only appeared when pBpa was present during growth and activated via UV-light (Fig. 54 A). It was detected at a height corresponding to about 55 kDa. The crosslink detectable when pBpa was incorporated at position L165 was also specific. In contrast to the crosslink detected at position L27 the crosslink at position L165 had a molecular weight of slightly more than 100 kDa. L27 as opposed to L165 is located on the surface of the dimerization domain. L165 is situated in the hydrophobic patch on the surface of the UBA domain. According to the size, two different crosslinks at these two positions were detected.

The crosslink appearing when pBpa was incorporated at position F103 on the surface of the dimerization domain of Egd1 had about the same size as the one observed for L27 in Egd2 (Fig. 54 B). This crosslink was specific as well as it only appeared in the combination of the presence of pBpa and exposure to UV-light. The crosslink at position I115 was detectable at the same height in the SDS-gel as the one for F103. This is not surprising as both positions are located in the same hydrophobic patch. The crosslink detected for I115 was also specific as were all others before.

In sum, first crosslinks of the subunits of NAC could be detected *in vivo*. For future experiments, the expression conditions need to be improved and the crosslinks need to be investigated more closely for example with mass spectrometry.

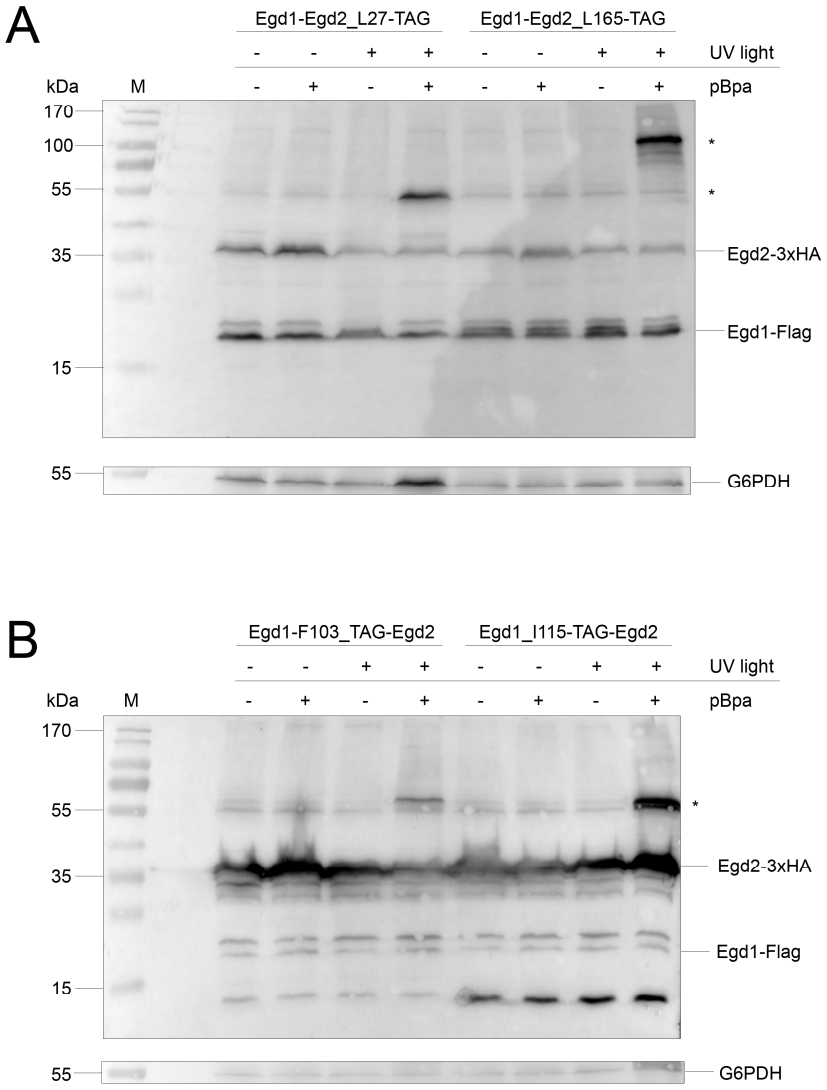

Fig. 54: Testing of the specificity of the crosslinks of four constructs. Cells were grown to an OD_{600} of 0.4 – 0.6. Cultures were then diluted and pBpa was added as indicated. Afterwards cells were grown to an OD_{600} of around 1.5. Cells were harvested by centrifugation, split in two and either subjected to UV-light or normal light. Samples were run on a 12% SDS-PAGE and blotted onto nitrocellulose membranes which were probed with an antibody against NAC. G6PDH was used as loading control. (A) Positions 27 and 165 in Egd2 were tested. (B) Positions 103 and 115 of Egd1 were tested. *: crosslink.

6. Discussion

NAC was first described in the early nineties (Wiedmann et al., 1994). Up to date, a lot of different functions were proposed for the individual subunits of NAC and the complex, amongst others a role in protein aggregation as well as in protein folding and transport (Bukau et al., 2000; Hartl and Hayer-Hartl, 2002; Rospert et al., 2002; Wegrzyn and Deuerling, 2005; Olzscha et al., 2011; Kirstein-Miles et al., 2013; Ott et al., 2015). NAC was recently observed to interact with artificial protein aggregates and our lab found NAC associating with ageing and heat shock dependent aggregates in *C. elegans* (Olzscha et al., 2011; Kirstein-Miles et al., 2013). We could further deduce a negative regulatory role for the UBA domain of α-NAC in prevention of protein aggregation in yeast (Ott et al., 2015). However, which region of NAC interacts with substrates is still unknown. To investigate the role and mechanisms of action of NAC in aggregation more closely, it was analysed in different *in vivo* and *in vitro* experiments.

6.1 Role of NAC in protein aggregation

Expression of highly aggregation prone polyglutamine-expansion proteins or Aβ-peptides depleted NAC from ribosomes in *C. elegans* and caused it to shift to the arising aggregates. The same was observed for aggregates induced by ageing. Subjecting the worms to heat shock also led to relocalization of NAC to aggregates. Lack of NAC greatly reduced the dissociation capability after heat shock of aggregated firefly luciferase (Kirstein-Miles et al., 2013). These observed effects are similar to the functions described for the yeast small heat shock protein Hsp26. It interacts with aggregating proteins and keeps them in a folding competent state. This interaction facilitates the subsequent resolubilization by Hsp104 and the Hsp70/40 system (Haslbeck et al., 1999; Haslbeck, 2002; Cashikar et al., 2005). In yeast, a chaperone function of NAC might be similar to that observed for Hsp26. Therefore it was tested, if NAC did behave like Hsp26 in *S. cerevisiae*.

First, aggregates were prepared from heat shocked yeast cells and investigated for Hsp26 association according to the protocol published by Cashikar et al. (2005). As described, Hsp26 was found to associate with the heat shock induced aggregates and their resolubilization depended on Hsp104 (Fig. 15) (Cashikar et al., 2005). The fact that this result was the same in wt and in *nacΔ* cells indicates that NAC and Hsp26 do not to work in the same pathway. No shift of the two NAC subunits to the pellet fraction upon heat shock occurred (Fig. 16). Only upon recovery a slight increase of Egd2 and Egd1 in the pellet fraction was detectable. This might indicate a role for NAC in the resolubilization of aggregates. Even so, the mechanism involved in such a function would be distinct from that

of Hsp26. Hsp26 needs to be present during the aggregation process and incorporates the aggregating proteins into higher oligomeric structures (Shashidharamurthy et al., 2005; Stengel et al., 2010; Braun et al., 2011; McHaowabet al., 2012; Hiltron et al., 2013; Peschek et al., 2013; Haslbeck and Vierling, 2015). This is plainly in contrast to the observed behaviour of NAC. In *hsp104Δ* cells, the increase of Egd2 in the pellet fraction upon recovery was significant when compared to untreated conditions. A greater need for the help of NAC in the resolubilization of aggregates may arise in yeast cells depleted of Hsp104. This would be consistent with the important role for NAC observed in nematodes (Kirstein-Miles et al., 2013), as higher eukaryotes do not possess a homologue to Hsp104.

The buffers used for aggregate preparation contained a detergent. Kirstein-Miles et al. (2013) had observed that NAC was washed off aggregates when detergent was present in the buffer. When analyzing the distribution of NAC in detergent-free buffer, no changes in its localization were observed (Fig. 17). Hence, in yeast cells the absence of an association of NAC with aggregates was not due to an influence of detergents.

Another possibility for the lack of a shift of NAC to aggregates upon heat shock might be the experimental protocol. The protocol used might not be suitable for detecting differences in NAC localization. To eliminate this option, another method for aggregate preparation was used. Again, no shift of NAC to the pellet fraction upon heat shock was detectable (Fig. 18). In addition, a shift to the pellet fraction upon recovery was only observable in *hsp104Δ* cells. When quantifying the amount of NAC in the pellet fraction, the mean standard deviation was much greater than the one observed for the other experiments.

In sum, no shift of NAC to aggregates upon heat shock was observed. Only during the recovery period a slight increase was detectable. This behaviour is unlike that observed for Hsp26. Higher eukaryotes do not contain a homologue to the Hsp104 disaggregase. Instead, a system comprised of Hsp40s, Hsp70 and Hsp110 was shown to be responsible for disaggregation in nematodes and humans (Nillegoda et al., 2015; Yu et al., 2015). An additional role for NAC in this system is conceivable. Hence, it might be possible that NAC also plays a role in disaggregation of heat shock induced aggregates in yeast albeit this role might not be as important for the survival of the cell in the presence of Hsp104.

No direct evidence for an interaction of NAC with aggregates upon heat shock was gained by these biochemical experiments. To validate this result, fluorescence microscopy was used for the investigation of NAC localization upon heat shock. To visualize aggregates, the aggregation prone model protein luciferase was tagged with the fluorophore mCherry (Bachelor thesis Lisa-Marie Haiber, 2015). NAC was tagged with yEGFP at the C-terminus of Egd1. The tag did not impair NAC function. It was still able to complement the pleiotropic growth defect of *nacΔssbΔ* cells (Fig. 19) and was still able to bind to ribosomes (Fig. 21).

Interestingly, when checking the expression levels of the tagged NAC construct, the band representing the tagged Egd1 subunit was much stronger than the untagged one (Fig. 20). The expression level of Egd2 was unchanged compared to untagged NAC. The most likely explanation would be an improved detection of the tagged subunit by the NAC antibody. Other reasons might be an increased stability of Egd1-yEGFP or that it is actually expressed at higher amounts than untagged Egd1. This seems to be unlikely, as the expression levels of Egd2 did not increase and the two subunits were expressed from the same plasmid. Furthermore, NAC was found to be present as a heterodimer *in vivo* (Reimann et al., 1999; Beatrix et al., 2000; Franke et al., 2001). Therefore it is likely, that just the detection by the antibody was improved by an unknown mechanism. To summarize, the C-terminal tag at the Egd1 subunit did not negatively influence NAC function. This is in contrast to what we observed in *C. elegans* (unpublished data of Dr. M. Gamerdinger) where a tag at the C-terminal end strongly impaired NAC function. Why a C-terminal tag can be used in yeast but not in *C. elegans* is unclear so far. However, data from our lab indicate that the structure of the αβ-NAC heterodimer is more labile in *C. elegans*.

As positive control for the fluorescence microscopy experiment Hsp104 was used. It is the main disaggregase in yeast where it works together with the Hsp70/40 system and should therefore be found at aggregates (Parsell et al., 1994 b). Indeed, Hsp104 co-localized with luciferase aggregates formed upon heat shock (Fig. 22). With time, aggregates were resolved and luciferase and Hsp104 resumed their cytosolic localization. To rule out a possible influence of the tag on the behavior of NAC it was expressed on its own under control of the *EGD1* promoter. Upon heat shock, yEGFP maintained its cytosolic localization and did not aggregate (Fig. 23). Hence, a potential co-localization of NAC would not be caused by aggregation of the fluorescent tag. Co-expression of NAC with luciferase during heat shock did not result in a shift of NAC localization: Luciferase was localized in aggregates, whereas NAC stayed evenly distributed throughout the cytosol (Fig. 24). Interestingly, after 90 min some cells did still contain one aggresome-like structure which was not observed in cells lacking NAC. This could also be observed when only the tagged Egd1 subunit without Egd2 was expressed (data not shown). This either hints that ribosome-association of NAC is necessary to form this structure or that Egd1 is sufficient. As Egd1 was found to associate with *EGD1* granules which also contain P-body components, it is feasible, that Egd1 might be responsible for this phenomenon (Hayashi et al., 2011). It might be an additional measure of protecting the cell under stress conditions. It seems therefore, that NAC interacts transiently with arising aggregates and has some sort of influence on them. This is in accordance with the data gained by the biochemical experiments.

6.2 *In vitro* analysis of NAC

NAC is described to be a heterodimer of one α- and one β-subunit. Functions for single subunits have been described (Zheng et al., 1997, Zheng et al., 1990; Parthun et al., 1992; Hu and Ronne, 1994; Yotov et al., 1996; Moreau et al., 1998; Yotov et al., 1998; Munz et al., 1999; Baghdoyan et al., 2000; Thiede et al., 2001; Goatley et al., 2002; Bloss et al., 2003; Stilo et al., 2003; Al-Shanti et al., 2004; Akhouayn et al., 2005; Freire 2005; Li et al., 2005; Arsenovic et al., 2012; Hradetzky et al., 2013; Zeng et al., 2014; Li et al., 2015) albeit they only seem to occur in living cells when the balance of α- and β-NAC is disrupted experimentally (Reimann et al., 1999; Beatrix et al., 2000; Franke et al., 2001). No higher oligomeric structures of NAC have been described so far. To analyse if purified NAC is able to form higher oligomers, analytical ultracentrifugation was performed (Fig. 31). The results showed that NAC is mainly present as a dimer. However, two smaller peaks were detected that correspond to a dimer and to a tetramer of heterodimers. Hence, NAC seems to form higher oligomeric structures *in vitro* even though the majority is present as dimers. As higher oligomeric structures of NAC have not been detected so far, a possible *in vivo* role of them is still obscure. It might be a possibility for cells to keep the balance of the NAC subunits intact. If one subunit gets depleted, the other might form higher oligomeric structures to avoid potentially harmful interactions. Another possibility might be that it is some kind of storage form. We showed that NAC acts as a sensor for proteostasis in *C. elegans*. Upon stress and formation of aggregates, NAC was depleted from ribosomes due to its association with aggregates and translation was reduced (Kirstein-Miles et al., 2013). In yeast NAC does not seem to interact with these aggregates in the same way. Nevertheless, it might still fulfil a role as proteostasis sensor. NAC may still dissociate from the ribosome but instead of associating with aggregates it might be stored in higher oligomeric structures until it is needed again, for example in disaggregation. Further experiments are required to test these hypotheses.

The biochemical and fluorescence microscopy experiments did not reveal a stable interaction of NAC with aggregates. This is consistent with the results gained from size exclusion chromatography (Fig. 33 and 34). Upon heat shock, the control protein Hsp26 associated with the aggregating model substrates citrate synthase and luciferase. NAC, however, did not stably associate with aggregates. Only transient interactions were evident in these experiments. This observation is in line with the data gained from fluorescence microscopy which implied a transient interaction of NAC with arising aggregates. In contrast, NAC was detected on different aggregates in *C. elegans* as well as on artificially constructed ones (Olzscha et al., 2011; Jacobson et al., 2012; Kirstein-Miles et al., 2013). These contradictory results might originate in a variable interaction behaviour of NAC with diverse aggregates.

This might even vary between yeast and higher eukaryotes as in *C.* elegans NAC was found to associate with heat shock aggregates (Kirstein-Miles et al., 2013). Another explanation could be that NAC needs additional factors to associate in a non-transient manner with aggregates which are absent in yeast as well as in *in vitro* experiments. Nevertheless, the observed transient interaction might still have an effect on the inactivation/aggregation or reactivation/disaggregation behaviour of proteins *in vitro*.

First, the influence of NAC on the inactivation of citrate synthase was investigated (Fig. 35). Hsp26, as expected, clearly slowed down the inactivation of citrate synthase. NAC hardly showed an effect when the same concentration as for Hsp26 was used. Only by doubling the amount of NAC a visible effect was accomplished. This effect, however, was still not as prominent as the one observed for Hsp26. These results do not support an important role of NAC in slowing down the inactivation of proteins supporting the results gained by the biochemical experiments that NAC does not associate with proteins in the process of aggregation. Interestingly, bovine serum albumin (BSA) also showed a dose-dependent slightly positive effect on the inactivation of citrate synthase. The interaction of another protein with citrate synthase might generally slow down the inactivation. This possibility needs to be investigated more closely in future.

Next, the influence of NAC on the reactivation of luciferase was tested (Fig. 36 B). NAC clearly improved reactivation of luciferase. If only NAC was present during reactivation it was already enhanced. This effect got more pronounced when the Hsp70/40 system was present as well. This pathway might be the one observed and possibly optimized in *C. elegans* (Kirstein-Miles et al., 2013) and the reason why NAC was found to interact with artificially induced aggregates and amyloid fibrils (Olzscha et al., 2011; Jacobson et al., 2012). When the whole reactivation system of yeast was present together with NAC, reactivation levels of luciferase were highest. NAC seems to be interacting with the Hsp70/40 system during reactivation which indicates a role for the complex in the disaggregation system discovered in higher eukaryotes (Nillegoda et al., 2015; Yu et al., 2015). This finding is also in accordance with the observed biochemical data, where more NAC was found in the pellet fraction upon recovery, supporting a role for NAC in reactivation. In Fig. 36 A, hardly any improvement of reactivation was observed even in the presence of the whole aggregation machinery. This is unexpected and indicates that luciferase might have formed aggregates which could no longer be resolved properly.

To directly monitor the aggregation process and a possible effect NAC might have on it, light scattering experiments with citrate synthase and luciferase were performed (fig 37). NAC was either expected to reduce aggregation or to have no effect whatsoever. Surprisingly, NAC increased the aggregation of both citrate synthase and luciferase dose-independently.

When NAC was incubated alone or with BSA at 43°C, no aggregation occurred indicating an effect specific for aggregation prone proteins. When Hsp26, which is known to suppress aggregation, was present in addition, aggregation was prevented. Pelleting of aggregates after light scattering revealed no shift of NAC to the pellet fraction. This indicates that the interaction of NAC with citrate synthase and luciferase during the process of aggregation seems to be a transient one which is in accordance with the results obtained via size exclusion chromatography and immunofluorescence. How NAC influences the aggregation of citrate synthase and luciferase is obscure so far. It might initialise the formation of larger aggregate frameworks, maybe even more loosely ones. These might then tend to form aggresome-like structures *in vivo*, which could be one possible explanation for the observed appearance in the fluorescence microscopy experiment. The formation of these structures might be beneficial under stress conditions, by keeping them in a folding-competent state without affecting native proteins. It could be one mechanism by which NAC supports resolubilization and refolding of aggregating proteins in higher eukaryotes.

The different NAC variants tested in light scattering, namely the ribosome binding deficient mutant, the Egd2 subunit alone as well as *C. elegans* NAC and a ribosome binding deficient mutant thereof, all displayed the same effect as native yeast NAC. Hence, the interaction site of NAC is not influenced when mutating the ribosomal binding site. Furthermore, Egd2 was sufficient for the observed NAC effect. In the fluorescence microscopy experiment Egd1 was sufficient for the formation of the aggresome-like structure. The two NAC subunits might function independently of each other in the process of aggregate resolubilization or both might have the same effect on the aggregated proteins rendering one subunit sufficient for this activity. This is in accordance with the many published roles for individual subunits for NAC which might also fulfil these roles being part of homodimers (Zheng et al., 1997, Zheng et al., 1990; Parthun et al., 1992; Hu and Ronne, 1994; Yotov et al., 1996; Moreau et al., 1998; Yotov et al., 1998; Munz et al., 1999; Baghdoyan et al., 2000; Thiede et al., 2001; Goatley et al., 2002; Bloss et al., 2003; Stilo et al., 2003; Al-Shanti et al., 2004; Akhouayn et al., 2005; Freire 2005; Li et al., 2005; Arsenovic et al., 2012; Hradetzky et al., 2013; Zeng et al., 2014; Li et al., 2015). No difference was found in the behaviour of yeast and *C. elegans* NAC even though an active role for NAC in the aggregation processes of nematodes was described (Kirstein-Miles et al., 2013). This might again point to missing factors *in vitro* necessary for this interaction.

Interestingly, BSA showed a slightly positive effect as was observed before during the inactivation of citrate synthase. This might again be just a general effect of the presence of another protein on luciferase or citrate synthase aggregation. It remains to be investigated if other non-chaperone proteins have the same effect as BSA.

6.3 Domain functions of the NAC subunits

So far, the only functional site identified for NAC is the ribosome binding site (Franke et al., 2001; Wegrzyn et al., 2006; Pech et al., 2010). How NAC binds its substrates is still not known. To gain further insights into the protein sequence and structure of NAC and to determine the substrate binding sites in the end, bioinformatics analysis was performed. This analysis was already part of my Master Thesis which I prepared in due course of the Konstanz Fast Track Programme. In addition to this analysis, limited proteolysis was performed to identify domain boundaries and easily accessible and therefore possibly very flexible regions of NAC. To analyze structural changes evoked by mutations, circular dichroism measurements were performed. These allowed detecting changes in the secondary structure composure in comparison to native NAC.

Proteinase K is an unspecific protease. When digesting a protein with it, proteinase K first cleaves it at easily accessible sites therefore allowing better insights into the structure of the digested protein. Detailed analysis of the alignments and the structure model were necessary for the interpretation of the results gained by limited proteolysis and subsequent mass spectrometry analysis. Limited proteolysis was performed with two different concentrations of NAC to investigate, if there exist concentration-dependent differences in the NAC structure. Using 0.5 mg/ml NAC, the NAC domain of Egd1 was very stable in contrast to the N- and C-terminal extensions (Fig. 42). When 1 mg/ml NAC was present, digestion per se proceeded more slowly and the N- and C-terminal regions were not cleaved as fast (Fig. 44). The most stable part of Egd1 seems to be the NAC domain responsible for dimerization. The N- as well as the C-terminal extensions are quite flexible. The structure of the subunit does not appear to change in a concentration-dependent manner.

In the other subunit, Egd2, the NAC domain was not as stable as in Egd1 (Fig. 43). Surprisingly, the most stable region appeared to be the linker region between the NAC and the UBA domain, even so the UBA domain itself was also quite stable. When using 1 mg/ml NAC the cutting pattern differed from the one observed for 0.5 mg/ml NAC (Fig. 45). This effect was in contrast to what was observed for Egd1. Cuts appeared in Egd2 at regions previously protected. One reason for this could be structural rearrangements in the subunit. During analytical ultracentrifugation of 0.87 mg/ml of NAC, higher oligomeric structures of it were detected. It is possible, that these structures were formed when 1 mg/ml NAC was present and, therefore, the accessibility for proteinase K changed. The experiments indicate that possible structural rearrangements would mainly occur in Egd2, which, therefore, might be responsible for the formation of higher oligomers, involving for example the UBA domain and the linker region. These potential structural rearrangements might also play a role in the observed effect of NAC on the aggregation of model proteins, by being responsible for the potential formation of an aggregate framework. Compatible with these observations, a role

for the UBA domain in regulating the stability of Egd2 as well as Egd1 was proposed (Panasenko et al., 2006).
The structural flexibility of NAC might be the reason for its reported interaction with a variety of different proteins and aggregates and might also be necessary to fulfil its various functions which, in part, may differ considerably.

To determine potential substrate binding sites from the sequence of NAC, the generated alignments were investigated. Considerable differences were observed in the C-termini of the two β-subunits of NAC (Egd1 and Btt1) (Fig. 50). The last 16 amino acids of Btt1 could not be aligned to the end of the C-termini of all other eukaryotes, including Egd1. In addition, the protein sequence of Btt1 is shorter than that of Egd1 by 8 amino acids. The similarity of the C-termini was only 30.8% with an identity of 10.3%. These values were clearly below the average for the whole sequence. Furthermore, the net charges of the C-termini also differ: Much more negatively charged amino acids are present in Egd1 than in Btt1. As different substrate specificities were already described for the two heterodimeric complexes in yeast (del Alamo et al., 2011) the observed differences in the C-termini strongly support a role in determining substrate specificity. However, no clear evidence for this suggestion exists so far. Initial experiments were performed by my colleague Ann-Kathrin Ott in her PhD thesis. Interestingly, the β-subunits of all other eukaryotes were aligned to Egd1, not to Btt1: Their C-termini were clearly more similar to that of Egd1. As higher eukaryotes do not possess a Btt1 homologue it stands to debate, whether the Egd1 homologue carries out the function of Btt1 in addition or whether another protein takes over.

In the limited proteolysis experiments, the UBA domain of Egd2 was revealed to be quite stable. The function of this domain was unknown for a long time. In Ott et al. (2015) we showed, that it plays a role in the aggregation prevention activity of NAC *in vivo*. A mutant lacking the UBA domain and part of the linker region was the most potent version in reducing aggregation levels in *nacΔssbΔ* cells. To investigate this finding more closely, *in vitro* studies with different ΔUBA variants were conducted. One of the variants was constructed based on the one used in Ott et al. (2015). For the second, the cutting site in the linker region determined with proteinase K was used and the third mutant lacked the UBA domain as well as the whole linker region. When comparing circular dichroism spectra of native NAC and the ΔUBA versions to reveal possible induced changes in the secondary structure, the most prominent feature was the covered range on the y-axis (Fig. 48). The mutants covered a much lower range than native NAC indicating a loss of secondary structure elements. The predicted amount of α-helices was below the amount predicted for native NAC. This is in accordance with the deletion of the UBA domain which consists mainly of three α-helices.

However, the amount of β-sheets was also predicted to be reduced in the mutants even though no β-sheets are present in the UBA domain. This indicates an influence of the deletions on the whole structure of NAC. The effect was most prominent in the mutant lacking the UBA domain and the complete linker region, where the predicted amount of β-sheets was reduced by half compared to native NAC. Substantial conformational changes seem to occur in this mutant. The mutant based on Ott et al. (2015) and the one created by using the cutting site identified by proteinase K were relatively similar. This was expected, as they differ in length by one amino acid only. However, the mutant with the proteinase K cutting site displayed shorter α-helices and longer β-sheets in comparison to the other mutant, even if the total number of α-helices and β-sheets was about the same. This indicates that even small differences in the protein sequence can visibly impact the secondary structure of NAC.

Next the mutants were tested for any differences in their effect on luciferase aggregation *in vitro* compared to native NAC (Fig. 49). However, nearly all mutants had the same effect as wt NAC: Aggregation of luciferase was increased. Only a twofold excess of the mutant with the proteinase K cutting site did not augment aggregation of luciferase. A fourfold excess led again to increased aggregation. It could be, that the interaction site in this mutant is somehow obscured which is compensated for at higher concentrations. Like native NAC, none of the mutants aggregated on its own when subjected to heat shock. Aggregation prevention of NACΔUBA *in vivo* affected aggregates caused by misfolding directly after translation (Ott et al., 2015). A possible effect on aggregates induced by heat shock was not investigated in that study. It could be that NAC directly intervenes with the misfolding of newly synthesized proteins at the ribosome. Lack of the UBA domain might be able to simplify the access for nascent chains to NAC. This mechanism is different to the one needed when native proteins start to aggregate providing a simple explanation for the observed effect *in vitro*. It is also possible, that the deletion of the UBA domain *in vivo* might prevent NAC from forming higher oligomeric structures upon stress if they are present in living cells. This would allow more NAC to tackle emerging aggregates. This explanation also supports the observed *in vitro* effects. The effects observed *in vitro* and *in vivo* (Ott et al., 2015) clearly point to two different functions or mechanisms of NAC.

6.4 Crosslinking of NAC to possible substrates and nascent chains *in vivo*

To deduce the substrate binding site(s) of NAC, *in vivo* crosslinking experiments were planned. First experiments to achieve this goal were performed in due course of this thesis. First, the modelled structure of yeast NAC was investigated for prominent hydrophobic

patches as it is most likely that NAC will interact with unfolded or aggregation prone proteins via such patches. As only the dimerization and the UBA domain could be modelled, these parts of the sequence could be searched. Three prominent patches were identified, one each on the surface of the dimerization domain of Egd1 and Egd2 and the UBA domain. The patches were then investigated for amino acids which could be replaced with the bulky unnatural amino acid pBpa. In addition to ten amino acids in the hydrophobic patches, four outside of them were chosen. Two of them were located in the C-terminus of Egd1, which is supposedly involved in substrate binding.

To pull at both subunits separately for immunoprecipitation they were both tagged C-terminally. Egd1 was tagged with Flag and Egd2 with 3xHA. Interestingly, this tagged version of NAC seemed to be more competent in complementing the pleiotropic growth phenotype of *nacΔssbΔ* cells than native NAC (Fig. 52). However, the cells expressing the native NAC construct were spotted at the plate border where nutrition is limiting. This might account for the observed growth deficiency.

All constructed mutants were tested for expression and ribosome binding. Mutations at two positions in Egd2 led to complete lack of NAC in the cell (L13 and M170). Not only Egd2 but also Egd1 was no longer expressed. These mutations probably affected the structure of Egd2 in a way that also affected Egd1 which then led to degradation of both subunits. Two further mutations, one in Egd2 (F66) and one in Egd1 (L27) abolished the expression of the respective subunits. The other subunit was still expressed, albeit at lower levels. This is in accordance with Reimann et al. (1999) which found, that if one NAC subunit is missing, the expression of the other subunits is downregulated. All other mutants were expressed and able to bind to ribosomes.

Incorporation of pBpa at position L142 of Egd2 or at the defined positions in the C-terminus (V147, V156), did not produce a detectable crosslink. It may be that at these positions no interactions with other proteins take place. It is still possible, however, that they might interact with nascent chains or the corresponding mRNA (del Alamo et al., 2011). In all other mutants crosslinks were detectable. Except for the one at position L165 in the UBA domain of Egd2, all crosslinks showed a molecular weight of 55 kDa. This size is too big for a heterodimer but too small for a higher oligomeric structure, indicating another interaction partner. The crosslink appearing at position L165 had a molecular weight of slightly more than 100 kDa. To determine the proteins crosslinked here, mass spectrometry analysis should be performed.

To study interaction kinetics of NAC with nascent chains, experiments with S^{35} need to be performed. S^{35} is incorporated into nascent chains and can be detected by autoradiography. Together with the detected crosslinks this could help analysing the kinetics of NAC interaction.

At the moment, the read-through of the integrated stop codon is quite high (Fig. 50). To reduce this read-through, another strain could be used for the experiment. The lab of Thomas Sommer, which kindly provided the plasmid encoding for the tRNA that incorporates pBpa, used the strain DF5 (Biederer et al., 1997) for *in vivo* experiments. To use this strain for the described crosslinking experiments, NAC needs to be deleted first in the chromosomal DNA.
In a next step, the interactome of NAC could be analysed with this method. Different conditions, for example heat shock, could be used to investigate the changes of NAC interaction upon environmental alterations *in vivo*.

No clear chaperone function of NAC could be identified in this study. It was clarified, that NAC does not function in the same way as the small heat shock protein Hsp26. However, a role for NAC in disaggregation processes is possible, maybe going hand in hand with structural rearrangements. NAC might even react differently to varying sorts of aggregates, as the lack of the UBA domain *in vivo* had a clear effect in aggregation prevention but no such effect was observed *in vitro* on aggregating luciferase. Crosslinking of NAC *in vivo* will shed further light on its interactome and help to unravel its potential various functions in the cell.

7. Material and Methods

7.1 Materials

7.1.1 Equipment and software

Equipment

Balances	Sartorius
Camera (microscope)	LEICA DFC 365 FX
CD instrument, J-815 super	Jasco
Centrifuges	Sorvall, Heraeus, Eppendorf
Cryofuge 8500 i	Heraeus
FastPrep	MP
FPLC-ÄKTA Purifier	GE Healthcare
French Press	SIM AMINCO
HPLC 2000 system	Jasco
Image Quant LAS 4000 mini	GE Healthcare
Incubators	Thermo Scientific, Infors HT, Heraeus
Microflex MALDI-TOF	Bruker
Microscope (fluorescence)	Leica DM5500B
Mini UZ M150SE	Sorvall
Multifuge 4	Heraeus
NanoPhotometer NP80	Implen
NanoVue	GE Healthcare
Objective (microscope)	HCX P2 FLUOTAR 100x 1.30 oil
Optima X-LA analytical ultracentrifugation	Beckmann
PCR	BioRad, analytic jena
pH-Meter 766	Knick
Scanner	Canon
SDS gel chamber	BioRad and custom made
Sonifier	Branson
Spectrophotometer Ultraspec 3100 pro	Amersham
Spectrophotometer Ultrospec 7000	GE Healthcare
Starion FLA 9000	FujiFilm
Tecan Reader GENios	Tecan
Thermomixer comfort	Eppendorf
Typhoon FLA 9500	GE Healthcare
UV-lamp	UVP

V-730 UV-Visible/NIR Spectrophotometer	Jasco
Western Blot apparatus, wet blot	BioRad and custom made

Software

Adobe Photoshop, Illustrator, Acrobat
PSI-BLAST (Position Specific Iterative-Basic Local Alignment and Search Tool)
alneditor
CLANS (cluster analysis of sequences)
EndNote
Fiji / Image J
ImageQuant LAS 4000.Ink
LAS AF (Leica)
Microsoft Office 2011
muscle
pyMOL
Serial Cloner 1-3
Sigma Plot
Jasco Spectra-Manager-Software-II
self-written perl programmes
SWIFT II Reaction Kinetics (GE Healthcare)

7.1.2 Chemicals

All chemicals were of analytical grade and ordered from Sigma Aldrich, Roth, Bachem, BD, Fluka, Merck, BioRad or AppliChem.

7.1.3 Lab buffers and solutions

Laemmli buffer	50 mM Tris-HCl, pH 6.8
	2 mM EDTA, pH 8.0
	1% (w/v) SDS
	1% (v/v) β-Mercaptoethanol
	10% (v/v) Glycerol
	7 mg/ml Bromophenol blue
Alkaline sample buffer	200 mM Tris-base
(solution 1)	20 mM EDTA, pH 8.8

Alkaline sample buffer (solution 2)	8.3% (w/v) SDS 83.3 mM Tris-base 29.2% (v/v) Glycerol 0.03% (w/v) Bromophenol blue
Alkaline sample buffer	Mixing of solution 1, solution 2 and H_2O in a ratio of 5:4:1 and addition of 2% (v/v) β-Mercaptoethanol
SDS running buffer	25 mM Tris 200 mM Glycine 1% (w/v) SDS
Western Blot transfer buffer	25 mM Tris 192 mM Glycine 0.02% (w/v) SDS 20% (v/v) Methanol
TBS	50 mM Tris-HCl, pH 8.0 150 mM NaCl
TBS-TT	50 mM Tris-HCl, pH 8.0 150 mM NaCl 0.2% (v/v) Tween-20
Coomassie blue staining solution	0.6% (w/v) Coomassie R250 50% (v/v) Methanol 10% (v/v) Acetic acid
Destaining solution	50% (v/v) Methanol 10% (v/v) Acetic acid
Fixation solution (sensitive Coomassie staining)	12% (w/v) Trichloroacetic acid
Coomassie G250 solution (sensitive Coomassie staining)	5% (w/v) Coomassie G250

Solution A (sensitive Coomassie staining)	12.5% (w/v) $(NH_4)_2SO_4$ 2.5% (v/v) H_3PO_4
Staining solution (sensitive Coomassie staining)	Mixing of Solution A and Methanol in a ratio of 4:1, addition of 2% Coomassie G250 solution
Destaining solution (sensitive Coomassie staining)	20% (w/v) $(NH_4)_2SO_4$
PonceauS staining solution	0.15% (w/v) PonceauS 5% (v/v) Acetic acid
Fixation solution (silver staining)	50% (v/v) Methanol 12% (v/v) Glacial acetic acid 0.05% (v/v) Formaldehyde
Pre-staining solution (silver staining)	0.02% (w/v) $Na_2S_2O_3$
Staining solution (silver staining)	0.1% (w/v) $AgNO_3$ 0.05% (v/v) Formaldehyde
Washing solution (silver staining)	50% Methanol
Developing solution (silver staining)	2% (w/v) Na_2CO_3 2 ml (v/v) of pre-staining solution 0.05% (v/v) Formaldehyde
4x SDS-stacking gel buffer	0.5 M Tris-HCl, pH 6.8 0.4% (w/v) SDS
4x SDS-separation gel buffer	1.5 M Tris-HCl, pH 8.8 0.4% (w/v) SDS

50x TAE buffer	2 M Tris 50 mM EDTA pH 8.0 with acetic acid
Phusion polymerase buffer	10 mM Tris-HCl, Ph 8.8 50 mM KCl 2 mM $MgCl_2$ 0.1% (v/v) Triton X-100
Pfu polymerase buffer	40 mM Tris, pH 8.0 200 mM KCl 0.2% (v/v) Triton X-100 0.2 mM EDTA 2 mM DTT
PBS	1.5 mM NaCl 22 mM Na_2HPO_4 3 mM NaH_2PO_4
50 mM PB	54.2 mM Na_2HPO_4 21.3 mM KH_2PO_4
TE buffer	50 mM Tris-HCl, pH 8.0 2 mM EDTA

7.1.4 Columns

Streptactin Sepharose	IBA
Protino Ni-IDA Resin	Machery-Nagel
ResourceQ (anion exchanger)	GE Healthcare - Amersham
ResourceS (cation exchanger)	GE Healthcare - Amersham
TSK gel 4000 PW	Tosoh Bioscience LLC

7.1.5 Markers

GeneRuler 1 kb DNA Ladder	Thermo Scientific
PageRuler Unstained Protein Ladder	Thermo Scientific

PageRuler Prestained Protein Ladder	Thermo Scientific

7.1.6 Proteins and antibodies

Proteins

Aprotinin	Genaxxon
Benzonase	Novagen
Bovine Serum albumin (BSA)	Roth
Citrate synthase	Sigma-Aldrich
Creatinephosphate	Roche
Creatine Phosphokinase	Roche
DNase I	Sigma-Aldrich
Egd2 (α-NAC)	Kind gift of Ann-Kathrin Ott
Fast Alkaline Phosphatase	Fisher Scientific (Fermentas)
His-Ulp1	AG Deuerling
Hsp26	This work and kind gift of Dr. M. Haslbeck (Buchner lab, TU Munich)
Hsp42	This work
Hsp104	This work
Leupeptinhemisulphate	Genaxxon
Luciferase	This work
NAC and NAC mutants	This work
Pepstatin A	Genaxxon
Pfu DNA Polymerase	AG Deuerling
Phosphoenolpyruvate	Sigma-Aldrich
Pyruvatekinase	Sigma-Aldrich
Phusion DNA Polymerase	AG Deuerling
Proteinase K	Sigma-Aldrich
Restriction enzymes	New England Biolabs
Shrimp Alkaline Phosphatase (SAP)	Fisher Scientific (Fermentas)
Ssa1	This work and kind gift of Dr. M. Haslbeck (Buchner lab, TU Munich)
Strep-Ulp1	This work
T4 DNA Ligase	Thermo Scientific
Taq DNA Polymerase	New England Biolabs
Ydj1	This work
Zymolyase 20T	amsbio

Antibodies

Anti-NAC, polyclonal antiserum, rabbit (1:5000)	Lab collection
Anti-NAC (*C. elegans)*, polyclonal antiserum, rabbit (1:5000)	Lab collection
Anti-Ssb, polyclonal antiserum, rabbit (1:20 000)	Lab collection
Anti-Ssa1, polyclonal antiserum, rabbit (1:10 000)	Lab collection
Anti-Hsp26, polyclonal antiserum, rabbit (1:10 000)	Kind gift of Dr. M. Haslbeck (Buchner lab TU Munich)
Anti-Hsp42, polyclonal antiserum, rabbit (1:10 000)	Kind gift of Dr. M. Haslbeck (Buchner lab TU Munich)
Anti-G6PDH, polyclonal, rabbit (1:10 000)	Sigma-Aldrich
Anti-mCherry, polyclonal, rabbit (1:10 000)	antikörper-online
Anti-GFP, monoclonal, mouse (1:10 000)	HISS-Diagnostics
Anti-RPL25, polyclonal antiserum, rabbit (1:10 000)	Lab collection
Anti-RPL17, polyclonal antiserum, rabbit (1:10 000)	Lab collection
Anti-L22, polyclonal antiserum, rabbit (1:10 000)	Lab collection
Anti-Pgk1, monoclonal, mouse (1:10 000)	Invitrogen
Anti-His6, monoclonal, mouse (1:10 000)	Dianova
Anti-HA.11, monoclonal, rabbit (1:10 000)	HISS-Diagnostics
Anti-Ha.11, monoclonal, mouse (1:10 000)	HISS-Diagnostics
Anti-FLAG, monoclonal, mouse (1:10 000)	Sigma-Aldrich
Anti-FLAG, polyclonal, rabbit (1:10 000)	Sigma-Aldrich

7.1.7 Primer

Sites for cutting with restriction endonucleases and bases changed via site directed mutagenesis are marked in lower case letters.

Primer	**Sequence (5' → 3')**
5'-(SpeI)-Prom(EGD1)	ggactagtccGGAGTAGAGAATACCTTAGGCC
EGD1-[BamHI]-rev	cgggatccTTCGACGTCAGCATCAAAAGTTTG
5'-(BamHI)-yEGFP	cgcggatccATGTCTAAAGGTGAAGAATTATTCACTG
3'-(Term(CYC1))-yEGFP	ACATAACTAATTACATGATGCTATTTGTACAATTCAT-CCA
5'-(yEGFP)-Term(CYC1)	TGGATGAATTGTACAAATAGCATCATGTAATTAGTT-ATGT
3'-(SmaI)-Term(CYC1)	tcccccgggggaCAAATTAAAGCCTTCGAGCGTC
5'-(SacI)-Prom(EGD2)	cgagctcgCGAAGGGCAGGGCTTCTAG
3'-(NotI)-Term(EGD2)	gcggccgcattcttatCAAGTTGGCAAAACTCCGTGC
5'-(BsaI)-HSP26	ccagtgggtctcaggtggtATGTCATTTAACAGTCCATTTTT-TGATTT
3'-(XhoI)-HSP26	ccgctcgagTTAGTTACCCCACGATTCTTGAG
5'-(BsmBI)-HSP42	ccagtgcgtctcaggtggtATGAGTTTTTATCAACCATCCCT-ATC
3'-(NotI)-HSP42	ataagaatgcggccgcTCAATTTTCTACCGTAGGGTTGG
5'-(BsmBI)-YDJ1	ccagtgcgtctcaggtggtATGGTTAAAGAAACTAAGTTTTA-CGATATT
3'-(XhoI)-YDJ1	ccgctcgagTCATTGAGATGCACATTGAACACC
5'-(BbsI)-HSP104	gatcgaagacgcggtggtATGAACGACCAAACGCAATTTA-CA
3'-(XhoI)-HSP104	ccgctcgagcggTTAATCTAGGTCATCATCAATTTCCA
5'-(BamHI)-P(EGD2)	cgcggatccGCTGCTATTGACGGTATTCTC
3'-EGD2_Fus(3xHA)	TCTGGTACGTCGTAGGGGTATTTAGACAAGGACAT-GATAGCG
5'-Fus(EGD2)-3xHA	CTATCATGTCCTTGTCTAAATACCCCTACGACGTA-CCA
3'-3xHA-Fus(T(EGD2))	TATAATATATTTTTATATCATTAAGCGTAATCTGGA-ACATCG
5'-Fus(3xHA)-T(EGD2)	ATGTTCCAGATTACGCTTAATGATATAAAAATATAT-TATATAGGGGTA
3'-T(EGD2)-(EcoRI)	ccgggaattcAGAGACCCACTATAATGCTACA

Primer	Sequence (5' → 3')
5'egd1-500bp(EagI)	ccggcggccgGGAGTAGAGAATACCTTAGGCC
3'-T(EGD1)-(BamHI)	cgggatccTTTGCCAGGAAGGATGCTCTAAAA
3'-T(EGD2)-(XmaI)	tcccccgggggaAGAGACCCACTATAATGCTACA
5'-(SpeI)-Prom(EGD2)	ggactagtccCGAAGGGCAGGGCTTCTAG
3'-EGD2-(BamHI)	cgggatccTTTAGACAAGGACATGATAGCGTT
5'-(BamHI)-mCherry_new	cgcggatccGTGAGCAAGGGCGAGGAG
3'-(Term(CYC1))-mCherry	ACATAACTAATTACATGATGTTACTTGTACAGCTCG-TCCATG
5'-mCherry-(Term(CYC1))	GAGCTGTACAAGTAACATCATGTAATTAGTTATGTC-ACGC
3'-(SmaI)-(Term(CYC1))	cccgggCAAATTAAAGCCTTCGAGCGTC
3'-(HindIII)-(Term(CYC1))	ccggaagcttCAAATTAAAGCCTTCGAGCGTC
5'-(SacI)-Prom(EGD1)	cgagctcgGGAGTAGAGAATACCTTAGGCC
3'-Term(EGD1)-(NotI)	gcggccgcAGCTCATCAAGGATGCGATAAAGA
3'-Prom(EGD2)-(BamHI)_new	cgggatccTATCAATTGAGTATGTGGGTGTGT
5'-SDM_EGD2_L23_to_TAG	GAACGAAAAGAAAGCCAGAGAAtagATTGGCAAATT-GGGTTTGAAG
3'-SDM_EGD2_L23_to_TAG	CTTCAAACCCAATTTGCCAATctaTTCTCTGGCTTTC-TTTTCGTTC
5'-SDM_EGD2_I24_to_TAG	CGAAAAGAAAGCCAGAGAATTGtagGGCAAATTGG-GTTTGAAGCAAATC
3'-SDM_EGD2_I24_to_TAG	GATTTGCTTCAAACCCAATTTGCCctaCAATTCTCTG-GCTTTCTTTTCG
5'-SDM_EGD2_L27_to_TAG	GCCAGAGAATTGATTGGCAAAtagGGTTTGAAGCAA-ATCCCAGG
3'-SDM_EGD2_L27_to_TAG	CCTGGGATTTGCTTCAAACCctaTTTGCCAATCAATT-CTCTGGC
5'-SDM_EGD2_F66_to_TAG	GCCGGTGGTAACTACGTTGTCtagGGTGAAGCTAA-GGTTGACAAC
3'-SDM_EGD2_F66_to_TAG	GTTGTCAACCTTAGCTTCACCctaGACAACGTAGTT-ACCACCGGC
5'-SDM_EGD2_L142_to_TAG	CTTGAATAAGGATGATATCGAGtagGTCGTTCAACA-AACTAACGTTTC
3'-SDM_EGD2_L142_to_TAG	GAAACGTTAGTTTGTTGAACGACctaCTCGATATCA-TCCTTATTCAAG

Primer	Sequence (5' → 3')
5'-SDM_EGD2_L165_to_TAG	CCTGAAAGCTCACAATGGTGACtagGTCAACGCTAT-CATGTCCTTG
3'-SDM_EGD2_L165_to_TAG	CAAGGACATGATAGCGTTGACctaGTCACCATTGTG-AGCTTTCAGG
5'-SDM_EGD2_M170_to_TAG	GGTGACTTAGTCAACGCTATCtagTCCTTGTCTAAA-TACCCCTACG
3'-SDM_EGD2_M170_to_TAG	CGTAGGGGTATTTAGACAAGGActaGATAGCGTTGA-CTAAGTCACC
5'-SDM_EGD1_F103_to_TAG	GGAAAAGAACTTGCAAGATTTGtagCCAGGTATTAT-CTCTCAATTGGG
3'-SDM_EGD1_F103_to_TAG	CCCAATTGAGAGATAATACCTGGctaCAAATCTTGC-AAGTTCTTTTCC
5'-SDM_EGD1_I107_to_TAG	GCAAGATTTGTTCCCAGGTATTtagTCTCAATTGGG-CCCTGAAGCC
3'-SDM_EGD1_I107_to_TAG	GGCTTCAGGGCCCAATTGAGActaAATACCTGGGAA-CAAATCTTGC
5'-SDM_EGD1_I115_to_TAG	CTCTCAATTGGGCCCTGAAGCCtagCAAGCCTTGTC-TCAATTGGCTG
3'-SDM_EGD1_I115_to_TAG	CAGCCAATTGAGACAAGGCTTGctaGGCTTCAGGG-CCCAATTGAGAG
5'-SDM_EGD1_V147_to_TAG	GGATGAAGCTATTCCAGAGTTAtagGAAGGTCAAAC-TTTTGATGCTG
3'-SDM_EGD1_V147_to_TAG	CAGCATCAAAAGTTTGACCTTCctaTAACTCTGGAAT-AGCTTCATCC
5'-SDM_EGD1_V156_to_TAG	GGTCAAACTTTTGATGCTGACtagGAAGACTACAAG-GACGACGATG
3'-SDM_EGD1_V156_to_TAG	CATCGTCGTCCTTGTAGTCTTCctaGTCAGCATCAA-AAGTTTGACC
5'-EGD1-TAG-to-TAA	GACTACAAGGACGACGATGACAAGtaaATAACTTAA-TCTTTAATTTTAACG
3'-EGD1-TAG-to-TAA	CGTTAAAATTAAAGATTAAGTTATttaCTTGTCATCG-TCGTCCTTGTAGTC
5'-SDM_EGD2_L13_to_TAG_nC	GAAAACGCCAACGTTACCGTCtagAACAAGAACGA-AAAGAAAGC
3'-SDM_EGD2_L13_to_TAG_nC	GCTTTCTTTTCGTTCTTGTTctaGACGGTAACGTTG-GCGTTTTC

Primer	Sequence (5' → 3')
5'-SDM_EGD1_L27_to_TAG_pC	TTGGTGGTACTAGAAGAAAGtagAACAAGAAGGCA-GGCTCTTC
3'-SDM_EGD1_L27_to_TAG_pC	GAAGAGCCTGCCTTCTTGTTctaCTTTCTTCTAGTA-CCACCAA
3'-(BamHI)-Prom(EGD1)	cgggatccTATGAATTATGAGTCGCGTCTGG
5'-(BamHI)-Luciferase	cgcggatccATGAGCCTCGAAGTTTATCTAAACTACCA-CC
3'-Luciferase-Fus-mCherry	TATCCTCCTCGCCCTTGCTCACTGATCCCACTGCG-ATCTTTCCGCCCTTCTTG
5'-Luciferase-Fus-mCherry	CAAGAAGGGCGGAAAGATCGCAGTGGGATCAGTG-AGCAAGGGCGAGGAGGATA
3'-mCherry-T(CYC1)-(SacI)	agatcgagctcCAAATTAAAGCCTTCGAGCGTCCCA
5'-(BamHI)-EGD2-UBA	cgcggatccCCACATACTCAATTGATAATGTCTG
3'-(SalI)-EGD2-UBA	gtcgacattaTTCGTCATCTTCTTCTGCTGC
3'-(SalI)-EGD2-linker-UBA	gtcgacattaAGCAGCGGCTAGCTTTTGGG
3'-(SalI)-EGD2-UBA-shorter	gtcgacattaATCAACTTCACCTTCTTCGTCATCT
3'-(SalI)-EGD2-UBA-Ansgar	gtcgacattaGTCAGCTTGGATGTCTTCTGG
5'-(XbaI)-EGD2-UBA_558	cctctaga AATAATTTTGTTTAACTTTAAG
EGD1-control-forw	GGTCGGTGTCCAAGTTGCTG
P492 5'SUMO-SSA1, BsaI	ccagtgggtctcaggtggtATGTCAAAAGCTGTCGGTATTG
P493 3'SSA1, SUMO XhoI	ccagtgctcgagTTAATCAACTTCTTCAACGGTTGG
P494 5'SUMO-SSE1, BsaI	ccagtgggtctcaggtggtATGAGTACTCCATTTGGTTTAG
P495 3'SSE1, SUMO XhoI	ccagtgctcgagTTAGTCCATGTCAACATCACCTTC
3'Sonde BTT1	CAGTGCAGTTGTACAGATTGCC
T3	ATTAACCCTCACTAAAGGGA
T7	TAATACGACTCACTATAGGG
pRSET-Rpnew	GGGTTATGCTAGTTATTGC
EGD2 Sonde fw	CTGCTATCCCAGAAAACGC
BTT1-seq-rev (#67)	GATATATCAACGGTGGTATATCCAG
3' EGD2 downstream	ACAAGTTCGCTCTCTCCCTTCA
3' EGD1 downstream	TCTCCATCAGCACACCTACACAT
mCherry_rev_seq	GGTCACCTTCAGCTTGGCGGT
mCherry forw	CCATCGTGGAACAGTACGAAC
P361 3'LUCIseq(697-721)	CAACACTTAAAATCGCAGTATCCGG
3'egd1(PstI)	cgaactgcagTTATTCGACGTCAGCATCAAAAGTTTGA-CC

7.1.8 Plasmids

Name	Description	Source
pRosetta	rare tRNAs, Cm^R	Novagen, Clontech
pSUMO	vector backbone: pET24; T7 promoter; Kan^R	Andréasson et al. (2008)
His6-SUMO-HSP26	His6-SUMO-Hsp26; T7 promoter; Kan^R	This study
His6-SUMO-HSP42	His6-SUMO-Hsp42; T7 promoter; Kan^R	This study
His6-SUMO-YDJ1	His6-SUMO-Ydj1; T7 promoter; Kan^R	This study
His6-SUMO-HSP104	His6-SUMO-Hsp104; T7 promoter; Kan^R	This study
pSUMO-SSA1	His6-SUMO-Ssa1; T7 promoter; Kan^R	Lab collection
His6-Egd2-Egd1	Operon: His6-SUMO-Egd2-Egd1 *C. elegans*); T7 promoter; Amp^R	Lab collection
pOP-H6-EGD2-EGD1	Operon: His6-Egd2, Egd1; T5 promoter; Amp^R	Wegrzyn et al. (2005)
pOP-H6-EGD2-BTT1 #4	Operon: His6-Egd2, Btt1; T5 promoter; Amp^R	Wegrzyn et al. (2005)
pOP-H6-EGD2-RRK/AAA/ EGD1	Operon: His6-Egd2, Egd1 with a mutation in the ribosome binding sequence (RRK to AAA)	Wegrzyn et al. (2005)
pOP-H6-EGD2-partLinker-UBA-EGD1	Operon: His6-Egd2ΔpartLinker ΔUBA, Egd1; T5 promoter; Amp^R	This study
pOP-H6-EGD2-partLinker-UBA(protK)-EGD1	Operon: His6-Egd2ΔpartLinker ΔUBA (protK cutting point); T5 promoter; Amp^R	This study
pOP-H6-EGD2-Linker-UBA-EGD1	Operon: His6-Egd2ΔLinkerΔUBA; T5 promoter; Amp^R	This study
pDS56-Luciferase (firefly)	His6-Luciferase; T5 promoter; Amp^R	Haslberger et al. (2008)

Name	Description	Source
pZA4	lacIq repressor; Spec^R	Lab collection
pRS316	CEN plasmid; Amp^R, URA3	Sikorski and Hieter (1989)
pRS315	CEN plasmid; Amp^R, LEU2	Sikorski and Hieter (1989)
pRS315-EGD1-yEGFP	yEGFP tagged Egd1; EGD1 promoter; Amp^R, LEU2	This study
pRS315-EGD2-EGD1-yEGFP	yEGFP tagged NAC; endogenous promoter; Amp^R, LEU2	This study
pRS315-P(EGD1)-yEGFP	yEGFP alone; EGD1 promoter; Amp^R, LEU2	This study
pRS315-EGD2-mCherry	mCherry tagged Egd2; EGD2 promoter; Amp^R, LEU2	This study
pRS315-EGD1-EGD2-mCherry	mCherry tagged NAC; endogenous promoter; Amp^R, LEU2	This study
pRS315-P(EGD2)-mCherry	mCherry alone, EGD2 promoter; Amp^R, LEU2	This study
p315-HSP104-mCherry	mCherry tagged Hsp104; endogenous promoter; Amp^R, LEU2	Lab collection
pJJ10-HSP104-sGFP	GFP tagged Hsp104; endogenous promoter; Amp^R, LEU2	Lab collection
pEM42-CUP1_N19AA-FFL*-sGFP	GFP tagged firefly luciferase; CUP1 promoter; Amp^R, LEU2	Lab collection
pRS316-FFL-mCherry	mCherry tagged firefly luciferase; CUP1 promoter; Amp^R, LEU2	Bachelor thesis L. Haiber
pRS316-EGD1-Flag-EGD2-3xHA	Flag tagged Egd1, 3xHA tagged Egd2; endogenous promoter; Amp^R, URA3	This study
pRS315-EGD1_TAA-Flag-EGD2-3xHA	Change of stop codon of EGD1 from TAG to TAA; endogenous promoter; Amp^R, LEU2	This study
pRS315-EGD1-Flag-EGD2_L13-3xHA	Incorporation of TAG at aa position	This study

Name	Description	Source
	L27 in EGD2; endogenous promoter; Amp^R, LEU2	
pRS315-EGD1-Flag-EGD2_L23-3xHA	Incorporation of TAG at aa position L23 in EGD2; endogenous promoter; Amp^R, LEU2	This study
pRS315-EGD1-Flag-EGD2_I24-3xHA	Incorporation of TAG at aa position I24 in EGD2; endogenous promoter; Amp^R; LEU2	This study
pRS315-EGD1-Flag-EGD2_L27-3xHA	Incorporation of TAG at aa position L27 in EGD2; endogenous promoter; Amp^R, LEU2	This study
pRS315-EGD1-Flag-EGD2_F66-3xHA	Incorporation of TAG at aa position F66 in EGD2; endogenous promoter; Amp^R, LEU2	This study
pRS315-EGD1-Flag-EGD2_L142-3xHA	Incorporation of TAG at aa position L142 in EGD2; endogenous promoter; Amp^R, LEU2	This study
pRS315-EGD1-Flag-EGD2_L165-3xHA	Incorporation of TAG at aa position L165 in EGD2; endogenous promoter; Amp^R, LEU2	This study
pRS315-EGD1-Flag-EGD2_M170-3xHA	Incorporation of TAG at aa position M170 in EGD2; endogenous promoter; Amp^R, LEU2	This study
pRS315-EGD1_L27-Flag-EGD2-3xHA	Incorporation of TAG at aa position L27 in EGD1; endogenous promoter; Amp^R, LEU2	This study
pRS315-EGD1_F103-Flag-EGD2-3xHA	Incorporation of TAG at aa position	This study

Name	Description	Source
pRS215-EGD1_I107-Flag-EGD2-3xHA	F103 in EGD1; endogenous promoter; Amp^R, LEU2 Incorporation of TAG at aa position I107 in EGD1; endogenous promoter; Amp^R, LEU2	This study
pRS315-EGD1_I115-Flag-EGD2-3xHA	Incorporation of TAG at aa position I115 in EGD1; endogenous promoter; Amp^R, LEU2	This study
pRS315-EGD1_V147-Flag-EGD2-3xHA	Incorporation of TAG at aa position V147 in EGD1; endogenous promoter; Amp^R, LEU2	This study
pRS315-EGD1_V156-Flag-EGD2-3xHA	Incorporation of TAG at aa position V156 in EGD1; endogenous promoter; Amp^R, LEU2	This study
pGK1-pBpa	3 tRNAs for incorporation of pBpa; PGK1 promoter; Amp^R, URA3	Chen et al. (2007)

7.1.9 *E. coli* strains

Strain	Genotype	Source
DH5αZ1	$lacI^q$, *PN25-tetR*, Sp^R, *deoR*, *supE44*, *Δ(lacZYA-argFV169)*, *Phi80 lacZ ΔM15*	Invitrogen
XL1-Blue	endA1 gyr A96(nal^R) thi-1 recA1 relA1 lac glnV44 F'[::Tn10 proAB+ $lacI^q$ Δ(kacZ)M15] hsdR17(r_K-m_K+)	Stratagene
BL21 (DE3)	*F-ara-14 leuB6 thi-1 fhuA31 lacY1 tsx-78 galK2 gakT22 supE44 hisG4 rpsL136 (Strr) xyl-5 mtl-1 dam13::tn9(CamR) dcm-6 mcrB1 hsdR2(rK-mK+) mcrA*	Invitrogen

Strain	Genotype	Source
MH1	*ΔfhuA Δptr ΔhhoAB ssh Δprc::kann degP::Tn10*	M. Ehrmann

7.1.10 *S. cerevisiae* strains

All strains were derivatives of BY4741.

Strain	Genotype	Source
BY4741	*MAT***a**, *his3Δ1 leu2Δ0 met15Δ0 ura3Δ0*	Euroscarf
hsp104Δ	*MAT***a**, *his3Δ1 leu2Δ0 met15Δ0 ura3Δ0 hsp104::kanMX*	Euroscarf
ssbΔ	*MAT***a**, *his3Δ1 leu2Δ0 met15Δ0 ura3Δ0 ssb1::kanMX4; ssb2::nat1*	Koplin et al. (2010)
nacΔ (1)	*MAT***a**, *his3Δ1 leu2Δ0 met15Δ0 ura3Δ0 egd1::hisMX6; btt1::phleo; egd2::LEU2*	Koplin et al. (2010)
nacΔ (2)	*MAT***a**, *his3Δ1 leu2Δ0 met15Δ0 ura3Δ0 btt1::hph; egd1:: ; egd2::*	Lab collection
nacΔssbΔ	*MAT***a**, *his3Δ1 leu2Δ0 met15Δ0 ura3Δ0 egd1::hisMX6; btt1::phleo; egd2:: ; ssb1::kanMX4; ssb2::nat1*	Lab collection

7.1.11 Acid washed glass beads

To 500 g of glass beads with a diameter of 0.5 mm, 500 ml of 5.8 M HCl were added. The beads were incubated over night at room temperature with continuous stirring. Afterwards, the beads were washed several times over the course of two days with ddH_2O to reach a physiological pH. They were dried at 37°C and autoclaved.

7.1.12 Media and antibiotics

7.1.12.1 Bacterial media

LB media:	Bacto Trypton:	1.24% (w/v)
	Yeast Extract:	0.52% (w/v)
	Sodium chloride:	0.52% (w/v)

For plates, 2% (w/v) agar was added.

For selection, antibiotics were added after autoclaving of the medium:

Ampicillin:	100 µg/ml	(stock: 100 mg/ml in ddH_2O)
Chloramphenicol:	25 µg /ml	(stock: 25 mg/ml in ddH_2O)
Kanamycin:	50 µg/ml	(stock: 50 mg/ml in ddH_2O)
Spectinomycin:	50 µg/ml	(stock: 50 mg/ml in ddH_2O)

7.1.12.2 Yeast media

YPD media:	Yeast Extract:	1% (w/v)
	Peptone:	2% (w/v)

For plates, 2% (w/v) agar was added.
After autoclaving, 2% (v/v) glucose (stock solution: 20%) was added.

Synthetic complete medium:

Difco Yeast Nitrogen base:	0.67% (w/v)
drop out mix:	0.2% (w/v)
Ade:	0.00553% (w/v)
His:	0.00629% (w/v)
Leu:	0.0219% (w/v)
Lys:	0.01803% (w/v)
Ura:	0.000224% (w/v)
Trp:	0.00817% (w/v)

Adjust to pH 5.6.
For plates, 2% (w/v) agar was added.
After autoclaving, 2% (v/v) glucose (stock solution: 20%) was added.
For selection medium, the respective amino acids were omitted.

Drop out mix:

Amino acid	Amount
L-Alanine	2.0 g
L-Arginine	2.0 g
L-Asparagine	2.0 g
L-Aspartic acid	2.0 g
L-Cysteine	2.0 g
L-Glutamic acid	2.0 g
L-Glutamine	2.0 g
Glycine	2.0 g
L-Methionine	2.0 g
L-Isoleucine	2.0 g
L-Phenylalanine	2.0 g
L-Proline	2.0 g
L-Serine	2.0 g
L-Threonine	2.0 g
L-Tyrosine	2.0 g
L-Valine	2.0 g
myo-Inositol	2.0 g
p-Aminobenzoic acid	0.2 g

For selection, Hygromycin B (10 µg/ml), L-Canavanine (0.25 µg/ml) or NaCl (0.4 M) were added to the medium. If L-Canavanine was used, L-Arginine was omitted in the drop out mix.

7.2 Methods

7.2.1 DNA

7.2.1.1 Cloning

Cloning was performed according to standard procedures described in Sambrook (2001). Synthetic oligonucleotides were HPLC-purified and obtained from biomers.net GmbH. Sequences of constructed plasmids were verified via sequencing performed by GATC Biotech AG, Germany.

7.2.1.2 PCR reaction

7.2.1.2.1 Standard-PCR

The following components were mixed:

400 nM of each primer
0.2 mM dNTPs
Phusion polymerase buffer
0.3 µl Phusion polymerase (stock: 2.2 mg/ml)
Template (100 – 400 ng)
ddH_2O to a final volume of 50 µl

Standard protocol:

Step	Procedure	Temperature	Time	Cycles
1	Initial denaturation	98°C	30 sec	
2	Denaturation	98°C	10 sec	30 x
3	Annealing	*	30 sec	
4	Elongation	72°C	°	
5	Final Elongation	72°C	10 min	
6	Storage	8°C		

* ((Melting temperature Primer 1 + Melting temperature Primer 2) / 2) + 3°C

° 30 sec/kb

7.2.1.2.2 Fusion-PCR

To fuse two constructs, first, two separate PCRs for the constructs were performed. Then, 200 ng DNA from each PCR reaction were mixed with 0.2 mM dNTPs, Phusion reaction buffer and 0.3 µl Phusion polymerase. The standard protocol was performed, but with 8 instead of 30 cycles. Afterwards, 3 µl of the fusion mixture were added to the standard components of the PCR reaction and the standard protocol was performed.

7.2.1.2.3 Colony-PCR

The following components were mixed:

400 nM of each primer
0.2 mM dNTPs
Thermopol buffer
0.3 µl Taq polymerase (5 units/ml)
Template (Colony)
ddH_2O to a final volume of 25 µl

Colony-PCR protocol:

Step	Procedure	Temperature	Time	Cycles
1	Initial denaturation	95°C	5 min	
2	Denaturation	95°C	20 sec	
3	Annealing	*	20 sec	30 x
4	Elongation	72°C	°	
5	Final Elongation	72°C	10 min	
6	Storage	8°C		

* (Melting temperature Primer 1 + Melting temperature Primer 2) / 2

° 1 min/kb

7.2.1.2.4 Site-directed mutagenesis

The following components were mixed:

40 nM of each primer
0.2 mM dNTPs
Pfu reaction buffer
1 µl Pfu polymerase (2.9 mg/ml)
Template (100 – 400 ng)
ddH_2O to a final volume of 50 µl

Site-directed mutagenesis protocol:

Step	Procedure	Temperature	Time	Cycles
1	Initial denaturation	98°C	2 min	
2	Denaturation	98°C	20 sec	
3	Annealing	55°C	20 sec	18 x
4	Elongation	72°C	10 min	
5	Final Elongation	72°C	10 min	
6	Storage	4°C		

To 10 µl of the PCR product 2 µl cut smart buffer (NEB), 1 µl Dpn1 (NEB) and 7 µl ddH_2O were added and incubated over night at 37°C.

7.2.1.3 Agarose gel electrophoresis and DNA preparation

DNA fragments were separated according to their size on a 1% agarose gel. DNA samples were supplemented with 6x loading dye. The gel contained Midori green to stain the DNA.

Samples were run at 70 – 120 V, depending on gel size. DNA fragments were visualized via UV light illumination.

DNA fragments were extracted from the gel according to the manufacturers' protocol (Qiagen: QIAquick Gel Extraction Kit / iNtRON Biotechnology: MEGA-spin™ Total Fragment DNA Purification Kit (cp column type)).

7.2.1.4 Digestion with restriction endonucleases

Type-II restriction enzymes (NEB) were used according to the recommendations of the manufacturer for each enzyme. In general, 3 µg of DNA (vector and insert separately) were digested in a final volume of 100 µl. 3 µl Fast Alkaline Phosphatase (Fast AP) was added to the vector after digestion to dephosphorylate the restriction sites and incubated for 1 h at 37°C. Fast AP was inactivated at 75°C for 5 min. The DNA fragments were purified via gel extraction purification (see 7.2.1.3).

7.2.1.5 Ligation

Vector and insert DNA were mixed in a 1:3 and a 1:5 ratio together with T4 DNA ligase and 1x T4 ligase buffer in a final volume of 20 µl. The reaction mixtures were incubated over night at 16 – 22°C.

7.2.1.6 Plasmid-DNA preparation

Plasmid-DNA was purified from bacterial DH5αZ1 cells according to the manufacturers' protocol (Qiagen: QIAprep Spin Miniprep Kit / iNtRON Biotechnology: DNA-spin™ Plasmid DNA Purification Kit).

7.2.2 Chemically competent cells

*7.2.2.1 Competent DH5α*Z1 /XL1-Blue

500 ml LB medium were inoculated with 2.5 ml of an overnight culture. Cells were grown at 37°C to an OD_{600} of 0.6. The culture was cooled on ice for 10 min prior to centrifugation (1,500 x g, 15 min, 4°C). Cell pellet was resuspended in 100 ml ice cold TFB1 buffer (30 mM KOAc, 50 mM $MnCl_2$, 100 mM KCl, 10 mM $CaCl_2$, 15% (v/v) glycerol) and centrifuged again. Pellet was then resuspended in 20 ml ice cold TFB2 buffer (10 mM MOPS pH 7.0, 75 mM $CaCl_2$, 10 mM KCl, 15% (v/v) glycerol). Aliquots à 500 µl were flash frozen in liquid nitrogen and stored at -80°C.

*7.2.2.2 Competent BL21*pRosetta*

100 ml LB medium containing chloramphenicol (Cm) were inoculated with 1 ml of an overnight culture and grown at 37°C to an OD_{600} of 0.5. Culture was cooled 10 min on ice before centrifugation (1,500 x g, 10 min, 4°C). Cell pellet was resuspended in 30 ml ice cold TFB1 buffer (100 mM RbCl, 50 mM $MnCl_2$, 30 mM KAc, 10 mM $CaCl_2$, 15% (v/v) glycerol) and incubated on ice for 90 min. Cell suspension was centrifuged again and the pellet was resuspended in 4 ml TFB2 buffer (10 mM MOPS, 10 mM RbCl, 75 mM $CaCl_2$, 15% (v/v) glycerol). Aliquots à 200 µl were flash frozen in liquid nitrogen and stored at -80°C.

7.2.3 Transformation

7.2.3.1 Transformation of E. coli

7.2.3.1.1 Transformation of chemically competent DH5αZ1 or XL1-Blue

Competent cells were thawed on ice. 100 µl were mixed with 10 µl of a ligation reaction or 3 µl plasmid DNA and incubated for 35 min on ice. Cells were then heat shocked at 42°C for 90 sec and subsequently incubated on ice for 20 min. 1 ml of LB medium was added and cells were incubated at 37°C for 60 min. They were then centrifuged at 600 x g for 5 min at room temperature. 900 µl of the supernatant were discarded and the pellet resuspended in the remaining medium. Then cells were plated on selective media.

7.2.3.1.2 Transformation of chemically competent BL21*pRosetta

Competent cells were thawed on ice. 10 µl of plasmid DNA were added to 100 µl competent cells and incubated on ice for 20 min. Cells were then heat shocked at 42°C for 90 sec. 500 µl Psi Broth (4 mM $MgSO_4$ and 10 mM KCl in LB medium) were added and the cells were incubated for 60 – 90 min at 37°C. Cells were centrifuged at 600 x g for 5 min at room temperature and the pellet was resuspended in the remaining medium. Then cells were plated on selective media.

7.2.3.1.3 TSS transformation of BL21*pRosetta or MH1

Overnight culture of the respective cell type was chilled on ice for 20 min. 100 µl cells were then mixed in a 1:1 ratio with 2x TSS (20% (w/v) PEG-6000, 10% (v/v) DMSO, 100 mM $MgSO_4$) and incubated on ice for 45 min. 5 µl plasmid DNA were added to 100 µl of competent cells and incubated for 20 min on ice. 900 µl LB medium were added and cells were incubated at 37°C/30°C for 1 h. After centrifugation (600 x g, 5 min, RT), cells were resuspended in the remaining medium and plated on selective media.

7.2.3.2 Transformation of S. cerevisiae

7.2.3.2.1 Quick transformation

To 100 µl of transformation mixture (400 mM LiOAc, 40% (w/v) PEG-3350, 132 mM β-Mercaptoethanol) 3 µl of heat denatured herring sperm carrier DNA and 1 µg of plasmid DNA were added. In this mixture one large yeast colony was resuspended and subsequently incubated at 37°C for 30 min. Cells were pelleted at 1,700 x g for 2 min, resuspended in 100 µl sterile ddH_2O and plated on selective media.

7.2.3.2.2 Transformation adapted from Güldener et al. (1996)

50 ml YPD were inoculated to an OD_{600} of 0.2. Cells were grown at 30°C to OD_{600}=0.8. Cells were centrifuged at 3,074 x g for 5 min at room temperature. Pellet was washed with 10 ml sterile ddH_2O and resuspended in 1 ml sterile ddH_2O. It was then centrifuged at 1,700 x g for 1 min at room temperature and washed with 1 ml TE/LiOAc buffer (100 mM LiOAc, 10 mM Tris/HCl pH 7.5, 1 mM EDTA pH 8.0). Finally, the pellet was resuspended in 200 µl TE/LiOAc buffer. To 50 µl of this cell suspension, 5 µl plasmid DNA, 5 µl heat denatured herring sperm carrier DNA and 300 µl 40% PEG (40% (w/v) PEG-3350, 3% (v/v) LiOAc, 3% (v/v) TE) were added. The mixture was incubated for 30 min at 30°C. Afterwards, it was heat shocked for 15 min at 42°C. 800 µl of sterile ddH_2O were added and the mixture was centrifuged at 1,700 x g for 1 min at room temperature. The pellet was resuspended in 1 ml YPD and incubated for 1 h at 30°C. Cells were pelleted at 1,700 x g for 1 min at room temperature, resuspended in 100 µl ddH_2O and plated on selective media.

7.2.4 Growth conditions

7.2.4.1 Growth conditions for E. coli

7.2.4.1.1 DH5*α*Z1 or XL1-Blue

If not described otherwise cells were grown at 37°C in LB medium containing the respective antibiotics. Plates were also incubated at 37°C.

7.2.4.1.2 BL21*pRosetta

Plates were generally grown at 37°C. To express proteins for purification, cells were grown overnight in LB medium containing the respective antibiotics at 30°C. Subsequently, 2 l of LB medium were inoculated to an OD_{600} of 0.1 and cells were grown to an OD_{600}=0.6. Then 1 mM isopropylthio *β*-D-1-galactopyrandoside (IPTG) was added and cells were grown for 4 h at 30°C. Cultures were then transferred to ice cold centrifuge beakers and harvested by centrifugation. Pellet was flash frozen in liquid nitrogen and stored at -80°C.

7.2.4.1.3 MH1

MH1 cells were grown at 30°C. Expression of proteins for purification was performed as described in 7.2.4.1.2.

7.2.4.2 Growth conditions for S. cerevisiae

If not described otherwise, yeast cells were grown at 30°C in YPD or defined synthetic complete media. Plates with freshly transformed yeast cells were incubated at 30°C or room temperature until colonies were visible. Afterwards, plates were incubated at 30°C.

7.2.5 Purification of proteins from *E. coli* cells

7.2.5.1 NAC and NAC mutants

To express yeast NAC in *E. coli* MH1 cells, they were first transformed with the plasmid pRARE/pRosetta via TSS transformation. To enable an induction of the expression of NAC, they were additionally transformed with a plasmid encoding for the lacIq repressor (pZA4). Finally, they were transformed with the plasmid encoding for yeast NAC (pOP-H6-EGD2-EGD1), NAC' (pOP-H6-EGD2-BTT1 #4) or the different mutants (pOP-H6-EGD2-RRK/AAA/EGD1, pOP-H6-EGD2-partLinker-UBA-EGD1, pOP-H6-EGD2-partLinker-UBA(protK)-EGD1, pOP-H6-EGD2-Linker-UBA-EGD1). Expression was performed as described in 7.2.4.1.3. Cell pellets were thawed on ice and resuspended in 25 ml of lysis buffer (50 mM Tris/HCl pH 7.0, 500/300 mM NaCl, 5 mM $MgCl_2$, 10% (v/v) glycerol, 1 mM phenylmethylsulfonyl fluoride (PMSF), 2 mM 1,4-dithiothreitol (DTT) and a spatula point of DNaseI). The lower salt concentration was used for NAC' and the NAC mutants. Cells were lysed via French Press (4x, 800-1000 psi). To clear the lysates they were centrifuged two times at 30,000 x g for 30 min at 4°C. Afterwards, the supernatant was incubated with 2 g Ni-IDA silica matrix (Protino) for 45 min at 4°C in an overhead roller. The matrix was washed five times with 20 ml high salt buffer (50 mM Tris/HCl pH 7.0, 1000/500 mM NaCl, 5 mM $MgCl_2$, 10% (v/v) glycerol, 2 mM DTT) and two times with 40 ml low salt buffer (50 mM Tris/HCl pH 7.0, 25 mM NaCl, 5 mM $MgCl_2$, 10% (v/v) glycerol, 2 mM DTT). NAC was eluted from the matrix three times with 25 ml elution buffer each (20 mM $NaPO_4$ pH 6.5, 25 mM NaCl, 250 mM Imidazol, 5 mM $MgCl_2$, 10% (v/v) glycerol, 2 mM DTT). The elution fractions were pooled and diluted 1:1 with elution buffer without Imidazol. Afterwards, cation ion exchange chromatography was performed, using Resource S, 6 ml. NAC was eluted using a linear gradient of buffer A (20 mM $NaPO_4$ pH 6.5, 25 mM NaCl, 5 mM $MgCl_2$, 10% (v/v) glycerol, 2 mM DTT) and buffer B (20 mM $NaPO_4$ pH 6.5, 1 M NaCl, 5 mM $MgCl_2$, 10% (v/v) glycerol, 2 mM DTT) over 17 column volumes. Fractions containing the NAC complex were pooled and dialysed over night into 50 mM Tris/HCl pH 7.0, 25 mM NaCl, 5 mM $MgCl_2$, 10%

(v/v) glycerol and 2 mM β-Mercaptoethanol. Aliquots were frozen in liquid nitrogen and stored at -80°C.

7.2.5.2 C. elegans NAC

To express *C.elegans* NAC in *E. coli* MH1 cells, they were first transformed with the plasmid pRARE/pRosetta via TSS transformation. Then they were transformed with the plasmid encoding for *C. elegans* NAC. Expression was essentially performed as described in 7.2.4.1.3, but after induction with IPTG cells were grown for 5 h at 30°C. Pellets were thawed on ice and resuspended in 25 ml of lysis buffer (20 mM $NaPO_4$ pH 7.5, 300 mM NaCl, 6 mM $MgCl_2$, 10% (v/v) glycerol, 2 mM PMSF, 2 mM DTT and a spatula point of DNaseI). Cells were lysed via French Press (4x, 800-1000 psi). To clear the lysates they were centrifuged two times at 30,000 x g for 30 min at 4°C. Afterwards, the supernatant was incubated with 2 g Ni-IDA silica matrix (Protino) for 45 min at 4°C in an overhead roller. The matrix was washed five times with 20 ml high salt buffer (20 mM $NaPO_4$ pH 7.5, 750 mM NaCl, 6 mM $MgCl_2$, 10% (v/v) glycerol, 2 mM PMSF, 2 mM DTT) and two times with 40 ml low salt buffer (20 mM $NaPO_4$ pH 7.5, 25 mM NaCl, 6 mM $MgCl_2$, 10% (v/v) glycerol, 2 mM PMSF, 2 mM DTT). NAC was eluted from the matrix four times with 20 ml elution buffer each (20 mM $NaPO_4$ pH 7.5, 250 mM Imidazol, 25 mM NaCl, 6 mM $MgCl_2$, 10% (v/v) glycerol, 2 mM DTT). The elution fractions were pooled and dialysed over night with 4 µg H6-Ulp1 per mg NAC to remove the His6-SUMO tag (20 mM $NaPO_4$ pH 7.5, 25 mM NaCl, 6 mM $MgCl_2$, 10% (v/v) glycerol, 2 mM DTT). Afterwards, protein solution was incubated with 3 g protino matrix to remove H6-Ulp1. Then anion ion exchange chromatography was performed, using Resource Q, 6 ml. NAC was eluted using a linear gradient of buffer A (20 mM $NaPO_4$ pH 7.5, 25 mM NaCl, 6 mM $MgCl_2$, 10% (v/v) glycerol, 2 mM DTT) and buffer B (20 mM $NaPO_4$ pH 7.5, 1 M NaCl, 6 mM $MgCl_2$, 10% (v/v) glycerol, 2 mM DTT) over 25 column volumes. Fractions containing the NAC complex were pooled and dialysed over night into 20 mM $NaPO_4$ pH 7.5, 25 mM NaCl, 6 mM $MgCl_2$, 10% (v/v) glycerol, 2 mM DTT. Aliquots were frozen in liquid nitrogen and stored at -80°C.

7.2.5.3 Hsp26

Hsp26 was expressed in BL21*pRosetta cells. Transformation of the chemically competent cell with His6-SUMO-HSP26 was accomplished via heat shock. Expression was performed as described in 7.2.4.1.2. Pellets were resuspended in 25 ml lysis buffer (30 mM HEPES-KOH pH 7.4, 500 mM KAc, 5 mM $MgCl_2$, 10% (v/v) glycerol, 1 mM PMSF, 1 mM β-Mercaptoethanol, protease inhibitor mix (10 µg/ml pepstatin, 5 µg/ml leupeptin, 8 µg/ml aprotinin) and a spatula point of DNaseI). Cells were lysed via French Press (4x, 800-1000 psi) and lysates were cleared via centrifugation (30,000 x g for 30 min at 4°C). The

lysate was then incubated with 2 g Ni-IDS silica matrix and washed five times with 20 ml high salt buffer (30 mM HEPES-KOH pH 7.4, 1 M KAc, 5 mM $MgCl_2$, 10% (v/v) glycerol, 1 mM β-Mercaptoethanol) and two times with 40 ml low salt buffer (30 mM HEPES-KOH pH 7.4, 50 mM KAc, 5 mM $MgCl_2$, 10% (v/v) glycerol, 1 mM β-Mercaptoethanol). Hsp26 was eluted from the matrix by washing it five times with 10 ml elution buffer (30 mM HEPES-KOH pH 7.4, 50 mM KAc, 250 mM Imidazol, 5 mM $MgCl_2$, 10% (v/v) glycerol, 1 mM β-Mercaptoethanol). Fractions containing the protein were pooled. To remove the His-Smt3-tag 5 – 7 µg of the Smt3 specific protease Ulp1 (1.95 mg/ml) were added. Dialysis was performed over night while fresh buffer was used after 2 h and after 4 h (30 mM HEPES-KOH pH 7.4, 50 mM KAc, 5 mM $MgCl_2$, 10% (v/v) glycerol, 1 mM β-Mercaptoethanol). His6-Ulp1 protease was removed by incubation with 3 g Ni-IDA silica matrix for 30 min at 4°C. Flowthrough was collected and applied to anion ion exchange chromatography using Resource Q, 6 ml. Hsp26 was eluted using a linear gradient of buffer A (30 mM HEPES-KOH pH 7.4, 50 mM KAc, 5 mM $MgCl_2$, 5% (v/v) glycerol, 1 mM β-Mercaptoethanol) and buffer B (30 mM HEPES-KOH pH 7.4, 1 M KAc, 5 mM $MgCl_2$, 5% (v/v) glycerol, 1 mM β-Mercaptoethanol) over 25 column volumes. Fractions containing Hsp26 were pooled and dialysed over night into 30 mM HEPES-KOH pH 7.4, 50 mM KAc, 5 mM $MgCl_2$, 10% (v/v) glycerol, 1 mM β-Mercaptoethanol. Aliquots were flash frozen in liquid nitrogen and stored at -80°C.

7.2.5.4 Ssa1

Ssa1 was expressed in BL21*pRosetta cells. The chemically competent cells were transformed with pSUMO-SSA1 via heat shock. To express Ssa1 for purification, 1.5 l LB media were inoculated to an OD_{600} of 0.1 and cells were grown to OD_{600}=0.8 at 30°C. Importantly, only 13 µg/ml instead of 25 µg/ml of chloramphenicol were used during expression. When OD_{600}=0.8 was reached, 1.5 ml of benzylalcohol were added and the culture was shifted to 20°C for 30 min. 0.5 mM IPTG was added and the cells were grown over night at 20°C. Cells were harvested via centrifugation and the pellet was flash frozen in liquid nitrogen and stored at -80°C. Purification was performed essentially as described in 7.2.5.2. In short, pellet was resuspended in lysis buffer (30 mM HEPES-KOH pH 7.4, 500 mM KAc, 5 mM $MgCl_2$, 10% (v/v) glycerol, 5 mM ATP, 1 mM PMSF, 1 mM β-Mercaptoethanol, protease inhibitor mix (10 µg/ml pepstatin, 5 µg/ml leupeptin, 8 µg/ml aprotinin) and a spatula point of DNaseI) and lysed via French Press. Lysate was cleared by centrifugation and incubated with 1.5 g Ni-IDA silica matrix. The matrix was washed five times with high salt buffer (30 mM HEPES-KOH pH 7.4, 1 M KAc, 5 mM $MgCl_2$, 10% (v/v) glycerol, 5 mM ATP, 1 mM β-Mercaptoethanol) and two times with low salt buffer (30 mM HEPES-KOH pH 7.4, 50 mM KAc, 5 mM $MgCl_2$, 10% (v/v) glycerol, 5 mM ATP, 1 mM β-

Mercaptoethanol). Ssa1 was eluted from the matrix by using five times 20 ml of elution buffer (30 mM HEPES-KOH pH 7.4, 50 mM KAc, 250 mM Imidazol, 5 mM $MgCl_2$, 10% (v/v) glycerol, 5 mM ATP, 1 mM β-Mercaptoethanol). Fractions containing Ssa1 were pooled, 5 – 7 µg of His6-Ulp1 were added, and the solution was dialysed over night (30 mM HEPES-KOH pH 7.4, 50 mM KAc, 5 mM $MgCl_2$, 10% (v/v) glycerol, 1 mM β-Mercaptoethanol). His6-Ulp1 was removed by incubation with 3 g Ni-IDA matrix. The Flowthrough was applied to anion ion exchange chromatography using Resource Q, 6 ml. Ssa1 was eluted using a linear gradient of buffer A (30 mM HEPES-KOH pH 7.4, 50 mM KAc, 5 mM $MgCl_2$, 5% (v/v) glycerol, 1 mM β-Mercaptoethanol) and buffer B (30 mM HEPES-KOH pH 7.4, 1 M KAc, 5 mM $MgCl_2$, 5% (v/v) glycerol, 1 mM β-Mercaptoethanol) over 25 column volumes. Fractions containing Ssa1 were pooled and dialysed over night into 30 mM HEPES-KOH pH 7.4, 50 mM KAc, 5 mM $MgCl_2$, 10% (v/v) glycerol, 1 mM β-Mercaptoethanol. Aliquots were flash frozen in liquid nitrogen and stored at -80°C.

7.2.5.5 Ydj1

Ydj1 was expressed in BL21*pRosetta cells. The chemically competent cells were transformed with His6-SUMO-YDJ1 via heat shock. Expression was performed as described in 7.2.4.1.2. Purification was performed as in 7.2.5.2 with minor alterations: after elution of the Ni-IDA silica matrix and addition of His6-Ulp1, dialysis was performed overnight without buffer changes. The composition of the buffers was the same as for Hsp26.

7.2.5.6 Hsp104

Hsp104 was expressed in BL21*pRosetta cells. The chemically competent cells were transformed via heat shock with His6-SUMO-HSP104. Expression was performed as described in 7.2.4.1.2. Purification was performed as in 7.2.5.5.

7.2.5.7 Luciferase

Luciferase was expressed in BL21*pRosetta cells transformed additionally with pZA4 encoding for the lacIq repressor. Next they were transformed with pDS56-Luciferase (firefly) via TSS transformation. Expression was performed as described in 7.2.4.1.2. For purification (similar to 7.2.5.5) the pellet was resuspended in lysis buffer (30 mM $NaPO_4$ pH 8.0, 500 mM NaCl, 5 mM $MgCl_2$, 10% (v/v) glycerol, 1 mM PMSF, 1 mM *β*-Mercaptoethanol, protease inhibitor mix (10 µg/ml pepstatin, 5 µg/ml leupeptin, 8 µg/ml aprotinin) and a spatula point of DNaseI) and lysed via French Press. The lysate was cleared via centrifugation and then incubated with 2 g Ni-IDA silica matrix. The matrix was washed five times with high salt (30 mM $NaPO_4$ pH 8.0, 1 M NaCl, 5 mM $MgCl_2$, 10% (v/v) glycerol, 1 mM *β*-Mercaptoethanol) and two times with low salt buffer (30 mM $NaPO_4$ pH 8.0, 50 mM NaCl,

5 mM $MgCl_2$, 10% (v/v) glycerol, 1 mM *β*-Mercaptoethanol). Luciferase was eluted from the matrix by using five times 5 ml of elution buffer (30 mM $NaPO_4$ pH 8.0, 1 M NaCl, 250 mM Imidazol, 5 mM $MgCl_2$, 10% (v/v) glycerol, 1 mM *β*-Mercaptoethanol). Afterwards fractions were again incubated with Ni-IDA matrix to remove remaining contaminants. It was washed one time with 25 ml high salt and one time with 25 ml low salt buffer. Luciferase was eluted with 10 times 2 ml. Fractions containing luciferase were pooled and dialysed over night (30 mM $NaPO_4$ pH 8.0, 50 mM NaCl, 5 mM $MgCl_2$, 10% (v/v) glycerol, 1 mM *β*-Mercaptoethanol). Aliquots were flash frozen in liquid nitrogen and stored at -80°C.

7.2.6 Alkaline lysis of yeast cells

1 ml of a stationary yeast culture was centrifuged (12,640 x g, 1 min, RT). The pellet was resuspended in 110 µl of 100 mM NaOH and the suspension was incubated at room temperature for 10 min. 10 µl were added to 990 µl of ddH_2O and OD_{600} was measured. Lysate was centrifuged and the pellet resuspended in SDS sample buffer, thereby adjusting protein concentration. For SDS-gel electrophoresis a volume corresponding to 0.1 OD_{600} was loaded.

7.2.7 Spot test

A volume corresponding to 1 OD_{600} of a stationary yeast culture was pelleted and resuspended in 1 ml sterile ddH_2O. 200 µl were transferred to a microtiter plate and five 5-fold serial dilutions were made. Dilutions were spotted onto selective media plates via a stamp. Plates were incubated at 30°C if not indicated otherwise.

7.2.8 Standard protein biochemical techniques

7.2.8.1 Bradford assay

The Bradford assay was used to determine protein concentrations. The binding of the anionic form of the Coomassie brilliant blue G-250 dye is specific to arginine, tryptophan, tyrosine, histidine and phenylalanine residues (Bradford, 1976). The absorbance maximum, which can be detected photometrically, is situated at 595 nm (blue). In solution, the free dye is in the cationic form and has an absorbance maximum at 470 nm (red).

7.2.8.2 SDS-PAGE

To separate proteins according to their size, Sodium Dodecyl Sulphate Polyacrylamide Gel Electrophoresis (SDS-PAGE) was used (Laemmli, 1970). Samples were supplemented with

Laemmli buffer (end concentration: 1x) and heated to 95°C. The samples were loaded onto 12%, 14% or 16% SDS-gels and run under denaturing conditions at 25 mA or 100 V for about 1.30 h to 1.40 h. To estimate the size of the samples, a molecular weight standard was included.

7.2.8.3 Coomassie brilliant blue staining

7.2.8.3.1 Regular protocol

SDS-gels were stained for 20 min in Coomassie staining solution. Afterwards, they were destained in Destaining solution until the bands were clearly visible. Solutions are described in 7.1.3.

7.2.8.3.2 Sensitive Coomassie staining

To detect protein bands with higher sensitivity Coomassie staining according to Neuhoff et al. (1988) was performed. SDS-gels were first fixed for 1 h at room temperature in the fixation solution. For staining, Solution A was mixed in a 1:5 ratio with methanol and 2% of Coomassie G250 solution were added. Gels were stained over night in this solution at room temperature. Afterwards, they were rinsed with ddH_2O and destained for 1 h in Destain solution. Finally, the gels were washed with ddH_2O.

7.2.8.4 PonceauS staining

After western blotting gels were stained for 10 min in PonceauS staining solution (7.1.3). The blots were washed with 1x TBS-T until discrete bands were visible. Blots could be scanned at this point and then be further destained using 1x TBS-T until no more bands were visible.

7.2.8.5 Silverstaining

SDS-gels were first fixed for 1 h in fixation solution (7.1.3). Afterwards they were washed for 12 min in washing solution and then two times for 5 min in ddH_2O. The gels were immersed in pre-staining solution for exactly 60 sec before washing again with ddH_2O (two times for 1 min). Gels were then stained at 4°C with pre-cooled staining solution for 25 min while covered with foil. Afterwards, gels were washed three times for 20 sec with ddH_2O and developing solution was added. The gels were incubated at room temperature until bands appeared. The reaction was stopped by immersing the gels in fixation solution for 5 min. Before scanning of the gels, they were washed three times for 1 min with ddH_2O.

7.2.8.6 Western blotting and immunostaining

To analyse samples via western blot and immunostaining, the samples were first run on a SDS-gel and then transferred onto a nitrocellulose membrane using wet blot technique. The

setup was run for 1.30 h at 300 mA. Blots were blocked with 3% milk or 5% BSA and then incubated with primary antibodies. Blots were washed with 1x TBS-T and a secondary antibody was applied. As secondary antibodies fluorescence-labelled (DY-682, Dyomics) or alkaline phosphatase coupled ones (Dianova) were used. They were detected using the Typhoon FLA 9500 or the LAS-4000 mini system (both GE Healthcare) respectively.

7.2.8.7 TCA precipitation of proteins

To precipitate proteins from solution, trichloroacetic acid was used. Ice cold TCA was added to the sample to a final concentration of 20% and the solution was incubated on ice for 1 h. Lysate was pelleted for 30 min at 16,000 x g, 4°C. The supernatant was discarded and the pellet washed twice with ice cold acetone. The pellet was dried for 10 min at 55°C and resuspended in 35 µl of alkaline sample buffer.

7.2.9 *Ex vivo* ribosome co-sedimentation assay

60 ml of the respective medium were inoculated to OD_{600}=0.1. Yeast cells were grown at 30°C to an OD_{600} of 0.8 – 1. A 50 ml volume of the culture was pelleted at 4°C, resuspended in ice cold ddH_2O, pelleted again and flash frozen in liquid nitrogen.

Pellets were thawed on ice and resuspended in lysis buffer (20 mM HEPES-KOH pH 7.4, 50 mM KAc, 2 mM MgAc, 2 mM DTT, 1x TM complete® (Roche Diagnostics), protease inhibitor mix (10 µg/ml pepstatin, 5 µg/ml leupeptin, 8 µg/ml aprotinin) and 1 mM PMSF). Cells were lysed via glass bead lysis using FastPrep24, 5x 20 sec, 5 M/s. In between, tubes were put on ice for 1 min. Lysates were centrifuged for 10 min at 16,000 x g, 4°C. Supernatant was transferred to a new reaction tube and centrifuged again. Supernatant was transferred to a new reaction tube and concentrations were adjusted using A_{260} values. Sample was taken (totals) and precipitated with TCA (7.2.8.7). 200 µl of the supernatant were loaded onto 20% sucrose cushion and centrifuged at 200,000 x g for 90 min at 4°C (S140AT rotor, Sorvall mini ultracentrifuge). Proteins present in the supernatant were precipitated with TCA and the pellet was resuspended in lysis buffer with SDS sample buffer (1x final concentration). Samples were all heat denatured by incubating at 95°C for 10 min.

7.2.10 Aggregate preparation

7.2.10.1 Aggregate preparation as described in Cashikar et al. (2005)

70 ml of YPD were inoculated to OD_{600}=0.05. Yeast cells were grown to an OD_{600} of 0.5. A 10 ml sample was taken, cells were pelleted and frozen in liquid nitrogen. Cultures were shifted for 30 min to 37°C for thermotolerance and subsequently to 46°C for 30 min. A 10 ml

sample was taken and 10 µg/ml cycloheximide was added to the culture. Regeneration took place at 30°C, samples were taken after 1 h and 2 h.
Pellets were thawed on ice and resuspended in 220 µl of lysis buffer (20 mM $NaPO_4$ pH 6.9, 10 mM DTT, 0.1% (v/v) Tween 20, 0.2 mg/ml zymolyase, 25 units of Benzonase™ nuclease, protease inhibitor mix (10 µg/ml pepstatin, 5 µg/ml leupeptin, 8 µg/ml aprotinin) and 1 mM PMSF). Cells were incubated at 25°C for 20 min. Afterwards, they were lysed via sonification (Branson tip sonifier: 6x, level 4, 50% duty cycle). Subsequently cell debris was pelleted by centrifugation and supernatant was transferred to a new reaction tube. Protein concentrations were adjusted using the Bradford assay. 100 µl were subjected to centrifugation (16,000 x g, 30 min, 4°C). Supernatant was transferred to a new reaction tube and the pellet was resuspended in 100 µl lysis buffer.
Statistical analysis was performed using ImageJ (Schneider et al., 2012) and SigmaPlot. One way ANOVA with post hoc Holm-Sidak-method was performed.

7.2.10.2 Standard lab protocol

70 ml of YPD were inoculated to OD_{600}=0.05. Yeast cells were grown to an OD_{600} of 0.5. To a 10 ml sample 50 µl of 3 M NaN_3 was added and cells were pelleted via centrifugation. The pellet was washed with 15 mM NaN_3 and flash frozen in liquid nitrogen. The cell culture was incubated at 37°C for 30 min and then heat shocked at 46°C for another 30 min. A 10 ml sample was taken and 10 µg/ml cycloheximide was added to the culture. Cells were subjected to regeneration at 30°C for 2 h. Samples were taken after 1 h and after 2 h.
Pellets were thawed on ice and resuspended in 200 µl of lysis buffer (20 mM KPO_4 pH 6.8, 10 mM DTT, 1 mM EDTA, 0.1% (v/v) Tween 20, protease inhibitor mix (20 µg/ml pepstatin, 10 µg/ml leupeptin, 16 µg/ml aprotinin), 2 mM PMSF; 3 mg/ml zymolyase T20 was added and the buffer was incubated at room temperature for 30 min, centrifuged and DNaseI (25 U/µl) was added). Cells were incubated for 15 min at room temperature and then shifted to ice for 5 min. Afterwards, cells were lysed via sonification (Branson tip sonifier: 8x, level 4, 50% duty cycle). Cell debris was pelleted by centrifugation and protein concentration of the supernatant was adjusted using the Bradford assay. 100 µl were subjected to centrifugation (16,000 x g, 30 min, 4°C). Pellet was washed two times with 750 µl 2% (v/v) NP40 (dissolved in 20 mM KPO_4 pH 6.8, protease inhibitor mix (10 µg/ml pepstatin, 5 µg/ml leupeptin, 8 µg/ml aprotinin), 2 mM PMSF), using sonification (6x, level 4, 50% duty cycle). In the third washing step, the pellet was washed with 750 µl of 20 mM KPO_4 pH 6.8, supplemented with 2 mM PMSF, protease inhibitor mix (10 µg/ml pepstatin, 5 µg/ml leupeptin, 8 µg/ml aprotinin) using Branson tip sonifier (4x, level 2, 65% duty cycle).

7.2.11 Measurement of potential chaperone activity

7.2.11.1 Inactivation of citrate synthase

Inactivation of citrate synthase was essentially performed as described previously (Srere, 1966; Buchner et al., 1998; Haslbeck et al., 1999). Citrate synthase was incubated without or with different concentrations of NAC at 43°C in 40 mM HEPES-KOH pH7.4. Samples were taken at different time points and the activity of citrate synthase was determined. The activity measurements were performed at 25°C in 50 mM Tris/HCl, 2 mM EDTA pH 8.0.

7.2.11.2 Reactivation of luciferase

The experiment was essentially performed as described in Dumitru et al. (2004); Haslbeck et al. (2005). Luciferase was either inactivated thermally or chemically. For thermal denaturation, 80 nM purified luciferase was incubated at 40°C for 30 min in buffer (50 mM Tris/HCl, 2 mM EDTA, pH 8.0) with or without NAC and/or Hsp26. 5 mM ATP, 320 nM Ssa1 and 320 nM Ydj1 were added. Kinetics of the reactivation was measured at 30°C. Gain of the reader was set to 85 and the signals of 240 cycles were accumulated.

For chemical denaturation, 184 nM luciferase was incubated for 2 h at room temperature in 8 M guanidinium hydrochloride. For reactivation it was diluted (1:100) into buffer (50 mM Tris/HCl, 2 mM EDTA, pH 8.0) with or without 320 nM NAC and containing different chaperones for reactivation (320 nM Ssa1, 320 nM Hsp104, 640 nM Ydj1). Kinetic interval of the reader was set to 165 sec and 60 cycles were accumulated.

7.2.11.3 Light scattering

7.2.11.3.1 Light scattering of citrate synthase

Light scattering was performed at 500 nm as complex formation of Hsp26 is not detected at this wavelength (Haslbeck et al., 1999). Thermal inactivation of citrate synthase was monitored at 43°C. Inactivation was performed in 40 mM HEPES-KOH, pH7.4 with or without different concentrations of NAC, Hsp26 and BSA. NAC was dialysed before the measurements into 40 mM HEPES-KOH, pH 7.4.

7.2.11.3.2 Light scattering of luciferase

As for citrate synthase, light scattering was measured at 500 nm (Haslbeck et al., 1999). Thermal inactivation was equally performed at 43°C. Luciferase was inactivated in buffer (25 mM HEPES-KOH pH 7.5, 5 mM MgAc, 50 mM KCl, 5 mM β-Mercaptoethanol) with or without different concentrations of NAC, NAC mutants, Hsp26 and BSA. NAC and its mutants were dialysed before measurements into 40 mM HEPES-KOH, pH 7.5.

7.2.12 Analytical ultracentrifugation

NAC solution at 0.87 mg/ml was subjected to analytical ultracentrifugation (Beckmann Optima X-LA, 34,000 rpm, 25°C). 600 scans à 2 min were made.

7.2.13 Gel filtration analysis

2.4 µM citrate synthase and 0.6 µM luciferase were used for gel filtration analysis. 9.6 µM NAC and Hsp26 were used. Components were either pre-incubated for 30 min at 25°C or 43°C. In addition, column (TSK gel 4000PW, Tosoh Biosciences) was always adjusted to the used temperature. Thyroglobulin, γ-globulin, ovalbumin and carbonic anhydrase were used as protein standards.

7.2.14 Limited proteolysis with proteinase K

For limited proteolysis, 0.5 – 1 mg/ml NAC and 1 µg/ml proteinase K were used. NAC was mixed with buffer (20 mM Tris/HCl pH 7.5, 2 mM $CaCl_2$, pH 8.0) and incubated at 30°C for 5 min. Sample for time point zero was taken, mixed with SDS-sample buffer containing PMSF and flash frozen in liquid nitrogen. Proteinase K was added and the reaction mixture was further incubated at 30°C. Samples were taken at different time points. The samples were then run on a 16% SDS gel, silver stained and bands were cut out for analysis by mass spectrometry performed at the Proteomics Facility at the University of Konstanz.

7.2.15 Microscopy of yeast cells

20 ml of selective medium were inoculated to OD_{600}=0.2. Copper sulphate was added to 50 µM for induction of luciferase expression. Cells were grown to an OD_{600} of 0.6. A volume corresponding to 1 OD_{600} was pelleted and 4% formaldehyde was added. Cells were incubated for 10 min at room temperature, pelleted, washed with 100 µl PBS and resuspended in 10 µl PBS. The fixed cells were stored on ice. The culture was shifted to 37°C for 30 min and then to 45°C for 30 min. Heat shock was performed and samples were taken directly afterwards and after 30 min, 60 min and 90 min of recovery at 30°C. Pictures were taken on a Leica fluorescence microscope, first differential interference contrast (DIC), then mCherry (excitation max.: 587 nm, emission max.: 610 nm), then GFP (excitation max.: 488 nm, emission max.: 509 nm).

Pictures were analysed using Fiji (Schindelin et al., 2012; Schindelin et al., 2015).

7.2.16 *In vivo* crosslinking

25 ml selective medium were inoculated to an OD_{600} of 0.1. The culture was grown to an OD_{600} = 0.4 – 0.6. Then 18 ml were transferred to 102 ml fresh medium, one time containing pBpa (1:1000 dilution from 0.4 M stock in 1 M NaOH) and one time not. Cells were then grown to an OD_{600} of 1.5 at 30°C. Of each culture 2x 50 ml were pelleted and washed two times with ddH_2O. Finally the pellets were resuspended in 2 ml Millipore and transferred to a 6-well plate. One plate was subjected to UV light (365 nm) for 45 min, one plate served as control. Afterwards, the cells were transferred to a reaction tube, pelleted and lysed in 110 µl of 0.1 M NaOH. Lysates were incubated for 10 min at room temperature, centrifuged and resuspended in SDS-sample buffer.

7.2.17 Circular dichroism measurement

Aliquots of NAC or NAC mutants were thawed at 30°C and then put on ice. They were centrifuged for 5 min at 18,000 x g. Protein concentration was adjusted to 5 µM using 50 mM phosphate buffer (PB). Then, NAC and its mutants were dialysed over night into 50 mM PB. After centrifugation, NAC solutions were measured in a J 815 super CD instrument in a 0.01 cm cell at 20°C. Analysis was performed by Dichroweb (Whitmore and Wallace, 2004; Whitmore and Wallace, 2008). CDSSTR (Compton and Johnson, 1986; Manavalan and Johnson, 1987; Sreerama and Woody., 2000) was used with SMP180 as reference dataset (Janes, 2008; Abdul-Gader et al., 2011).

7.2.18 Synthesis of Acetyl-CoA

35 mg Coenzyme A were dissolved in 30 ml ice cold ddH_2O and stored on ice. 3 µl acetic anhydrid were added at soft shaking. pH was adjusted to 7.25 using 1 M sodium bicarbonate. The mixture was incubated in an ice-water bath for 4 h and lyophilized over night. Product was analysed by HPLC-MS. Acetyl-CoA was stored at -20°C.

7.2.19 Bioinformatics

7.2.19.1 Generation of alignments

The protein sequences of the 3 yeast NAC subunits were used as query sequences: Egd2 (α-NAC), Egd1 (β-NAC) and Btt1 (β'-NAC). First, a PSI-BLAST (Position Specific Iterative – Basic Local Alignment and Search Tool) search of the NCBI protein database, downloaded from the NCBI homepage in November 2010, was performed. With a self-written perl-programme the full names of the sequences were extracted from the NCBI homepage. The

resulting 600 sequences were further analysed using CLANS (Cluster Analysis of Sequences) (Frickey and Lupas, 2004). Egd1 and Btt1 were found in one cluster, Egd2 in another. The sequences were extracted from CLANS and aligned using 'muscle' (Edgar, 2004). The full names of the sequences were extracted again and the alignments were analysed manually to find the biologically optimal solution. Finally, an external HMM profile was created and all respective sequences were aligned to it. The HMMER3 was downloaded from the HMMI homepage http://hmmmer.org/ in December 2010. To better compare the sequences especially concerning conservation they were sorted according to their kingdoms (Master Thesis Lisa Locher: Towards a molecular understanding of the mechanism of action of the nascent-polypeptide associated complex (NAC), 15th June 2012; work belonged already to the PhD thesis in course of the Konstanz fast track programme).

7.2.19.2 Generation of the structure model of yeast NAC

The modelling of the dimerization domain of yeast (and also *C. elegans*) NAC was done using the resolved structure of human NAC with HHPred, which is a structure prediction programme freely available on the homepage of the Max-Planck Institute for Developmental Biology in Tübingen, Germany. It uses HMM-HMM comparison and known structures of homologous sequences as profiles to model the 3D-structure of the query sequence. So far, the dimerization domain is the only part crystallized of NAC (Spreter et al., 2005; Liu et al., 2010; Wang et al., 2010). Using PyMOL, the structure could be edited to highlight different regions or check for steric hindrance by the incorporation of pBpa for example.

8. References

8.1 Publication

Ann-Kathrin Ott, Lisa Locher, Miriam Koch and Elke Deuerling (2015)

Functional Dissection of the Nascent Polypeptide-Associated Complex in *Saccharomyces cerevisiae*.

PLoS ONE 10: e0143457

Contribution:

For this publication I contributed the alignment of the β-NAC subunits and the similarity and identity analysis of the C-termini of β (Egd1) and β' (Btt1) of *S. cerevisiae*. Additionally I was responsible for the statistical analyses of the presented data.

8.2 Bibliography

Abdul-Gader A, Miles AJ, Wallace BA (2011) A reference dataset for the analyses of membrane protein secondary structures and transmembrane residues using circular dichroism spectroscopy. *Bioinformatics* 27: 1630-1636

Adams JM (1968) On the release of the formyl group from nascent protein. *J Mol Biol* 33: 571-589

Agrawal RK, Penczek P, Grassucci RA, Frank J (1998) Visualization of elongation factor G on the *Escherichia coli* 70S ribosome: the mechanism of translocation. *Proc Natl Acad Sci U S A* 95: 6134-6138

Aguilaniu H, Gustafsson L, Rigoulet M, Nystrom T (2003) Asymmetric inheritance of oxidatively damaged proteins during cytokinesis. *Science* 299: 1751-1753

Albanèse V, Reissmann S, Frydman J (2010) A ribosome-anchored chaperone network that facilitates eukaryotic ribosome biogenesis. *J Cell Biol* 189: 69-81

Al-Shanti N, Aldahoodi Z (2006) Inhibition of alpha nascent polypeptide associated complex protein may induce proliferation, differentiation and enhance the cytotoxic activity of human CD8(+) T cells. *J Clin Immunol* 26: 457-464

Al-Shanti N, Steward CG, Garland RJ, Rowbottom AW (2004) Investigation of alpha nascent polypeptide-associated complex function in a human CD8(+) T cell *ex vivo* expansion model using antisense oligonucleotides. *Immunology* 112: 397-403

Andersen KM, Semple CA, Hartmann-Petersen R (2007) Characterization of the nascent polypeptide-associated complex in fission yeast. *Mol Biol Rep* 34: 275-281

Andréasson C, Fiaux J, Rampelt H, Druffel-Augustin S, Bukau B (2008) Insights into the structural dynamics of the Hsp110-Hsp70 interaction reveal the mechanism for nucleotide exchange activity. *Proc Natl Acad Sci U S A* 105: 16519-16524

Anfinsen CB (1973) Principles that govern the folding of protein chains. *Science* 181: 223-230

Anger AM, Armache JP, Berninghausen O, Habeck M, Subklewe M, Wilson DN, Beckmann R (2013) Structures of the human and Drosophila 80S ribosome. *Nature* 497: 80-85

Arnesen T, Van Damme P, Polevoda B, Helsens K, Evjenth R, Colaert N, Varhaug J.E, Vandekerckhove J, Lillehaug J.R, Sherman F, Gevaert K (2009) Proteomics analyses reveal the evolutionary conservation and divergence of N-terminal acetyltransferases from yeast and humans. *Proc Natl Acad Sci U S A* 106: 8157-8162

Arsenovic PT, Maldonado AT, Colleluori VD, Bloss TA (2012) Depletion of the *C. elegans* NAC engages the Unfolded Protein Response, Resulting in Increased Chaperone Expression and Apoptosis. *PLoS ONE* 7(9): e44038

Baghdoyan S, Dubreuil P, Eberlé F, Gomez S (2000) Capture of cytokine-responsive genes (NACA and RBM3) using a gene trap approach. *Blood* 95: 3750-3757

Bagneris C, Bateman OA, Naylor CE, Cronin N, Boelens WC, Keep NH, Slingsby C (2009) Crystal structures of α-crystallin domain dimers of αB-crystallin and Hsp20. *J Mol Biol* 392: 1242-1252

Baldwin RL, Williams JW (1950) Boundary spreading in sedimentation velocity experiments. *J Am Chem Soc* 72: 4325

Baldwin TO (1999) Protein folding in vivo: the importance of ribosomes. *Nat Cell Biol* 1: E154-155

Ball LA, Kaesberg P (1973) Cleavage of the N-terminal formylmethionine residue from a bacteriophage coat protein in vitro. *J Mol Biol* 79: 531-537

Ban N, Nissen P, Hansen J, Capel M, Moore PB, Steitz TA (1999) Placement of protein and RNA structures into a 5 A-resolution map of the 50S ribosomal subunit. *Nature* 400: 841-847

Ban N, Nissen P, Hansen J, Moore PB, Steitz TA (2000) The complete atomic structure of the large ribosomal subunit at 2.4 A resolution. *Science* 289: 905-920

Baranova EV, Weeks SD, Beelen S, Bukach OV, Gusev NB, Strelkov SV (2011) Three-dimensional structure of α-crystallin domain dimers of human small heat shock proteins HSPB1 and HSPB6. *J Mol Biol* 411: 110-122

Basha E, O'Neill H, Vierling E (2012) Small heat shock proteins and α-crystallins: dynamic proteins with flexible functions. *Cell* 37: 106-117

Bashan A, Yonath A (2008) Correlating ribosome function with high-resolution structures. *Trends Microbiol* 16: 326-335

Beatrix B, Sakai H, Wiedmann M (2000) The alpha and beta subunit of the nascent polypeptide-associated complex have distinct functions. *J Biol Chem* 275: 37838-37845

Becker T, Bhushan S, Jarasch A, Armache JP, Funes S, Jossinet F, Gumbart J, Mielke T, Berninghausen O, Schulten K, Westhof E, Gilmore R, Mandon EC, Beckmann R (2009) Structure of monomeric yeast and mammalian Sec61 complexes interacting with the translating ribosome. *Science* 326: 1369-1373

Ben-Shem A, Jenner L, Yusupova G, Yusupov M (2010) Crystal structure of the eukaryotic ribosome. *Science* 330: 1203-1209

Bentley NJ, Fitch IT, Tuite MF (1992) The small heat-shock protein Hsp26 of *Saccharomyces cerevisiae* assembles into a high molecular weight aggregate. *Yeast* 8: 95-106

Bepperling A, Alte F, Kriehuber T, Braun N, Weinkauf S, Groll M, Haslbeck M, Buchner J (2012) Alternative bacterial two-component small heat shock protein systems. *Proc Natl Acad Sci USA* 109: 20407-20412

Bergman LW, Kuehl WM (1979) Formation of intermolecular disulfide bonds on nascent immunoglobulin polypeptides. *J Biol Chem* 254: 5690-5694

Bernabeu C, Lake JA (1982) Nascent polypeptide chains emerge from the exit domain of the large ribosomal subunit: immune mapping of the nascent chain. *Proc Natl Acad Sci U S A* 79: 3111-3115

Beringer M (2008) Modulating the activity of the peptidyl transferase center of the ribosome. *RNA* 14: 795-801

Bhushan S, Gartmann M, Halic M, Armache JP, Jarasch A, Mielke T, Berninghausen O, Wilson DN, Beckmann R (2010) alpha-Helical nascent polypeptide chains visualized within distinct regions of the ribosomal exit tunnel. *Nat Struct Mol Biol* 17: 313-317

Biederer T, Volkwein C, Sommer T (1997) Role of Cue1p in ubiquitination and degradation at the ER surface. *Science* 278: 1806-1809

Bingel-Erlenmeyer R, Kohler R, Kramer G, Sandikci A, Antolic S, Maier T, Schaffitzel C, Wiedmann B, Bukau B, Ban N (2008) A peptide deformylase-ribosome complex reveals mechanism of nascent chain processing. *Nature* 452: 108-111

Blobel G, Sabatini DD (1970) Controlled proteolysis of nascent polypeptides in rat liver cell fractions. I.Location of the polypeptides within ribosomes. *J Cell Biol* 45: 130-145

Bloss TA, Witze ES, Rothman JH (2003) Suppression of CED-3-independent apoptosis by mitochondrial betaNAC in *Caenorhabditis elegans*. *Nature* 424: 1066-1071

Bosl B, Grimminger V, Walter S (2006) The molecular chaperone Hsp104 - a molecular machine for protein disaggregation. *J Struct Biol* 156: 139-148

Borgia MB, Borgia A, Best RB, Steward A, Nettels D, Wunderlich B, Schuler B, Clarke J (2011) Singlemolecule fluorescence reveals sequence-specific misfolding in multidomain proteins. *Nature* 474: 662-665

Borgia A, Kemplen KR, Borgia MB, Soranno A, Shammas S, Wunderlich B, Nettels D, Best RB, Clarke J, Schuler B (2015) Transient misfolding dominates multidomain protein folding. *Nat Commun* 6: 8861

Boutin JA (1997) Myristoylation. *Cell Signal* 9: 15-35

Braakman I, Hebert DN (2013) Protein folding in the endoplasmic reticulum. *Cold Spring Harb Perspect Biol* 5: a013201

Bradford MM (1976) A rapid and sensitive method for the quantitation of microgram quantities of protein utilizing the principle of protein-dye binding. *Anal Biochem* 72: 248-254

Brahms S, Brahms J (1980) Determination of protein secondary structure in solution by vacuum ultraviolet circular dichroism. *J Mol Biol* 138: 149-178

Brandvold KR, Morimoto RI (2015) The Chemical Biology of Molecular Chaperones-Implications for Modulation of Proteostasis. *J Mol Biol* 427: 2931-2947

Braun JE, Huntzinger E, Fauser M, Izaurralde E (2011) GW182 proteins directly recruit cytoplasmic deadenylase complexes to miRNA targets. *Mol Cell* 44: 120-133

Braun N, Zacharias M, Peschek J, Kastenmuller A, Zou J, Hanzlik M, Haslbeck M, Rappsilber J, Buchner J, Weinkauf S (2011) Multiple molecular architectures of the eye lens chaperone αB-crystallin elucidated by a triple hybrid approach. *Proc Natl Acad Sci USA* 108: 20491-20496

Brengues M, Teixeira D, Parker R (2005) Movement of eukaryotic mRNAs between polysomes and cytoplasmic processing bodies. *Science* 310: 486-489

Bridgman WB (1942) Some physical characteristics of glycogen. *J Am Chem Soc* 64: 2349-2356

Brockstedt E, Otto A, Rickers A, Bommert K, Wittman-Liebold B (1999) Preparative high-resolution two-dimensional electrophoresis enables the identification of RNA polymerase B transcription factor 3 as an apoptosis-associated protein in the human BL60-2 Burkitt lymphoma cell line. *J Protein Chem* 18: 225-231

Brockwell DJ, Radford SE (2007) Intermediates: ubiquitous species on folding energy landscapes? *Curr Opin Struct Biol* 17: 30-37

Bryngelson JD, Onuchic JN, Socci ND, Wolynes PG (1995) Funnels, pathways, and the energy landscape of protein folding: a synthesis. *Proteins* 21: 167-195

Buchan JR, Muhlrad D, Parker R (2008) P bodies promote stress granule assembly in *Saccharomyces cerevisiae*. *J Cell Biol* 183: 441-455

Buchan JR, Nissan T, Parker R (2010) Analyzing P-bodies and stress granules in *Saccharomyces cerevisiae*. *Methods Enzymol* 470: 619-640

Buchan JR, Yoon JH, Parker R (2011) Stress-specific composition, assembly and kinetics of stress granules in *Saccharomyces cerevisiae*. *J Cell Sci* 124: 228-239

Buchner J (1996) Supervising the fold: functional principles of molecular chaperones. *The FASEB journal* 10: 10-19

Buchner J, Grallert H, Jakob U (1998) Analysis of chaperone function using citrate synthase as nonnative substrate protein. *Methods Enzymol* 290: 323-338

Buchner GS, Murphy RD, Buchete NV, Kubelka J (2011) Dynamics of protein folding: probing the kinetic network of folding-unfolding transitions with experiment and theory. *Biochim et biophys acta* 1814: 1001-1020

Bukau B (2005) Ribosomes catch Hsp70s. *Nat Struct Biol* 12: 472-473

Bukau B, Deuerling E, Pfund C, Craig EA (2000) Getting newly synthesized proteins into shape. *Cell* 101: 119-122

Bukau B, Horwich AL (1998) The Hsp70 and Hsp60 chaperone machines. *Cell* 92: 351-366

Cabrita LD, Dobson CM, Christodoulou J (2010) Protein folding on the ribosome. *Curr Opin Struct Biol* 20: 33-45

Cary GA, Vinh DBN, May P, Kuestner R, Dudley AM (2015) Proteomic analysis of Dhh1 complexes reveals a role for Hsp40 chaperone Ydj1 in yeast P-body assembly. *G3 (Bethesda)* 5: 2497-2511

Cashikar AG, Duennwald M, Lindquist SL (2005) A Chaperone Pathway in Disaggregation: Hsp26 alters the nature of protein aggregates to facilitate reactivation by Hsp104. *J Biol Chem* 280: 23869-23875

Cate JH, Yusupov MM, Yusupova GZ, Earnest TN, Noller HF (1999) X-ray crystal structures of 70S ribosome functional complexes. *Science* 285: 2095-2104

Chandramouli P, Topf M, Menetret JF, Eswar N, Cannone JJ, Gutell RR, Sali A, Akey CW (2008) Structure of the mammalian 80S ribosome at 8.7 A resolution. *Structure* 16: 535-548

Chen S, Schultz, PG, Brock A (2007) An Improved System for the Generation and Analysis of Mutant Proteins Containing Unnatural Amino Acids in *Saccharomyces cerevisiae*. *J Mol Biol* 371: 112-122

Chiti F, Dobson CM (2006) Protein misfolding, functional amyloid, and human disease. *Annu Rev Biochem* 75: 333-366

Ciechanover A, Brundin P (2003) The ubiquitin proteasome system in neurodegenerative diseases: sometimes the chicken, sometimes the egg. *Neuron* 40: 427-446

Clark AR, Naylor CE, Bagneris C, Keep NH, Slingsby C (2011) Crystal structure of R120G disease mutant of human αB-crystallin domain dimer shows closure of a groove. *J Mol Biol* 408: 118-134

Clerico EM, Tilitsky JM, Meng W, Gierasch LM (2015) How hsp70 molecular machines interact with their substrates to mediate diverse physiological functions. *J Mol Biol* 427: 1575-1588

Compton LA, Johnson WC (1986) Analysis of protein circular dichroism spectra for secondary structure using a simple matrix multiplication. *Anal Biochem* 155: 155-167

Conz C, Otto H, Peisker K, Gautschi M, Wolfle T, Mayer MP, Rospert S (2007) Functional characterization of the atypical Hsp70 subunit of yeast ribosome-associated complex. *J Biol Chem* 282: 33977-33984

Cowie DB, Spiegelman S, Roberts RB, Duerksen JD (1961) Ribosome-bound beta-galactosidase. *Proc Natl Acad Sci U S A* 47: 114-122

Craig EA, Eisenman HC, Hundley HA (2003) Ribosome-tethered molecular chaperones: the first line of defense against protein misfolding? *Curr Opin Microbiol* 6: 157-162

Cross BC, Sinning I, Luirink J, High S (2009) Delivering proteins for export from the cytosol. *Nat Rev Mol Cell Biol* 10: 255-264

Cuchillo R, Michel J (2012) Mechanisms of small-molecule binding to intrinsically disordered proteins. *Biochem Soc Trans* 40: 1004-1008

Dalley JA, Selkirk A, Pool MR (2008) Access to ribosomal protein Rpl25p by the signal recognition particle is required for efficient cotranslational translocation. *Mol Biol Cell* 19: 2876-2884

Das KP, Surewicz, WK (1995) Temperature-induced exposure of hydrophobic surfaces and its effect on the chaperone activity of alpha-crystallin. *FEBS Lett* 369: 321-325

Decker CJ, Parker R (2012) P-bodies and stress granules: possible roles in the control of translation and mRNA degradation. *Cold Spring Harb Perspect Biol* 4(9): a012286

De Jong WW, Leunissen JA, Voorter CE (1993) Evolution of the alpha-crystallin/small heat-shock protein family. *Mol Biol Evol* 10: 103-126

del Alamo M, Hogan DJ, Pechmann S, Albanese V, Brown PO, Frydman J (2011) Defining the specificity of cotranslationally acting chaperones by systematic analysis of mRNAs associated with ribosome-nascent chain complexes. *PLoS Biol* 9: e1001100

Delbecq P, Calvo O, Filipkowski RK, Pierard A, Messenguy F (2000) Functional analysis of the leader peptide of the yeast gene CPA1 and heterologous regulation by other fungal peptides. *Curr Genet* 38: 105-112

Delbecq SP, Klevit RE (2013) One size does not fit all: the oligomeric states of αB crystallin. *FEBS Lett* 587: 1073-1080

Deng JM, Behringer RR (1995) An insertional mutation in the BTF3 transcription factor gene leads to an early postimplantation lethality in mice. *Transgenic Res* 4: 264-269

Deuerling E, Bukau B (2004) Chaperone-assisted folding of newly synthesized proteins in the cytosol. *Crit Rev Biochem Mol Biol* 39: 261-277

Douglas PM, Dillin A (2010) Protein homeostasis and aging in neurodegeneration. *J Cell Biol* 190: 719-729

Dragovic Z, Broadley SA, Shomura Y, Bracher A, Hartl FU (2006) Molecular chaperones of the Hsp110 family act as nucleotide exchange factors of Hsp70s. *Embo J* 25: 2519-2528

Drescher M, Huber M, Subramaniam V (2012) Hunting the chameleon: structural conformations of the intrinsically disordered protein alpha-synuclein. *Chembiochem* 13: 761-768

Doyle S M, Wickner S (2009) Hsp104 and ClpB: protein disaggregating machines. *Trends Biochem Sci* 34: 40-48

Dumitru GL, Groemping Y, Klostermeier D, Restle T, Deuerling E, Reinstein J (2004) DafA cycles between the DnaK chaperone system and translational machinery. *J Mol Biol* 339: 1179-1189

Dunker AK, Silman I, Uversky VN, Sussman JL (2008) Function and structure of inherently disordered proteins. *Curr Opin Struct Biol* 18: 756-764

Duttler S, Pechmann S, Frydman J (2013) Principles of cotranslational ubiquitination and quality control at the ribosome. *Mol Cell* 50: 379-393

Ebeling W, Hennrich N, Klockow M, Metz H, Orth, HD, Lang H (1974) Proteinase K from *Tritirachium album Limber*. *Eur J Biochem* 47: 91-97

Edgar RC (2004) MUSCLE: multiple sequence alignment with high accuracy and high throughput. *Nucleic Acids Res* 32: 1792-1797

Eichmann C, Preissler S, Riek R, Deuerling E (2010) Cotranslational structure acquisition of nascent polypeptides monitored by NMR spectroscopy. *Proc Natl Acad Sci U S A* 107: 9111-9116

Eifert C, Burgio MR, Bennett, PM, Salerno JC, Koretz, JF (2005) N-terminal control of small heat shock protein oligomerization: changes in aggregate size and chaperone-like function. *Biochim Biophys Acta* 1748: 146-156

Ellis RJ (1996) Revisiting the Anfinsen cage. *Fold Des* 1: R9-15

Ellis RJ, Hartl FU (1999) Principles of protein folding in the cellular environment. *Curr Opin Struct Biol* 9: 102-110

Ellis RJ, Minton AP (2006) Protein aggregation in crowded environments. *Biol Chem* 387: 485-497

Escusa-Toret S, Vonk WI, Frydman J (2013) Spatial sequestration of misfolded proteins by a dynamic chaperone pathway enhances cellular fitness during stress. *Nat Cell Biol* 15: 1231-1243

Eulalio A, Behm-Ansmant I, Schweizer D, Izaurralde E (2007) P-body formation is a consequence, not the cause, of RNA-mediated gene silencing. *Mol Cell Biol* 27: 3970-3981

Evans MS, Ugrinov KG, Frese MA, Clark PL (2005) Homogeneous stalled ribosome nascent chain complexes produced in vivo or in vitro. *Nat Methods* 2: 757-762

Falb M, Aivaliotis M, Garcia-Rizo C, Bisle B, Tebbe A, Klein C, Konstantinidis K, Siedler F, Pfeiffer F, Oesterhelt D (2006) Archaeal N-terminal protein maturation commonly involves N-terminal acetylation: a large-scale proteomics survey. *J Mol Biol* 362: 915-924

Farazi TA, Waksman G, Gordon JI (2001) The biology and enzymology of protein N-myristoylation. *J Biol Chem* 276: 39501-39504

Fry KT, Lamborg MR (1967) Amidohydrolase activity of Escherichia coli extracts with formylated amino acids and dipeptides as substrates. *J Mol Biol* 28: 423-433

Fedorov AN, Baldwin TO (1997) Cotranslational protein folding. *J Biol Chem* 272: 32715-32718

Fedorov AN, Baldwin TO (1999) Process of biosynthetic protein folding determines the rapid formation of native structure. *J Mol Biol* 294: 579-586

Fiaux J, Horst J, Scior A, Preissler S, Koplin A, Bukau B, Deuerling E (2010) Structural analysis of the ribosome-associated complex (RAC) reveals an unusual Hsp70/Hsp40 interaction. *J Biol Chem* 285: 3227-3234

Frank J, Zhu J, Penczek P, Li Y, Srivastava S, Verschoor A, Radermacher M, Grassucci R, Lata RK, Agrawal RK (1995) A model of protein synthesis based on cryo-electron microscopy of the *E. coli* ribosome. *Nature* 376: 441-444

Franke J, Reimann B, Hartmann E, Kohlerl M, Wiedmann B (2001) Evidence for a nuclear passage of nascent polypeptide-associated complex subunits in yeast. *J Cell Sci* 114: 2641-2648

Freire MA (2005) Translation initiation factor (iso) 4E interacts with BTF3, the beta subunit of the nascent polypeptide-associated complex. *Gene* 345: 271-277

Frickey T, Lupas AN (2004) CLANS: A Java application for visualizing protein families based on pairwise similarity. *Bioinformatics* 20: 3702-3704

Frydman J, Erdjument-Bromage H, Tempst P, Hartl FU (1999) Co-translational domain folding as the structural basis for the rapid de novo folding of firefly luciferase. *Nat Struct Biol* 6: 697-705

Fuentealba LC, Eivers E, Geissert D, Taelman V, De Robertis EM (2008) Asymmetric mitosis: Unequal segregation of proteins destined for degradation. *Proc Natl Acad Sci U S A* 105: 7732-7737

Fünfschilling U, Rospert S (1999) Nascent polypeptide-associated complex stimulates protein import into yeast mitochondria. *Mol Biol Cell* 10: 3289-3299

Gabashvili IS, Gregory ST, Valle M, Grassucci R, Worbs M, Wahl MC, Dahlberg AE, Frank J (2001) The polypeptide tunnel system in the ribosome and its gating in erythromycin resistance mutants of L4 and L22. *Mol Cell* 8: 181-188

Gaczynska M, Osmulski PA, Ward WF (2001) Caretaker or undertaker? The role of the proteasome in aging. *Mech Ageing Dev* 122: 235-254

Gamerdinger M, Hanebuth MA, Frickey T, Deuerling E (2015) The principle of antagonism ensures protein targeting specificity at the endoplasmic reticulum. *Science* 348: 201-207

García-Mata R, Bebok Z, Sorscher EJ, Sztul ES (1999) Characterization and dynamics of aggresome formation by a cytosolic GFP-chimera. *J Cell Biol* 146: 1239-1254

Garmendia-Torres C, Skupin A, Michael SA, Ruusuvuori P, Kuwada NJ, Falconnet D, Cary GA, Hansen C, Wiggins PA, Dudley AM (2014) Unidirectional P-body transport during the yeast cell cycle. *PLoS ONE* 9(6): e99428

Gautschi M, Just S, Mun A, Ross S, Rucknagel P, Dubaquie Y, Ehrenhofer-Murray A, Rospert S (2003) The yeast N(alpha)-acetyltransferase NatA is quantitatively anchored to the ribosome and interacts with nascent polypeptides. *Mol Cell Biol* 23: 7403-7414

Gautschi M, Lilie H, Funfschilling U, Mun A, Ross S, Lithgow T, Rucknagel P, Rospert S (2001) RAC, a stable ribosome-associated complex in yeast formed by the DnaK-DnaJ homologs Ssz1p and zuotin. *Proc Natl Acad Sci U S A* 98: 3762-3767

Gautschi M, Mun A, Ross S, Rospert S (2002) A functional chaperone triad on the yeast ribosome. *Proc Natl Acad Sci U S A* 99: 4209-4214

Genest O, Hoskins JR, Kravats AN, Doyle SM, Wickner S (2015) Hsp70 and Hsp90 of *E. coli* Directly Interact for Collaboration in Protein Remodelling. *J Mol Biol* 427: 3877-3889

George R, Beddoe T, Landl K, and Lithgow T (1998) The yeast nascent polypeptide-associated complex initiates protein targeting to mitochondria in vivo. *Proc Natl Acad Sci U S A* 95: 2296-2301

George R, Walsh P, Beddoe T, Lithgow T (2002) The nascent polypeptide-associated complex (NAC) promotes interaction of ribosomes with the mitochondrial surface *in vivo*. *FEBS Lett* 516: 213-216

Gershenson A, Gierasch LM (2011) Protein folding in the cell: challenges and progress. *Curr Opin Struct Biol* 21: 32-41

Ghaemmaghami S, Huh WK, Bower K, Howson RW, Belle A, Dephoure N, O'Shea EK, Weissman JS (2003) Global analysis of protein expression in yeast. *Nature* 425: 737-741

Gidalevitz T, Ben-Zvi A, Ho KH, Brignull HR, Morimoto RI (2006) Progressive disruption of cellular protein folding in models of polyglutamine diseases. *Science* 311: 1471-1474

Giglione C, Boularot A, Meinnel T (2004) Protein N-terminal methionine excision. *Cell Mol Life Sci* 61: 1455-1474

Giglione C, Fieulaine S, Meinnel T (2009) Cotranslational processing mechanisms: towards a dynamic 3D model. *Trends Biochem Sci* 34: 417-426

Giglione C, Fieulaine S, Meinnel T (2015) N-terminal protein modifications: Bringing back into play the ribosome. *Biochimie* 114: 134-146

Gloge F, Becker AH, Kramer G, Bukau B (2014) Co-translational mechanisms of protein maturation. *Curr Opin Struct Biol* 24: 24-33

Goatley LC, Twigg SR, Miskin JE, Monaghan P, St-Arnaud R, Smith GL, Dixon LK (2002) The African swine fever virus protein j4R binds to the alpha chain of nascent polypeptide associated complex. *J Virol* 76: 9991-9999

Greene MK, Maskos K, Landry SJ (1998) Role of the J-domain in the cooperation of Hsp40 with Hsp70. *Proc Natl Acad Sci U S A* 95: 6108-6113

Gruebele M (2005) Downhill protein folding: evolution meets physics. *Comptes Rendus Biol* 328: 701-712

Guerra-Moreno A, Isasa M, Bhanu MK, Waterman DP, Eapen, VV, Gygi SP, Hanna J (2015) Proteomic Analysis Identifies Ribosome Reduction as an Effective Proteotoxic Stress Response. *J Biol Chem* 290: 29695-29706

Güldener U, Heck S, Fielder T, Beinhauer J, Hegemann JH (1996) A new efficient gene disruption cassette for repeated use in budding yeast. *Nucleic Acids Res* 24: 2519-2524

Gundersen V (2010) Protein aggregation in Parkinson's disease. *Acta Neurol Scand Suppl* s190: 82-87

Guo B, Huang J, Wu W, Feng D, Wang X, Chen Y, Zhang H (2014) The nascent polypeptide-associated complex is essential for autophagic flux. *Autophagy* 10: 1738-1748

Haiber, L-M (2015) Analyse der Ko-Lokalisation von Firefly Luciferase und Chaperonen in *S. cerevisiae*. *Bachelor Thesis*

Halic M, Becker T, Pool MR, Spahn CM, Grassucci RA, Frank J, Beckmann R (2004) Structure of the signal recognition particle interacting with the elongation-arrested ribosome. *Nature* 427: 808-814

Halic M, Blau M, Becker T, Mielke T, Pool MR, Wild K, Sinning I, Beckmann R (2006a) Following the signal sequence from ribosomal tunnel exit to signal recognition particle. *Nature* 444: 507-511

Halic M, Gartmann M, Schlenker O, Mielke T, Pool MR, Sinning I, Beckmann R (2006b) Signal recognition particle receptor exposes the ribosomal translocon binding site. *Science* 312: 745-747

Hamlin J, Zabin I (1972) -Galactosidase: immunological activity of ribosome-bound, growing polypeptide chains. *Proc Natl Acad Sci U S A* 69: 412-416

Hanazono Y, Takeda K, Oka T, Abe T, Tomonari T, Akiyama N, Aikawa Y, Yohda M, Miki K (2013) Nonequivalence observed for the 16-meric structure of a small heat shock protein, SpHsp16.0, from *Schizosaccharomyces pombe*. *Structure* 21: 220-228

Hanson PI, Whiteheart SW (2005) AAA+ proteins: have engine, will work. *Nat Rev Mol Cell Biol* 6: 519-529

Hartl FU (1996) Molecular chaperones in cellular protein folding. *Nature* 381: 571-579

Hartl FU, Bracher A, Hayer-Hartl M (2011) Molecular chaperones in protein folding and proteostasis. *Nature* 475: 324-332

Hartl FU, Hayer-Hartl M (2009) Converging concepts of protein folding in vitro and in vivo. *Nat Struct Mol Biol* 16: 574-581

Hartl FU, Hayer-Hartl M (2002) Molecular chaperones in the cytosol: from nascent chain to folded protein. *Science* 295: 1852-1858

Haslbeck M (2002) sHsps and their role in the chaperone network. *Cell Mol Life Sci* 59: 1649-1657

Haslbeck M, Miess A, Stromer T, Walter S, Buchner J (2005) Disassembling Protein Aggregates in the Yeast Cytosol: The Cooperation of Hsp26 with Ssa1 and Hsp104. *J Biol Chem* 280: 23861-23868

Haslbeck M, Walke S, Stromer T, Ehrnsperger M, White HE, Chen S, Saibil HR, Buchner J (1999) Hsp26: a temperature-regulated chaperone. *EMBO J* 18: 6744-6751

Haslbeck M, Vierling E (2015) A first line of stress defense: small heat shock proteins and their function in protein homeostasis. *J Mol Biol* 427: 1537-1548

Haslberger T, Zdanowicz A, Brand I, Kirstein J, Turgay K, Mogk A, Bukau B (2008) Protein disaggregation by the AAA+ chaperone ClpB involves partial threading of looped polypeptide segments. *Nat Struct Mol Biol* 15: 641-650

Hayashi S, Andoh T, Tani T (2011) *EGD1* (β-NAC) mRNA is localized in a novel cytoplasmic structure in *Saccharomyces cerevisiae*. *Genes to Cells* 16: 316-329

Henderson KA, Gottschling DE (2008) A mother's sacrifice: what is she keeping for herself? *Curr Opin Cell Biol* 20: 723-728

Herbst R, Gast K, Seckler R (1998) Folding of firefly (Photinus pyralis) luciferase: aggregation and reactivation of unfolding intermediates. *Biochemistry* 37: 6586-6597

Hershko A, Ciechanover A (1992) The ubiquitin system for protein degradation. *Annu Rev Biochem* 61: 761-807

Hilton GR, Lioe H, Stengel F, Baldwin AJ, Benesch JL (2013) Small heat-shock proteins: paramedics of the cell. *Top Curr Chem* 328: 69-98

Hingorani KS, Gierasch LM (2014) Comparing protein folding in vitro and in vivo: foldability meets the fitness challenge. *Curr Opin Struct Biol* 24: 81-90

Hipp MS, Park SH, Hartl FU (2014) Proteostasis impairment in protein-misfolding and –aggregation diseases. *Trends Cell Biol* 24: 506-514

Hiraishi H, Shimada T, Ohtsu I, Sato TA, Takagi H (2009) The yeast ubiquitin ligase Rsp5 downregulates the alpha subunit of nascent polypeptide-associated complex Egd2 under stress conditions. *FEBS J* 276: 5287-5297

Hochberg GK, Benesch, JL (2014) Dynamical structure of αB-crystallin. *Prog Biophys Mol Biol* 115: 11-20

Holcik M, Sonenberg N (2005) Translational control in stress and apoptosis. *Nat Rev Mol Cell Biol* 6: 318-327

Holtkamp W, Kokic G, Jäger M, Mittelstaet J, Komar AA, Rodnina MV (2015) Cotranslational protein folding on the ribosome monitored in real time. *Science* 350: 1104-1107

Hotokezaka Y, Katayama I, van Leyen K, Nakamura T (2015) GSK-3β-dependent downregulation of γ-taxilin and αNAC merge to regulate ER stress response. *Cell Death Differ* 6: e1719

Hotokezaka Y, van Leyen K, Lo EH, Beatrix B, Katayama I, Jin G, Nakamura T (2009) αNAC depletion as initiator of ER stress-induced apoptosis in hypoxia. *Cell Death Differ* 16: 1505-1514

Hoyle NP, Castelli LM, Campbell SG, Holmes LE, Ashe MP (2007) Stress-dependent relocalization of translationally primed mRNPs to cytoplasmic granules that are kinetically and spatially distinct from P-bodies. *J Cell Biol* 179: 65-74

Hradetzky S, Balaji H, Roesner LM, Heratizadeh A, Mittermann I, Valenta R, Werfel T (2013) The human skin-associated autoantigen α-NAC activates monocytes and dendritic cells via TLR-2 and primes an IL-12-dependent Th1 response. *J Invest Dermatol* 133: 2289-2292

Hsu ST, Cabrita LD, Fucini P, Christodoulou J, Dobson CM (2009) Probing side-chain dynamics of a ribosome-bound nascent chain using methyl NMR spectroscopy. *J Am Chem Soc* 131: 8366-8367

Hsu ST, Fucini P, Cabrita LD, Launay H, Dobson CM, Christodoulou J (2007) Structure and dynamics of a ribosome-bound nascent chain by NMR spectroscopy. *Proc Natl Acad Sci U S A* 104: 16516-16521

Hu G-Z, Ronne H (1994) Yeast BTF3 protein is encoded by duplicated genes and inhibits the expression of some genes *in vivo*. *Nucleic Acids Res* 22: 2740-2743

Huang P, Gautschi M, Walter W, Rospert S, Craig EA (2005) The Hsp70 Ssz1 modulates the function of the ribosome-associated J-protein Zuo1. *Nat Struct Mol Biol* 12: 497-504

Hundley H, Eisenman H, Walter W, Evans T, Hotokezaka Y, Wiedmann M, Craig E (2002) The in vivo function of the ribosome-associated Hsp70, Ssz1, does not require its putative peptide-binding domain. *Proc Natl Acad Sci U S A* 99: 4203-4208

Hundley HA, Walter W, Bairstow S, Craig EA (2005) Human Mpp11 J protein: ribosome-tethered molecular chaperones are ubiquitous. *Science* 308: 1032-1034

Hutt DM, Powers ET, Balch WE (2009) The proteostasis boundary in misfolding diseases of membrane traffic. *FEBS Lett* 583: 2639-2646

Hwang CS, Shemorry A, Varshavsky A (2010) N-terminal acetylation of cellular proteins creates specific degradation signals. *Science* 327: 973-977

Ingolia NT, Lareau LF, Weissman JS (2011) Ribosome profiling of mouse embryonic stem cells reveals the complexity and dynamics of mammalian proteomes. *Cell* 147: 789-802

Ito K, Chiba S, Pogliano K (2010) Divergent stalling sequences sense and control cellular physiology. *Biochem Biophys Res Commun* 393: 1-5

Jackson SE (1998) How do small single-domain proteins fold? *Fold Des* 3: R81-91

Jacobson T, Navarrete C, Sharma SK, Sideri TC, Ibstedt S, Priya S, Grant CM, Christen P, Goloubinoff P, Tamás MJ (2012) Arsenite interferes with protein folding and triggers formation of protein aggregates in yeast. *J Cell Sci* 125: 5073-5083

Jahn TR, Radford SE (2008) Folding versus aggregation: polypeptide conformations on competing pathways. *Arch Biochem Biophys* 469: 100-117

Jaiswal H, Conz C, Otto H, Wolfle T, Fitzke E, Mayer MP, Rospert S (2011) The chaperone network connected to human ribosome-associated complex. *Mol Cell Biol* 31: 1160-1173

Janes RW (2008) Reference Datasets Circular Dichroism and Synchrotron Radiation Circular Dichroism Spectroscopy of Proteins in: Modern Techniques in Circular Dichroism and Synchrotron Radiation Circular Dichroism Spectroscopy. Wallace BA and Janes RW, eds. *IOS Press, 2009* ISBN-10: 1607500000

Jaya N, Garcia V, Vierling E (2009) Substrate binding site flexibility of the small heat shock protein molecular chaperones. *Proc Natl Acad Sci U S A* 106: 15604-15609

Jehle S, van Rossum B, Stout JR, Noguchi SM, Falber K, Rehbein K, Oschkinat H, Klevit RE, Rajagopal P (2009) αB-crystallin: a hybrid solid-state/solution-state NRM investigation reveals structural aspects of the heterogeneous oligomer. *J Mol Biol* 385: 1481-1497

Jehle S, Vollmar BS, Bardiaux B, Dove KK, Rajagopal P, Gonen T, Oschkinat H, Klevit RE (2011) N-terminal domain of αB-crystallin provides a conformational switch for multimerization and structural heterogeneity. *Proc Natl Acad Sci U S A* 108: 6409-6414

Jenni S, Ban N (2003) The chemistry of protein synthesis and voyage through the ribosomal tunnel. *Curr Opin Struct Biol* 13: 212-219

Johnston JA, Ward CL, Kopito RR (1998) Aggresomes: a cellular response to misfolded proteins. *J Cell Biol* 143: 1883-1898

Kaganovich D, Kopito R, Frydman J (2008) Misfolded proteins partition between two distinct quality control compartments. *Nature* 454: 1088-1095

Kalies KU, Görlich D, Rapoport TA (1994) Binding of ribosomes to the rough endoplasmic reticulum mediated by the Sec61p-complex. *J Cell Biol* 124: 925-934

Kampinga HH, Craig EA (2010) The HSP70 chaperone machinery: J proteins as drivers of functional specificity. *Nat Rev Mol Cell Biol* 11: 579-592

Kanki T, Wang K, Baba M, Bartholomew CR, Lynch-Day MA, Du Z, Geng J, Mao K, Yang Z, Yen WL, Klionsky DJ (2009) A genomic screen for yeast mutants defective in selective mitochondrial autophagy. *Mol Biol Cell* 20: 4730-4738

Kappe G, Leunissen JA, De Jong WW (2002) Evolution and diversity of prokaryotic small heat shock proteins. *Prog Mol Subcell Biol* 28:01-17

Karplus M (1997) The Levinthal paradox: yesterday and today. *Fold Des* 2: S69-75

Karzai AW, McMacken R (1996) A bipartite signaling mechanism involved in DnaJ-mediated activation of the Escherichia coli DnaK protein. *J Biol Chem* 271: 11236-11246

Kaschner LA, Sharma R, Shrestha OK, Meyer AE, Craig EA (2015) A conserved domain important for association of eukaryotic J-protein co-chaperones Jjj1 and Zuo1 with the ribosome. *Biochim Biophys Acta* 1853: 1035-1045

Katranidis A, Atta D, Schlesinger R, Nierhaus KH, Choli-Papadopoulou T, Gregor I, Gerrits M, Buldt G, Fitter J (2009) Fast biosynthesis of GFP molecules: a single-molecule fluorescence study. *Angew Chem Int Ed Engl* 48: 1758-1761

Kaushik S, Cuervo AM (2015) Proteostasis and aging. *Nat Med* 21: 1406-1415

Kedersha N, Anderson P (2009) Regulation of translation by stress granules and processing bodies. *Prog Mol Biol Transl Sci* 90: 155-185

Kedersha N, Invanov P, Anderson P (2013) Stress granules and cell signaling: more than just a passing phase? *Trends Biochem Sci* 38: 494-506

Keenan RJ, Freymann DM, Stroud RM, Walter P (2001) The signal recognition particle. *Annu Rev Biochem* 70: 755-775

Kettern N, Dreiseidler M, Tawo R, Hohfeld J (2010) Chaperone-assisted degradation: multiple paths to destruction. *Biol Chem* 391: 481-489

Khatter H, Myasnikov AG, Natchiar SK, Klaholz BP (2015) Structure of the human 80S ribosome. *Nature* 520: 640-645

Kiho Y, Rich A (1964) Induced Enzyme Formed on Bacterial Polyribosomes. *Proc Natl Acad Sci U S A* 51: 111-118

Kim HK, Kim RR, Oh JH, Cho H, Varshavsky A, Hwang CS (2014) The N-terminal methionine of cellular proteins as a degradation signal. *Cell* 156: 158-169

Kim R, Kim KK, Yokota H, Kim SH (1998) Small heat shock protein of *Methanococcus jannaschii*, a hyperthermophile. *Proc Natl Acad Sci U S A* 95: 9129-9133

Kim SY, Craig EA (2005) Broad sensitivity of Saccharomyces cerevisiae lacking ribosome-associated chaperone ssb or zuo1 to cations, including aminoglycosides. *Eukaryot Cell* 4: 82-89

Kim YE, Hipp MS, Bracher A, Hayer-Hartl M, Hartl FU (2013) Molecular chaperone functions in protein folding and proteostasis. *Annu Rev Biochem* 82: 323-355

Kirstein-Miles J, Scior A, Deuerling E, Morimoto RI (2013) The nascent polypeptide-associated complex is a key regulator of proteostasis. *Embo J* 32: 1451-1468

Kitamura A, Kubota H (2010) Amyloid oligomers: dynamics and toxicity in the cytosol and nucleus. *FEBS J* 277: 1369-1379

Kleizen B, van Vlijmen T, de Jonge HR, Braakman I (2005) Folding of CFTR is predominantly cotranslational. *Mol Cell* 20: 277-287

Kolb VA, Makeyev EV, Spirin AS (2000) Co-translational folding of an eukaryotic multidomain protein in a prokaryotic translation system. *J Biol Chem* 275: 16597-16601

Komar AA (2009) A pause for thought along the co-translational folding pathway. *Trends Biochem Sci* 34: 16-24

Komar AA, Kommer A, Krasheninnikov IA, Spirin AS (1997) Cotranslational folding of globin. *J Biol Chem* 272: 10646-10651

Koplin A, Preissler S, Ilina Y, Koch M, Scior A, Erhardt M, Deuerling E (2010) A dual function for chaperones SSB-RAC and the NAC nascent polypeptide-associated complex on ribosomes. *J Cell Biol* 189: 57-68

Kosolapov A, Deutsch C (2009) Tertiary interactions within the ribosomal exit tunnel. *Nat Struct Mol Biol* 16: 405-411

Kosolapov A, Tu L, Wang J, Deutsch C (2004) Structure acquisition of the T1 domain of Kv1.3 during biogenesis. *Neuron* 44: 295-307

Koteiche HA, Chiu S, Majdoch RC, Stewart PL, Mchaourab HS (2005) Atomic models by cryo-EM and site-directed spin labeling: application to the N-terminal region of Hsp16.5. *Structure* 13: 1165-1171

Kramer G, Boehringer D, Ban N, Bukau B (2009) The ribosome as a platform for co-translational processing, folding and targeting of newly synthesized proteins. *Nat Struct Mol Biol* 16: 589-597

Kramer G, Guilbride DL, Bukau B (2015) Finding nascent proteins the right home. A protein complex prevents promiscuous targeting of nascent polypeptides in the cell. *Cell Biol* 348: 182-183

Kraus E, Femfert U (1976) Proteinase K from the mold *Tritirachium album Limber*. Specificity and mode of action. *Hoppe Seyler Z Physiol Chem* 357: 937-947

Krause SA, Xu H, Gray JV (2008) The synthetic genetic network around PKC1 identifies novel modulators and components of protein kinase C signaling in *Saccharomyces cerevisiae*. *Eukaryot Cell* 7: 1880-1887

Kriehuber T, Rattei T, Weinmaier T, Bepperling A, Haslbeck M, Buchner J (2010) Independent evolution of the core domain and its flanking sequences in small heat shock proteins. *FASEB J* 24: 3633-3642

Krishna MM, Englander SW (2005) The N-terminal to C-terminal motif in protein folding and function. *Proc Natl Acad Sci U S A* 102: 1053-1058

Kubelka J, Hofrichter J, Eaton WA (2004) The protein folding 'speed limit'. *Curr Opin Struct Biol* 14: 76-88

Kudlicki W, Chirgwin J, Kramer G, Hardesty B (1995) Folding of an enzyme into an active conformation while bound as peptidyl-tRNA to the ribosome. *Biochemistry* 34: 14284-14287

Kundu M, Thompson CB (2008) Autophagy: basic principles and relevance to disease. *Annu Rev Pathol* 3: 427-455

Laemmli UK (1970) Cleavage of structural proteins during the assembly of the head of bacteriophage T4. *Nature* 227: 680-685

Laganowsky A, Benesch JL, Landau M, Ding L, Sawaya MR, Cascio D, Huang Q, Robinson CV, Horwitz J, Eisenberg D (2010) Crystal structures of truncated αA and αB crystallins reveal structural mechanisms of polydispersity important for eye lens function. *Protein Sci* 19: 1031-1043

Land A, Zonneveld D, Braakman I (2003) Folding of HIV-1 envelope glycoprotein involves extensive isomerization of disulfide bonds and conformation-dependent leader peptide cleavage. *FASEB J* 17: 1058-1067

Laufen T, Mayer MP, Beisel C, Klostermeier D, Mogk A, Reinstein J, Bukau B (1999) Mechanism of regulation of hsp70 chaperones by DnaJ cochaperones. *Proc Natl Acad Sci U S A* 96: 5452-5457

Lauring B, Kreibich G, Weidmann M (1995a) The intrinsic ability of ribosomes to bind to endoplasmic reticulum membranes is regulated by signal recognition particle and nascent-polypeptide-associated complex. *Proc Natl Acad Sci U S A* 92: 9435-9439

Lauring B, Sakai H, Kreibich G, Wiedmann M (1995b) Nascent polypeptide-associated complex protein prevents mistargeting of nascent chains to the endoplasmic reticulum. *Proc Natl Acad Sci U S A* 92: 5411-5415

Lee U, Wie C, Escobat M, Williams B, Hong SW, Vierling E (2005) Genetic analysis reveals domain interactions of *Arabidopsis* Hsp100/ClpB and cooperation with the small heat shock protein chaperone system. *Plant Cell* 17: 559-571

Leeds JA, Dean CR (2006) Peptide deformylase as an antibacterial target: a critical assessment. *Curr Opin Pharmacol* 6: 445-452

Leidig C, Bange G, Kopp J, Amlacher S, Aravind A, Wickles S, Witte G, Hurt E, Beckmann R, Sinning I (2013) Structural characterization of a eukaryotic chaperone--the ribosome-associated complex. *Nat Struct Mol Biol* 20: 23-28

Lesnik C, Cohen Y, Atir-Lande A, Schuldiner M, Arava Y (2014) OM14 is a mitochondrial receptor for cytosolic ribosomes that supports co-translational import into mitochondria. *Nat Commun* 6: 6813

Li D, Wang X, Ding J, Yu J-P (2005) NACA as a Potential Cellular Target of Hepatitis B Virus PreS1 Protein. *Dig Dis Sci* 50:1156-1160

Li S, Chen X, Geng X, Zhan W, San J (2015) Identification and expression analysis of nascent polypeptide-associated complex alpha gene in response to immune challenges in Japanese flounder *Paralichthys olivaceus*. *Fish Shellfish Immunol* 46: 261-267

Lim VI, Spirin AS (1986) Stereochemical analysis of ribosomal transpeptidation. Conformation of nascent peptide. *Journal of molecular biology* 188: 565-574

Lindner AB, Madden R, Demarez A, Stewart EJ, Taddei F (2008) Asymmetric segregation of protein aggregates is associated with cellular aging and rejuvenation. *Proc Natl Acad Sci U S A* 105: 3076-3081

Liu B, Larsson L, Caballero A, Hao X, Oling D, Grantham J, Nystrom T (2010a) The polarisome is required for segregation and retrograde transport of protein aggregates. *Cell* 140: 257-267

Liu Y, Hu Y, Li X, Niu L, Teng M (2010b) The crystal structure of the human nascent polypeptideassociated complex domain reveals a nucleic acid-binding region on the NACA subunit. *Biochemistry* 49: 2890-2896

Lizardi PM, Engelberg A (1974) Rapid isolation of RNA using proteinase K and sodium perchlorate. *Anal Biochem* 98: 116-122

Locher, L (2012) Towards a molecular understanding of the mechanism of action of the nascent-polypeptide associated complex (NAC). *Master thesis*

Lopez S, Stuhl L, Fichelson S, Dubart-Kupperschmitt A, St-Arnaud R, Galindo JR, Murati A, Berda N, Dubreuil P, Gomez S (2005) NACA is a positive regulator of human erythroid-cell differentiation. *J Cell Sci* 118: 1595-1605

Lowther WT, Matthews BW (2002) Metalloaminopeptidases: common functional themes in disparate structural surroundings. *Chem Rev* 102: 4581-4608

Lu J, Deutsch C (2005a) Folding zones inside the ribosomal exit tunnel. *Nat Struct Mol Biol* 12: 1123- 1129

Lu J, Deutsch C (2005b) Secondary structure formation of a transmembrane segment in Kv channels. *Biochemistry* 44: 8230-8243

Lu J, Deutsch C (2008) Electrostatics in the ribosomal tunnel modulate chain elongation rates. *J Mol Biol* 384: 73-86

Lu J, Kobertz WR, Deutsch C (2007) Mapping the electrostatic potential within the ribosomal exit tunnel. *J Mol Biol* 371: 1378-1391

Luirink J, Sinning I (2004) SRP-mediated protein targeting: structure and function revisited. *Biochim Biophys Acta* 1694: 17-35

Macario AJ, Conway De Macario E (2001) The molecular chaperone system and other anti-stress mechanisms in archaea. *Front Biosci* 6: D262-283

Maiti P, Manna J, Veleri S, Frautschy S (2014) Molecular chaperone dysfunction in neurodegenerative diseases and effects of curcumin. *Biomed Res Int* 2014: 495091

Makeyev EV, Kolb VA, Spirin AS (1996) Enzymatic activity of the ribosome-bound nascent polypeptide. *FEBS Lett* 378: 166-170

Malinovska L, Kroschwald S, Munder MC, Richter D, Alberti S (2012) Molecular chaperones and stress-inducible protein-sorting factors coordinate the spatiotemporal distribution of protein aggregates. *Mol Biol Cell* 23: 3041-3056

Malkin LI, Rich A (1967) Partial resistance of nascent polypeptide chains to proteolytic digestion due to ribosomal shielding. *J Mol Biol* 26: 329-346

Manavalan P, Johnson WC Jr (1987) Variable selection method improves the prediction of protein secondary structure from circular dichroism spectra. *Anal Biochem* 167: 76-85

Mankin A (2006) Antibiotic blocks mRNA path on the ribosome. *Nat Struct Mol Biol* 13: 858-860

Mao D, Wachter E, Wallace BA (1982) Folding of the H+-ATPase Proteolipid in Phospholipid Vesicles. *Biochemistry* 21: 4960-4968

Marino J, von Heijne G, Beckmann R (2016) Small protein domains fold inside the ribosome exit tunnel. *FEBS Lett* 590: 655-660

Markesich DC, Gajewski KM, Nazimiec ME, Beckingham K (2000) bicaudal encodes the Drosophila beta NAC homolog, a component of the ribosomal translational machinery*. *Development* 127: 559-572

Martinez A, Traverso JA, Valot B, Ferro M, Espagne C, Ephritikhine G, Zivy M, Giglione C, Meinnel T (2008) Extent of N-terminal modifications in cytosolic proteins from eukaryotes. *Proteomics* 8: 2809-2831

Mayer MP (2010) Gymnastics of molecular chaperones. *Mol Cell* 39: 321-331

Mayer MP (2013) Hsp70 chaperone dynamics and molecular mechanism. *Trends Biochem Sci* 38: 507-514

Mayer MP, Bukau B (2005) Hsp70 chaperones: cellular functions and molecular mechanism. *Cell Mol Life Sci* 62: 670-684

Mayer MP, Kityk R (2015) Insights into the molecular mechanism of allostery in Hsp70s. *Front Mol Biosci* 2: 58

Mayer MP, Schroder H, Rudiger S, Paal K, Laufen T, Bukau B (2000) Multistep mechanism of substrate binding determines chaperone activity of Hsp70. *Nat Struct Biol* 7: 586-593

McHaourab HS, Lin YL, Spiller BW (2012) Crystal structure of an activated variant of small heat shock protein Hsp16.5. *Biochemistry* 51: 5105-5112

Meinnel T, Giglione C (2008) Tools for analyzing and predicting N-terminal protein modifications. *Proteomics* 8: 626-649

Meinnel T, Mechulam Y, Dardel F, Schmitter JM, Hountondji C, Brunie S, Dessen P, Fayat G, Blanquet S (1990) Methionyl-tRNA synthetase from *E. coli* - a review. *Biochimie* 72: 625-632

Miller SB, Mogk A, Bukau B (2015) Spatially organized aggregation of misfolded proteins as cellular stress defense strategy. *J Mol Biol* 427: 1564-1574

Minton AP (1980) Excluded volume as a determinant of protein structure and stability. *Biophys J* 32: 77-79

Minton AP (2001) The influence of macromolecular crowding and macromolecular confinement on biochemical reactions in physiological media. *J Biol Chem* 276: 10577-10580

Minton AP (2005) Influence of macromolecular crowding upon the stability and state of association of proteins: predictions and observations. *J Pharm Sci* 94: 1668-1675

Misselwitz B, Staeck O, Rapoport TA (1998) J proteins catalytically activate Hsp70 molecules to trap a wide range of peptide sequences. *Mol Cell* 2: 593-603

Mittermann I, Reininger R, Zimmermann M, Gangl K, Reisinger J, Aichberger KJ, Greisenegger EK, Niederberger V, Seipelt J, Bohle B, Kopp T, Akdis CA, Spitzauer S, Valent P, Valenta R (2008) The IgE-reactive autoantigen Hom s 2 induces damage of respiratory epithelial cells and keratinocytes via induction of IFN-γ. *J Invest Dermatol* 128: 1451-1459

Mogk A, Deuerling E, Vorderwulbecke S, Vierling E, Bukau B (2003) Small heat shock proteins, ClpB and the DnaK system form a functional triade in reversing protein aggregation. *Mol Microbiol* 50: 858-595

Mogk A, Kummer E, Bukau B (2015) Cooperation of Hsp70 and Hsp100 chaperone machines in protein disaggregation. *Front Mol Biosci* 2: 22

Möller I, Beatrix B, Kreibich G, Sakai H, Lauring B, Wiedmann M (1998a) Unregulated exposure of the ribosomal M-site caused by NAC depletion results in delivery of non-secretory polypeptides to the Sec61 complex. *FEBS Lett* 441: 1-5

Möller I, Jung M, Beatrix B, Levy R, Kreibich G, Zimmermann R, Wiedmann M, Lauring B (1998b) A general mechanism for regulation of access to the translocon: competition for a membrane attachment site on ribosomes. *Proc Natl Acad Sci U S A* 95: 13425-13430

Moreau A, Yotov WV, Glorieux FH, St-Arnaud R (1998) Bone-Specific Expression of the Alpha Chain of the Nascent Polypeptide-Associated Complex, a Coactivator Potentiating c-Jun-Mediated Transcription. *Mol Cell Biol* 18: 1312-1321

Moro F, Fernandez-Saiz V, Muga A (2004) The lid subdomain of DnaK is required for the stabilization of the substrate-binding site. *J Biol Chem* 279: 19600-19606

Mossabeb R, Seiberler S, Mittermann I, Reininger R, Spitzauer S, Natter S, Verdino P, Keller W, Kraft D, Valenta R (2002) Characterization of a novel isoform of alpha-nascent polypeptide-associated complex as IgE-defined autoantigen. *J Invest Dermatol* 119: 820-829

Mueller TD, Kamionka M, Feigon J (2004) Specificity of the interaction between ubiquitin-associated domains and ubiquitin. *J Biol Chem* 279: 11926-11936

Munz B, Wiedmann M, Lochmüller H, Werner S (1999) Cloning of Novel Injury-related Genes – Implications for an important role of the muscle-specific protein skNAC in muscle repair. *J Biol Chem* 274: 13305-13310

Naylor DJ, Hartl FU (2001) Contribution of molecular chaperones to protein folding in the cytoplasm of prokaryotic and eukaryotic cells. *Biochem Soc Symp*: 45-68

Nelson RJ, Ziegelhoffer T, Nicolet C, Werner-Washburne M, Craig EA (1992) The translation machinery and 70 kd heat shock protein cooperate in protein synthesis. *Cell* 71: 97-105

Netzer WJ, Hartl FU (1997) Recombination of protein domains facilitated by co-translational folding in eukaryotes. *Nature* 388: 343-349

Neuhof A, Rolls MM, Jungnickel B, Kalies KU, Rapoport TA (1998) Binding of signal recognition particle gives ribosome/nascent chain complexes a competitive advantage in endoplasmic reticulum membrane interaction. *Mol Biol Cell* 9: 103-115

Neuweiler H, Doose S, Sauer M (2005) A microscopic view of miniprotein folding: enhanced folding efficiency through formation of an intermediate. *Proc Natl Acad Sci U S A* 102: 16650-16655

Nijholt DA, De Kimpe L, Elfrink HL, Hoozemans JJ, Scheper W (2011) Removing protein aggregates: the role of proteolysis in neurodegeneration. *Curr Med Chem* 18: 2459-2476

Nillegoda NB, Kirstein J, Szlachcic A, Berynskyy M, Stank A, Stengel F, Arnsburg K, Gao X, Scior A, Aebersold R, Guilbride DL, Wade RC, Morimoto RI, Mayer MP, Bukau B (2015) Crucial HSP70 cochaperone complex unlocks metazoan protein disaggregation. *Nature* 524: 247-251

Nilsson OB, Hedman R, Marino J, Wickles S, Bischoff L, Johansson M, Müller-Lucks A, Trovato F, Puglisi JD, O'Brien EP, Beckmann R, von Heijne G (2015) Cotranslational Protein Folding inside the Ribosome Exit Tunnel. *Cell Rep* 12: 1533-1540

Nissen P, Hansen J, Ban N, Moore PB, Steitz TA (2000) The structural basis of ribosome activity in peptide bond synthesis. *Science* 289: 920-930

Novoa EM, Ribas de Pouplana L (2012) Speeding with control: codon usage, tRNAs, and ribosomes. *Trends Genet* 28: 574-581

Nyathi Y, Pool MR (2015) Analysis of the interplay of protein biogenesis factors at the ribosome exit site reveals new role for NAC. *J Cell Biol* 210: 287-301

Nyström T (2005) Role of oxidative carbonylation in protein quality control and senescence. *Embo J* 24: 1311-1317

O'Brien EP, Hsu ST, Christodoulou J, Vendruscolo M, Dobson CM (2010) Transient tertiary structure formation within the ribosome exit port. *J Am Chem Soc* 132: 16928-16937

Oka OB, Bulleid NJ (2013) Forming disulfides in the endoplasmic reticulum. *Biochim Biophys Acta* 1833: 2425-2429

Olzscha H, Schermann SM, Woerner AC, Pinkert S, Hecht MH, Tartaglia GG, Vendruscolo M, Hayer-Hartl M, Hartl FU, Vabulas RM (2011) Amyloid-like aggregates sequester numerous metastable proteins with essential cellular functions. *Cell* 144: 67-78

Onuchic JN, Luthey-Schulten Z, Wolynes PG (1997) Theory of protein folding: the energy landscape perspective. *Annu Rev Phys Chem* 48: 545-600

Onuchic JN, Socci ND, Luthey-Schulten Z, Wolynes PG (1996) Protein folding funnels: the nature of the transition state ensemble. *Fold Des* 1: 441-450

Ott A-K, Locher L, Koch M, Deuerling E (2015) Functional Dissection of the Nascent Polypeptide-Associated Complex in *Saccharomyces cerevisiae*. *PLoS ONE* 10: e0143457

Otto H, Conz C, Maier P, Wolfle T, Suzuki CK, Jeno P, Rucknagel P, Stahl J, Rospert S (2005) The chaperones MPP11 and Hsp70L1 form the mammalian ribosome-associated complex. *Proc Natl Acad Sci U S A* 102: 10064-10069

Palmiter RD, Gagnon J, Walsh KA (1978) Ovalbumin: a secreted protein without a transient hydrophobic leader sequence. *Proc Natl Acad Sci U S A* 75: 94-98

Panasenko OO, David FP, Collart MA (2009) Ribosome association and stability of the nascent polypeptide-associated complex is dependent upon its own ubiquitination. *Genetics* 181: 447-460

Panasenko O, Landrieux E, Feuermann M, Finka A, Paquet N, Collart MA (2006) The yeast Ccr4-Not complex controls ubiquitination of the nascent-associated polypeptide (NAC-EGD) complex. *J Biol Chem* 281: 31389-31398

Park SH, Kukushkin Y, Gupta R, Chen T, Konagai A, Hipp MS, Hayer-Hartl M, Hartl FU (2013) PolyQ proteins interfere with nuclear degradation of cytosolic proteins by sequestering the Sis1p chaperone. *Cell* 154: 134-145

Parsell DA, Kowal AS, Lindquist S (1994a) *Saccharomyces cerevisiae* Hsp104 protein: Purification and characterization of ATP induced structural changes. *J Biol Chem* 11: 4480-4487

Parsell DA, Kowal AS, Singer MA, Lindquist S (1994b) Protein disaggregation mediated by the heat-shock protein Hsp104. *Nature* 372: 475-478

Parthun MR, Mangus DA, Jaehning JA (1992) The *EGD1* product, a yeast homolog of human BTF3, may be involved in GAL4 DNA binding. *Mol Cell Biol* 12: 5683-5689

Pech M, Spreter T, Beckmann R, Beatrix B (2010) Dual binding mode of the nascent polypeptideassociated complex reveals a novel universal adapter site on the ribosome. *J Biol Chem* 285: 19679-19687

Peisker K, Braun D, Wölfle T, Hentschel J, Fünfschilling U, Fischer G, Sickmann A, Rospert S (2008) Ribosome-associated complex binds to ribosomes in close proximity of Rpl31 at the exit site of the polypeptide tunnel in yeast. *Mol Biol Cell* 19: 5279-5288

Peisker K, Chiabudini M, Rospert S (2010) The ribosome-bound Hsp70 homolog Ssb of *Saccharomyces cerevisiae*. *Biochim Biophys Acta* 1803: 662-672

Pellecchia M, Szyperski T, Wall D, Georgopoulos C, Wuthrich K (1996) NMR structure of the J-domain and the Gly/Phe-rich region of the Escherichia coli DnaJ chaperone. *J Mol Biol* 260: 236-250

Peschek J, Braun N, Rohrberg J, Back KC, Kriehuber T, Kastenmüller A, Weinkauf S, Buchner J (2013) Regulated structural transitions unleash the chaperone activity of αB-crystallin. *Proc Natl Acad Sci* 110: E3780-3789

Pestana A, Pitot HC (1975) Acetylation of nascent polypeptide chains on rat liver polyribosomes *in vivo* and *in vitro*. *Biochemistry* 14: 1404-1412

Pfund C, Lopez-Hoyo N, Ziegelhoffer T, Schilke BA, Lopez-Buesa P, Walter WA, Wiedmann M, Craig EA (1998) The molecular chaperone Ssb from *Saccharomyces cerevisiae* is a component of the ribosome-nascent chain complex. *Embo J* 17: 3981-3989

Picking WD, Picking WL, Odom OW, Hardesty B (1992) Fluorescence characterization of the environment encountered by nascent polyalanine and polyserine as they exit *Escherichia coli* ribosomes during translation. *Biochemistry* 31: 2368-2375

Pine MJ (1969) Kinetics of maturation of the amino termini of the cell proteins of Escherichia coli. *Biochim Biophys Acta* 174: 359-372

Plath K, Rapoport TA (2000) Spontaneous release of cytosolic protein from posttranslational substrates before their transport into the endoplasmic reticulum. *J Cell Biol* 151: 167-178

Polevoda B, Arnesen T, Sherman F (2009) A synopsis of eukaryotic Nalpha-terminal acetyltransferases: nomenclature, subunits and substrates. *BMC proceedings* 3 Suppl 6: S2

Polevoda B, Brown S, Cardillo TS, Rigby S, Sherman F (2008) Yeast N(alpha)-terminal acetyltransferases are associated with ribosomes. *J Cell Biochem* 103: 492-508

Polevoda B, Sherman F (2000) Nalpha -terminal acetylation of eukaryotic proteins. *J Biol Chem* 275: 36479-36482

Powers ET, Morimoto RI, Dillin A, Kelly JW, Balch WE (2009) Biological and chemical approaches to diseases of proteostasis deficiency. *Annu Rev Biochem* 78: 959-991

Powers T, Walter P (1996) The nascent polypeptide-associated complex modulates interactions between the signal recognition particle and the ribosome. *Curr Biol* 6: 331-338

Preissler S (2011) Insights into cotranslational protein folding and protein quality control systems on ribosomes. *PhD thesis*

Preissler S, Deuerling E (2012) Ribosome-associated chaperones as key players in proteostasis. *Trends Biochem Sci* 37: 274-283

Qian YQ, Patel D, Hartl FU, McColl DJ (1996) Nuclear magnetic resonance solution structure of the human Hsp40 (HDJ-1) J-domain. *J Mol Biol* 260: 224-235

Quélo I, Akhouayri O, Prud'homme J, St-Arnaud R (2004a) GSK3β-Dependent Phosphorylation of the αNAC Coactivator Regulates Its Nuclear Translocation and Proteasome-Mediated Degradation. *Biochemistry* 43: 2906-2914

Quélo I, Gauthier C, Hannigan GE, Dedhar S, St-Arnaud R (2004b) Integrin-linked kinase regulates the nuclear entry of the c-Jun coactivator α-NAC and its coactivation potency. *J Biol Chem* 279: 43893-43899

Queitsch C, Hong SW, Vierling E, Lindquist S (2000) Heat shock protein 101 plays a crucial role in thermotolerance in *Arabidopsis*. *Plant Cell* 12: 479-492

Raasi S, Varadan R, Fushman D, Pickart C (2005) Diverse polyubiquitin interaction properties of ubiquitin-associated domain. *Nat Struct Mol Biol* 12: 708-714

Rabl J, Leibundgut M, Ataide SF, Haag A, Ban N (2011) Crystal structure of the eukaryotic 40S ribosomal subunit in complex with initiation factor 1. *Science* 331: 730-736

Raden D, Gilmore R (1998) Signal recognition particle-dependent targeting of ribosomes to the rough endoplasmic reticulum in the absence and presence of the nascent polypeptide-associated complex. *Mol Biol Cell* 9: 117-130

Rajabi K, Ashcroft AE, Radford SE (2015a) Mass spectrometric methods to analyze the structural organization of macromolecular complexes. *Methods*

Rajabi K, Reuther J, Deuerling E, Radford SE, Ashcroft AE (2015b) A comparison of the folding characteristics of free and ribosome-tethered polypeptide chains using limited proteolysis and mass spectrometry. *Protein Sci* 24: 1282-1291

Rajala RV, Datla RS, Moyana TN, Kakkar R, Carlsen SA, Sharma RK (2000) N-myristoyltransferase. *Mol Cell Biochem* 204: 135-155

Rakwalska M, Rospert S (2004) The ribosome-bound chaperones RAC and Ssb1/2p are required for accurate translation in *Saccharomyces cerevisiae*. *Mol Cell Biol* 24: 9186-9197

Rampelt H, Kirstein-Miles J, Nillegoda NB, Chi K, Scholz SR, Morimoto RI, Bukau B (2012) Metazoan Hsp70 machines use Hsp110 to power protein disaggregation. *EMBO J 31: 4221-4235*

Ramu H, Vazquez-Laslop N, Klepacki D, Dai Q, Piccirilli J, Micura R, Mankin AS (2011) Nascent peptide in the ribosome exit tunnel affects functional properties of the A-site of the peptidyl transferase center. *Mol Cell* 41: 321-330

Rapoport TA (2007) Protein translocation across the eukaryotic endoplasmic reticulum and bacterial plasma membranes. *Nature* 450: 663-669

Ratajczak E, Zietkiewicz S, Liberek K (2009) Distinct activities of *Escherichia coli* small heat shock proteins IbpA and IbpB promote efficient protein disaggregation. *J Mol Biol* 386: 178-189

Raue U, Oellerer S, Rospert S (2007) Association of protein biogenesis factors at the yeast ribosomal tunnel exit is affected by the translational status and nascent polypeptide sequence. *J Biol Chem* 282: 7809-7816

Raviol H, Sadlish H, Rodriguez F, Mayer MP, Bukau B (2006) Chaperone network in the yeast cytosol: Hsp110 is revealed as an Hsp70 nucleotide exchange factor. *Embo J* 25: 2510-2518

Reimann B, Bradsher J, Franke J, Hartmann E, Wiedmann M, Prehn S, Wiedmann B (1999) Initial characterization of the nascent polypeptide-associated complex in yeast. *Yeast* 15: 397-407

Richter K, Haslbeck M, Buchner J (2010) The heat shock response: life on the verge of death. *Mol Cell* 40: 253-266

Rospert S, Dubaquie Y, Gautschi M (2002) Nascent-polypeptide-associated complex. *Cell Mol Life Sci* 59: 1632-1639

Ross S, Giglione C, Pierre M, Espagne C, Meinnel T (2005) Functional and developmental impact of cytosolic protein N-terminal methionine excision in Arabidopsis. *Plant Physiol* 137: 623-637

Rubin N, Perugia E, Goldschmidt M, Fridkin M, Addadi L (2008) Chirality of amyloid suprastructures. *J Am Chem Soc* 130: 4602-4603

Rüdiger S, Germeroth L, Schneider-Mergener J, Bukau B (1997) Substrate specificity of the DnaK chaperone determined by screening cellulose-bound peptide libraries. *Embo J* 16: 1501-1507

Rujano MA, Bosveld F, Salomons FA, Dijk F, van Waarde MA, van der Want JJ, de Vos RA, Brunt ER, Sibon OC, Kampinga HH (2006) Polarised asymmetric inheritance of accumulated protein damage in higher eukaryotes. *PLoS Biol* 4: e417

Rutkowska A, Mayer MP, Hoffmann A, Merz F, Zachmann-Brand B, Schaffitzel C, Ban N, Deuerling E, Bukau B (2008) Dynamics of trigger factor interaction with translating ribosomes. *J Biol Chem* 283: 4124-4132

Saibil H (2013) Chaperone machines for protein folding, unfolding and disaggregation. *Nat Rev Mol Cell Biol* 14: 630-642

Sambrook J, R.D. (2001). Molecular cloning: a laboratory manual.

Schaffitzel C, Oswald M, Berger I, Ishikawa T, Abrahams JP, Koerten HK, Koning RI, Ban N (2006) Structure of the *E. coli* signal recognition particle bound to a translating ribosome. *Nature* 444: 503-506

Schindelin J, Arganda-Carreras I, Frise E, Kaynig V, Longair M, Pietzsch T, Preibisch S, Rueden C, Saalfeld S, Schmid B, Tinevez JY, White DJ, Hartenstein V, Eliceiri K, Tomancak P, Cardona A (2012) Fiji: an open-source platform for biological-image analysis. *Nat Methods* 9: 676-682

Schindelin J, Rueden CT, Hiner MC, Eliceiri KW (2015) The ImageJ ecosystem: An open platform for biomedical image analysis. *Mol Reprod Dev* 82: 518-529

Schiene C, Fischer G (2000) Enzymes that catalyse the restructuring of proteins. *Curr Opin Struct Biol* 10: 40-45

Scholte TG (1968) Molecular weights and molecular weight distribution of polymers by equilibrium ultracentrifugation. Part II. Molecular weight distribution. *J Polymer Sci* 6: 111-127

Seidelt B, Innis CA, Wilson DN, Gartmann M, Armache JP, Villa E, Trabuco LG, Becker T, Mielke T, Schulten K, Steitz TA, Beckmann R (2009) Structural insight into nascent polypeptide chain-mediated translational stalling. *Science* 326: 1412-1415

Selvakumar P, Lakshmikuttyamma A, Shrivastav A, Das SB, Dimmock JR, Sharma RK (2007) Potential role of N-myristoyltransferase in cancer. *Prog Lipid Res* 46: 1-36

Shashidharamurthy R, Koteiche HA, Dong J, McHaourab HS (2005) Mechanism of chaperone function in small heat shock proteins: dissociation of the HSP27 oligomer is required for recognition and binding of destabilized T4 lysozyme. *J Biol Chem* 280: 5281-5289

Shemorry A, Hwang CS, Varshavsky A (2013) Control of protein quality and stoichiomietries by N-terminal acetylation and the N-end rule pathway. *Mol Cell* 50: 540-551

Sheth U, Parker R (2003) Decapping and decay of messenger RNA occur in cytoplasmic processing bodies. *Science* 300: 805-808

Shi X, Parthun MR, Jaehning JA (1995) The yeast *EGD2* gene encodes a homologue of the αNAC subunit of the human nascent polypeptide-associated complex. *Gene* 165: 199-202

Shorter J (2011) The mammalian disaggregase machinery: Hsp110 synergizes with Hsp70 and Hsp40 to catalyze protein disaggregation and reactivation in a cell-free system. *PLoS One* 6: e26319

Shulga N, James P, Craig EA, Goldfarb DS (1999) A nuclear export signal prevents *Saccharomyces cerevisiae* Hsp70 Ssb1p from stimulating nuclear localization signal-directed nuclear transport. *J Biol Chem* 274: 16501-16507

Signer R, Gross H (1934) Ultrazentrifugale Polydispersitätsbestimmungen an hochpolymeren Stoffen. *Helv Chim Acta* 17: 726

Sikorski RS, Hieter P (1989) A system of shuttle vectors and yeast host strains designed for efficient manipulation of DNA in Saccharomyces cerevisiae. *Genetics* 122: 19- 27

Simpson CE, Ashe MP (2012) Adaptation to stress in yeast: to translate or not? *Biochem Soc Trans* 40: 794-799

Slavov N, Semrau S, Airoldi E, Budnik B, van Oudenaarden A (2015) Differential Stoichiometry among Core Ribosomal Proteins. *Cell Rep* 13: 865-873

Slepenkov SV, Witt SN (2002) Kinetic analysis of interdomain coupling in a lidless variant of the molecular chaperone DnaK: DnaK's lid inhibits transition to the low affinity state. *Biochemistry* 41: 12224-12235

Smith WP, Tai PC, Davis BD (1978) Interaction of secreted nascent chains with surrounding membrane in Bacillus subtilis. *Proc Natl Acad Sci U S A* 75: 5922-5925

Sontag EM, Vonk WI, Frydman J (2014) Sorting out the trash: the spatial nature of eukaryotic protein quality control. *Curr Opin Cell Biol* 26: 139-146

Soppa, J. (2010). Protein acetylation in archaea, bacteria, and eukaryotes. *Archaea* 2010 pii: 820681

Spahn CM, Beckmann R, Eswar N, Penczek PA, Sali A, Blobel G, Frank J (2001). Structure of the 80S ribosome from Saccharomyces cerevisiae--tRNA-ribosome and subunit-subunit interactions. *Cell* 107: 373-386

Specht S, Miller SB, Mogk A, Bukau B (2011) Hsp42 is required for sequestration of protein aggregates into deposition sites in *Saccharomyces cerevisiae*. *J Cell Biol* 195: 617-629

Spreter T, Pech M, Beatrix B (2005) The crystal structure of archaeal nascent polypeptide-associated complex (NAC) reveals a unique fold and the presence of a ubiquitin-associated domain. *J Biol Chem* 280: 15849-15854

Squires CL, Pedersen S, Ross BM, Squires C (1991) ClpB is the Escherichia coli heat shock protein F84.1. *J Bacteriol* 173: 4254-4262

Sreerama N, Woody RW (2000) Estimation of protein secondary structure from CD spectra: Comparison of CONTIN, SELCON and CDSSTR methods with an expanded reference set. *Anal Biochem* 287: 252-260

Srere PA (1966) Citrate-condensing enzyme-oxalacetate binary complex. Studies on its physical and chemical properties. *J Biol Chem* 241: 2157-2165

Stafford WF (1992) Boundary analysis in sedimentation transport experiments: a procedure for obtaining sedimentation coefficient distributions using the time derivative of the concentration profile. *Anal Biochem* 203: 295-301

Stark H, Rodnina MV, Rinke-Appel J, Brimacombe R, Wintermeyer W, van Heel M (1997) Visualization of elongation factor Tu on the *Escherichia coli* ribosome. *Nature* 389: 403-406

Stengel F, Baldwin AJ, Painter AJ, Jaya N, Basha E, Kay LE, Vierling E, Robinson CV, Benesch JL (2010) Quaternary dynamics and plasticity underlie small heat shock protein chaperone function. *Proc Natl Acad Sci U S A* 107: 2007-2012

Stilo R, Liguoro D, di Jeso B, Leonardi A, Vito P (2003) The α-chain of the nascent polypeptide-associated complex binds to and regulates FADD function. *Biochem Biophys Res Commun* 303: 1034-1041

Sun Y, MacRae TH (2005) Small heat shock proteins: molecular structure and chaperone function. *Cell Mol Life Sci* 62: 2460-2476

Sunde M, Serpell LC, Bartlam M, Fraser PE, Pepys MB, Blake CC (1997) Common core structure of amyloid fibrils by synchrotron X-ray diffraction. *J Mol Biol* 273: 729-739

Svedberg T, Pederson KO (1940) The Ultracentrifuge. Edited by Fowler RH and Kapitza P. *Oxford University press, London, U.K.*

Szyperski T, Pellecchia M, Wall D, Georgopoulos C, Wuthrich K (1994) NMR structure determination of the *Escherichia coli* DnaJ molecular chaperone: secondary structure and backbone fold of the Nterminal region (residues 2-108) containing the highly conserved J domain. *Proc Natl Acad Sci U S A* 91: 11343-11347

Taylor DJ, Devkota B, Huang AD, Topf M, Narayanan E, Sali A, Harvey SC, Frank J (2009) Comprehensive molecular structure of the eukaryotic ribosome. *Structure* 17: 1591-1604

Teilum K, Maki K, Kragelund BB, Poulsen FM, Roder H (2002) Early kinetic intermediate in the folding of acyl-CoA binding protein detected by fluorescence labeling and ultrarapid mixing. *Proc Natl Acad Sci U S A* 99: 9807-9812

Teixeira D, Sheth U, Valencia-Sanchez MA, Brengues M, Parker R (2005) Processing bodies require RNA for assembly and contain nontranslating mRNAs. *RNA* 11: 371-382

Thiede B, Dimmler C, Siejak F, Rudel T(2001) Predominant identification of RNA-binding proteins in Fas-induced apoptosis by proteome analysis. *J Biol Chem* 276: 26044-26050

Tompa P, Schad E, Tantos A, Kalmar L (2015) Intrinsically disordered proteins: emerging interaction specialists. *Curr Opin Struct Biol* 35: 49-59

Tsai J, Douglas MG (1996) A conserved HPD sequence of the J-domain is necessary for YDJ1 stimulation of Hsp70 ATPase activity at a site distinct from substrate binding. *J Biol Chem* 271: 9347-9354

Tu L, Khanna P, Deutsch C (2014) Transmembrane segments form tertiary hairpins in the folding vestibule of the ribosome. *J Mol Biol* 426: 185-198

Tu LW, Deutsch C (2010) A folding zone in the ribosomal exit tunnel for Kv1.3 helix formation. *J Mol Biol* 396: 1346-1360

Tyedmers J, Mogk A, Bukau B (2010) Cellular strategies for controlling protein aggregation. *Nat Rev Mol Cell Biol* 11: 777-788

Ugrinov KG, Clark PL (2010) Cotranslational folding increases GFP folding yield. *Biophys J* 98: 1312-1320

van Damme P, Arnesen T, Gevaert K (2011) Protein alpha-N-acetylation studied by N-terminomics. *FEBS J* 278: 3822-3834

van Holde KE, Weischet WO (1978) Boundary analysis of sedimentation velocity experiments with monodisperse and paucidisperse solutes. *Biopolymers* 17: 1387-1403

van Montfort RL, Basha E, Friedrich KL, Slingsby C, Vierling E (2001) Crystal structure and assembly of a eukaryotic small heat shock protein. *Nat Struct Biol* 8: 1025-1030

van Montfort R, Slingsby C, Vierling E (2002) Strucutre and function of the small heat shock protein/α-crystallin family of molecular chaperones. *Adv Protein Chem* 59: 105-156

Varenne S, Buc J, Lloubes R, Lazdunski C (1984) Translation is a non-uniform process. Effect of tRNA availability on the rate of elongation of nascent polypeptide chains. *J Mol Biol* 180: 549-576

Vetro JA, Chang YH (2002) Yeast methionine aminopeptidase type 1 is ribosome-associated and requires its N-terminal zinc finger domain for normal function in vivo. *J Cell Biochem* 85: 678-688

Vinograd J, Bruner R (1966) Band centrifugation of macromolecules in self-generating density gradients: II. Sedimentation and diffusion of macromolecules in bands. *Biopolymers* 4: 131-156

Vogel M, Bukau B, Mayer MP (2006a) Allosteric regulation of Hsp70 chaperones by a proline switch. *Mol Cell* 21: 359-367

Vogel M, Mayer MP, Bukau B (2006b) Allosteric regulation of Hsp70 chaperones involves a conserved interdomain linker. *J Biol Chem* 281: 38705-38711

Voss NR, Gerstein M, Steitz TA, Moore PB (2006) The geometry of the ribosomal polypeptide exit tunnel. *J Mol Biol* 360: 893-906

Wall D, Zylicz M, Georgopoulos C (1994) The NH2-terminal 108 amino acids of the *Escherichia coli* DnaJ protein stimulate the ATPase activity of DnaK and are sufficient for lambda replication. *J Biol Chem* 269: 5446-5451

Wallace BA, Lees J, Orry AJW, Lobley A, Janes RW (2003) Analyses of circular dichroism spectra of membrane proteins. *Protein Sci* 12: 875-884

Wallin E, von Heijne G (1998) Genome-wide analysis of integral membrane proteins from eubacterial, archaean, and eukaryotic organisms. Protein science : a publication of the *Prot Soc* 7: 1029-1038

Wals, P, Bursac D, Law YC, Cyr D, Lithgow T (2004) The J-protein family: modulating protein assembly, disassembly and translocation. *EMBO Rep* 5: 567-571

Walter P, Blobel G (1980) Purification of a membrane-associated protein complex required for protein translocation across the endoplasmic reticulum. *Proc Natl Acad Sci U S A* 77: 7112-7116

Walter P, Blobel G (1982) Signal recognition particle contains a 7S RNA essential for protein translocation across the endoplasmic reticulum. *Nature* 299: 691-698

Walter P, Johnson AE (1994) Signal sequence recognition and protein targeting to the endoplasmic reticulum membrane. *Annu Rev Cell Biol* 10: 87-119

Walters RW, Muhlrad D, Garcia J, Parker R (2015) Differential effects of Ydj1 and Sis1 on Hsp70-mediated clearance of stress granules in *Saccharomyces cerevisiae*. *RNA* 21: 1660-1671

Wang S, Sakai H, Wiedmann M (1995) NAC covers ribosome-associated nascent chains thereby forming a protective environment for regions of nascent chains just emerging from the peptidyl transferase center. *J Cell Biol* 130: 519-528

Wang E, Wang J, Chen C, Xiao Y (2015) Computational evidence that fast translation speed can increase the probability of cotranslational protein folding. *Sci Rep* 5: 15316

Wang L, Zhang W, Zhang XC, Li X, Rao Z (2010) Crystal structures of NAC domains of human nascent polypeptide-associated complex (NAC) and its alphaNAC subunit. *Protein Cell* 1: 406-416

Waters ER, Lee GJ, Vierling E (1996) Evolution, structure and function of the small heat shock proteins in plants. *J Exp Bot* 47: 325-338

Wegrzyn RD, Deuerling E (2005) Molecular guardians for newborn proteins: ribosome-associated chaperones and their role in protein folding. *Cell Mol Life Sci* 62: 2727-2738

Wegrzyn RD, Hofmann D, Merz F, Nikolay R, Rauch T, Graf C, Deuerling E (2006) A conserved motif is prerequisite for the interaction of NAC with ribosomal protein L23 and nascent chains. *J Biol Chem* 281: 2847-2857

White HE, Orlova EV, Chen S, Wang L, Ignatiou A, Gowen B, Stromer T, Franzmann TM, Haslbeck M, Buchner J, Saibil HR (2006) Multiple distinct assemblies reveal conformational flexibility in the small heat shock protein Hsp26. *Structure* 14: 1197-1204

Whitmore L, Wallace BA (2004) DICHROWEB, an online server for protein secondary structure analyses from circular dichroism spectroscopic data. *Nucleic Acids Res* 32: W668-W673

Whitmore L, Wallace BA (2008) Protein secondary structure analyses from circular dichroism spectroscopy: methods and reference databases. *Biopolymers* 89: 392-400

Wiedmann B, Sakai H, Davis TA, Wiedmann M (1994) A protein complex required for signalsequence- specific sorting and translocation. *Nature* 370: 434-440

Wilkinson CR, Seeger M, Hartmann-Petersen R, Stone M, Wallace M, Semple C, Gordon C (2001) Proteins containing the UBA domain are able to bind to multi-ubiquitin chains. *Nat Cell Biol* 3: 939-943

Willmund F, del Alamo M, Pechmann S, Chen T, Albanese V, Dammer EB, Peng J, Frydman J (2013) The cotranslational function of ribosome-associated Hsp70 in eukaryotic protein homeostasis. *Cell* 152: 196-209

Wilson DN, Beckmann R (2011) The ribosomal tunnel as a functional environment for nascent polypeptide folding and translational stalling. *Curr Opin Struct Biol* 21: 274-282

Wilson D, Bhushan S, Becker T, Beckmann R (2011) Nascent polypeptide chains within the ribosomal tunnel analyzed by cryo-EM. In *Ribosomes*, Rodnina M, Wintermeyer W, Green R (eds), 31, pp 393- 404. Springer Vienna

Wilson DN, Nierhaus KH (2005) Ribosomal proteins in the spotlight. *Crit Rev Biochem Mol Biol* 40: 243-267

Wimberly BT, Brodersen DE, Clemons WM, Jr., Morgan-Warren RJ, Carter AP, Vonrhein C, Hartsch T, Ramakrishnan V (2000) Structure of the 30S ribosomal subunit. *Nature* 407: 327-339

Winkler J, Tyedmers J, Bukau B, Mogk A (2012) Chaperone networks in protein disaggregation and prion propagation. *J Struct Biol* 179: 152-160

Woerner AC, Frottin F, Hornburg D, Feng LR, Meissner F, Patra M, Tatzelt J, Mann M, Winklhofer KF, Hartl FU, Hipp MS (2016) Cytoplasmic protein aggregates interfere with nucleocytoplasmic transport of protein and RNA. *Science* 351: 173-176

Wolynes PG, Onuchic JN, Thirumalai D (1995) Navigating the folding routes. *Science* 267: 1619-1620

Wool IG (1996) Extraribosomal functions of ribosomal proteins. *Trends Biochem Sci* 21: 164-165

Woolhead CA, Johnson AE, Bernstein HD (2006) Translation arrest requires two-way communication between a nascent polypeptide and the ribosome. *Mol Cell* 22: 587-598

Woolhead CA, McCormick PJ, Johnson AE (2004) Nascent membrane and secretory proteins differ in FRET-detected folding far inside the ribosome and in their exposure to ribosomal proteins. *Cell* 116: 725-736

Wright PE, Dyson HJ (2015) Intrinsically disordered proteins in cellular signalling and regulation. *Nat Rev Mol Cell Biol* 16: 18-29

Xu G, Gonzales V, Borchelt DR (2002) Rapid detection of protein aggregates in the brains of Alzheimer patients and transgenic mouse models of amyloidosis. *Alzheimer Dis Assoc Disord* 16: 191-195

Yan W, Schilke B, Pfund C, Walter W, Kim S, Craig EA (1998) Zuotin, a ribosome-associated DnaJ molecular chaperone. *EMBO J* 17: 4809-4817

Yogev O, Karniely S, Pines O (2007) Translation-coupled Translocation of Yeast Fumarase into Mitochondria *in Vivo*. *J Biol Chem* 282: 29222-29229

Yonath A, Leonard KR, Wittmann HG (1987) A tunnel in the large ribosomal subunit revealed by three-dimensional image reconstruction. *Science* 236: 813-816

Yoshida K, Nogami S, Satoh S, Tanaka-Nakadate S, Hiraishi H, Terano A, Shirataki H (2005) Interaction of the taxilin family with the nascent polypeptide-associated complex that is involved in the transcriptional and translational processes. *Genes Cells* 10: 465-476

Yotov WV, Moreau A, St-Arnaud R (1998) The Alpha Chain of the Nascent Polypeptide-Associated Complex Functions as a Transcriptional Coactivator. *Mol Cell Biol* 18: 1303-1311

Yotov WV, St-Arnaud R(1996) Differential splicing-in of a proline-rich exon converts αNAC into a muscle-specific transcription factor. *Genes Dev* 10: 1763-1772

Yu HY, Ziegelhoffer T, Craig EA (2015) Functionality of Class A and Class B J-protein co-chaperones with Hsp70. *FEBS Lett* 589: 2825-2830

Yusupov MM, Yusupova GZ, Baucom A, Lieberman K, Earnest TN, Cate JH, Noller HF (2001) Crystal structure of the ribosome at 5.5 A resolution. *Science* 292: 883-896

Yusupova G, Yusupov M (2014) High-resolution structure of the eukaryotic 80S ribosome. *Annu Rev Biochem* 83: 467-486

Zeng W, Zhang J, Qi M, Peng C, Su J, Chen X, Yuan Z (2014) αNAC inhibition of the FADD-JNK axis plays anti-apoptotic role in multiple cancer cells. *Cell Death Dis* 5: e1282

Zhang K, Ezemaduka A N, Wang Z, Hu H, Shi X, Liu C, Lu X, Fu X, Chang Z, Yin C-C (2015a) A Novel Mechanism for Small Heat Shock Proteins to Function as Molecular Chaperones. *Sci Rep* 5: 8811

Zhang G, Hubalewska M, Ignatova Z (2009) Transient ribosomal attenuation coordinates protein synthesis and co-translational folding. *Nat Struct Mol Biol* 16: 274-280

Zhang G, Ignatova Z (2011) Folding at the birth of the nascent chain: coordinating translation with cotranslational folding. *Curr Opin Struct Biol* 21: 25-31

Zhang X, Gao X, Coots RA, Conn CS, Liu B, Qian S-B (2015b) Translational control of the cytosolic stress response by mitochondrial ribosomal protein L18. *Nat Struct Mol Biol* 22: 404-410

Zhang Y, Berndt U, Golz H, Tais A, Oellerer S, Wolfle T, Fitzke E, Rospert S (2012) NAC functions as a modulator of SRP during the early steps of protein targeting to the endoplasmic reticulum. *Mol Biol Cell* 23: 3027-3040

Zhang Y, Ma C, Yuan Y, Zhu J, Li N, Chen C, Wu S, Yu L, Lei J, Gao N (2014) Structural basis for interaction of a cotranslational chaperone with the eukaryotic ribosome. *Nat Struct Mol Biol* 21: 1042- 1046

Zheng XM, Black D, Chambon P, Egly JM (1990) Sequencing and expression of complementary DNA for the general transcription factor BTF3. *Nature* 344: 556-559

Zheng XM, Monocollin V, Egly JM, Chambon P (1987) A General Transcription Factor Forms a Stable Complex with RNA Polymerase B (II). *Cell* 50: 361-368

Zhong L, Zhou W, Wang H, Ding S, Lu Q, Wen X, Peng L, Zhang L, Lu C (2013) Chloroplast small heat shock protein HSP21 interacts with plastid nucleoid protein pTAC5 and is essential for chloroplast development in Arabidopsis under heat stress. *Plant Cell* 25: 2925-2543

Zhu X, Zhao X, Burkholder WF, Gragerov A, Ogata CM, Gottesman ME, Hendrickson WA (1996) Structural analysis of substrate binding by the molecular chaperone DnaK. *Science* 272: 1606-1614

Zimmerman SB, Trach SO (1991) Estimation of macromolecule concentrations and excluded volume effects for the cytoplasm of *Escherichia coli*. *J Mol Biol* 222: 599-620

Zwanzig R, Szabo A, Bagchi B (1992) Levinthal's paradox. *Proc Natl Acad Sci U S A* 89: 20-22

9. Acknowledgements

Zunächst möchte ich Prof. Elke Deuerling danken. Sie hat mich herzlich in Ihre Arbeitsgruppe aufgenommen und mir ermöglicht, die Promotion im fast track Progamm zu machen. Sie war immer offen für Diskussionen und hat mich stets unterstützt.
Bedanken möchte ich mich auch bei den ehemaligen und jetzigen Mitgliedern der Arbeitsgruppe, allen voran bei Dr. Jeannette Juretschke. Sie stand mir immer mit Rat und Tat zur Seite. Ein Dankeschön geht auch an Ann-Kathrin Ott für die gute Zusammenarbeit.
Ein herzliches Dankeschön geht an Gabi Witz. Zusätzlich möchte ich mich auch bei Gundula Hunaeus, Uli Dahl und Renate Schlömer bedanken.
Bei der Graduiertenschule Chemische Biologie bedanke ich mich für die Unterstützung während der Doktorarbeit. Der DFG danke ich für die finanzielle Unterstützung im Rahmen des SFB969.

Ein weiteres Dankeschön geht an Prof. Johannes Buchner und Dr. Martin Haslbeck die mich zweimal in Ihrem Labor aufgenommen haben.
Bedanken möchte ich mich auch bei Prof. Valentin Wittmann sowie Ivan Zemskoff die mir bei der Synthese von Acetyl-CoA geholfen haben. Dank geht auch an Prof. Bernhard Schink, Prof. Jörg Hartig und Prof. Hans-Jürgen Apell dafür, dass ich bei Ihnen im Labor Messungen durchführen durfte.
Ebenso möchte ich meinen Studenten für ihre Mitarbeit danken.

Ein großes Dankeschön geht an Ina Schlatterer und Elke Deuerling für das Korrekturlesen dieser Arbeit.
Bedanken möchte ich mich auch bei meinem Thesis Committee bestehend aus Prof. Elke Deuerling, Prof. Karin Hauser und Prof. Alexander Bürkle, welches mich über die Zeit der Promotion begleitet hat.
Zudem danke ich Prof. Elke Deuerling und Prof. Karin Hauser für die Erstellung der Gutachten sowie Prof. Alexander Bürkle für die Übernahme des Prüfungsvorsitzes.

Ganz herzlich möchte ich mich bei meiner Familie bedanken, allen voran meinen Eltern. Sie haben mich immer unterstützt auf meinem Weg und mir gezeigt, dass nichts unmöglich ist. Auch meine Schwester war immer für mich da, wofür ich ihr ganz herzlich danken möchte! Ebenso möchte ich mich bei meiner Oma und vor allem bei meinem Gette bedanken, ohne die das alles nicht möglich gewesen wäre.
Bedanken möchte ich mich auch bei Christine Ruff, Christine Ziese, Grzegorz Kubik und Gundula Hunaeus für die vielen Diskussionen und Gespräche.

10. Appendix

- Ott A-K, Locher L, Koch M, Deuerling E (2015) Functional Dissection of the Nascent Polypeptide-Associated Complex in *Saccharomyces cerevisiae*. *PLoS ONE* 10: e0143457

PLOS ONE

RESEARCH ARTICLE

Functional Dissection of the Nascent Polypeptide-Associated Complex in *Saccharomyces cerevisiae*

Ann-Kathrin Ott[1,2], Lisa Locher[1,2], Miriam Koch[1,2¤], Elke Deuerling[1]*

1 Molecular Microbiology, Department of Biology, University of Konstanz, 78457, Konstanz, Germany,
2 Konstanz Research School of Chemical Biology, University of Konstanz, 78457, Konstanz, Germany

¤ Current address: Department of Chemistry and Biochemistry, University of Bern, Freiestrasse 3, 3012, Bern, Switzerland
* Elke.Deuerling@uni-konstanz.de

OPEN ACCESS

Citation: Ott A-K, Locher L, Koch M, Deuerling E (2015) Functional Dissection of the Nascent Polypeptide-Associated Complex in *Saccharomyces cerevisiae*. PLoS ONE 10(11): e0143457. doi:10.1371/journal.pone.0143457

Editor: Jeffrey L Brodsky, University of Pittsburgh, UNITED STATES

Received: August 28, 2015

Accepted: November 4, 2015

Published: November 30, 2015

Data Availability Statement: All relevant data are within the paper and its Supporting Information files.

Funding: This work was supported by a research grant from the German Science Foundation (DFG; SFB969/A01) to ED.

Competing Interests: The authors have declared that no competing interests exist.

Abstract

Both the yeast **n**ascent polypeptide-**a**ssociated **c**omplex (NAC) and the Hsp40/70-based chaperone system RAC-Ssb are systems tethered to the ribosome to assist cotranslational processes such as folding of nascent polypeptides. While loss of NAC does not cause phenotypic changes in yeast, the simultaneous deletion of genes coding for NAC and the chaperone Ssb (*nacΔssbΔ*) leads to strongly aggravated defects compared to cells lacking only Ssb, including impaired growth on plates containing L-canavanine or hygromycin B, aggregation of newly synthesized proteins and a reduced translational activity due to ribosome biogenesis defects. In this study, we dissected the functional properties of the individual NAC-subunits (α-NAC, β-NAC and β'-NAC) and of different NAC heterodimers found in yeast (αβ-NAC and αβ'-NAC) by analyzing their capability to complement the pleiotropic phenotype of *nacΔssbΔ* cells. We show that the abundant heterodimer αβ-NAC but not its paralogue αβ'-NAC is able to suppress all phenotypic defects of *nacΔssbΔ* cells including global protein aggregation as well as translation and growth deficiencies. This suggests that αβ-NAC and αβ'-NAC are functionally distinct from each other. The function of αβ-NAC strictly depends on its ribosome association and on its high level of expression. Expression of individual β-NAC, β'-NAC or α-NAC subunits as well as αβ'-NAC ameliorated protein aggregation in *nacΔssbΔ* cells to different extents while only β-NAC was able to restore growth defects suggesting chaperoning activities for β-NAC sufficient to decrease the sensitivity of *nacΔssbΔ* cells against L-canavanine or hygromycin B. Interestingly, deletion of the **ub**iquitin-**a**ssociated (UBA)-domain of the α-NAC subunit strongly enhanced the aggregation preventing activity of αβ-NAC pointing to a negative regulatory role of this domain for the NAC chaperone activity *in vivo*.

Introduction

The folding of newly synthesized proteins requires the assistance of molecular chaperones. At the forefront are ribosome-associated chaperones, which contact nascent polypeptides to control early protein folding processes and to prevent aggregation or degradation of newly synthesized proteins [1, 2]. Yeast ribosomes are transiently associated with two different types of chaperone systems. One is a Hsp70/Hsp40-based chaperone system consisting of the **r**ibosome-**a**ssociated **c**omplex (RAC), a heterodimer formed by Zuo(tin) and Ssz, and Ssb. The second system is the **n**ascent polypeptide-**a**ssociated **c**omplex (NAC). Both systems bind transiently to the large ribosomal subunit for interaction with nascent polypeptides early during protein biogenesis (Fig 1A).

NAC reversibly binds to ribosomes and is described as the first factor that interacts with nascent polypeptides emerging from the ribosome to prevent them from incorrect interactions [3]. The complex is widely conserved from archaea to man, however, archaea only have a homodimeric NAC formed by two α-NAC subunits while yeast and higher eukaryotes mainly form a stable αβ-NAC heterodimer (Fig 1A). Crystal structures of NAC deletion variants from archaea and humans suggest that the two NAC subunits dimerize via their homologous six-stranded β-barrel-like NAC domains (Fig 1B). Only α-NAC contains an additional UBA (ubiquitin-associated) domain with unknown function at its C-terminus (Fig 1B) [4–6]. Ribosome binding of eukaryotic NAC is mediated by the N-terminus of β-NAC involving a conserved ribosome-binding motif (Fig 1B) and probably an adjacent helix element [7–9]. Mutations in this region of β-NAC ($\beta^{RRK/AAA}$-NAC, Fig 1C) diminish ribosome binding of the entire complex [9]. Crosslinking data suggest different binding sites for NAC on the ribosome including the ribosomal proteins Rpl31 (eL31) and Rpl25 (uL23), which have been shown to be functional docking sites for other ribosome-attached factors as well, including Zuotin or bacterial Trigger Factor, SRP, and the ER-translocon, respectively [5, 9–11]. Moreover, both subunits of αβ-NAC crosslink to nascent polypeptides [7], suggesting that both can contact substrates, but the substrate binding sites in the individual subunits have not been elucidated yet.

In contrast to other eukaryotic organisms, the *Saccharomyces cerevisiae* genome encodes three NAC subunits: One α-NAC subunit encoded by the *EGD2* gene and two alternative β-NAC paralogues, β-NAC and β'-NAC, encoded by the *EGD1* and the *BTT1* gene, respectively. Hence, two different types of heterodimers, αβ-NAC and αβ'-NAC, are formed in yeast with potentially different substrate pools and functions [12]. However, β'-NAC *(BTT1)* is approximately 100-fold less expressed than β-NAC and thus, the heterodimeric αβ-NAC seems to be the dominant species in yeast. Moreover, it is suggested that to a minor extent also homodimers of both subunits exist *in vivo* [10, 13, 14].

While yeast NAC is not important for growth, NAC is essential in higher eukaryotes and a loss of its function induces early embryonically lethal phenotypes or developmental defects in mice, fruit flies, and *C. elegans* [15–17]. Recent data show that NAC is a member of the chaperone network in yeast and in *C. elegans* [12, 18, 19]. The simultaneous deletion of all three NAC genes in yeast does not cause growth defects while the combined deletion of NAC genes together with genes encoding the Ssb chaperone (*SSB1* and *SSB2*) leads to synthetic defects including impaired growth under protein folding stress, enhanced aggregation of newly synthesized proteins and accelerated defects in ribosomal biogenesis and translation [18]. Two recent studies revealed the functions of NAC in metazoans [19, 20]. Depletion of NAC in *C. elegans* results in enhanced protein aggregation of folding-sensitive polyQ proteins. Moreover, NAC was shown to be associated with heat-induced aggregates of firefly luciferase in transgenic *C. elegans* strains and loss of NAC prevents the efficient re-solubilization of aggregated luciferase at permissive temperature in these animals [19]. In addition, NAC plays an essential role as a

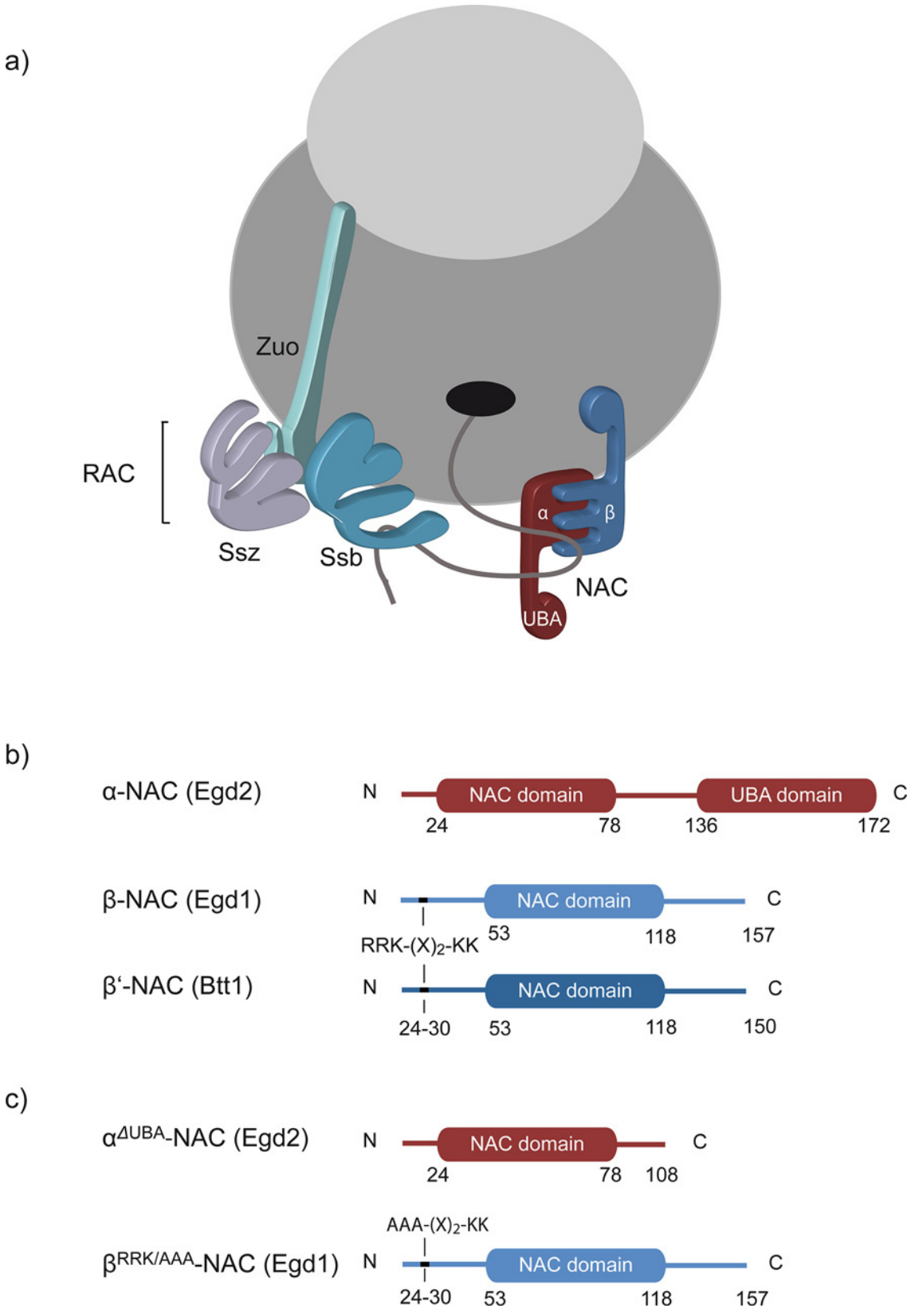
a)
Zuo
RAC
Ssz
Ssb
α
β
NAC
UBA
b)
α-NAC (Egd2)
N
NAC domain
UBA domain
C
24
78
136
172
β-NAC (Egd1)
N
NAC domain
C
RRK-(X)2-KK
53
118
157
β'-NAC (Btt1)
N
NAC domain
C
24-30
53
118
150
c)
αΔUBA-NAC (Egd2)
N
NAC domain
C
24
78
108
AAA-(X)2-KK
βRRK/AAA-NAC (Egd1)
N
NAC domain
C
24-30
53
118
157

Fig 1. Ribosome-associated chaperones from *S. cerevisiae*. a) The Hsp70/Hsp40-chaperone system that consists of RAC (Ssz and Zuo), shown in purple and light green, and Ssb, shown in light blue, forms a functional triad at the ribosome. In addition, β-NAC (shown in blue) and α-NAC (shown in red) that contains a C-terminal UBA (ubiquitin-associated) domain constitute the stable heterodimeric αβ-NAC complex which binds to the ribosome via the ribosome-binding motif in the β-subunit. Both, NAC and Ssb can interact directly with the nascent chain. b) Schematic representation of the different NAC subunits. α-NAC (shown in red) contains a NAC domain and a UBA domain. Besides the NAC domain the two different β-subunits (shown in light and dark blue) also contain a conserved ribosome-binding motif present in their N-termini. c) Schematic drawing of the two NAC mutants investigated in this study. $\alpha^{\Delta UBA}$-NAC (shown in red) lacks the C-terminal UBA domain and part of the linker region. In $\beta^{RRK/AAA}$-NAC (shown in blue) the conserved RRK-$(X)_2$-KK motif was mutated to AAA-$(X)_2$-KK to abolish ribosome binding.

doi:10.1371/journal.pone.0143457.g001

negative regulator in cotranslational protein targeting to the ER in metazoans. Bound to ribosomes, NAC shields the high affinity binding site of ribosomes for the Sec61 translocon and thereby prevents incorrect ribosome-nascent chain complexes from association with the ER-translocon and the erroneous import of incorrect cargo in the ER [20]. However, this function is less well understood in yeast where *in vivo* studies showed no aberrant translocation phenotype upon NAC deletion [10, 14, 21], perhaps due to the fact that yeast cells use a distinct post-translational ER targeting system in addition.

In this study we set out to better understand the function of NAC and its individual subunits in yeast. To this end, we expressed individual subunits or heterodimeric complexes of NAC in cells lacking NAC and Ssb and investigated which subunits of NAC are potent to complement the phenotypic changes of *nacΔssbΔ* cells.

Results

The β-subunit of NAC is essential and sufficient to ameliorate growth

The loss of NAC does not result in a growth phenotype, while *nacΔssbΔ* cells lacking all NAC and Ssb chaperone encoding genes (*EGD1Δ*, *EGD2Δ*, *BTT1Δ*, *SSB1Δ*, *SSB2Δ)* show a strong growth deficiency compared to wild type (wt) or *ssbΔ* cells at 30°C, in particular in the presence of drugs which impair protein synthesis or folding like the arginine analogue L-canavanine or the translation inhibitor hygromycin B [18]. To understand which NAC subunits are essential for growth, we expressed NAC subunits encoded on centromeric plasmids (Fig 2A) individually or in combinations and tested their ability to complement the growth defects of *nacΔssbΔ* cells (Fig 2B). Expression of NAC genes was driven by the respective authentic promoter (Fig 2A) and protein levels were probed by Western blotting revealing similar expression levels as in the wt (S2B Fig).

Expression of the αβ-NAC heterodimer complemented the growth defect of *nacΔssbΔ* cells in the presence of L-canavanine or hygromycin B (Fig 2B, lane 4). This finding is in agreement with an earlier report [18]. Interestingly, also the expression of β-NAC alone as well as in combination with an α-NAC variant lacking the C-terminal 64 amino acid residues including the UBA domain (called hereafter $\alpha^{\Delta UBA}$-NAC, see Fig 1C) ameliorated growth of *nacΔssbΔ* cells in the presence of both drugs (Fig 2B, lanes 4, 5 and 9). In contrast, the expression of the ribosome-binding mutant $\beta^{RRK/AAA}$-NAC alone (Fig 1C) or in combination with α-NAC did not decrease sensitivity to L-canavanine or hygromycin B compared to the vector control (Fig 2B, lanes 3, 7 and 8). This data suggests that expression of the β-NAC subunit is sufficient to restore growth defects of *nacΔssbΔ* cells back to the growth properties of *ssbΔ* cells. Based on the finding that $\alpha\beta^{RRK/AAA}$-NAC did not restore growth, we conclude that the α-NAC subunit is not sufficient to promote growth and ribosome-binding of β-NAC is crucial for the activity of αβ-NAC. In contrast to β-NAC, the expression of β'-NAC did not ameliorate growth of *nacΔssbΔ* cells in presence of L-canavanine or hygromycin B (Fig 2B, lane 6) implying that the paralogous β'-NAC subunit is either functionally distinct from β-NAC in yeast or, due to its low expression, the level of β'-NAC is not sufficient to support growth under these conditions.

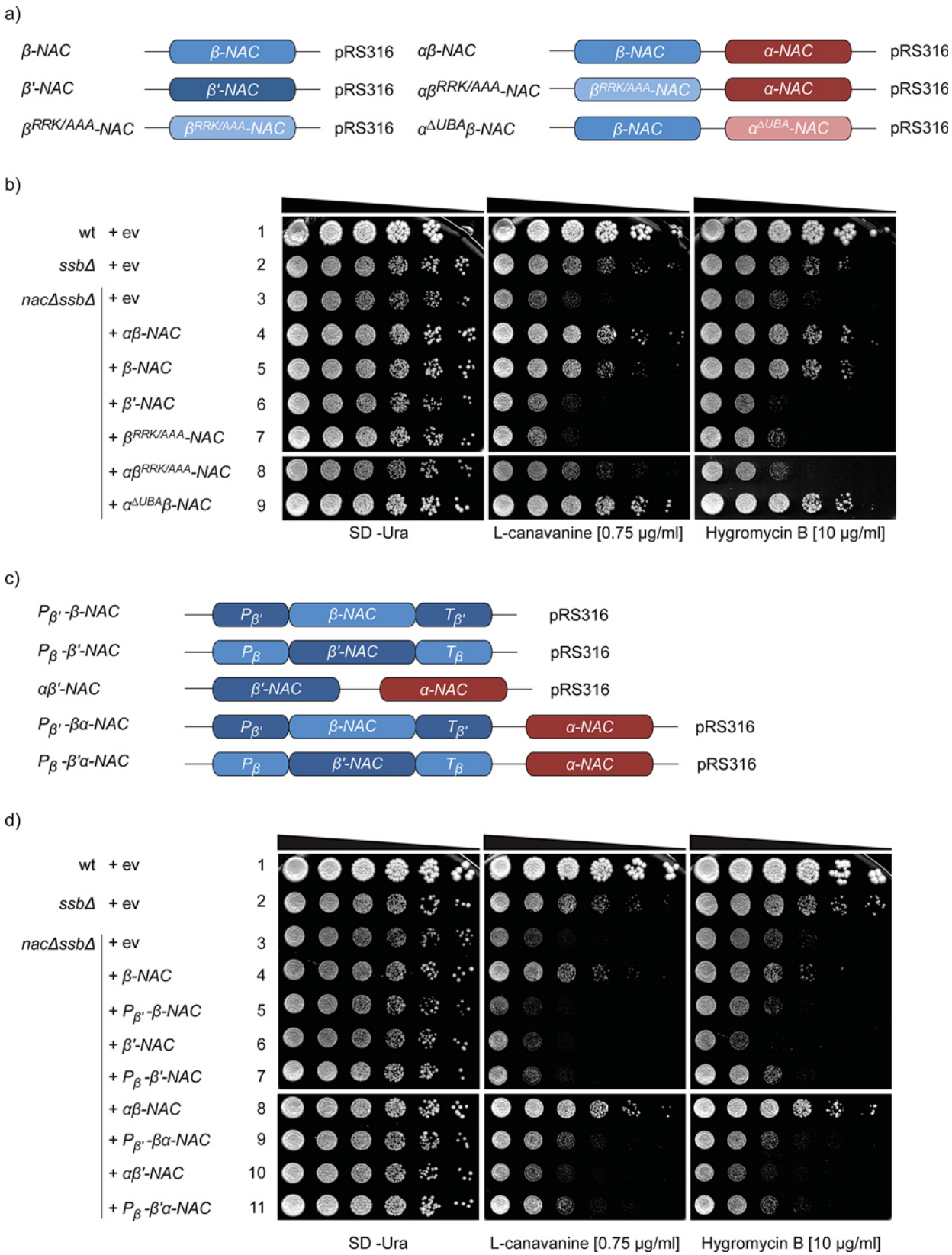
a)
β-NAC
β-NAC
pRS316
β′-NAC
β′-NAC
pRS316
βRRK/AAA-NAC
βRRK/AAA-NAC
pRS316
αβ-NAC
β-NAC
α-NAC
pRS316
αβRRK/AAA-NAC
βRRK/AAA-NAC
α-NAC
pRS316
αΔUBAβ-NAC
β-NAC
αΔUBA-NAC
pRS316
b)
wt + ev 1
ssbΔ + ev 2
nacΔssbΔ + ev 3
+ αβ-NAC 4
+ β-NAC 5
+ β′-NAC 6
+ βRRK/AAA-NAC 7
+ αβRRK/AAA-NAC 8
+ αΔUBAβ-NAC 9
SD -Ura
L-canavanine [0.75 μg/ml]
Hygromycin B [10 μg/ml]
c)
Pβ′-β-NAC
Pβ′
β-NAC
Tβ′
pRS316
Pβ-β′-NAC
Pβ
β′-NAC
Tβ
pRS316
αβ′-NAC
β′-NAC
α-NAC
pRS316
Pβ′-βα-NAC
Pβ′
β-NAC
Tβ′
α-NAC
pRS316
Pβ-β′α-NAC
Pβ
β′-NAC
Tβ
α-NAC
pRS316
d)
wt + ev 1
ssbΔ + ev 2
nacΔssbΔ + ev 3
+ β-NAC 4
+ Pβ′-β-NAC 5
+ β′-NAC 6
+ Pβ-β′-NAC 7
+ αβ-NAC 8
+ Pβ′-βα-NAC 9
+ αβ′-NAC 10
+ Pβ-β′α-NAC 11
SD -Ura
L-canavanine [0.75 μg/ml]
Hygromycin B [10 μg/ml]

Fig 2. The αβ-NAC complex and β-NAC under control of their endogenous promoter complement the growth defect of *nacΔssbΔ* cells. a) Schematic drawing of the different plasmid-encoded NAC constructs used in this study. Plasmids encoding wild type (wt) and mutant αβ-NAC, either alone or in complex, were cloned in the vector backbone pRS316 reported by [18]. b) Growth analysis of wt and mutant yeast cells expressing different NAC versions from plasmids as indicated. Serial dilutions were spotted on synthetic complete media without uracil (SD-Ura) containing the indicated drugs. When cells were plated on the arginine analogue L-canavanine, arginine was omitted. The cells were incubated for 3 days at 30°C. c) The promoter (P)—and terminator (T)- regions of *EGD1* were replaced with the corresponding regions of *BTT1* and *vice versa* and cloned in the vector backbone of pRS316 with or without *EGD2*. *BTT1* under its endogenous promoter and terminator was also cloned into pRS316 together with *EGD2*. d) Growth analyses were performed as described in b).

doi:10.1371/journal.pone.0143457.g002

Expression levels of β-NAC but not β'-NAC are important for growth

The expression ratio of β-NAC *(EGD1)* and β'-NAC *(BTT1)* in yeast cells is about 100:1 [13, 14]. To investigate whether the expression levels of β-NAC and β'-NAC are important for their ability to complement the growth defects of *nacΔssbΔ* cells, we exchanged the promoter and terminator region of *BTT1* with regions from the *EGD1* gene and *vice versa* (Fig 2C) and tested these constructs in *nacΔssbΔ* cells (Fig 2D).

When the *BTT1* promoter and terminator regions were fused to the *EGD1* gene, which results in strongly reduced *β-NAC* mRNA levels (S1A Fig), the growth defect of *nacΔssbΔ* cells on plates containing translation inhibitory drugs could not be complemented (Fig 2D, compare lane 4 with lane 5). Similarly, low expression of β-NAC in combination with wt levels of α-NAC did no longer enhance growth under these conditions (Fig 2D, lane 9). We conclude from these results that the high expression level of β-NAC is crucial for enhanced growth of *nacΔssbΔ* cells on plates containing L-canavanine or hygromycin B.

In turn, expression of β'-NAC under control of the *EGD1* promoter and terminator led to significantly higher levels of *BTT1* mRNA (S1B Fig). The high level expression of β'-NAC alone or in combination with wt levels of α-NAC enhanced growth of *nacΔssbΔ* cells on plates containing drugs compared to αβ'-NAC expressing cells (Fig 2D, compare lanes 6 and 7, 10 and 11), however, only slightly compared to cells expressing β-NAC or αβ-NAC (Fig 2D, lanes 4 and 8). It should be mentioned that the expression levels of the β-NAC variants with exchanged promoter and terminator regions were tested on the mRNA level due to the lack of specific antibodies. Thus, we cannot exclude that some variations on the protein level may contribute to the observed effects as well.

In summary, the data suggest that the paralogous ribosome-associated β-NAC and β'-NAC execute distinct functions *in vivo* even when expressed at similar levels.

Ribosomal defects in *nacΔssbΔ* cells are suppressed by αβ-NAC

Previous studies revealed that *nacΔssbΔ* cells show a defect in ribosome biogenesis leading to the formation of ribosomal halfmers and a reduced translational activity [18]. This defect in ribosome biogenesis can be investigated by separating total cell lysate on a sucrose gradient using ultracentrifugation and subsequent fractionation of the gradient monitoring ribosomal species by measuring the absorption at 254 nm. The peak heights of the absorption traces detected at 254 nm could be used as sensitive indicators for the levels of each ribosomal species because equal absorption units of the samples were loaded. Thereby, the shoulder in the 80S and polysome peaks of the double knockout cells represents the presence of ribosomal halfmers in such fractionation experiments (Fig 3C, arrows). Such halfmers consist of an uncomplexed 40S subunit bound to the mRNA and are typically caused by an impaired balance of 40S and 60S ribosomal subunits due to defects in the assembly of 60S particles [22, 23]. Indeed, higher levels of 40S subunits were detected in *nacΔssbΔ* cells compared to the wild type. Moreover, the 80S monosome and polysome peaks were significantly reduced and ribosomal halfmers were present in *nacΔssbΔ* cells compared to wt cells indicating the reduced translational activity

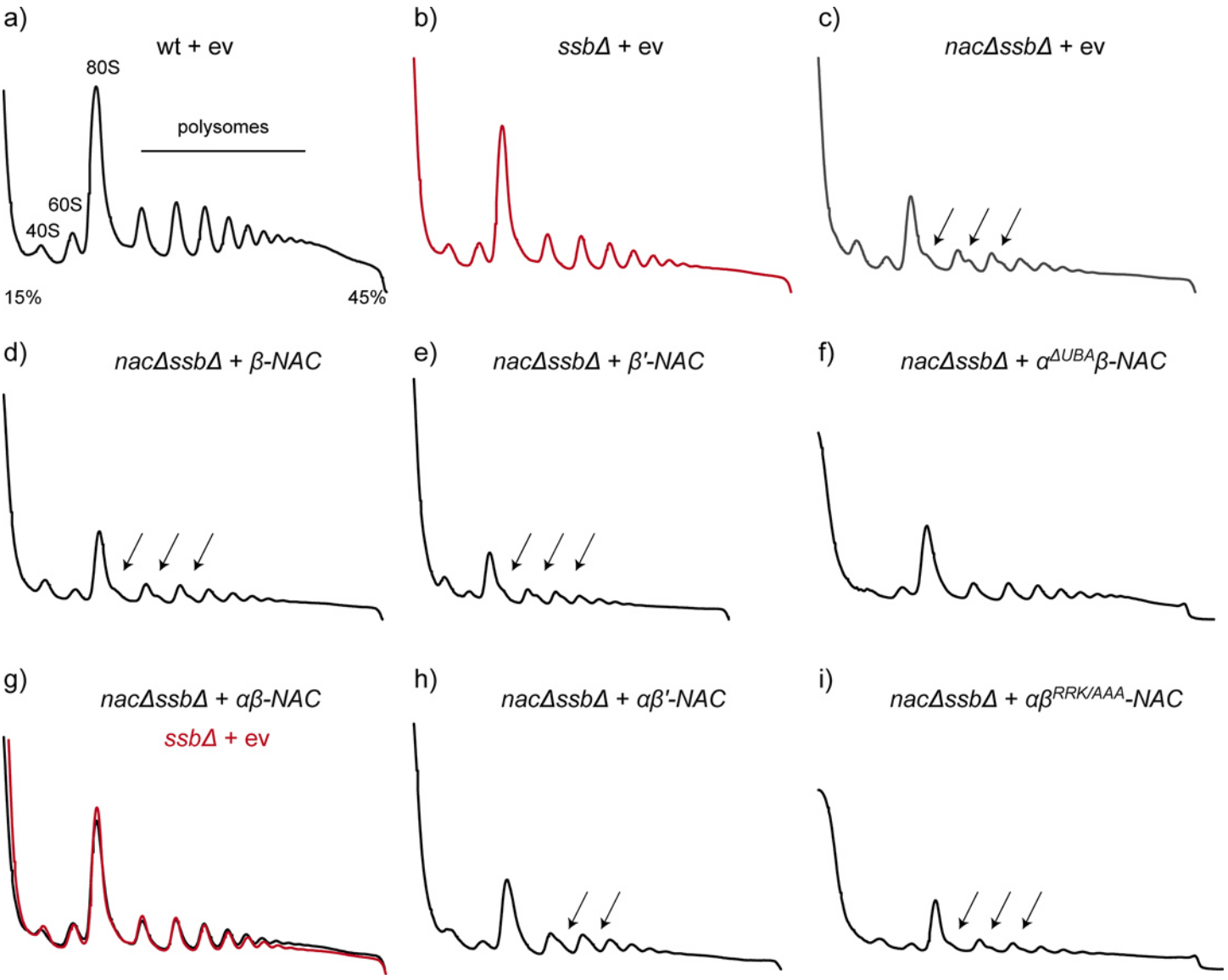

Fig 3. Halfmer formation of *nacΔssbΔ* knockout cells can be prevented by expression of *αβ-NAC*. a-i) Polysome profiles derived from wild type (wt) or mutant yeast cells. Absorbance traces at 254 nm are shown. Cells were grown to an optical density (OD_{600}) of 0.8 in SD-Ura medium. 10 A_{260} units of lysates of indicated cells were loaded onto 15–45% linear sucrose gradients to isolate ribosomal fractions (40S, 60S, 80S and polysomes) as indicated by centrifugation and subsequent fractionation. Polysome profiles show: a) wt + empty vector (ev), b) *ssbΔ* cells + ev, c-i) *nacΔssbΔ* cells + ev (c), + *β-NAC* (d), *β'-NAC* (e), $\alpha^{\Delta UBA}\beta$-*NAC* (f), *αβ-NAC* (g) + *αβ'-NAC* (h) and $\alpha\beta^{RRK/AAA}$-*NAC* (i) The profiles are representative for three independent experiments.

doi:10.1371/journal.pone.0143457.g003

(Fig 3A and 3C). As reported earlier [18], these ribosomal defects are clearly less pronounced in cells lacking only Ssb (Fig 3B).

To test which subunit(s) of NAC complement(s) the ribosomal defects, ribosome profiles were generated from *nacΔssbΔ* cells expressing different NAC variants. We found that in contrast to the growth analysis, only the expression of the αβ-NAC heterodimer could restore the ribosome biogenesis defects observed in *nacΔssbΔ* cells (Fig 3G). This is demonstrated by a decreased amount of halfmers, a reduced 40S peak and enhanced 80S and polysome peaks resulting in a profile that is similar to *ssbΔ* cells (Fig 3B, 3C and 3G). Importantly, expression of the ribosome-binding deficient $\alpha\beta^{RRK/AAA}$-NAC version did not suppress these deficiencies in

ribosome biogenesis and translation (Fig 3I). Moreover, neither expression of β-NAC nor β'-NAC alone cured the ribosomal defects (Fig 3D and 3E). A small reduction in the amount of halfmers could be observed upon expression of αβ'-NAC (Fig 3H). We also investigated whether the expression levels of β-NAC and β'-NAC are crucial for the suppression of ribosomal defects in *nacΔssbΔ* cells (Fig 4). High level expression of β'-NAC driven by the *EGD1* promoter and terminator elements with or without coexpression of α-NAC resulted also in a very mild reduction of ribosomal halfmers confirming again that the β'-NAC subunit and consequently also the αβ'-NAC heterodimer are functionally distinct from β-NAC and αβ-NAC, respectively, even when expressed at similar levels (Fig 4C and 4F). Moreover, a reduced expression of αβ-NAC did not complement the aberrant translation phenotype (Fig 4B and 4E) and also α-NAC itself could not prevent halfmer formation of *nacΔssbΔ* knockout cells (Fig 4D). Interestingly, the expression of the $\alpha^{\Delta UBA}$β-NAC mutant version in *nacΔssbΔ* cells (Fig 3F) reduced the halfmer formation whereas the 80S and polysome peaks were still reduced compared to *ssbΔ* cells, suggesting that the UBA domain functionally contributes to the function of αβ-NAC in translation.

Taken together, these data show that, in contrast to the growth analyses where ribosome-bound β-NAC is sufficient for complementation, exclusively the αβ-NAC heterodimer expressed at high levels is able to support proper ribosome biogenesis and translation in yeast cells.

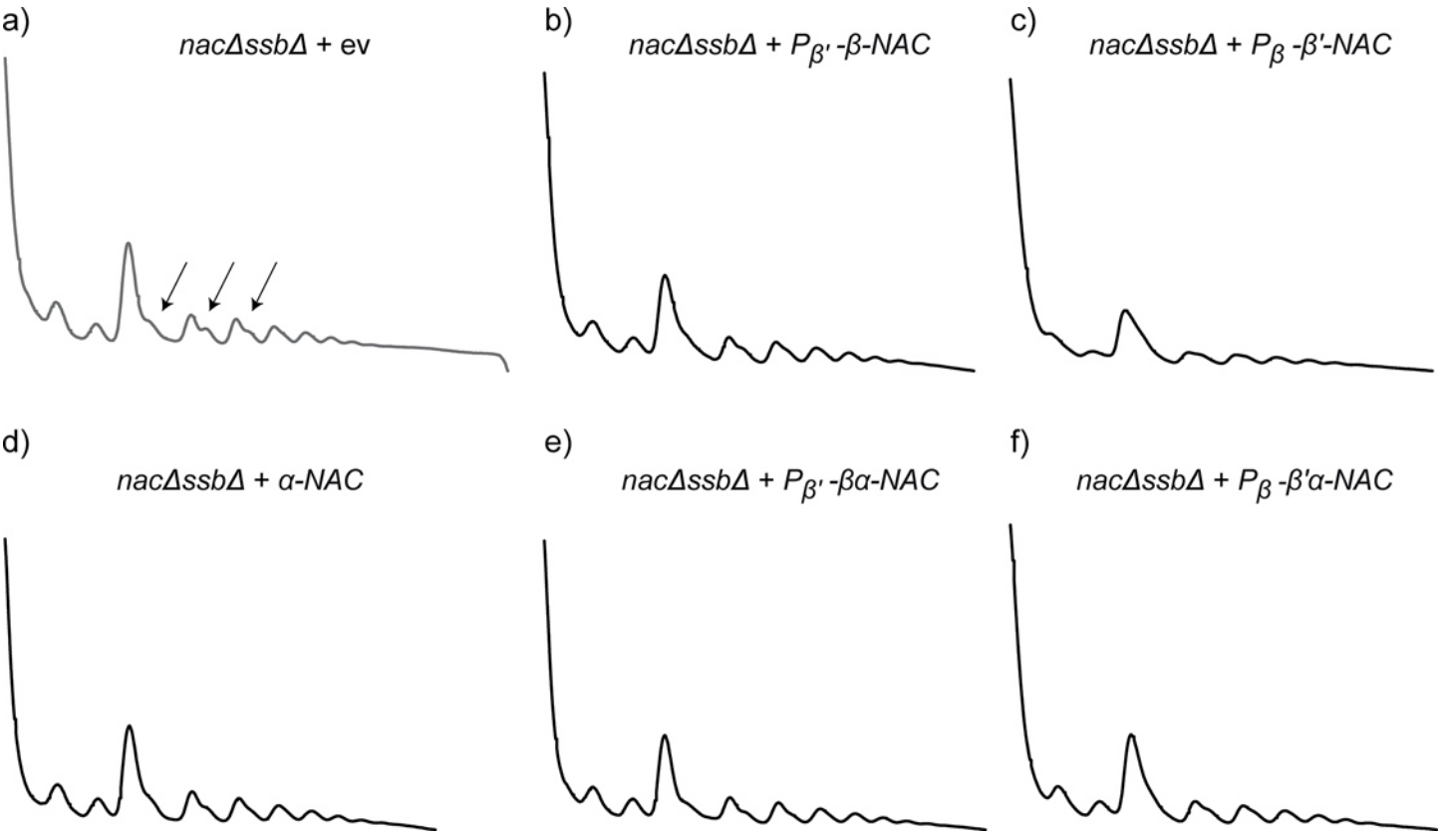

Fig 4. Expression levels of *β-NAC* are important for complementation of *nacΔssbΔ* halfmers. Polysome profiling with wild type (wt) or mutant yeast cells. Absorbance traces at 254 nm are shown. 10 A_{260} units of lysates of indicated yeast cells were loaded onto 15–45% linear sucrose gradients similar to Fig 3. a) Polysome profile of *nacΔssbΔ* cells + empty vector control (ev) (in grey). b) and c) Complementation of *nacΔssbΔ* cells with promoter-swapped *β-NAC* constructs alone. d) *nacΔssbΔ* cells expressing α-NAC alone. e) and f) Polysome profiles of *nacΔssbΔ* cells expressing promoter-swapped β-NAC constructs in combination with α-NAC. Arrows indicate halfmers. The profiles are representative for three independent runs.

doi:10.1371/journal.pone.0143457.g004

NAC is transcriptionally not coregulated with components of the translation apparatus

The expression of genes encoding proteins involved in ribosome biogenesis is often coregulated with genes coding for ribosomal proteins [24]. This has been reported also for the ribosome-associated chaperone Ssb [25]. As the ribosomal biogenesis and translation defects of cells lacking NAC and Ssb are more pronounced than in the cells lacking only Ssb, we wondered whether the genes *EGD1*, *BTT1* and *EGD2* coding for NAC are also coregulated with ribosomal genes. In a previous study from Albanèse et al. [26] where transcriptional analysis of gene expression in response to environmental stress, e.g. heat shock or nitrogene depletion, was performed, NAC was found to be corepressed together with components of the translational apparatus and ribosome biogenesis chaperones such as Ssb and RAC. To further address this question under non-stress conditions, wt cells were grown in medium containing glycerol as carbon source until they reached an OD_{600} of 0.6 (time point zero). Then the cells were washed and transferred into medium containing glucose because ribosomal genes are upregulated upon carbon upshift from glycerol- to glucose-containing medium. Total RNA was isolated after various time points and followed by quantitative real-time PCR. We found, in agreement with earlier studies [25], that the mRNAs of *SSB1* and the ribosomal protein *RPL5* as well as the mRNA of the ribosome biogenesis factor *JJJ1* were upregulated about 2- to 3.5-fold upon carbon shift (Fig 5A). However, no significantly enhanced transcription of mRNA coding for any of the three NAC subunits was detected. The mRNA levels of *EGD1* and *EGD2* remained almost constant in comparison to *SSB1* or *JJJ1* and the mRNA level of *BTT1* was even slightly reduced upon carbon shift (Fig 5A). Hence, NAC is not coregulated with ribosomal proteins under these conditions, which is a typical characteristic for ribosomal biogenesis factors and chaperones directly involved in this process, such as Jjj1 or Ssb. It is known that loss of Jjj1 causes a slow growth phenotype and the combined deletion of the *SSB1*,*2* genes and *JJJ1* results in synthetic lethality [18]. To further investigate the role of NAC in ribosome biogenesis, we generated *jjj1Δ* and *nacΔjjj1Δ* knockout strains to test for a genetic interaction. The *nacΔjjj1Δ* cells lacking Jjj1 and all three genes encoding NAC showed no synthetic growth phenotype compared to *jjj1Δ cells* under the conditions tested (Fig 5B). Ribosome profiles of *jjj1Δ* and *nacΔjjj1Δ* cells (Fig 5C–5F) revealed that the deletion of *JJJ1* resulted in a decrease of 60S subunits and in the appearance of halfmers (Fig 5E), indicating that this strain has a ribosome biogenesis defect as described previously [27, 28]. Loss of NAC in *jjj1Δ* cells did neither enhance the halfmer formation nor cause a further reduction of 60S, 80S or polysome peaks. This suggests that NAC and Jjj1 do not display overlapping functions in ribosome biogenesis and indicates together with the lack of transcriptional coregulation that NAC supports the activity of the translation apparatus by a mechanism distinct from classical ribosome biogenesis factors.

Suppression of protein aggregation by NAC

The loss of NAC does not provoke protein aggregation while cells lacking the Ssb chaperone activity accumulate misfolded and insoluble proteins. However, defects in protein folding are much more pronounced in *ssbΔ* cells upon additional loss of NAC suggesting that these two ribosome-associated systems act in overlapping pathways to support the folding of newly synthesized proteins [18]. Therefore, we finally examined if NAC subunits expressed alone or in combination reduce the level of protein aggregation in *nacΔssbΔ* cells. Mutant cells were grown to exponential phase, harvested and after lysis the insoluble protein material was isolated by centrifugation (Fig 6). Equalized total lysates are shown in S2A Fig and served as a loading control. Three biologically independent experiments were conducted for each NAC variant to test the chaperone activity by analyzing the suppression of protein aggregation in *nacΔssbΔ* cells.

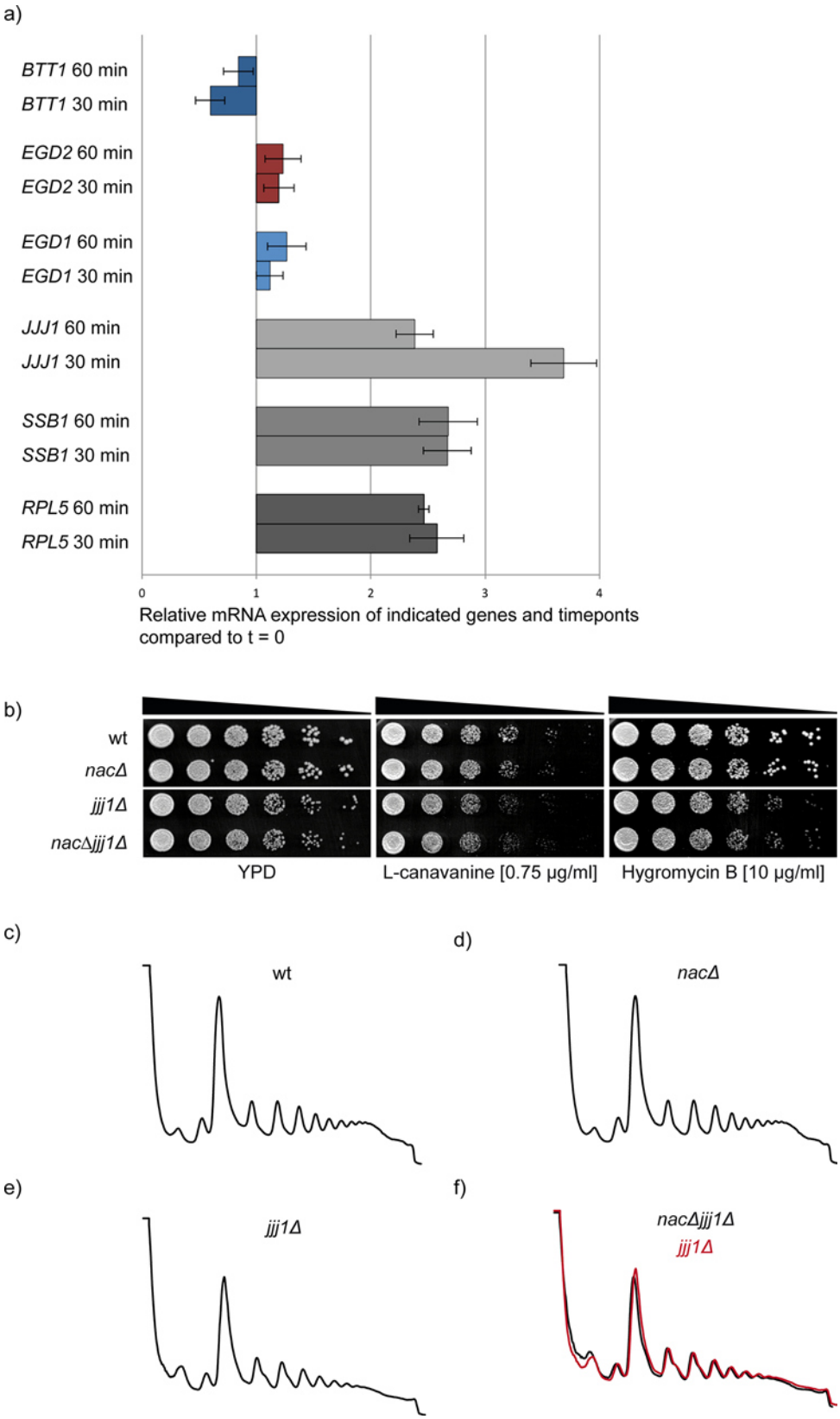
a)
BTT1 60 min
BTT1 30 min
EGD2 60 min
EGD2 30 min
EGD1 60 min
EGD1 30 min
JJJ1 60 min
JJJ1 30 min
SSB1 60 min
SSB1 30 min
RPL5 60 min
RPL5 30 min
0
1
2
3
4
Relative mRNA expression of indicated genes and timeponts compared to t = 0
b)
wt
nacΔ
jjj1Δ
nacΔjjj1Δ
YPD
L-canavanine [0.75 µg/ml]
Hygromycin B [10 µg/ml]
c)
wt
d)
nacΔ
e)
jjj1Δ
f)
nacΔjjj1Δ
jjj1Δ

Fig 5. *NAC* is not coregulated with genes encoding ribosomal proteins. a) X-axis: Relative mRNA levels of indicated genes and time points compared to timepoint zero (t = 0, before glucose addition) and normalized to an internal control (housekeeping gene). Cells were harvested at 0 min, 30 min and 60 min after glucose addition and mRNA was extracted. cDNA was obtained by reverse transcription and used for qRT-PCR. b) Serial dilutions of wild type (wt) and chaperone mutant cells were spotted on YPD plates and plates containing the indicated drugs for growth analysis. When cells were plated on the arginine analogue L-canavanine, arginine was omitted. The cells were incubated for 3 days at 30°C. c) Polysome profiles of wt and mutant cells. 10 A_{260} units of lysates of indicated yeast strains were loaded onto 15–45% linear sucrose gradients as shown in Fig 3. The profiles are representative for three independent runs.

doi:10.1371/journal.pone.0143457.g005

The data were analyzed using one-way-between-groups ANOVA with post-hoc Tukey test [29] to assess significance. As shown previously, cells lacking Ssb and NAC revealed enhanced levels of insoluble protein material compared to *ssbΔ* cells (Fig 6A, lanes 1–3). We found that expression of αβ-NAC at wt levels significantly reduced protein aggregation in *nacΔssbΔ* cells (Fig 6A, lane 8; quantification in Fig 6C and S1 Table ($p = 0$)) suggesting that this heterodimer is a potent chaperone *in vivo*. The expression of the single NAC-subunits or of αβ'-NAC ameliorated protein aggregation as well, with some variances compared to the expression of αβ-NAC (Fig 6A, lanes 4, 7, 11 and S1 Table). This suggests that chaperone activity can be displayed by individual subunits and does not necessarily rely on the heterodimeric NAC complex. The chaperone activity of αβ-NAC and β-NAC critically depends on ribosome association as protein aggregation could not be prevented in *nacΔssbΔ* cells expressing the $\alpha\beta^{RRK/AAA}$-NAC or $\beta^{RRK/AAA}$-NAC subunit (Fig 6A, lanes 6 and 9, Fig 6C, S1 Table ($p = 0.24$ and 0.921, respectively)).

Surprisingly, the most potent NAC version in preventing protein aggregation was $\alpha^{\Delta UBA}\beta$-NAC (Fig 6A, lane 10 and S1 Table, $p = 0$, highly significant). Fig 6A and 6B show the SDS-PAGES of the isolated and Coomassie-stained aggregated protein species from *nacΔssbΔ* cells expressing either $\alpha^{\Delta UBA}\beta$-NAC or αβ-NAC in comparison to controls for all three biological replicates. Expression of $\alpha^{\Delta UBA}\beta$-NAC ameliorated protein aggregation even more than αβ-NAC (Fig 6A and 6B; compare lanes 10 and 8) to a level similar to wt cells (S1 Table, $p = 0.633$, not significant). This data suggests an enhanced chaperone activity for $\alpha^{\Delta UBA}\beta$-NAC and suggests that the UBA domain negatively regulates the chaperone activity of αβ-NAC *in vivo*.

Discussion

The eukaryotic conserved heterodimer αβ-NAC was discovered in 1994 by Wiedmann and colleagues [7] and has since then been studied *in vitro* and *in vivo* to better understand the diverse roles of this complex e.g. in protein folding and transport [2, 30]. NAC is not essential in yeast but displays a strong genetic and functional interaction with the Ssb chaperone as is evident by the amplification of the pleiotropic defects found in cells lacking Ssb upon additional deletion of NAC encoding genes [18]. In contrast to other eukaryotes, *Saccharomyces cerevisiae* encodes besides the universally conserved α-NAC and β-NAC subunits that form the stable and abundant αβ-NAC heterodimer, a second paralogous β'-NAC subunit that forms the alternative αβ'-NAC dimer. In this study, we dissected the functions of the individual NAC subunits and the two different heterodimers by their ability to complement the pleiotropic phenotype of *nacΔssbΔ* cells. In addition, our results demonstrate the importance of ribosome binding of NAC and identify for the first time a potential role for the UBA-domain of α-NAC in regulating the chaperone activity of αβ-NAC.

We found major functional differences between αβ-NAC and αβ'-NAC. Only αβ-NAC but not αβ'-NAC (even when expressed at similar levels as αβ-NAC) can suppress all defects found in *nacΔssbΔ* cells including the high sensitivity against translation inhibitory drugs, ribosomal deficiencies that result in halfmer formation, reduced amounts of 80S particles and polysomes,

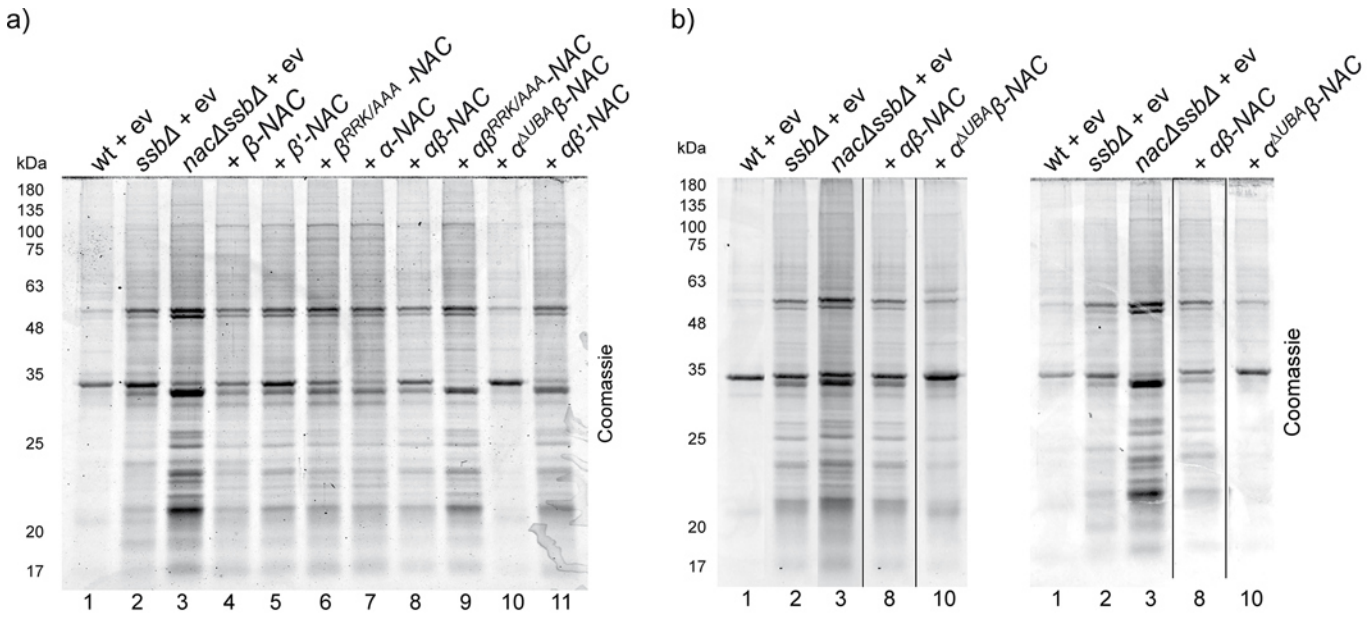
a)
wt + ev
ssbΔ + ev
nacΔssbΔ + ev
+ β-NAC
+ β'-NAC
+ β^RRK/AAA -NAC
+ α-NAC
+ αβ-NAC
+ αβ^RRK/AAA-NAC
+ α^ΔUBAβ-NAC
+ αβ'-NAC
kDa
180
135
100
75
63
48
35
25
20
17
Coomassie
1 2 3 4 5 6 7 8 9 10 11
b)
wt + ev
ssbΔ + ev
nacΔssbΔ + ev
+ αβ-NAC
+ α^ΔUBAβ-NAC
kDa
180
135
100
75
63
48
35
25
20
17
1 2 3 8 10
1 2 3 8 10
Coomassie

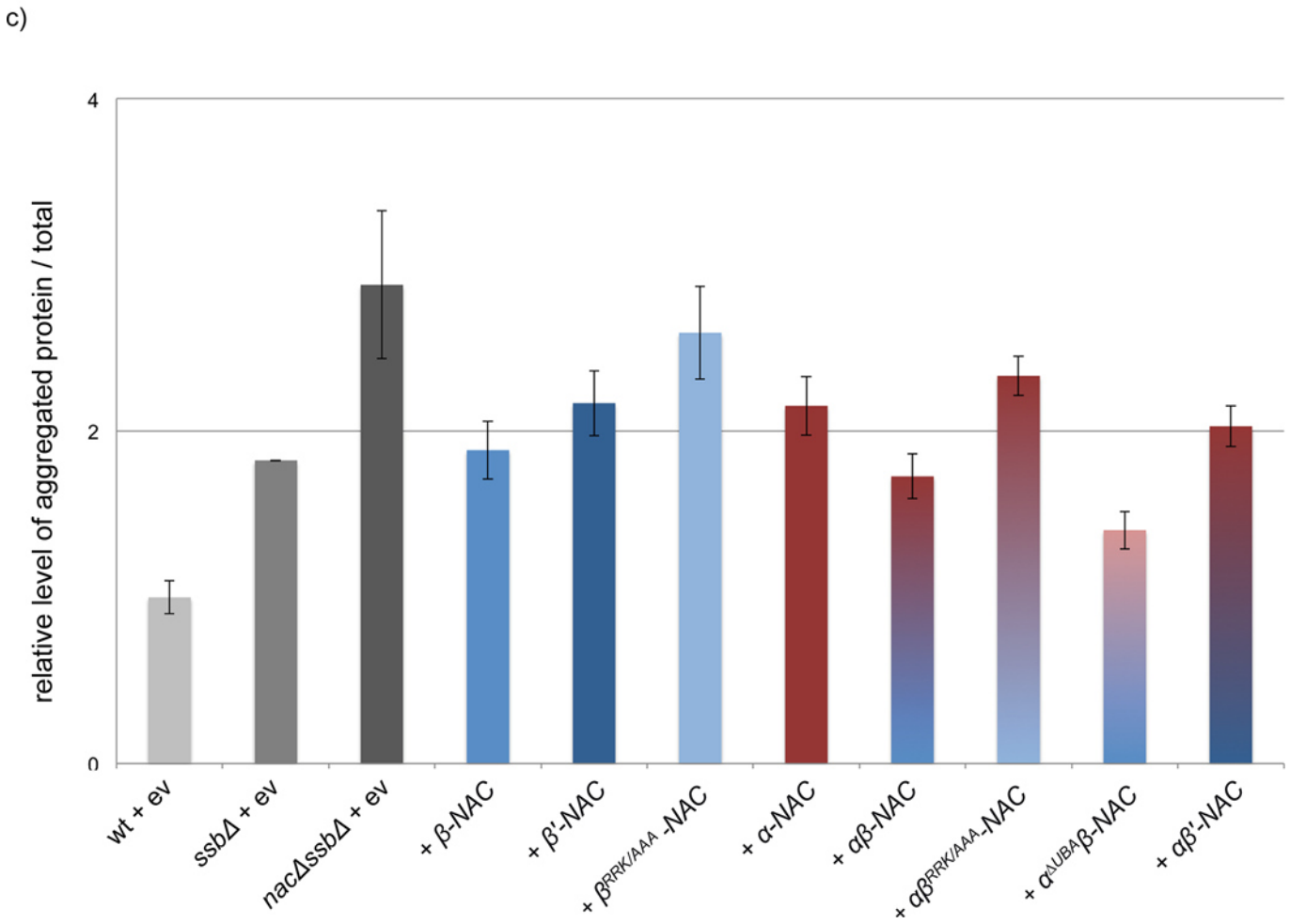
c)
relative level of aggregated protein / total
4
2
0
wt + ev
ssbΔ + ev
nacΔssbΔ + ev
+ β-NAC
+ β'-NAC
+ β^RRK/AAA -NAC
+ α-NAC
+ αβ-NAC
+ αβ^RRK/AAA-NAC
+ α^ΔUBAβ-NAC
+ αβ'-NAC

Fig 6. Analysis of protein aggregation in *nacΔssbΔ* suppressed by *NAC* variants. a) 50 OD_{600} units of transformed yeast cells expressing the indicated NAC variants in the logarithmic phase were lysed and the aggregated protein material was isolated by sedimentation. Isolated aggregated fractions were separated by SDS-PAGE and visualized by Coomassie staining. b) Biological replicates of the experiment shown in a) for aggregated proteins of wt, *ssbΔ* and *nacΔssbΔ* cells (lanes 1–3), *nacΔssbΔ* + *αβ-NAC* (lane 8) and + $\alpha^{\Delta UBA}\beta$-*NAC* (lane 10). The experiment was performed as in a). For better visualization the corresponding lanes were cut out from the same SDS-PAGE after Coomassie staining as indicated by black lines. c) Quantification of aggregated material using ImageJ shows the relative level of aggregated protein in relation to total protein amount, normalized to the mean value of wt replicates. Mean ± SD is shown from three experiments (n = 3).

doi:10.1371/journal.pone.0143457.g006

as well as protein aggregation. This suggests that αβ-NAC is functionally most important for yeast vitality. Our results are in agreement with a recent study by Frydman and colleagues analyzing the nascent interactome of NAC [12]. They showed that αβ-NAC has a preference for ribosomes translating metabolic enzymes as well as secretory and membrane proteins while αβ'-NAC preferentially binds to ribosomes translating mitochondrial or ribosomal proteins. This finding implies different substrate pools of αβ-NAC and αβ'-NAC. Both heterodimers are ribosome-associated by the conserved ribosome-binding motif found in β-NAC as well as in β'-NAC (Figs 1B and 7A). In addition, both subunits possess the conserved NAC domain involved in dimerization (Fig 7B). The two different β-subunits display an overall similarity of 64.3% with an identity of 46.5% on their amino acid level. However, β-NAC and β'-NAC obviously reveal strong differences at their C-terminal ends (Fig 7C) as the similarity of this region is only 30.8% with an identity of 10.3%. Both C-termini are predicted to be rather unstructured, however, the C-terminus of β'-NAC is shorter by 8 amino acid residues compared to β-NAC and the last 16 amino acids show no homology to β-NAC at all (Fig 7C). Moreover, β'-NAC has a lower amount of charged amino acids in its C-terminus: 5 negatively charged residues (Asp + Glu) and 2 positively charged residues (Arg + Lys) compared to β-NAC with 11 negatively charged residues (Asp + Glu) and 4 positively charged residues (Arg + Lys). Thus, we speculate that the diverse C-termini of β- and β'-NAC might be involved in substrate selectivity and thus contribute to the functional differences of αβ-NAC and αβ'-NAC. Interestingly, the C-termini of β-NAC subunits from *C. elegans* and humans also contain a high number of charged residues and are clearly more similar to yeast β-NAC than to β'-NAC (Fig 7C).

Obviously, αβ-NAC can only display its function *in vivo* when bound to ribosomes and expressed at high levels. This conclusion is strongly supported by the findings that neither $\alpha\beta^{RRK/AAA}$-NAC, that forms a stable heterodimer but is deficient in ribosome binding, nor the low expression of αβ-NAC driven by the *BTT1* promoter could complement all phenotypic defects of *nacΔssbΔ* cells.

Interestingly, expression of ribosome-bound β-NAC but not of β'-NAC was sufficient to restore growth but both versions could lower the aggregation propensity of newly synthesized proteins. This suggests some residual chaperoning activities of ribosome-bound β-NAC and β'-NAC subunits, probably as a homodimer which, in the case of β-NAC, is sufficient to promote growth of *nacΔssbΔ* cells.

The α-NAC subunit contains a conserved UBA (ubiquitin–associated) domain at its C-terminal end (Fig 1). UBA domains can bind ubiquitin and thus are often found in proteins associated with the ubiquitin-mediated degradation pathway. However, UBA domains can also act as protein-protein interaction or dimerization surfaces by exposing a hydrophobic patch [31]. That far, no ubiquitin binding of the NAC UBA domain could be demonstrated and the role of this domain is enigmatic. In this study, we discovered a potential role for the NAC UBA domain by studying the $\alpha^{\Delta UBA}\beta$-NAC version, a heterodimer with a wild type (wt) β-NAC subunit and a mutant α-NAC lacking the C-terminal 64 amino acid residues including the complete UBA domain and part of the flexible linker between the UBA and the NAC domain (Fig 1B and 1C). The $\alpha^{\Delta UBA}\beta$-NAC mutant complemented growth defects of *nacΔssbΔ* cells similar

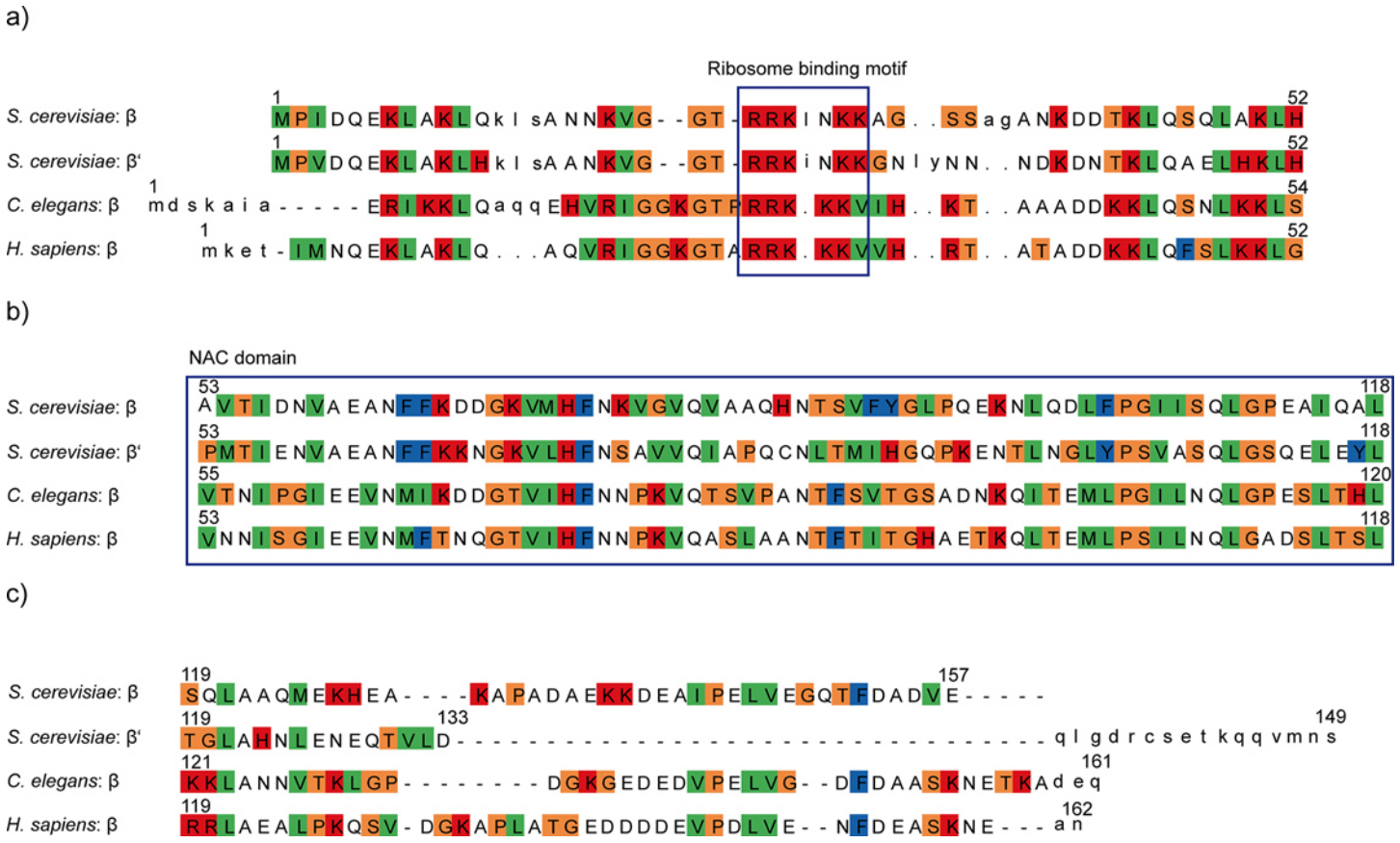

Fig 7. β-NAC and β'-NAC show differences in their C-termini. First, a PSI-BLAST search of the NCBI database was performed. Then the sequences were sorted using CLANS [34] and aligned with the alignment programme muscle [35]. An HMM (http://hmmer.org/) was constructed of the fungi sequences and all sequences were aligned against the HMM. The sequences are shown for a) the N-terminus, b) the NAC-domain and c) the C-terminus of β-NAC and β'-NAC of *S. cerevisiae*, and of β-NAC from *C. elegans* and *H. sapiens*. Amino acids are depicted in the one letter-code. β-NAC of *S. cerevisiae* could be aligned completely to the β-sequences of all kingdoms, but the end of the C-terminus of β' from *S. cerevisiae* could not be aligned with the other sequences and was marked as an insert (small letters at the end of the alignment). Colour legend: orange = small hydrophilics, green = small hydrophobics, red = bases, blue = aromatics and colourless = acids/amides and sulphhydrils.

doi:10.1371/journal.pone.0143457.g007

to αβ-NAC, but was significantly more potent to suppress protein aggregation in these cells suggesting a higher chaperone activity of $\alpha^{\Delta UBA}$β-NAC compared to αβ-NAC. This led us to conclude that the UBA domain attached via a highly flexible linker to the α-NAC subunit may regulate the chaperone activity of αβ-NAC. How can we envision such a role for the UBA domain? We speculate that the hydrophobic and surface-exposed stretch of the UBA domain may contact and transiently cover a hydrophobic substrate binding site in the αβ-NAC heterodimer. Enhanced exposure of such a binding site in $\alpha^{\Delta UBA}$β-NAC may allow NAC to associate more efficiently with misfolded proteins to prevent their aggregation. However, such a "hyper" chaperone activity might be harmful as well, e.g. by binding too tight or in an unregulated manner to certain substrates. This may explain why the $\alpha^{\Delta UBA}$β-NAC is not as efficient as wt αβ-NAC in suppressing defects in translation. Another possibility would be that the UBA domain contributes to dimerization or oligomerization of αβ-NAC and thereby affects its chaperone activities.

Future *in vivo* and *in vitro* experiments are required to evaluate this interesting hypothesis and to shed more light on the chaperone activity of NAC. This study provides the framework to pursue such analyses.

Materials and Methods

Strains, plasmids and growth conditions

The genotypes of the yeast strains are listed in S2 Table. Strains carrying gene deletions were constructed by PCR-based gene disruption [32, 33] and clones were analyzed by PCR. Gene deletions in yeast strains obtained from EUROSCARF were confirmed by growth on YPD-G418 and PCR. All plasmids were generated using standard molecular cloning techniques and are listed in S3 Table. Plasmids encoding wild type (wt) NAC and mutants of NAC were described in [18]. To generate plasmids where the two β-NAC subunits were expressed with the promoter and terminator region originally belonging to the other subunit, the PCR-amplified promoter and terminator regions as well as the coding regions of *EGD1* and *BTT1* (derived from yeast genomic DNA of BY4741) were cloned into pRS316 or pRS316-α-NAC in the desired combinations. All plasmids used are listed in S3 Table. Unless indicated otherwise, yeast cells were grown at 30°C in YPD (1% yeast extract, 2% peptone and 2% dextrose) or defined synthetic complete media (6.7 g/liter YNB, 2 g/liter drop out mix and 2% dextrose). Analysis of cell growth was performed four times.

Density gradient ultracentrifugation and ribosomal profiling

For yeast ribosome profiling 200 ml cultures in–Ura medium were grown at 30°C to an OD_{600} = 1. Cycloheximide was added to a final concentration of 100 μg/ml. Immediately afterwards, the treated cultures were transferred into centrifuge bottles containing 100 g crushed ice and centrifuged at 5000 x g for 5 min. The cell pellets were frozen in liquid nitrogen and stored at -80°C. Cell pellets were resuspended in lysis buffer (20 mM Hepes-KOH, pH 7.4, 100 mM KAc, 2 mM MgAc, 100 μg/ml cycloheximide, 0.5 mM DTT, 1 mM PMSF, and protease inhibitor cocktail) and 1 g of acid-washed glass beads was added. The cells were lysed mechanically by glass bead disruption. Triton X-100 and sodium deoxycholate were added to a final concentration of 0.25% each after cell lysis. 10 A_{260} absorption units of each lysate in 500 μl volume were loaded onto an 11 ml linear sucrose gradient (15–45% in lysis buffer) and centrifuged for 2 hours at 4°C at 200.000 x g. The gradients were fractionated from top to bottom with a density gradient fractionator (Teledyne Isco, Inc.) and ribosome profiles were monitored at 254 nm. Data were recorded and processed with PeakTrak V1.1 (Teledyne ISco, Inc.). Experiments were performed four times.

Antibodies and Western Blot analysis

Rabbit polyclonal antibody against the NAC complex was described in [18]; antibodies recognizing PGK1 were obtained from Invitrogen. Protein samples were separated by SDS-PAGE and transferred to a nitrocellulose membrane (GE Healthcare) by Western blotting (wet blot). Primary antibodies were diluted 1:10.000. Fluorescence-labeled secondary anti-rabbit antibodies (DY-682; Dyomics) were applied and visualized with the FLA-9000 system (Fujifilm). Experiments were repeated at least three times.

RNA isolation and quantitative real-time PCR

Total RNA was isolated from yeast wild type strain using RNeasy Mini Kit (Qiagen) according to the manufacturer's protocol and transcribed into cDNA according to the QuantiTect reverse transcription kit protocol (Qiagen). For quantitative real-time PCR 20 μl triplicate reactions with 1 μl of 1:5 diluted cDNA were used together with 0.2 mM of the primer pair and 1x GoTaq®qPCR Master Mix (Promega). For detection the ABI 7500 Fast Real-Time PCR

System (Applied Biosystems) was used. Data were analyzed using the comparative 2ΔΔCT method and *TAF10* as a reference gene. Experiments were repeated at least three times.

Isolation of aggregated proteins

Overnight cultures of yeast cells transformed with the indicated plasmids encoding the different NAC subunits were grown in synthetic complete medium without uracil. The main culture was grown in YPD to the logarithmic stage and 50 OD_{600} units were harvested. The cell pellets were resuspended in lysis buffer (20 mM potassium phosphate, pH 6.8, 10 mM DTT, 1 mM EDTA, 0.1% Tween, 1 mM PMSF, protease inhibitor cocktail, 3 mg/ml zymolyase 20T and 25 u/μl DNaseI) and incubated at room temperature for 15 minutes. After chilling on ice for 5 minutes, the samples were treated by tip sonication (Branson, eight times at level 4 and duty cycle 50%) and centrifuged at 4°C for 20 minutes and 200 x g. Protein levels were adjusted to identical concentrations and aggregated proteins were pelleted at 16.000 x g for 20 min at 4°C. Aggregated proteins were washed twice with 2% NP-40 (in 20 mM potassium phosphate, pH 6.8, 1 mM PMSF and protease inhibitor cocktail), sonicated six times at level 4 and 50% duty cycle and centrifuged as described above. The final washing step was performed in buffer without NP-40, samples were sonicated for four times at level 2 with 65% duty cycle and subsequently boiled in SDS sample buffer. The total and aggregated proteins were separated by SDS-PAGE and analyzed by Coomassie staining. Experiments were performed three times. Quantification was performed using ImageJ; mean +/- SD is shown.

Statistical analysis

Statistical analysis was performed using one-way-between-groups ANOVA with post-hoc Tukey test [29]. All the data from the aggregation experiment were normalized to the mean raw value of the wt data set. A Levenes test for homogeneity of Variance was performed followed by one-Way ANOVA. Tukeys post-hoc test compared the aggregation level of every strain to the other to check for statistically significant differences.

Supporting Information

S1 Fig. mRNA levels of β-NAC subunits are changed when expressed under different promoters. a) Yeast *nacΔssbΔ* mutant cells transformed with the indicated plasmids were grown to an optical density (OD_{600}) of 0.8 and mRNA was isolated. cDNA was obtained by reverse transcription and used for qRT-PCR with *EGD1*-specific primer pairs. The samples were normalized to an internal control (housekeeping gene) and compared to wild type. b) Experiment performed as in a) with *BTT1*-specific primer pairs.
(TIF)

S2 Fig. Equalized protein levels of lysates used for aggregate isolation. a) 50 OD_{600} units of transformed yeast cells in the logarithmic phase were lysed and the aggregated protein material was quantitatively isolated. 15 μg of total lysates were separated by SDS-PAGE and visualized by Coomassie staining. b) Total lysates prepared in a) were used for Western blotting to analyse the expression levels of the different NAC-encoding plasmids. Pgk1 served as loading control. The asterisks mark a degradation product of α-NAC (*) and an unspecific protein band (**).
(TIF)

S1 Table. The levels of aggregated proteins were analysed by one-way-between-groups ANOVA followed by Tukeys test. ANOVA Statistics: One-way-between-groups ANOVA assessed a statistically significant divergence of the portions of aggregated proteins between the different strains. Tukey honest significant difference comparison: the levels of isolated

aggregates of each strain were compared with the ones of the respective other strain to test for statistically significant differences.
(DOCX)

S2 Table. Yeast strains used in this study. All yeast strains used in this work were isogenic derivatives of BY4741 and are listed by their genotypes.
(DOCX)

S3 Table. Plasmids used for complementation studies of the *nacΔssbΔ* phenotypes. All plasmids were generated using standard molecular cloning techniques.
(DOCX)

Acknowledgments

We thank Tancred Frickey, Julia Reuther, Christina Schlatterer and E. Oberer-Bley for their discussion and valuable help with the manuscript. This work was supported by a research grant from the German Science Foundation (DFG; SFB969/A01) to E. D.

Author Contributions

Conceived and designed the experiments: A-KO MK LL ED. Performed the experiments: A-KO MK LL. Analyzed the data: A-KO MK LL ED. Contributed reagents/materials/analysis tools: A-KO MK LL. Wrote the paper: A-KO ED.

References

1. Bukau B, Weissman J, Horwich A. Molecular chaperones and protein quality control. Cell. 2006; 125: 443–451. doi: 10.1016/j.cell.2006.04.014 PMID: 16678092.
2. Preissler S, Deuerling E. Ribosome-associated chaperones as key players in proteostasis. Trends Biochem Sci. 2012; 37: 274–283. doi: 10.1016/j.tibs.2012.03.002 PMID: 22503700.
3. Wang S, Sakai H, Wiedmann M. NAC covers ribosome-associated nascent chains thereby forming a protective environment for regions of nascent chains just emerging from the peptidyl transferase center. J Cell Biol. 1995; 130: 519–528. PMID: 7622554; PubMed Central PMCID: PMCPMC2120527.
4. Spreter T, Pech M, Beatrix B. The crystal structure of archaeal nascent polypeptide-associated complex (NAC) reveals a unique fold and the presence of a ubiquitin-associated domain. J Biol Chem. 2005; 280: 15849–15854. doi: 10.1074/jbc.M500160200 PMID: 15665334.
5. Wang L, Zhang W, Wang L, Zhang XC, Li X, Rao Z. Crystal structures of NAC domains of human nascent polypeptide-associated complex (NAC) and its alphaNAC subunit. Protein Cell. 2010; 1: 406–416. doi: 10.1007/s13238-010-0049-3 PMID: 21203952.
6. Liu Y, Hu Y, Li X, Niu L, Teng M. The crystal structure of the human nascent polypeptide-associated complex domain reveals a nucleic acid-binding region on the NACA subunit. Biochemistry. 2010; 49: 2890–2896. doi: 10.1021/bi902050p PMID: 20214399.
7. Wiedmann B, Sakai H, Davis TA, Wiedmann M. A protein complex required for signal-sequence-specific sorting and translocation. Nature. 1994; 370: 434–440. doi: 10.1038/370434a0 PMID: 8047162.
8. Franke J, Reimann B, Hartmann E, Kohlerl M, Wiedmann B. Evidence for a nuclear passage of nascent polypeptide-associated complex subunits in yeast. J Cell Sci. 2001; 114: 2641–2648. PMID: 11683391.
9. Wegrzyn RD, Hofmann D, Merz F, Nikolay R, Rauch T, Graf C, et al. A conserved motif is prerequisite for the interaction of NAC with ribosomal protein L23 and nascent chains. J Biol Chem. 2006; 281: 2847–2857. doi: 10.1074/jbc.M511420200 PMID: 16316984.
10. Nyathi Y, Pool MR. Analysis of the interplay of protein biogenesis factors at the ribosome exit site reveals new role for NAC. J Cell Biol. 2015; 210: 287–301. doi: 10.1083/jcb.201410086 PMID: 26195668; PubMed Central PMCID: PMCPMC4508901.
11. Pech M, Spreter T, Beckmann R, Beatrix B. Dual binding mode of the nascent polypeptide-associated complex reveals a novel universal adapter site on the ribosome. J Biol Chem. 2010; 285: 19679–19687. Epub 2010/04/23. doi: 10.1074/jbc.M109.092536 PMID: 20410297; PubMed Central PMCID: PMC2885246.

12. del Alamo M, Hogan DJ, Pechmann S, Albanese V, Brown PO, Frydman J. Defining the specificity of cotranslationally acting chaperones by systematic analysis of mRNAs associated with ribosome-nascent chain complexes. PLoS Biol. 2011; 9: e1001100. doi: 10.1371/journal.pbio.1001100 PMID: 21765803; PubMed Central PMCID: PMCPMC3134442.
13. George R, Beddoe T, Landl K, Lithgow T. The yeast nascent polypeptide-associated complex initiates protein targeting to mitochondria in vivo. Proc Natl Acad Sci U S A. 1998; 95: 2296–2301. PMID: 9482879; PubMed Central PMCID: PMCPMC19325.
14. Reimann B, Bradsher J, Franke J, Hartmann E, Wiedmann M, Prehn S, et al. Initial characterization of the nascent polypeptide-associated complex in yeast. Yeast. 1999; 15: 397–407. doi: 10.1002/(SICI)1097-0061(19990330)15:5<397::AID-YEA384>3.0.CO;2-U PMID: 10219998.
15. Bloss TA, Witze ES, Rothman JH. Suppression of CED-3-independent apoptosis by mitochondrial betaNAC in Caenorhabditis elegans. Nature. 2003; 424: 1066–1071. doi: 10.1038/nature01920 PMID: 12944970.
16. Deng JM, Behringer RR. An insertional mutation in the BTF3 transcription factor gene leads to an early postimplantation lethality in mice. Transgenic Res. 1995; 4: 264–269. PMID: 7655515.
17. Markesich DC, Gajewski KM, Nazimiec ME, Beckingham K. Bicaudal encodes the *Drosophila* beta NAC homolog, a component of the ribosomal translational machinery. Development. 2000; 127: 559–572. PMID: 10631177.
18. Koplin A, Preissler S, Ilina Y, Koch M, Scior A, Erhardt M, et al. A dual function for chaperones SSB-RAC and the NAC nascent polypeptide-associated complex on ribosomes. J Cell Biol. 2010; 189: 57–68. doi: 10.1083/jcb.200910074 PMID: 20368618; PubMed Central PMCID: PMCPMC2854369.
19. Kirstein-Miles J, Scior A, Deuerling E, Morimoto RI. The nascent polypeptide-associated complex is a key regulator of proteostasis. EMBO J. 2013; 32: 1451–1468. doi: 10.1038/emboj.2013.87 PMID: 23604074; PubMed Central PMCID: PMCPMC3655472.
20. Gamerdinger M, Hanebuth MA, Frickey T, Deuerling E. The principle of antagonism ensures protein targeting specificity at the endoplasmic reticulum. Science. 2015; 348: 201–207. doi: 10.1126/science.aaa5335 PMID: 25859040.
21. Wiedmann B, Prehn S. The nascent polypeptide-associated complex (NAC) of yeast functions in the targeting process of ribosomes to the ER membrane. FEBS Lett. 1999; 458: 51–54. PMID: 10518932.
22. Sydorskyy Y, Dilworth DJ, Yi EC, Goodlett DR, Wozniak RW, Aitchison JD. Intersection of the Kap123p-mediated nuclear import and ribosome export pathways. Mol Cell Biol. 2003; 23: 2042–2054. PMID: 12612077; PubMed Central PMCID: PMCPMC149464.
23. Basu U, Si K, Warner JR, Maitra U. The Saccharomyces cerevisiae TIF6 gene encoding translation initiation factor 6 is required for 60S ribosomal subunit biogenesis. Mol Cell Biol. 2001; 21: 1453–1462. doi: 10.1128/MCB.21.5.1453–1462.2001 PMID: 11238882; PubMed Central PMCID: PMCPMC86691.
24. Gorenstein C, Warner JR. Coordinate regulation of the synthesis of eukaryotic ribosomal proteins. Proc Natl Acad Sci U S A. 1976; 73: 1547–1551. PMID: 775493; PubMed Central PMCID: PMCPMC430334.
25. Lopez N, Halladay J, Walter W, Craig EA. SSB, encoding a ribosome-associated chaperone, is coordinately regulated with ribosomal protein genes. J Bacteriol. 1999; 181: 3136–3143. PMID: 10322015; PubMed Central PMCID: PMCPMC93769.
26. Albanese V, Yam AY, Baughman J, Parnot C, Frydman J. Systems analyses reveal two chaperone networks with distinct functions in eukaryotic cells. Cell. 2006; 124: 75–88. doi: 10.1016/j.cell.2005.11.039 PMID: 16413483.
27. Meyer AE, Hung NJ, Yang P, Johnson AW, Craig EA. The specialized cytosolic J-protein, Jjj1, functions in 60S ribosomal subunit biogenesis. Proc Natl Acad Sci U S A. 2007; 104: 1558–1563. doi: 10.1073/pnas.0610704104 PMID: 17242366; PubMed Central PMCID: PMCPMC1785244.
28. Demoinet E, Jacquier A, Lutfalla G, Fromont-Racine M. The Hsp40 chaperone Jjj1 is required for the nucleo-cytoplasmic recycling of preribosomal factors in Saccharomyces cerevisiae. RNA. 2007; 13: 1570–1581. doi: 10.1261/rna.585007 PMID: 17652132; PubMed Central PMCID: PMCPMC1950757.
29. Wessa P. Free Statistics Software, Office for Research Development and Education [URL]. 2015. Available: http://www.wessa.net/.
30. Rospert S, Dubaquie Y, Gautschi M. Nascent-polypeptide-associated complex. Cell Mol Life Sci. 2002; 59: 1632–1639. PMID: 12475173.
31. Hartmann-Petersen R, Semple CA, Ponting CP, Hendil KB, Gordon C. UBA domain containing proteins in fission yeast. Int J Biochem Cell Biol. 2003; 35: 629–636. PMID: 12672455.
32. Brachmann CB, Davies A, Cost GJ, Caputo E, Li J, Hieter P, et al. Designer deletion strains derived from Saccharomyces cerevisiae S288C: a useful set of strains and plasmids for PCR-mediated gene

disruption and other applications. Yeast. 1998; 14: 115–132. doi: 10.1002/(SICI)1097-0061(19980130)14:2<115::AID-YEA204>3.0.CO;2–2 PMID: 9483801.

33. Goldstein AL, McCusker JH. Three new dominant drug resistance cassettes for gene disruption in Saccharomyces cerevisiae. Yeast. 1999; 15: 1541–1553. Epub 1999/10/09. doi: 10.1002/(SICI)1097-0061(199910)15:14<1541::AID-YEA476>3.0.CO;2-K PMID: 10514571.

34. Frickey T, Lupas A. CLANS: a Java application for visualizing protein families based on pairwise similarity. Bioinformatics. 2004; 20: 3702–3704. doi: 10.1093/bioinformatics/bth444 PMID: 15284097.

35. Edgar RC. MUSCLE: multiple sequence alignment with high accuracy and high throughput. Nucleic Acids Res. 2004; 32: 1792–1797. doi: 10.1093/nar/gkh340 PMID: 15034147; PubMed Central PMCID: PMCPMC390337.